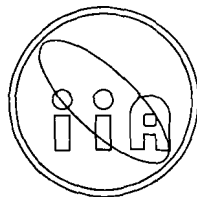


Effects of the Poor Cluster Environment on Galaxies

*A thesis
submitted for the degree of
Doctor of Philosophy
in the Faculty of Science
University of Calicut, India*

Mangala Sharma



Indian Institute of Astrophysics
Bangalore, India


July 2002

Dr. K. Neelakandan
Professor

Department of Physics
University of Calicut

Certificate

This is to certify that the thesis entitled '*Effects of the Poor Cluster Environment on Galaxies*' is a bona fide record of research work carried out by *Mangala Sharma* at the Indian Institute of Astrophysics under my supervision for the award of the degree of Doctor of Philosophy of the University of Calicut and that no part of this thesis has been presented elsewhere for the award of any degree, diploma or other similar title.


(K. Neelakandan)

University of Calicut
Calicut, India

Date: 17-9-2002

Declaration

I hereby declare that this thesis entitled '*Effects of the Poor Cluster Environment on Galaxies*', submitted to the University of Calicut for the award of a Ph.D. degree, is a bona fide record of the research work carried out by me at the Indian Institute of Astrophysics, Bangalore (a recognised Research Center of the University of Calicut). No part of this thesis has been presented before for the award of any degree, diploma or other similar title.



Mangala Sharma

Indian Institute of Astrophysics
Bangalore, India

Date:

Acknowledgments

*Writing is easy. All you do is stare at a blank sheet of paper
until drops of blood form on your forehead.*

– Gene Fowler

I can hardly believe that I've completed my thesis. The relief is so overwhelming that I am at a loss for words to acknowledge all the people who sailed with me through these years of my doctoral work. Let me therefore take recourse to the conventional, and begin at the beginning.

I thank Prof. R. Cowshik, director, Indian Institute of Astrophysics, for giving me the opportunity to work toward my doctoral degree. Prof. T. P. Prabhhu, my supervisor at IIA, gave me valuable advice and encouraged me to chart my own course among the galaxies. My sincere gratitude goes to Prof. K. Neelakandan, my supervisor at Calicut University, Prof. S. S. Hasan (IIA) and Dr. B. R. S. Babu (Calicut University) for their constant support and great help with my Ph.D. registration and university formalities.

I owe a debt of gratitude to the Time Allocation Committee of the Vainu Bappu Observatory for allotting — year after year — dark nights for my observations. The observing assistants and technical support staff of the VBT were most helpful, supplying me generous, competent assistance and hot tea during the observations on clear runs, as well as commiseration on the (too many!) clouded nights. S. G. Bhargavi gave me some 20 minutes of a photometric night in March 2000 that helped me nail the *B*-band calibration of the cluster MS 0735.6+7421.

To R. Srikanth and S. Rajaguru — fellow eclipse watchers, friends at work and beyond, and companions at countless lunches — my gratitude is infinite. With them, and Holger Merlitz and B. S. Ramachandra, I could not only discuss work but also be myself and share the feeling that doing astronomy is not just about making a living.

I acknowledge useful interactions with Dr. J. Bagchi, Profs. S. Bhavsar, B. Guiderdoni, C. Sivaram, Dr. P. Shastri, and Prof. K. P. Singh, all of whom directly increased my knowledge of astronomy and cosmology. Many thanks also to my colleagues and fellow students at IIA; over the course of these years, we have had many rich exchanges. A great benefit to me came from some astronomy meetings and schools I attended; I am obliged, in particular, to Profs. A. K. Kembhavi and B. Guiderdoni for having invited me to a couple of the excellent meetings they organized.

This research has made use of NASA's Astrophysics Data System Bibliographic Services.

This research has made use of the NASA/IPAC Extra-galactic Database (NED) which is operated by the Jet Propulsion Laboratory, Caltech, under contract with the National Aeronautics and Space Administration.

This research has made use of the SIMBAD database, operated at CDS, Strasbourg, France.

This research has made use of the USNOFS Image and Catalogue Archive operated by the United States Naval Observatory, Flagstaff Station.

This research has made use of the APS Catalog of POSS I which is supported by the National Aeronautics and Space Administration and the University of Minnesota.

We made use of the database CATS (Verkhodanov et al., 1997) of the Special Astrophysical Observatory.

Figure 1.1 used scanned images from the Digitized Sky Surveys. The Digitized Sky Surveys were produced at the Space Telescope Science Institute under U.S. Government grant NAGW-2166. The images of these surveys are based on photographic data obtained using the Oschin Schmidt Telescope on Palomar Mountain and the UK Schmidt Telescope.

I must not forget to mention the immense influence upon my Ph.D. of the Weather Gods working overtime at Kavalur. They taught me patience (though I still haven't got the hang of the best-to-be-resigned bit), allowed me to discover what sort of clouds I like best (cirrus, for the spectacular array of colors they bring out at sunset), and gave me ample time to become au courant with ARAA articles.

Hard though to believe, especially while proof-reading a thesis, life exists, indeed has always existed, outside academia. I happen to know some wonderful people whose roles in my life I'd like to acknowledge with great pleasure.

My confidantes for heaven knows how long – Sunitha, Siri, Vasu and Rahool, with whom a strong sense of belonging and acceptance prevails. It sounds almost silly to thank you. Instead I quote from my favorite Basho:

*Don't touch my plum tree!
Said my friend, and saying so
Broke the branch for me*

A soft white bouquet of affection and thanks to Lakshmi and Ashok. You share so generously of yourselves, and you believed in me when even I sometimes had doubts. You will always be special to me!

Other special folks get special mention: Stephane who introduced me to Doisneau's superb photographs and French poetry, Jam for twinkling haiku, and Ramkiran for those Sunday action matinees. Rahul, at his most pre-occupied, organized hikes and concert tickets. Jean-Marc empathized. Jyotsna understood the part about gittin' a thorn with every rose but ain't the roses sweet. Ted hid ax murderers in the mists at the observatory. Thanks, everyone, for all these and oh-so-much more!

I managed to remain unblinker during my thesis writing thanks also to my association with Suchitra Film Society and Friends of CRY. My creative, committed and enthusiastic friends in these places, I am delighted and gratified to know you. May your tribe increase!

I've saved the most for last. My family, who make it all possible. Amma, Appa, Avva and Sona, you give me steadfast support, endless caring, patience and generosity. I wonder if I could have achieved any of this without your unquestioning belief in me! This chatterbox has run out of words to express her immeasurable gratitude to you. You'll just have to settle for all my love instead.

This work is dedicated to all who have stars in their eyes.

Synopsis

Galaxies are rarely isolated “island universes”; they reside in environments that span a continuum of densities, from rarefied voids and the isolated “field”, to binary galaxies, then triplets and small groups of galaxies, through poor clusters and finally, to crowded rich clusters. A galaxy naturally interacts with its surroundings. Its environment — the number of neighbors, their spatial distribution and relative velocities — exerts influence on the galactic characteristics and evolution; in turn, the release of material and energy from a galaxy into the surroundings affects the systems to which it belongs. Observations do indeed give weight to variations existing in galaxy properties such as morphological fractions, star formation, luminosity function, etc., in different environments. The variations may have been set *ab initio*, and/or may arise due to the different relative impact of processes such as galaxy interactions and mergers, ram-pressure stripping or gas infall in the different environments. This is the so-called “nature vs. nurture” debate about galaxy properties.

Galaxies within rich clusters evince the most dramatic environmental forcing: for instance, spiral and irregular galaxies are hardly found in the centers of dense clusters, whereas they are the most common component of the field. Further, cluster spirals show only about one-third the star-formation as their kin in the field. However, comprising $< 5\%$ of the total galaxy population and subject to exceptionally strong environmental effects, rich cluster members represent a minority population. Now, a much larger fraction of galaxies are members of poorer systems.

Such “poor clusters” (PCs), a few of which we study in the present thesis, are aggregates of a few tens of galaxies with velocity dispersion of about $300\text{--}700 \text{ km s}^{-1}$ (Beers et al. 1995). They are intermediate environs between small groups (with fewer than five galaxies brighter than L^*) and crowded rich clusters (which contain upto several hundred galaxies brighter than the average luminosity L^*), and contain about 20% of the galaxies in the nearby universe (White et al. 1999). A large fraction of poor clusters show luminous, extended X-ray emission presumably arising from the diffuse intracluster medium; the galaxy distribution traces the X-ray structure in these systems (Dell’Antonio et al. 1995). Poor clusters form a natural and continuous extension to lower richness, mass, size, and X-ray luminosity from the rich and rare clusters (Bahcall 1980; White et al. 1999), bridging the gap between the well-studied environments of the rich clusters and the special groups such as the Hickson Compact Groups. It is then interesting to examine how galaxies evolve in such small clusters where, in comparison with rich clusters, the effects of the intracluster plasma are comparable but the tidal perturbations due to the global potential are weaker, but where, in comparison with small groups, the velocity dispersions are higher and the global potential deeper. If the kinematics and dynamical youth of poor clusters (e.g., Beers et al. 1995; Ledlow et al. 1996) make them preferred sites for galaxy-galaxy interaction (some of which may culminate in mergers), the morphologies and star formation histories of some member galaxies may be altered, leading to variations in the bulk properties of cluster galaxies.

Moreover, galaxy groups and poor clusters are effective tracers of the large-scale galaxy distribution, with the group centers following the distribution of all galaxies (Ramella, Geller, & Huchra 1989), and their principal axis being aligned with their neighbors on scales extending to about $15\text{--}30 \text{ h}^{-1} \text{ Mpc}$ (West 1989). X-ray data show that in superclusters, massive Abell clusters are

linked together by groups and poor clusters of galaxies (Mulchaey 2000). If clusters and super-clusters formed hierarchically from smaller associations, poor clusters, as the building blocks, provide a natural focus to understand the formation and evolution of large-scale structure in the universe.

In this thesis we present an observational study — primarily through optical imaging — of galaxy properties within four X-ray luminous poor clusters at moderate redshifts ($0.08 < z < 0.25$). In the literature there are many definitions of poor clusters; our working definition of a poor cluster is that its bright galaxy population within the central 0.5 Mpc must number > 5 but \leq the Abell (1958) richness 0 criterion of between 30 and 49 galaxies within two magnitudes of the third brightest cluster member. We select our sample as luminous, extended X-ray sources identified with galaxy overdensities that are noted as being optically poor in the EMSS catalog of clusters of galaxies (Gioia & Luppino 1994). Selection of clusters by means of their (extended) X-ray emission has a major advantage over optical selection in that X-ray observations are far less contaminated by projection effects — especially important for poorly populated galaxy systems — thereby avoiding spurious detections.

We acquired optical images of the poor clusters at the prime focus of the 2.34-m Vainu Bappu Telescope, operated by the Indian Institute of Astrophysics, using a CCD detector and broadband B, V, R and I filters. We performed standard CCD data pre-processing, and then co-added the individual cluster images within each filter. We used the FOCAS suite of programs (Valdes 1982) to detect objects and classify them into stars or extended objects. Our final catalogs contain all the extended objects detected in the fields of the individual clusters; we shall refer to these objects as galaxies. We performed aperture photometry on all the objects using 3.5 arcsecond diameter apertures, and calculated total magnitudes by applying aperture corrections. We then transformed the photometry from the instrumental system into the Johnson B, V and Kron-Cousins R, I standard systems using the open cluster M67 and several Standard Area stars from Landolt (1992) for photometric calibration. For an object of $m_v = 20$ mag, the total photometric error is ≈ 0.7 mag. We corrected the photometry for Galactic extinction, and employed the spectro-evolutionary models of Poggianti (1997) to compute K-corrections to derive rest-frame magnitudes. The final galaxy catalogs are complete to about $M_V = -18$ in the cluster rest-frame. We describe the details of the above in Chapter 2.

We study in Chapters 3, 4 and 5 several statistical properties of the galaxies in these four poor clusters using the optical photometry mentioned above. The questions we address are:

- How do colors of galaxies in poor clusters compare with those in the field and rich clusters?
- What is the nature of the luminosity function in the poor clusters?
- What is the morphology of the poor clusters?

In Chapter 4 we study the stellar content of the cluster galaxies using their colors as tracers of stellar ages and populations. We derive the relation between the optical magnitudes and colors of the early-type galaxies, the so-called color-magnitude relation (CMR), as $B-V$ vs. V , $V-R$ vs. V and $R-I$ vs. V . A significant fraction of objects in the lines-of-sights to the various poor clusters

fall within narrow ridges in the color-magnitude plane. This is similar to the situation in rich clusters; in fact, virtually all rich clusters observed so far have a tight sequence of red early-type galaxies (e.g., Stanford et al. 1998). Further, the poor cluster CMRs have slope and scatter unchanged with respect to local clusters such as Virgo, within the observational errors. This is circumstantial evidence that the poor cluster environment suppresses star formation, since cluster ellipticals are typically redder than their field counterparts. The smallness of the scatter in the CMR and near constancy of its slope over the admittedly modest redshift range of our poor cluster sample implies also that the bulk of the stars in these cluster early-type galaxies is coeval and has perhaps formed at $z > 2 - 3$. We then use this well-defined ridge or “sequence” to identify cluster members; such a cluster red sequence, even if it has significant scatter, generally represents a distribution not found in the cumulative field that would span a large redshift range (Gladders & Yee 2000).

A substantial fraction of bright galaxies in the clusters are bluer than can be ascribed to the existence of a CMR and predictions of passive evolution. The blue galaxy fractions ($f_b \approx 0.1$) in the EMSS poor clusters are similar to those of low redshift richness 0 clusters, which are themselves higher than those of rich clusters at similar redshifts. These blue galaxies could be field galaxies in the process of infall into the cluster. Or interactions between galaxies (clearly visible in a few of the blue galaxies) and internal tides in the cluster may have induced recent excess star formation resulting in the blueing of these small number of galaxies.

We study another statistical property of galaxies in Chapter 3 – their luminosity function (LF), i.e, the relative abundance distribution of galaxies within a given volume according to their brightness. The LF stands in for the distribution of galaxy masses and is thus a fundamental measure in extra-galactic astronomy and cosmology.

If the LF is universal or consistent in shape across the different galaxian environments, it argues for the galaxy mass function being insensitive to global neighborhood. On the other hand, if the dwarf-to-giant galaxy ratio increases significantly with the richness of the environment (e.g., Phillipps et al. 1998), one expects the poor cluster LF to be steeper than those in the field and small groups, and flatter than that of much richer clusters. The “nature versus nurture” debate is valid here as well: is it the early environment or subsequent influences that determines the differences in LF? Since galaxy interactions or mergers that lead to changes in the number and luminosity of galaxies occur on different timescales in different environments, galaxy LF may behave differently in the field, galaxy groups and clusters. Further, if star-formation and galaxy evolution in poor clusters are different from (or more recent than) that in the cores of rich clusters or the field, it may have a noticeable effect on the poor cluster LF. If there are differences in the bright-end of the LFs of rich and poor clusters, then, is it this factor that renders some cluster rich and others poor?

A study of the poor cluster LF has two main purposes: (1) to test for “universality” of the LF of different poor clusters, and (2) to compare the galaxy LF in the EMSS poor clusters with those in the field and rich clusters, and thus study the influence of the environment on galaxy formation or in modifying the primordial LF through dynamical processes either during or after cluster collapse.

Again, using the tightness of the CMR as a tool to distinguish cluster members from the background, we construct the cluster galaxy luminosity functions to a faint limit of $M_V = -18$. Since our I band data are not so deep nor so complete as the V and R filter images, we shall exclude this band from the present analysis. Non-parametric statistical tests show that the individual cluster V and R -band LFs (to $M_V = -18$) are not significantly different from each other. We then construct composite LFs in B , V , and R bands by a simple combinations of the individual cluster sequence LFs. Again, non-parametric tests indicate that these composite LFs are reasonably good representations of the individual LFs. Both argue for galaxy luminosity distributions being similar in the poor clusters (whose X-ray luminosities vary by a factor of twenty).

We use another technique to construct the LFs that is independent of the “sequence” selection. We select galaxies within a particular metric radius of the brightest cluster galaxy, and bin the galaxy counts by magnitude into 0.5 mag bins. To derive the cluster, i.e., field-corrected LFs, we subtract binned field galaxy counts from the literature from the cluster galaxy counts. The composite LFs created by weighted addition of the individual cluster LFs are in all cases falling steeply in the brighter magnitudes and are relatively shallow at faint luminosities. We fit the Schechter (1976) function to the composite LFs of both the sequence galaxies and the background-corrected magnitude data. Since the brightest cluster galaxies are unlikely to have all arisen from a Schechter LF (Schechter 1976; Bhavsar 1989), we remove them from the individual catalogs prior to fitting the analytical function. Schechter fits to these composite LFs generated using the two different methods have similar parameters, attesting to the robustness of our cluster galaxy selection. The LF slopes are flat ($\alpha \approx -1$) in the different colors. They are thus similar to V -band LF of MKW/AWM poor clusters (Yamagata & Maehara 1986). In the R -band, the poor cluster LF is steeper than that of field galaxies (e.g., Lin et al. 1996) but not so steep as in either poor groups (Zabludoff & Mulchaey 2000) or richer clusters (e.g., Colless 1989; Trentham 1998).

There is evidence that optical morphology, the presence of a dominant D or cD galaxy in the cluster center, and X-ray emission of the clusters correlate with their richness and dynamical states (e.g., Bahcall 1980, Forman & Jones 1984), and influence the ratio of dwarf galaxies to bright ones (Lopez-Cruz 1997). In Chapter 5 we present analyses related to the morphology of the four EMSS poor clusters. We study the cluster morphology at various levels: qualitatively by visual assessment and through a simple comparison of the optical image with the contours of X-ray emission; and in a quantitative manner using maps of the projected galaxy distribution. We look at the spatial arrangement of the galaxies as a function of their colors to evaluate the radial trend of morphology. We check if the clustering properties of the cluster galaxies depends on their brightness by estimating the amount of luminosity segregation. We then discuss the alignment effect wherein the brightest cluster member points in the same direction as the distribution of cluster galaxies.

We discover that our poor clusters are similar to rich clusters in terms of a significant number of faint galaxies in the cluster “sequence”, their central concentration, the coincidence of the position of the BCM and extended X-ray emission, and reasonable coincidence of X-ray and galaxy density isocontours. We find, not surprisingly, that the core and halo sizes for our poor clusters are typically one third and one quarter of the corresponding sizes for Abell clusters (Hickson 1977). Their concentration factor is smaller than the average for Abell clusters. The poor cluster

morphologies are irregular and show some substructure, suggesting they are relatively unevolved. However, the dynamical youth of the cluster does not seem to rule out galaxy segregation by luminosity (for which the evidence is marginally significant). Further, luminosity segregation responds marginally more strongly to cluster-centric distance rather than to local environment, suggesting that its dominant driver is the global (dynamic) potential of the cluster. As for morphological segregation, the evidence is subtle and not very tractable to our analysis.

We also find that the first-ranked cluster member is frequently collimated with the distributions of galaxies and the intracluster gas. In particular, for MS0002 and MS0735, the optical major axis of the BCM, the isocontours of the galaxy distribution and the X-ray emission (from the intracluster hot gas which, outside the cooling radius, traces the cluster gravitational potential) are clearly elongated in approximately the same direction. The collimation of the BCM major axis with the galaxy distribution in the parent cluster and with the diffuse X-ray emission follows the statistical behavior of cD galaxies in rich clusters. This similarity between our X-ray luminous poor clusters, much poorer groups, and cD clusters offers support to the insensitivity of the alignment effects to system richness.

Many clusters – rich and poor – harbor gigantic galaxies at their centers (defined by the centroid of either the galaxy distribution or the X-ray emission, which may frequently coincide). Dynamical friction, mergers, and tidal stripping together give rise to galactic cannibalism whose end product is an extremely luminous first-ranked galaxy along with a deficit of normal bright galaxies. To explore if the first-ranked galaxies in poor and rich clusters similar, we perform multicolor CCD surface photometry for the brightest cluster members (BCMs) of three of our sample of poor clusters (the exclusion being MS0735). This is the subject of Chapter 6 of the thesis. We use the standard package STSDAS layered onto IRAF to interactively fit ellipses to the isophotes of the galaxies following the method of Jedrzejewski (1987). We account for errors due to sky subtraction and seeing effects. All galaxies show a monotonous increase in ellipticity with radius, but no significant changes in position angle. The BCMs have surface brightness profiles that can be described by a de Vaucouleurs law; none show the envelopes characteristic of cD galaxies. However, the BCMs have enlarged characteristic radii and lower central surface brightness in comparison with normal ellipticals. One of the BCMs (of MS1306) has an anomalous color profile that reddens with increasing galactocentric distance. The observed color gradients for the other two galaxies imply a decrease in the metallicity by a factor of about 2 per decade in radius. The BCMs are aligned with the X-ray emission and galaxy distribution as mentioned above. The alignments suggest that the formation and/or evolution of the central galaxy is linked to the shape of the global cluster potential. Our observations suggest in toto that the poor clusters BCMs have grown dynamically, with mergers having been important at early epochs.

Overall, in terms of the statistical properties of their galaxies, poor cluster appear to be extensions of their rich counterparts to lower masses and lower or comparable X-ray luminosities.

Contents

1	Introduction	1
1.1	Galaxian Environments	1
1.2	Environmental Influences on Galaxies	5
1.2.1	Galaxy Formation in Different Environments	5
1.2.2	Drivers of Galaxian Properties and Evolution	5
1.2.3	Signatures of Environmental Variations in Galaxy Properties	8
1.3	Background on Poor Clusters	11
1.3.1	Motivation for Studying Poor Clusters	12
1.3.2	Definitions and Catalogs	13
1.3.3	Content: Galaxies and Intracluster Medium	16
1.3.4	Are Poor Clusters Real? Bound? Virialized?	18
1.3.5	Simulations	19
1.4	Objectives and Presentation of the Thesis	20
2	Observations and Data Analysis	22
2.1	Avant-Propos	22
2.2	Sample Selection	23
2.2.1	Poor Clusters : Operational Definition	23
2.2.2	Other work done with the EMSS cluster sample	24
2.2.3	Sample Selection: Caveats	25
2.2.4	Preliminary Richness Estimates	26
2.3	Observations : Optical Imaging	28
2.3.1	Telescope: the Vainu Bappu Telescope	28
2.3.2	Filters: Broad-band B, V, R and I	29
2.3.3	Detector: CCD	29
2.3.4	Gainful Imaging: the Shift-and-Stare Technique	31
2.3.5	Imaging Sequence at the VBT	31
2.4	Image Analysis	32
2.4.1	CCD Data Pre-Processing	33
2.4.2	Image Registration and Co-Addition	34
2.4.3	Object Detection and Classification	35
2.4.4	Optical Photometry	38
2.4.5	Galactic Extinction Correction	40
2.5	Cluster Galaxy Catalogs	40
2.5.1	Individual Cluster Catalogs	41
2.5.2	Completeness and Misclassifications	41
2.6	Discussion and Summary	44

3	Galaxy Luminosity Functions	48
3.1	Avant-Propos	48
3.2	Analysis	51
3.2.1	Extraction of Cluster Galaxies	51
3.2.2	Conversion to Rest-Frame Magnitudes	54
3.2.3	Construction of the Individual Luminosity Functions	56
3.2.4	Estimation of Completeness	56
3.2.5	Errors in Construction of the Individual LFs	57
3.2.6	Construction of Composite Luminosity Functions	58
3.2.7	Nonparametric Tests	59
3.2.8	Schechter Function Fits and Parametric Tests	60
3.3	Results	61
3.3.1	Cluster Richness	62
3.3.2	Binned Galaxy LFs for Individual Clusters	64
3.3.3	Direct Comparisons of Unbinned LFs	65
3.3.4	Binned Composite LFs and Schechter Parameters	68
3.3.5	LF over Different Cluster Radii	71
3.3.6	Schechter Parameters: Comparison with Other Environments	73
3.4	Summary and Discussion	75
3.4.1	Is there a universal LF?	75
3.4.2	Is the LF determined by Nature or Nurture?	77
4	Evolutionary State of the Cluster Galaxies	80
4.1	Avant-Propos	80
4.2	The Color–Magnitude Relation	81
4.2.1	The Form and Causes of the Correlation	82
4.2.2	Analysis	82
4.2.3	Results	83
4.3	Cluster “Sequence” Galaxies	89
4.4	Photometric Blue Galaxy Fraction	94
4.4.1	The Butcher–Oemler Effect	94
4.4.2	Analysis	96
4.4.3	Results	98
4.5	Red Galaxies	101
4.6	Discussion and Conclusions	103
5	Cluster Morphology	104
5.1	Avant-Propos	104
5.2	Visual and X-Ray Morphologies	105
5.3	Spatial Distribution of Galaxies	113
5.3.1	Galaxy Isopleths	113
5.3.2	Structural Parameters	115
5.4	Galaxy Segregation	121
5.4.1	Luminosity Segregation	123

5.4.2	Color Segregation	124
5.5	Alignment Effect	126
5.6	Summary and Discussions	130
6	The Brightest Cluster Galaxies	133
6.1	Avant-Propos	133
6.2	Techniques: Isophotal Analysis and Color Maps	136
6.2.1	Pre-Processing	136
6.2.2	Photometric Calibration	136
6.2.3	Ellipse Fitting	137
6.2.4	Residual and Color Maps	138
6.2.5	Errors in Isophotal Analyses	139
6.3	Morphological and Structural Parameters	140
6.3.1	Visual Morphology	140
6.3.2	Isophotal Geometry	141
6.3.3	Deviations from Elliptical Structure	144
6.3.4	Surface Brightness Profiles	148
6.4	Stellar Populations and Interstellar Matter	153
6.4.1	Color Gradients	153
6.4.2	Presence of Dust and Fine Structure	158
6.5	Further about Individual Galaxies	160
6.5.1	Dwarf Galaxies of MS 1306.7-0121	160
6.5.2	The VSSS in MS 0735.6+7421	161
6.6	Discussion	162
7	Conclusions	165
7.1	Recapitulation of our Results	165
7.2	Future Investigations	167
A	Catalog of Galaxies	183
B	Cosmological Parameters	192
C	Image Reduction Software	193

List of Figures

1.1	A gallery of galaxy environments	2
1.2	X-ray-optical overlay for AWM7	17
2.1	Completeness of detection	41
2.2	Star-galaxy separation	43
2.3	Number counts of stars and galaxies	44
3.1	Galaxy counts in “local” backgrounds	52
3.2	“Global” background subtraction for luminosity functions	54
3.3	$N_{0.5}$ vs. L_X	64
3.4	LFs for the EMSS poor clusters using “sequence” galaxies	65
3.5	Composite LFs for the poor clusters	69
3.6	LFs of EMSS poor cluster versus other environments	74
4.1	Color-magnitude diagrams for MS0301 and MS1306	85
4.2	Color-magnitude diagrams for MS0002 and MS0735	86
4.3	Scatter about the color-magnitude relations	88
4.4	$(B - V)$ vs. $(V - R_C)$ color-color diagrams	90
4.5	$(R_C - I_C)$ vs. $(V - R_C)$ color-color diagrams	91
4.6	Blue galaxy fractions	99
4.7	Red galaxies in the EMSS fields.	102
5.1	Optical-X-ray image and isopleths of MS 0002.8+1556	106
5.2	Optical-X-ray image and isopleths of MS 0301.7+1516	107
5.3	Optical-X-ray image and isopleths of MS 0735.6+7421	108
5.4	Optical-X-ray image and isopleths of MS 1306.7-0121	109
5.5	Galaxy counts centered on the BCMs	115
5.6	Radial extent of the poor clusters	116
5.7	Distribution of galaxies according to color	125
6.1	Images of the brightest cluster members	140
6.2	BCM ellipticity and position angles	142
6.3	Third- and fourth-order deviations from ellipticity	146
6.4	BCM surface brightness profiles	150
6.5	BCM color profiles	155
6.6	Color map of the central region of MS1306	159
6.7	Radio maps of 4C +74.13	163
B.1	Important parameters in different cosmologies.	192

List of Tables

1.1	Galactic morphological distribution in different environments	9
1.2	Typical properties of clusters and groups.	17
2.1	Possible poor clusters in the EMSS catalog	25
2.2	Cast of characters	26
2.3	Preliminary richness measurements	28
2.4	CCD parameters	30
2.5	Galactic extinction corrections	40
2.6	Objects detected and classified by FOCAS	40
2.7	Photometric transformation using M67.	46
2.8	Journal of cluster observations	47
3.1	K-corrections for elliptical galaxies from Poggianti (1997).	55
3.2	Cluster richness estimates using “sequence” galaxies	63
3.3	Inter-comparisons between individual LFs	66
3.4	Non-parametric tests on the composite LFs	67
3.5	Schechter parameters for the composite LFs	70
3.6	Schechter parameters for LFs in various environments	75
4.1	The linear fits to the color-magnitude relations.	84
4.2	Cluster blue galaxy fractions.	98
5.1	Optical mosaic images of the clusters	110
5.2	Core and halo sizes, concentration factor, and clumpiness	119
5.3	Intergalactic separations at different magnitude ranges	123
5.4	Intergalactic separations for different color ranges	126
5.5	Position angles to examine alignment effect	128
6.1	BCM isophote geometrical parameters	143
6.2	Fit parameters for the de Vaucouleurs law.	151
6.3	Color gradients in the BCMs	156
6.4	Properties of the candidate dwarf galaxies around MS1306.	160
6.5	The VSSS 4C +74.13	162
A.1	Catalog of galaxies in the field of MS0002.	185
A.2	Catalog of galaxies in the field of MS0301.	187
A.3	Catalog of galaxies in the field of MS0735	189
A.4	Catalog of galaxies in the field of MS1306.	191

Chapter 1

Introduction

... the realm of the nebulae is the universe ...

– Edwin Hubble

If galaxies are “island universes” then they prefer to reside in archipelagos whose populations span a wide range from only a few to a few thousand members¹. After formation, a galaxy may evolve as an isolated entity, governed entirely by internal processes such as feedback from supernovae, galactic winds, etc. A present-day galaxy then has attributes that are at least partially determined by those of its protogalactic precursor(s). But far from evolving in splendid isolation, galaxies naturally interact with their surroundings. The **environment** — the number of neighbors a galaxy has, their spatial distribution and relative velocities — exerts influence on galactic characteristics and evolution; in turn, the release of material and energy from a galaxy into the surroundings affects the systems to which it belongs. Controversy persists about the extent to which the initial conditions (“nature”) and the galactic environment (“nurture”) affect the properties and evolution of galaxies². An additional important issue is the relative contribution of the environment at galaxy formation versus that at the present epoch.

Studies of galaxy properties as a function of environs (and look-back time) are extremely important in constraining any theoretical understanding of their formation and evolution, and in cosmology. In this thesis, we study a particular galaxian environment, the **poor cluster**, and some of its effects on the properties of galaxies.

1.1 Galaxian Environments

Galaxies occur in neighborhoods that span a continuum of densities, from rarefied voids to crowded rich clusters (see Fig. 1.1). Compared to the cosmic mean space density of ≈ 0.02 bright galaxies per cubic megaparsec (Zombeck 1990), the density in voids is depressed by about a factor of four; at the other extreme of the cores of rich clusters the galaxy density is enhanced by $\geq 10^4$. In this section, we shall briefly describe the diverse environments in which galaxies are located.

Isolated galaxies are in the simplest environments; these objects have no known optical companions within about one megaparsec (Mpc) and within recession velocities ± 1000 km s⁻¹ of their own. The top left panel in Fig. 1.1 shows the isolated spiral galaxy IC 1269 ($z = 0.02$, $m_B = 13.4$). However, deep observations show that even isolated galaxies are connected with

¹Though galaxies cluster together at small separations, their distribution on the largest scales (> 100 Mpc) is homogeneous. This corroborates the Cosmological Principle that states that the universe is everywhere isotropic and homogeneous, i.e., it looks the same in all directions and presents the same aspect from all places. Galaxies are also receding from each other at the largest scales, implying an expanding universe.

²Evrard (1993) suggests that for a galaxy of mass M_{gal} , processes operating on mass scales $M \leq M_{gal}$ may be ascribed to “nature” while those arising from $M > M_{gal}$ are “nurture” processes; environmental effects fall into the latter category.

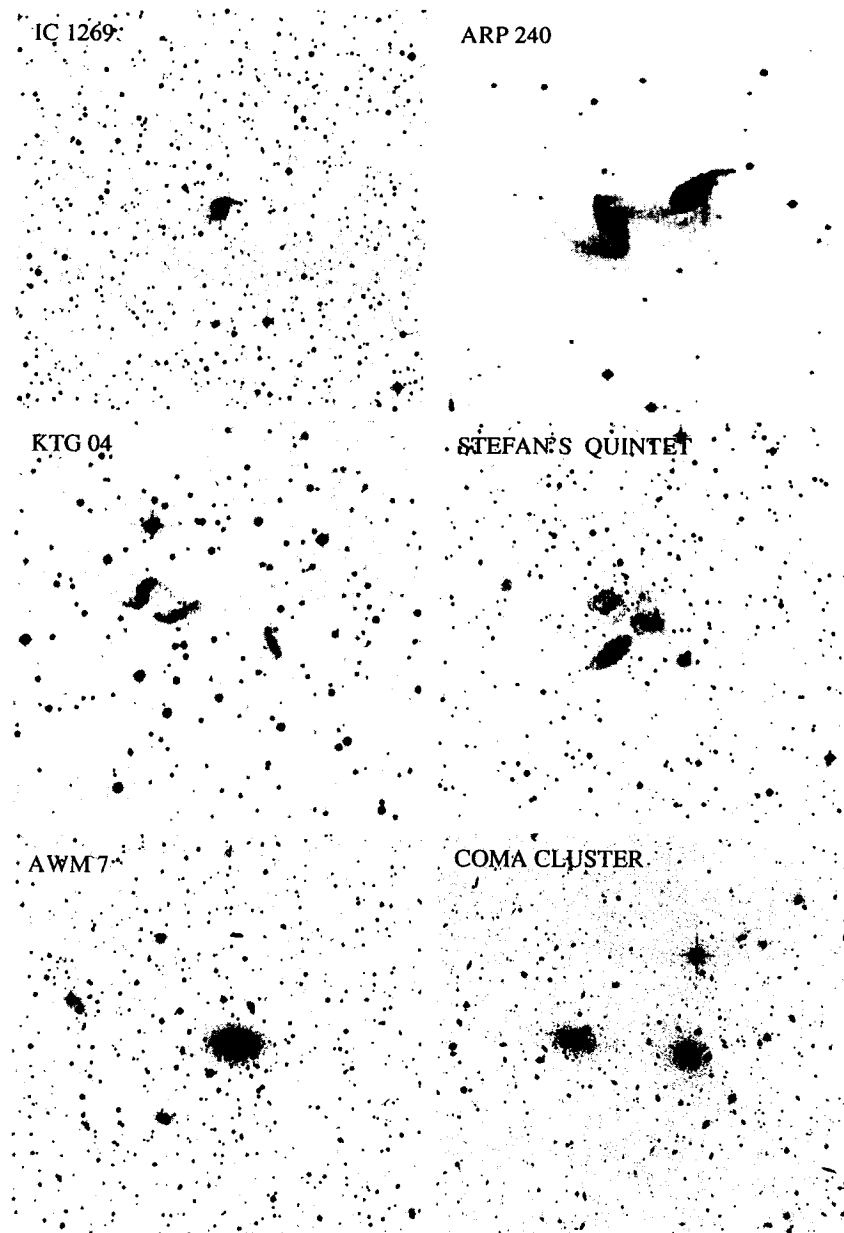


Figure 1.1: The different neighborhoods in which galaxies are located. Going from upper left to bottom right: isolated “field”, pair, triplet, compact group, poor cluster, and rich cluster. All the galaxies are at similar distances ($z \approx 0.02$). The optical images cover on a side 250 kpc for the isolated and paired galaxies, 500 kpc for the triplet, group and poor cluster, and 1 Mpc across the Coma Cluster. The little dots in all the images are stars of the Milky Way, except in the Coma region where they are mostly faint galaxies. Images are from the Digitized Sky Surveys.

diffuse systems of galaxies (Einasto 1990) or have dwarf satellites (e.g., Zaritsky et al. 1993), implying that a population of really isolated galaxies probably does not exist. Some “isolated” ellipticals may actually be end products of runaway mergers in small galaxy groups (Ponman et al. 1994; Mulchaey & Zabludoff 1999).

Pairs of galaxies are interesting because the mutual gravity of the members makes possible collisions or even mergers. Binary spiral galaxies, for instance, can merge into large featureless

elliptical galaxies within 10^9 years, a time scale that is short relative to the age of the universe. Shown in the top right panel of Fig. 1.1 is the galaxy pair Arp 240 ($z = 0.022$).

Triplets are the smallest groups of galaxies, important because of the question of their stability: two galaxies can form a stable configuration but a triple system cannot. Therefore, triplets are likely to be transitory configurations that eventually decay due to one body being ejected and leaving a residual binary system. Or they could be in a state of ongoing collapse. The left panel of the middle row in Fig. 1.1 shows the galaxy triplet KTG 04 ($z = 0.017$) which contains the interacting galaxy pair VV 769.

Small groups are small-scale structures with radii typically in the range of $0.2 - 1$ Mpc. They consist of three to five bright galaxies with relatively small projected separations between members and low relative velocities of $< 500 \text{ km s}^{-1}$. These systems may well contain a population of faint galaxies.

Groups can be “compact” or “loose” depending on whether the typical intergalactic distances are of the order of a galaxy diameter or more, respectively. Most groups are loose and may be only weakly gravitationally bound. Our Galaxy resides in the sparsely populated Local Group, which it dominates along with its spiral neighbor Messier 31. Other members of the Local Group are a few bright irregular galaxies such as the Magellanic Clouds, and plenty of dwarf ellipticals (see review by van den Bergh 2000). A small fraction of galaxies appear to reside in dense compact groups (reviewed by Hickson 1997), whose inferred crossing times are much shorter than the lifetime of the universe. The small intergalaxy separations (of the order of a galaxy diameter) and relative velocities found in compact groups result in strong tidal interactions. The first example of compact groups was found over one hundred years ago by Stephan (1877) as a small configuration of five nebulae, three of which show gravitational interaction (Fig. 1.1, middle row right panel).

Galaxy groups have potential wells deep enough to trap and heat an intragroup medium which then emits in X-ray (see review by Mulchaey 2000). The origin of this gas is still debated, but likely sources are primordial material and material divested or ejected from galaxies (shown by the presence of heavy elements particularly iron which could only have been created in supernovae).

Clusters of galaxies are the urban environment of the galaxy world and the largest gravitationally-bound structures in the universe (see Sarazin 1988 for an extensive review of cluster properties). They contain several tens to several thousands of optically-observable galaxies swimming in a hot ($kT = 3 - 9 \text{ keV}$) bath of X-ray emitting intracluster medium (ICM). The space density of galaxies in clusters is on average about a hundred times higher than the mean density in the universe and in particular, 10^5 to 10^6 times higher in the central (“core”) region of a few hundred kiloparsec in radius. The galaxies move with high random velocities³ of typically $\sim 750 \text{ km s}^{-1}$, implying virial masses of $\sim 5 \times 10^{14} h^{-1} M_{\odot}$. The diffuse ($10^{-3} - 10^{-2} \text{ particles cm}^{-3}$) intracluster plasma trapped in the potential well of the cluster radiates in X-rays (with luminosities 10^{43} to $10^{45} \text{ erg s}^{-1}$) due to thermal bremsstrahlung, and has 2-10 times the mass of the galaxies. The total mass contributed by the galaxies and gas does not provide sufficient gravity to hold groups or clusters together; the requisite remainder is in dark matter. Most of the ICM is probably primor-

³The urban setting of rich clusters turns out to be, in the description of Evrard (1993), “fast-paced”.

dial, either part of the cluster when it first formed or accreted afterward from the intergalactic medium. However, the metal abundance of the ICM is around 30% that of the Sun, implying that elements produced in stars within galaxies must have been driven out into it. Many clusters show substructures in both galaxy and ICM distribution, evidence for their formation by mergers of smaller systems.

Clusters of galaxies are classified by their properties such as richness (“rich” or “poor” depending on the number of member galaxies), shape (regular or irregular), and galactic content (spiral-rich, spiral-poor, or elliptical-rich). The high density rich clusters are relatively rare objects, with a spatial number density of $\sim 10^{-5}$ clusters Mpc^{-3} (Bahcall 1977), and containing fewer than 5% of all the galaxies in the universe (Dressler 1984). The nearest very massive rich cluster is the Coma Cluster (shown in the bottom right panel of Fig. 1.1), 130 megaparsec from the Milky Way. It contains about 2500 galaxies, mostly ellipticals, and radiates 10^{44} erg s^{-1} in X-rays.

Poor clusters are systems which have too few galaxies to meet the criterion to be “rich” clusters such as those in the Abell catalog. They bridge the continuum of environments between groups of a few galaxies and rich clusters. For example, the bright galaxy population of poor clusters is typically less than 50 whereas rich clusters may contain several hundred members; and their typical velocity dispersions are between 100 and 600 km s^{-1} (Beers et al. 1995) compared to 600 to 2000 km s^{-1} for rich clusters. The ICM of poor clusters, at $\approx 1 - 3$ keV, is usually cooler than that of rich clusters, while its metallicity is of the same order at $\approx 0.3Z_{\odot}$ (Mulchaey 2000 and references therein). One of the most X-ray luminous poor clusters containing a supergiant cD galaxy at the center is AWM 7 shown in the bottom left panel of the gallery in Fig. 1.1. Poor clusters span a great range in richness and exhibit a great diversity in structures and kinematics. We shall describe poor clusters in detail subsequently in Sec. 1.3.

The apparent separations of galaxies in a cluster are only a few times larger than their diameters; this proximity leads to mutual gravitational interactions. The cluster crossing time⁴ (as well as galaxy ages) is comparable to or a little smaller than the lifetime of the universe. Further, in the core of the cluster, the ICM may sometimes lose so much energy through X-ray emission (depending on the metal abundance) that it cools noticeably over a Hubble time. The cooling leads to the slow loss of pressure and causes the ICM to gradually condense into a central cooling flow (see Fabian 1994). If this cooling flow (of a few to a few hundred $M_{\odot} \text{ yr}^{-1}$) can persist without being disrupted by magnetic fields or explosive events, it may ultimately provide raw material to form future generations of stars or small galaxies. The residents of the dense clusters or groups are therefore likely to have their stellar and gas contents shaped by cluster-specific processes.

On scales of several megaparsec, the Universe reveals large inhomogeneities and a complicated void-supercluster network. **Superclusters**, the largest known systems of galaxies, typically contain 3–10 rich clusters and extend to $\sim 100h^{-1}$ Mpc (the clusters themselves fill very little of the supercluster volume). They highlight the large-scale structure of the universe, many appearing to form long filaments (see reviews by Oort 1983; Bahcall 1988). **Voids** are regions underdense by factors of a few relative to the mean cosmic density (see review by Rood 1988). Even voids

⁴Crossing time = radius of the cluster / velocity dispersion of the galaxies

are unlikely to be empty, being instead populated by faint dwarf galaxies tracing the underlying dark matter (more below). On scales of a few megaparsec void galaxies are gravitationally bound, forming interacting galaxy pairs, loose pairs, and loose groups (Szomoru et al. 1996).

Sky surveys show that a majority (nearly 70%) of galaxies in the nearby universe occur in small modestly populated groupings such as the Local Group; fewer than 1% of galaxies are isolated (e.g., Tully 1987) and only about 5% occur in rich clusters (Dressler 1984). We note that the literature frequently applies the term “field galaxy” to denote all “non-cluster” galaxies.

1.2 Environmental Influences on Galaxies

The literature on the effect of the environment on galaxies is too vast to summarize comprehensively into a section of a chapter, obliging us to limit the discussion here. Fortunately, many reviews are available to which we shall refer: Dressler (1984), Oemler (1992) and Irwin (1995), and Schweizer (1998) focussing largely on observational work; White (1982), Barnes & Hernquist (1992), Evrard (1993), whose themes are the physical processes that affect galaxies.

1.2.1 Galaxy Formation in Different Environments

The origin of galaxies is closely tied with the formation of cosmological structures, driven by “gravitational instability” of the density fluctuations at early epochs in the history of the Universe. Clumps of dark matter collapse in regions of slightly elevated densities and merge to form galaxies. The primordial baryonic gas of hydrogen and helium cool radiatively and condense within the parent dark halos, become self-gravitating and light up as stars. In hierarchical structure formation scenarios, galaxies then gather to form progressively larger systems such as groups and clusters of galaxies, filaments and walls. The primordial gas left over from galaxy formation remains bound within the cluster as the intracluster medium. The ICM can be heated nongravitationally through supernova ejecta and galaxy winds and become enriched with metals.

Biased galaxy formation scenarios (e.g., Kaiser 1984) predict that the efficiency of galaxy formation is enhanced in dense environments. Further, giant galaxies are more likely to be formed in regions of the highest density, while faint low-mass galaxies preferentially occupy voids (Dekel & Silk 1986). A general assumption, then, is that the efficiency of galaxy formation is determined by properties (e.g., density) of the local environment.

1.2.2 Drivers of Galaxian Properties and Evolution

The coupling of the galaxies to their environs post-formation (i.e., when the bulk of the gas has been turned into stars, and the galaxy has relaxed) occurs through various processes broadly classifiable into two categories: (i) stellar-dynamical, e.g., galaxy interactions, minor collisions, harassment, tidal stripping, mergers and cannibalism, and (ii) gas-dynamical, e.g., ram-pressure stripping by the intracluster medium, gas infall and cooling flows mass deposition, etc. These astrophysical processes, described rather tersely below, have different relative influence in the different environments.

The average separation between galaxies in groups or clusters is of the order of their own dimensions. **Tidal interactions**, since gravity is always attractive, could hence be frequent. The interaction or collision timescale for galaxies, treating a cluster of galaxies as a thermodynamic state in a closed volume, may be parametrized as (Bothun 1998):

$$\tau_{coll} = 10^9 \text{ yr} \left[\left(\frac{V_r}{1000 \text{ km s}^{-1}} \right) \left(\frac{N_d}{100 \text{ gal Mpc}^{-3}} \right) \left(\frac{R_{gal}^2}{100 \text{ kpc}^2} \right) \right]^{-1}. \quad (1.1)$$

Tidal interactions are usually inelastic; they increase the internal energies of the galaxies at the expense of their relative (orbital) motions. Interactions may be weak or strong, their outcome depending on the orbital (e.g., impact parameter) as well as internal characteristics (masses and compactness, structure of the dark matter halos) of the colliding galaxies. Multi-frequency observations, from radio to X-ray energies, have made it abundantly clear that interactions between galaxies, as well as between galaxies and their surroundings, occur in at least 10% of objects (see review by Barnes & Hernquist 1992). Gravitational forces and torques between galaxies in close passage can alter the stellar distribution and dynamics, e.g., creating tails and bridges of material (Zwicky 1957) and heating the galactic disk (e.g., Toth & Ostriker 1992) or warping their spiral structure (see review by Binney 1992), and could even result in the individual galaxies merging into a larger elliptical galaxy which then drives evolution along the Hubble sequence (see below). Galactic collisions can also wreak havoc on the interstellar gas in the systems, driving shocks into the molecular clouds, heating and compressing the gas which could then fragment into a new batch of luminous stars (the “starburst” phenomenon, see Larson & Tinsley 1978; Kennicutt 1998), or lead to bars which may fuel gas into the centers and incite energetic activity (the “active galactic nuclei” phenomenon, e.g., Sanders et al. 1988).

Repeated high-velocity encounters between a massive galaxy and its much smaller companions, termed **galaxy harassment** (Moore et al. 1996), may be frequent in the cluster environment. Harassment mostly affects the smaller galaxies; each episode may cause only modest disturbances, but over a Hubble time, can transform faint spirals into dwarf ellipticals. Within clusters, collisions between galaxies leave the galaxy cores relatively unaffected, but change the envelopes significantly by **tidal stripping** (e.g., Richstone 1976). The effect of stripping may be strong during the initial cluster collapse (Merritt 1984) when the cross-sections for dynamical friction and galaxy-galaxy interactions would be larger; once the dark matter halo is stripped from a galaxy, its interaction cross-section reduces, and subsequent communication with the environment would be negligible. Tidal stripping of the outer halos of galaxies could generate a population of stars floating free of their host galaxies but still bound to the cluster in which the galaxies reside, and thus give rise to an extended halo around the central galaxy or create very diffuse intracluster light. Just as galaxy-galaxy encounters generate tidal forces, so do the variations in the gradient of the global group/cluster potential. The latter depend on the galactic orbit around the cluster, and results in tidal truncation of the galaxies such that the mean density of their outer regions are of the order of the mean cluster density (see Chapter 7 of Binney & Tremaine 1987).

A massive galaxy traveling through a sea of small cluster members (and a smooth background of dark matter) also suffers a steady deceleration in the direction of its motion due to **dynamical friction**. The dynamical friction timescale for the decay of an object on a circular orbit is (Bothun

1998):

$$\tau_{fric} = \left(\frac{5.0 \times 10^{10} \text{ yr}}{\ln \Lambda} \right) \left(\frac{R}{300 \text{ kpc}} \right)^2 \left(\frac{V_{rel}}{1000 \text{ km s}^{-1}} \right) \left(\frac{M/L}{10} \right)^{-1} \left(\frac{L}{10^{11} L_{\odot}} \right)^{-1}. \quad (1.2)$$

Note that the dynamical friction force depends only on the total density of the particles in the “sea”, not on their individual masses. Further, it preferentially slows down the more massive galaxies, which spiral in toward the cluster center, creating mass/luminosity segregation within a small core.

Kinetic energy losses due to dynamical friction or inelastic tidal interactions could lead to contraction of the relative orbits of the galaxies until “the two components form practically one object” (Holmberg 1941). But not every close encounter results in such a **merger**; only repeated encounters that are slow relative to the internal stellar velocity dispersion of the galaxies culminate in mergers. An extreme case of merging, termed **galactic cannibalism**, occurs at the centers of (mainly poor) clusters, where a giant central galaxy (see below) forms through a succession of such mergers and accretion of smaller companions. Some of the consequences of a merger are the following: (i) tidally-stripped stars (and dark matter) remain bound to the merger remnant, forming a common envelop or plumes and tails of stellar material; (ii) violent relaxation following the merger of two equally massive gas-rich spirals may redistribute the stars into the characteristic $r^{1/4}$ law of elliptical galaxies (Toomre & Toomre 1977; Barnes & Hernquist 1992; Schweizer 1998, and references therein), thus transforming the Hubble type; (iii) dissipative effects on dense, cold gas leads to enormous central concentration of molecular gas that may fuel nuclear starbursts and activity (Kennicutt 1999). Galaxies that exhibit severe tidal disturbances usually have colors anomalously blue compared to undisturbed galaxies (e.g., Larson & Tinsley 1978), implying a young stellar population. Triggered massive starbursts in tidal tails may also lead to the formation of tidal dwarf galaxies, and/or globular cluster systems; (iv) remnants of gas accumulated in the center may appear as kinematic subsystems: disks in the cores of ellipticals, oddly-rotating or kinematically decoupled cores, or polar rings; (v) starbursts, supernovae, shocks at the interface of the colliding disk galaxies, galactic wind, etc., could heat up the ISM and possibly form X-ray coronae around the elliptical remnant. Merger processes seem to have been visibly affected between 5% and 50% of all galaxies (Schweizer 1998).

The cluster galaxies constantly plow through the hot intracluster medium, and can experience **ram pressure** (Gunn & Gott 1972) that could entirely strip the diffuse gas from a spiral. It would be difficult to strip dense molecular clouds (Valluri & Jog 1990), but easy enough to remove the outer parts of atomic gas disks (Kundic, Hernquist, & Gunn 1992). The consequences of ram pressure include (i) compression of the galaxian ISM leading to enhanced star formation; (ii) evaporation of the ISM and suppressed star formation; (iii) formation of emission line nebulae in cooling flows due to the stripped gas; (iv) changes in the properties of cluster radio sources leading to narrow-angle tailed radio sources (e.g., O’Dea & Owen 1985; Venkatesan et al. 1995).

Besides the above influences, galaxies may be subject to mass accretion of several M_{\odot} over a Hubble time from their surrounding dark matter halo or via a possible cooling flow in the cluster (see Fabian 1994). Galaxies in turn affect their environment via outflows (see Irwin 1995) of mass (as in radio jets), chemically-enriched material (through galactic winds, supernova ejecta), and

energy which heats the ICM to X-ray emitting temperatures.

The nature and frequency of interactions depend strongly on the immediate environment. A field galaxy — which is not affected by dramatic gravitational encounters with massive neighbors or processes that strip its stars or gas — may remain embedded in its nascent dark halo and the primordial neutral gas (mainly H and He) from which it was formed. This gas may be infalling into the galaxy, as a consequence of which the star formation may proceed continuously enriching the interstellar medium in a way completely different from that happening in a galaxy cluster.

Galaxy groups and clusters have galaxy densities large enough to lead galaxies into vigorous interaction, and potentials deep enough to retain much of the material detached or ejected as a consequence. The cluster environment can alter the effects of galaxy collisions. The random velocities of the galaxies in clusters are usually greater than their internal velocities. So, the time the two galaxies are close together is correspondingly shorter, and the probability of dynamical friction bringing galaxies into a bound orbit that may decay is also smaller than for an isolated pair. Therefore, the perturbation on cluster galaxies due to collision is weaker due to its inverse dependence on relative velocity and direct dependence on the duration of the collision. Ram pressure stripping declines in proportion to the velocity dispersion (squared), so plays a relatively less important role in groups than in large clusters (e.g., Abadi, Moore, & Bower 1999). Generally, in a cluster the density of galaxies falls off as a function of distance from the center. Therefore, depending on the current location and orbit of a galaxy (i.e., on the local cluster galaxy density and velocity dispersion, and on the density and temperature of the ICM), a particular object may experience different degrees of interactions as a function of time. However, unlike in rich clusters, group velocity dispersions (or equivalently, virial temperatures) are similar to those of individual galaxies (roughly 200 km s^{-1}). So energetic events within galaxies can have a significant impact on the properties of the modest groups as a whole. The mass distribution within the system (group or poor cluster) greatly influences galaxy interaction and merger timescales. If the dominant mass (50-90%) is in dark matter distributed generally through the group rather than in the individual galaxy halos, the times between mergers are increased (Bode et al. 1994). As already mentioned, tidal phenomena and mergers may have enhanced probability at cluster formation and high redshifts when galaxy density is high and velocity dispersion low and may be ineffective currently within clusters where the velocity dispersion is high (Merritt 1984; Dubinski 1998).

1.2.3 Signatures of Environmental Variations in Galaxy Properties

Galaxy-galaxy and galaxy-cluster interactions — whose strengths vary from mild to completely disruptive, as seen above — have profound consequences on the morphology and evolution of galaxies as well as their environments. Notable manifestations of the role of environment in the formation and evolution of galaxies are in the differences between the members of rich clusters contrasted with objects in the field, in terms of the distribution of galaxy types, the gas content, star formation and related activity of galaxies.

Averaged over all environments, spiral and irregular galaxies comprise $\approx 70\%$ of all galaxies, the rest being elliptical and SO galaxies. An important observation of the variations in bulk galaxy properties with environment is the **galaxy morphology–density relation** (see Table 1.1) which

shows that elliptical, spheroidal, and early-type spiral galaxies are preferentially found in dense environments (e.g., cores of clusters), while late-type spirals and irregulars are found mostly in low density (i.e., field) environments (see Dressler 1984; Oemler 1992). A related phenomenon is the morphology–radius correlation, seen through the increasing fraction of early-type galaxies at smaller clustrocentric radii (see Whitmore 1992). Indeed, the origin of the spheroidal (i.e., S0) galaxies is itself a controversial subject with the “nature” *vs.* “nurture” theme (covered in the review by Dressler 1984). In addition, the spiral fraction of a cluster is inversely correlated with the X-ray luminosity (e.g., Bahcall 1977) and velocity dispersion (e.g., Bahcall 1978). In X-ray luminous poor groups with fewer than 6 members, the morphological fraction varies from 25% to 55%, similar to the situation in substructures within some rich clusters (Zabludoff & Mulchaey 1998). In fact, the dependence of morphology on density does not extend to very low densities. For local galaxy densities of $n_g \sim 5$ galaxies Mpc^{-3} , the morphological fractions remain approximately constant at the average field fraction (Postman & Geller 1984). This density corresponds to groups in which the crossing time is close to the Hubble time, suggesting that dynamical interactions between galaxies after formation, and ram-pressure evaporation of the gaseous medium in galaxies may be responsible for the differences in early-type fractions, perhaps through the transformation of Hubble types in the harsh environment of cluster cores.

Table 1.1: Galactic morphological distribution in different environments

Environment	% E	% S0	% S
Field	10	20	70
Rich groups	10	30	60
Rich clusters	20	40	40

The most luminous, most massive, gigantic relaxed objects in the universe, the **cD galaxies**, are found exclusively close to the centers of clusters or groups of galaxies that are rich, high density regions. Whereas a typical giant elliptical galaxy may have a luminosity of about $1.5L^*$, where L^* is the characteristic luminosity of the Schechter luminosity function (see Chapter 3), a cD galaxy shines at $10 - 12L^*$ (Kormendy & Djorgovski 1989). These cD galaxies have surface brightness profiles in their inner regions similar to ellipticals, but in addition have extensive (several 100 kpc) luminous halos or envelopes, which can contain as much light as the rest of the galaxy (Schombert 1988, and references therein). Some cDs are surrounded by a population of faint galaxies that are bound to the cD itself, rather than to the general cluster potential (e.g., Bothun & Schombert 1990). The buildup of these dominant cluster galaxies occurs due to a combination of repeated mergers that create the main body, and tidal disruption of numerous smaller cluster galaxies that supplies stellar material for the extended halo. The properties of these objects seem to be modulated by the richness of the global environment: cD galaxies in poor cluster are brighter than in rich clusters but lack the megaparsec-sized envelopes seen in their rich cluster cousins (Thuan & Romanishin 1981). This difference may be due to the low tidal stripping rate in poor clusters compared with richer domains. We shall inquire into this topic further in Chapter 6 where we subject the brightest galaxies of our poor cluster to close scrutiny.

Several classes of **cluster radio sources** are known to exhibit morphological and physical properties that are dramatically influenced by their environments. Wide-angle tailed radio sources

(e.g., Gomez et al. 1997) and narrow-angle tailed radio sources (e.g., Bliton et al. 1998) are unique to cluster environments. As the radio galaxy plunges through the ICM, the ram pressure bends the radio lobes, creating the tails. Poor groups also host tailed radio galaxies in numbers more than one would expect from their ICM densities and velocity dispersions (Burns et al. 1987; Doe et al. 1995).

Galaxies in close pairs have higher **star formation rates** (SFRs) than isolated galaxies (Kennicutt et al. 1987), testifying to interaction being able to induce star formation. But cluster galaxy star formation rates are on the average smaller than those in field galaxies, with a monotonic decline to the cluster center (Dressler 1980; Whitmore 1992; Balogh et al. 1999). Even in (high velocity dispersion) groups, the SFR in galaxies (corrected for Hubble type) is inversely proportional to the local galaxy density (Hashimoto et al. 1998; Allam et al. 1999). In Hickson Compact Groups, galaxies show evidence for tidal disturbances, but few contain young stellar populations (Zepf & Whitmore 1993). The quenching of star formation in higher density environs may be due in part to ram-pressure stripping of the cluster galaxies which denudes them of their interstellar medium, and partly because star formation is inherently less effective in the tidal fields of dense environs (which remove low density gas in galactic halos as well as gas-rich satellites/companions which could be accreted by large galaxies).

Early-type galaxies in clusters tend to have integrated colors that are closely correlated with their luminosities, such that brighter galaxies are redder. It turns out that the **color-magnitude diagrams** of galaxies in “irregular” clusters — no matter rich or poor — are less tight compared to those of “regular” clusters (Garilli et al. 1996), indicating the influence of the cluster dynamical state on the galaxy population. In Sec. 4.2 of this thesis, we shall explore the color-magnitude relation for poor cluster galaxies.

At higher redshifts, clusters contain a large **fraction of blue galaxies** (the Butcher-Oemler effect), quite in contrast to nearby rich clusters where red ellipticals predominate. The blue galaxies consist mostly of star-forming disk galaxies, a few peculiar (interacting) galaxies and hardly any merger remnants, favoring the galaxy harassment explanation for their origin (Oemler, Dressler & Butcher 1997). We shall delve further into the topic of blue galaxies in Sec. 4.4 of this thesis. Another peculiar phenomenon, the rare “ $E + A$ ”, or post-starburst, galaxies first identified in high-redshift clusters (Dressler & Gunn 1992) being also found in the field (Zabludoff et al. 1996) attests to interactions of paired galaxies rather than any global environmental effect being important.

Galaxies in groups are deficient in **neutral hydrogen (HI)** alike their kin in cluster cores (see van Gorkom 1996), although to a lesser extent. In some Virgo cluster spirals, “ram-pressure stripping has done serious damage to the HI disks, while in other galaxies turbulent viscous stripping and thermal conductivity have caused a mild, but global HI deficiency...” (Cayatte et al. 1994). But the HI deficiency does not translate to changes in molecular gas masses which are not greatly deficient or otherwise unusual (e.g., Kenney & Young 1989).

Galaxies that reside within the lowest density voids — mostly late-type, gas-rich systems — are similar to field galaxies of the same morphological type in their optical properties and neutral Hydrogen content (Szomoru et al. 1996). So, there are no strong variations between void galaxies

and those in more normal environments, in contrast to the situation in clusters where there are dramatic differences in galaxy star-formation properties as a function of local density.

The differential probability distribution of galaxies over luminosity or absolute magnitude is termed the **luminosity function** (LF). The LF — for a given mass-to-light ratio — serves as a first approximation to the mass function of galaxies. If environmental influences are not important, and if galaxy formation occurred with the same efficiency everywhere in the universe, the LF would then be a universal function. But we have seen that galaxies are different in the two extreme density domains of the field and cluster. Further, if clusters are dynamically active, their occupant galaxies are evolving in luminosity and number density. So LF estimates of cluster galaxies might be as informative of cluster-related influences on the bulk properties of galaxies as about cosmological parameters such as the shape of the primordial mass spectrum. Controversy persists as to whether the LF is universal or varies with environment; observational studies have suggested both. We shall postpone further discussion about this topic to Chapter 3.

Rotation curves of spirals in the cores of clusters exhibit a decline at the outer radii, in contrast with the asymptotically flat, or even rising, rotation curves of galaxies in the field or in the peripheries of clusters (Whitmore, Ford, & Rubin 1988). This effect is marginal for early-type spirals but is marked for the late-type spirals (Adami et al. 1999). Falling rotation curves suggest that the dark matter halos of the core galaxies may have suffered stripping due to galaxy-galaxy or galaxy-cluster interactions (see e.g., Balkowski 1992).

Elliptical galaxies lie on a **fundamental plane** defined by bivariate correlations between their global properties of radius, velocity dispersion and mean surface brightness (Dressler et al. 1987; Djorgovski & Davis 1987). However, field ellipticals and cluster elliptical galaxies populate different fundamental planes (de Carvalho & Djorgovski 1992). The differences are particularly noticeable for correlations that include stellar population variables sensitive to both the galaxian history of star formation and metal enrichment, and suggest different formation histories and epochs for ellipticals in the two extreme environments. In Sec. 6.3.4, we shall examine the brightest cluster members in the light of an equivalent of the fundamental plane.

We see that galaxy properties show marked differences among different environments. A wide variety of mechanisms may be affecting the structure and dynamics of galaxies it is uncertain which of these are actually operating, and to what degree they are important. The above discussion also shows that there is not a one-to-one correspondence between a given observation and its causes; secular or stochastic effects of dissimilar dynamical and evolutionary histories might present similar present-day galaxies. To catch the environmental processes in action, one has to compare galaxies across the field, small associations and rich clusters at various epochs.

1.3 Background on Poor Clusters

“Poor clusters” (PCs), which we study in the present thesis, are aggregates of a few tens of galaxies with velocity dispersion of about $300\text{--}700\text{ km s}^{-1}$ (Beers et al. 1995). They are intermediate environs between small groups (with fewer than five galaxies brighter than L^*) and crowded rich clusters (which contain upto several hundred galaxies brighter than L^*), and contain about 20%

of the galaxies in the nearby universe. A large fraction of poor clusters are luminous, extended X-ray sources; the galaxy distribution traces the X-ray structure (Dell'Antonio et al. 1995). The mass in galaxies is about half the mass in the ICM, and together these add up to about 5-10% of the total mass of the cluster.

1.3.1 Motivation for Studying Poor Clusters

Many, if not all, theories of galaxy formation and evolution are tied in some way to cluster properties such as velocity dispersion, total cluster mass, baryon fraction, galaxy population, and galaxy density. Galaxies within rich cluster evince the most dramatic environmental forcing; however, comprising only a few percent of the total galaxy population, and subject to exceptionally strong environmental effects, rich cluster denizens represent a minority population. Poor clusters are not so massive as rich clusters, but are far more numerous. They form a natural and continuous extension to lower richness, mass, size, and luminosity from the rich and rare clusters (Bahcall 1980; White et al. 1999; see also Table 1.2). Hence they contribute a significant quantity to the mass and baryonic fraction of the universe, contain a larger fraction of the galaxy population than do their richer versions, and bridge the gap between the well-studied environments of the rich clusters and the special groups such as the Hickson Compact Groups.

A majority of rich clusters show substructures in their galaxy distribution as well as in X-ray (White, Forman & Jones 1997, and references therein). Moreover, poor clusters are effective tracers of the large-scale galaxy distribution, with the group centers following the distribution of all galaxies (Ramella, Geller, & Huchra 1989), and their principal axis being aligned with their neighbors on scales extending to about 15-30 h^{-1} Mpc (West 1989). X-ray data (Mulchaey 2000) show that in superclusters, massive Abell clusters are linked together by groups and poor clusters of galaxies. If clusters and superclusters formed hierarchically from smaller associations, poor clusters, as the building blocks, provide a natural focus to understand the formation and evolution of large-scale structure in the universe.

Further, poor clusters provide a sample of galaxies in medium-sized communities with populations and velocity dispersions that support galaxy interactions. It is then interesting to examine how galaxies evolve in such small clusters where, in comparison with rich clusters, the effects of the intracluster plasma is comparable but the tidal perturbations due to the global potential are weaker, but where, in comparison with small groups, the velocity dispersions are higher and the global potential deeper. If the kinematics and dynamical youth of poor clusters (e.g., Beers et al. 1995; Ledlow et al. 1996) make them preferred sites for galaxy-galaxy interaction (some of which may culminate in mergers), one expects that the morphologies and star formation histories of some member galaxies to be altered, leading to variations in the bulk properties of cluster galaxies.

Among the statistical properties of galaxies is their luminosity function (LF). If, as mentioned in Sec. 1.2.3, the shape of the LF varies with environment, it agrees with the prediction of standard biased galaxy formation models. Then, for example, the dwarf-to-giant galaxy ratio increases significantly with the richness of the environment (e.g., Phillipps et al. 1998), one expects the poor cluster LF to be steeper than those in the field and small groups, and flatter than that

of much richer clusters. Instead, if the LF is universal or consistent in shape within different environments, it argues for the galaxy mass function being insensitive to global neighborhood. If galaxy evolution in poor clusters is different from (and more recent than) that in the cores of rich clusters or the field, it may have a noticeable effect on the poor cluster LF.

Many poor clusters also harbor gigantic galaxies at their centers (defined by the centroid of either the galaxy distribution or the X-ray emission, which may frequently coincide). As discussed in Chapter 6, these central galaxies are “special” objects, end-points of extensive merging or cannibalism (e.g., Merritt 1984; Dubinski 1998). Comparison of poor cluster dominant galaxies with their rich cluster equivalents would shed light on the dynamical processes that affect cluster galaxies, and on the formation of extremely massive galaxies, including cD galaxies.

Therefore, poor clusters provide an important niche for testing theories of galaxy formation and evolution in different environments. Though very numerous and cosmologically significant, poor clusters do not proffer themselves to detailed study easily, mainly due to their low relief against the background. Further, as poor systems are best identified and usually studied in our immediate neighborhood, remarkably little is known about these systems at intermediate or high redshift. But, local as well as moderately distant poor clusters are crucial for interpretation of systems at high redshift. It is only recently — thanks largely to X-ray surveys that are beginning to detect poor systems at increasingly larger redshifts although their goal is usually to find distant rich clusters (e.g., Jones et al. 1998; Vikhlinin et al. 1998) — that these entities have started receiving the attention they merit. It is important for statistical studies of groups and poor clusters to develop a broad reach like that of rich cluster studies.

1.3.2 Definitions and Catalogs

“When I use a word,” Humpty Dumpty said, in rather a scornful tone,

“it means just what I choose it to mean – neither more nor less.”

– Lewis Carroll

When can a galaxy agglomeration be labelled a poor cluster? While the assignment of galaxies into the “field” or “rich clusters” is fairly unambiguous, arbitrariness persists about when a spatial over-density of galaxies can be identified as a “poor cluster”. Generally, a grouping of galaxies is termed poor if its population *fails* to satisfy some limiting (say, Abell’s) number criterion for a *rich* cluster⁵. Small multi-galaxy systems are called “groups” or “clusters”, with each term further qualified by a plethora of adjectives such as “poor”, “rich”, “loose”, “compact”. It emerges, then, that poor clusters would span the entire gamut of galaxy populations from triplets,

⁵Rich clusters contain, by traditional definition (Abell 1958), at least 50 galaxies brighter than $m_3 + 2$ mag (where m_3 is the magnitude of the third brightest cluster member) within a radius of $R = 1.5 h^{-1}$ Mpc of the cluster center. This galaxy count within the specified area around the cluster center and within the luminosity range of a factor of about six of the third brightest member generally goes by the tag of the *richness* of the cluster. Richness is thus also a measure of the mean surface galaxy density of the cluster. Included in the Abell catalog are clusters of richness 0 that contain between 30 and 50 galaxies, and which the literature commonly refers to as “poor clusters”. These clusters are part of the nonstatistical compilation of Abell, included in his catalog merely to enhance its value as a finding list, and thus are incomplete in an unknown way. Abell issued a warning in his original catalog that there is nothing sacred about the richness criteria, and that dispersion in cluster richness estimates may be about one richness class.

through quintets, through systems like the Local Group, upto (and including) the threshold of rich clusters. Today, the distinction between “groups” and “clusters” is itself becoming fuzzier, and retaining the nomenclature of old “would obscure the continuous spectrum of properties possessed by these objects” (White et al. 1999). *An operational definition of a poor cluster is that its bright galaxy population must number > 5 but \leq the Abell (1958) richness 0 criterion of between 30 and 49 galaxies within two magnitudes of the third brightest cluster member.* The typical region for counting the galaxies would have a radius about 0.5 Mpc around the cluster center (Sec. 3.3.1 includes detailed discussions about richness of poor clusters).

Existing poor cluster catalogs have both overlapping and widely divergent selection criteria such as population or richness, density contrast over the background, compactness, presence of extended matter between the galaxies, etc. Though varied and often subjective, these catalogs testify to four major ways of identifying poor clusters:

1. in 2-D through **projected enhancements in galaxy counts** over the background, (i) by visual inspection of photographic plates, e.g., de Vaucouleurs (1975), similar to the creation of the catalogs of rich clusters of Abell (1958) and Zwicky (1951-56) and the compact groups of Shakhbazian (1973), Rose (1977) and Hickson (1980), or (ii) through automated searches using the Friends-of-Friends algorithm, e.g., Turner & Gott (1976), White et al. (1999).
2. by **the presence of a special galaxy** such as (i) a cD galaxy, e.g., the thirty-odd poor clusters of Morgan et al. (MKW; 1975) and Albert et al. (AWM; 1977) collectively called the Yerkes clusters, or (ii) a strong radio source, e.g., Allington-Smith et al. (1993) similar to the approach for finding distant rich clusters of Dickinson (1995), or on the basis of visible signs of interaction between galaxies as in the peculiar galaxy groups of Vorontsov-Velyaminov (1959) and Arp (1966).
3. in 3-D using **both positional and velocity information**, or equivalently, volume rather than surface density enhancements, using (i) the hierarchical method – Tully 1987; Gourgoulhon, Chamaraux, & Fouque 1992, or (ii) the percolation method – Huchra & Geller (1982); Maia, da Costa, & Latham (1989); Trasarti-Battistoni (1998); Tucker et al. (2000), or (iii) both – Garcia et al. (1993); Giuricin et al. (2000). Note that these catalogs usually pick out small groups of about 4-8 galaxies.
4. by **the presence of an intracluster medium** that is detected in X-ray, followed by optical identification of galaxy overdensities in the same regions. Though most cluster catalogs from X-ray surveys have focused on detecting rich clusters, they inevitably include many poor clusters, e.g., the serendipitous cluster detections in the *Einstein* Medium Sensitivity Survey (EMSS; Gioia & Luppino 1994); and the catalog of Vikhlinin et al. (1998), the Wide Angle *ROSAT* Pointed Survey (WARPS; Scharf et al. 1997; Jones et al. 1998), the bright Serendipitous High-Redshift Archival Cluster survey (SHARC; Collins et al. 1997).

An important uncertainty in discovering poor clusters through projected galaxy overdensity in the optical is in their very identification: even at moderate redshifts, their contrast against the background (of random fluctuations in surface number density of field galaxies) is weak. Thus,

some poor systems identified as projected overdensities are likely to be chance superpositions of galaxies. On the other hand, optical richness of $\approx 5\%$ of “rich” clusters are likely to be significantly overestimated (Struble & Rood 1991) due to interloping galaxies (which also explains the unexpectedly low X-ray luminosity of such clusters which are preferentially found in denser or supercluster environments).

An improved way of detecting poor clusters is to supplement the projected spatial overdensity with distance information. The advantage of using objective searches such as the Friends-of-Friends method is that few real systems are missed, at the risk of including some spurious ones (Frederic 1995; Diaferio 1999). Though the algorithm is well-defined, the use of different parameters leads to catalogs with overlapping groups with different numbers of galaxies. In fact, many cataloged groups or poor clusters may not be real physical systems (e.g., Walke & Mamon 1988; Hernquist et al. 1995; Ramella et al. 1997), but rather pairs chance superpositions of galaxies, or large-scale structure filaments viewed edge-on.

The observation that over 80% all rich clusters (richness ≥ 0) are X-ray sources (Briel & Henry 1993) and that about 50% of all nearby groups of galaxies (regardless of whether they are compact or loose) contain a hot intragroup medium (e.g., Ponman et al. 1996; Burns et al. 1996) motivates a method of cluster selection that is more secure than in the optical. X-ray emission implies the presence of a deep potential well such as that of a massive galaxy system, to contain the high-energy $10^7 K$ plasma. X-ray luminosity (L_X) of the hot ICM is proportional to the square of the gas density, making X-ray selection less susceptible to the projection effects that plague optical selection by galaxy overdensity. Poor clusters that contain a few tens of galaxies are X-ray emitters with L_X ranging from several $10^{41} \text{erg s}^{-1}$ to several $10^{43} \text{erg s}^{-1}$ (Schwartz et al. 1980; Kriss et al. 1983; Burns et al. 1981; Price et al. 1991; Dell’Antonio et al. 1994; Doe et al. 1995; Dahlem & Thiering 2000). Even poorer galaxy groups also contain intergalactic material (Mulchaey et al. 1993; Ponman & Bertram 1993; Pildis et al. 1995; Ponman et al. 1996; Mulchaey & Zabludoff 1998; Helsdon & Ponman 2000). The L_X of poor systems are consistent with their being scaled-down versions of more massive clusters; the X-ray luminosity function (XLF) for poor clusters is a smooth extrapolation of the rich cluster XLF (Burns et al. 1996, for the WBL poor clusters), and is also consistent with that of an X-ray-selected sample of smaller groups (Henry et al. 1995).

In this thesis, therefore, we choose to use an X-ray-selected sample from the catalog of clusters of galaxies (Gioia & Luppino 1994, GL94 here onwards) detected in the *Einstein* Observatory Medium Sensitivity Survey (EMSS; Gioia et al. 1990; Stocke et al. 1991). GL94 noted that 19 of the nearly one hundred EMSS clusters displayed morphologies and galaxy counts that were best described as that of poor clusters; we have selected these poor clusters as the objects for our study. Such selection is then not entirely objective, for the optical richness is merely a visual estimate. In Chapter 2 we provide details of the sample of poor clusters we have studied in this thesis. We shall estimate that the typical population of the EMSS poor clusters is about 10 galaxies, and their velocity dispersions (from the correlation of the same with X-ray luminosity) are about 500-800 km s^{-1} . In the present section we merely delineate another valid method of constructing a set of poor clusters.

But is cluster selection through the X-ray luminosity of the ICM flawless, and does it unearth a

complete set of poor clusters? The shape of the XLF is similar for different Abell richness classes, but manifests a luminosity–richness relation: the characteristic luminosities increase by about twice for an increase by one in richness class (Briel & Henry 1993). Thus, flux-limited surveys tend to pick out the more luminous objects. Moreover, galactic content and cluster dynamical age may dictate the X-ray visibility of the galaxy multiplets; for instance, small galaxy groups tend not to be X-ray detected if they are composed exclusively of spiral galaxies (see Mulchaey 2000), and even among Abell rich clusters, irregular clusters tend to be weaker X-ray emitters (see, e.g., Forman & Jones 1984). Further selection effects may persist because X-ray fluxes from gas-poor clusters may be low, causing incompleteness in catalogs; and clusters in which the gas distribution is compact (unresolved) usually find themselves excluded from cluster catalogs. Another important consideration is that clusters comprise only about 10%-20% of the total source population detected in X-ray surveys (e.g., Stocke et al. 1991; Vikhlinin et al. 1998). On the other hand, X-ray surveys have found intriguing objects such as “fossil groups” wherein bright galaxies have merged to form a single bright galaxy with extended X-ray emission (Ponman et al. 1994), and “dark clusters” (e.g., Hattori et al. 1997). Exploration of a sample of X-ray-selected poor clusters should in any case prove profitable.

The lower spiral fractions of X-ray selected galaxy groups (see Mulchaey 2000) suggests that such a choice may produce a more dynamically evolved sample of groups (Henry et al. 1995). So, our sample is necessarily biased toward the more evolved poor clusters wherein the ICM is heated enough to emit high-energy radiation. The average bright galaxy populations of the systems in catalogs mentioned above range from about ten (e.g., the Allington-Smith et al. radio groups, WBL clusters), to the equivalent of Abell Richness 0 to -2 (in the definition of Bahcall 1978) for the MKW/AWM poor clusters (Bahcall 1980), while the number of comparably bright galaxies in Hickson Compact Groups, for instance, is typically about 4. We shall see in Sec. 3.3.1 that the EMSS poor clusters we study bracket the same richness range as the Yerkes poor clusters.

We see that in the literature on poor clusters, there exist many catalogs with varied selection criteria of galaxy population and density, compactness, etc., testifying to the diversity of this environment. Thus, poor clusters are probably a mixed bag⁶ of galaxy aggregates important in the study of galaxy formation, evolution, cluster formation and dynamics as well as in cosmology.

1.3.3 Content: Galaxies and Intracluster Medium

To first order, galaxy groups and poor clusters appear to be successively scaled-down versions of rich clusters (see Table 1.2). The optical properties (richness, central galactic density, galaxy spatial distribution, and galactic content) of poor clusters represent a smooth continuation from the properties of Abell (rich) clusters to lower richness (e.g., Bahcall 1980; Ledlow et al. 1996).

The median velocity dispersion of poor clusters ($\approx 350 \text{ km s}^{-1}$) is about half of that found in richer environs, and their radii are typically also half that of the rich clusters. The X-ray emission ($L_X \sim 10^{41} - 10^{44} \text{ erg s}^{-1}$) often extends to radii of $\sim 0.5h_{100}^{-1} \text{ Mpc}$, and beyond the visible galaxy distribution with a size typically half that of rich clusters. The intracluster medium has temperatures of 1-3 keV (Hwang et al. 1999) which are at the lower end of the range occupied

⁶All authors believe that the poor clusters in their particular catalog are “representative” of the class as a whole.

by rich clusters, and somewhat higher than that of smaller galaxy groups (about 1 keV). ICM metallicities are $< 10\%$ of the solar metallicity (compared with 20-30% solar for clusters; see Mulchaey 2000 for more about interrelationships between X-ray and dynamical characteristics of galaxy groups). The poor cluster X-ray luminosity function (XLF) is also a smooth extrapolation of the rich cluster XLF (Burns et al. 1996).

Table 1.2: Typical properties of clusters and groups.

Property	Rich clusters	Poor clusters/Groups
Richness	50–300 galaxies	3–50 galaxies
Radius	(1–2) h^{-1} Mpc	(0.1–1) h^{-1} Mpc
Radial velocity dispersion	400–1400 km s^{-1}	100–500 km s^{-1}
X-ray luminosity	$(10^{42.5} - 10^{45})h^{-2} \text{ erg s}^{-1}$	$\sim 10^{43}h^{-2} \text{ erg s}^{-1}$
X-ray temperature	2–14 keV	~ 2 keV
Fraction of galaxies in the Universe	$\sim 5\%$	$\sim 55\%$

Poor clusters possess total masses of a few to ten times $10^{13}M_{\odot}$. The gas-to-stellar mass ratio is $\approx 1.5h^{-0.5}$, similar to the value for rich clusters, while the baryon fraction ($\sim 10\%$) is about half that in rich clusters (e.g., dell’Antonio, Geller, & Fabricant 1995; but see Roussel, Sadat, & Blanchard 2000). Furthermore, the baryonic masses are a small fraction of the total mass, indicating that such mid-sized galaxy aggregates are dominated by dark matter.

For poor clusters, richness, optical properties of the first-ranked cluster galaxies and X-ray luminosities are correlated (Bahcall 1980; Yamagata & Maehara 1986). But for small groups of galaxies, such relationships are not strong (see Mulchaey 2000 and references therein). However, the bulk morphological composition of all small galaxy systems — small groups or poor clusters — show appreciable correspondence with the X-ray luminosity such that the fraction of early-type galaxies increases with L_X (Bahcall 1980; Mahdavi et al. 1997; Hickson 1997; Mulchaey 2000).

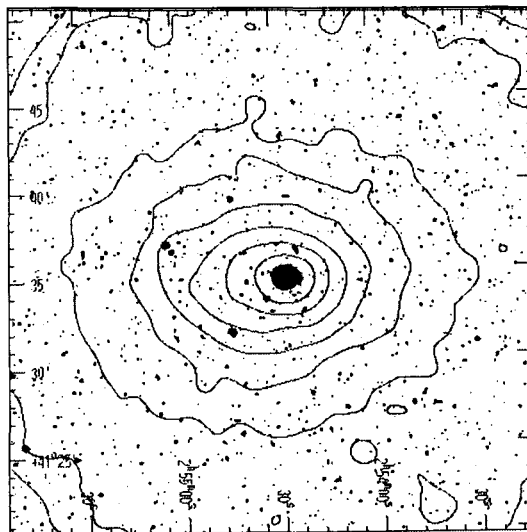


Figure 1.2: Digitised Sky Survey optical image of the poor cluster AWM7 ($z = 0.017$) overlaid with ROSAT X-ray contours. Notice that the high-energy emission is extended and peaked on the brightest cluster galaxy.

The cD galaxies in poor clusters are usually at the kinematic centers, as shown by their small relative velocities vis-a-vis the mean velocity of the cluster, and by the coincidence of their position with the cluster galaxy isopleth and peak of X-ray emission.

Tailed radio galaxies are found in the poor groups in larger numbers than expected through extrapolation from rich clusters (Burns et al. 1987; Venkatesan et al. 1994; Doe et al. 1995). Furthermore, these objects are similar in physical characteristics related to the radio jet, spectral indices, etc. This fact supports the following: the radio objects have high velocities (possible due to poor clusters being dynamically young) and their local environments are strikingly similar in density, magnetic field structures, etc., irrespective of the global richness.

The smooth, symmetrical X-ray emission from the ICM that fills poor clusters shows a sharp peak on the central galaxy (e.g., Kriss et al. 1983). Though a few X-ray-luminous poor clusters (e.g., the cD-dominated poor cluster AWM7; Neumann & Boehringer 1995) and even lower-mass systems (e.g., the NGC 5044 group; David et al. 1994) show the central excess in electron density and drop in temperature characteristic of cooling flows, it is unlikely the majority of them host cooling flows. The central X-ray luminosity excesses are probably unresolved emission from the brightest cluster galaxies (Doe et al. 1995; Mulchaey & Zabludoff 1998). Whereas cooling flows in rich clusters tend to be inhomogeneous, with a significant amount of the gas cooling out at large radii (cf. Fabian 1994), they are nearly homogeneous in small groups (David et al. 1994). This is in keeping with the plasma temperature being significantly higher in rich clusters than in groups, where it is comparable to the virial temperature of both the group itself and the central galaxy. X-ray emission in the cooling flow region may be provided by the gravitational energy in groups, whereas central mass deposition dominates in rich clusters. Overall, poor clusters represent the transition between poor groups and rich clusters.

1.3.4 Are Poor Clusters Real? Bound? Virialized?

Many galaxy associations, especially small groups, have non-negligible chances of being mere projection effects. This could be due to accidental over-population of field galaxies in the line-of-sight (Sulentic 1987), or due to galaxy pairs projected close to field galaxies (Walke & Mamon 1988), or due to large-scale cosmic structures such as filaments and sheets of galaxies (e.g., Ramella et al. 1997). As an instance, only 40% of the groups identified by Huchra & Geller are extended X-ray sources, with the remaining 60% being either accidental superpositions or systems devoid of X-ray plasma (Mahdavi et al. 2000). Even optical-X-ray identification of poor clusters is not without pitfalls. The existence of diffuse X-ray emitting gas is not necessarily evidence that a galaxy association is real or bound; especially in very poor groups, X-ray emission could be from sparser systems in filaments along the line of sight (Ostriker, Lubin & Hernquist 1995) or through shock-heating of primordial gas (Hernquist et al. 1995).

So, are poor clusters real, gravitationally bound galaxy aggregates? There is considerable observational support for a large fraction of small- and mid-sized galaxy systems being real, physical systems and not merely chance superpositions or large-scale filaments viewed edge-on. Such evidence includes (i) a large population of spectroscopically-confirmed faint member galaxies (Ledlow et al. 1996; Zabludoff & Mulchaey 1998), (ii) the presence of a first-ranked galaxy as luminous

and large as any seen in rich clusters, and which could only have arisen from multiple mergers of several bound galaxies (N.B.: the MKW/AWM clusters were *identified* on such a basis), and (iii) extended X-ray halos due to a confined, diffuse intracluster/intragroup medium (e.g., in the Yerkes clusters – Kriss et al. 1983; Price et al. 1991; in small groups – Ponman et al. 1996; Mulchaey & Zabludoff 1998; Mahdavi et al. 1999, Helsdon & Ponman 2000) similar to those seen in rich clusters. As mentioned already, X-ray selection is generally secure because X-ray luminosity increases as the square of the gas density (and depends also on the X-ray temperature which is an index of the total potential). Though the velocity distribution of galaxies within small systems is frequently non-Maxwellian, most ($\approx 70 - 100\%$) poor clusters are likely to be bound (Ramella et al. 1989; Beers et al. 1995; Barton et al. 1998; Zabludoff & Mulchaey 1998).

Poor cluster crossing times of a few 10^9 years are shorter than the Hubble time; after a few crossing times, it is likely that clusters would be relaxed. However, though bound, not all poor clusters may be virialized; many are likely to be part of larger, bound systems such as larger, more diffuse clusters or filaments of galaxies (e.g., Beers et al. 1995; Doe et al. 1995). This attests to continuing hierarchical growth of large-scale structure on all scales; small groups and poor clusters fall into large clusters. It is likely that a few Yerkes clusters and most elliptical-dominated galaxy groups are relaxed systems; their diffuse ICM extends to hundreds of kiloparsecs and appears smooth, reflecting perhaps the equally smooth system potential well (see Mulchaey 2000). Further, cooling flows exist in some of these aggregates, suggesting the hydrostatic equilibrium of the long-lived intragroup gas (see Sarazin 1988; Fabian 1984). In contrast, it is likely that some groups with low X-ray luminosity and temperature, that tend to have irregular X-ray morphologies, are still dynamically restless and not virialized. Several MWK/AWM poor clusters (Beers et al. 1995), approximately half the sample of WBL poor clusters (Ledlow et al. 1996), and a few poor groups (Zabludoff & Mulchaey 1998) also exhibit complex substructures in the velocity distributions. The member galaxies of these systems may then be on different orbits, and may not have mixed well enough to validate a virial analysis for such systems. In effect, the optical morphology, large-scale environment, presence of tailed radio sources (Venkatesan et al. 1994) and substructure in the velocity field and X-ray emission of many of these objects suggest that poor clusters belong to a class of “young, dynamically evolving clusters” (Ledlow et al. 1996).

Regardless of their diversity, poor clusters represent the same genre of objects - largely bound, dynamically active entities in the regime of intermediate clustering strength.

1.3.5 Simulations

N-body simulations of poor clusters with enough particles to resolve the individual galaxies are becoming feasible only of late. While each suite of simulations has its own characteristic features and limitations, they evince some processes and phenomena in common as summarized below. Dynamical evolution reveals itself as substructures in the galaxy counts and in the projected density of the intracluster medium (ICM) except in isolated clusters where substructure is less pronounced (Lima Neto & Baier 1997). So long as the centers of the galaxy groups are reasonably dense, under widely different initial conditions — spherical or non-spherical, isotropic or anisotropic collapse, virialised or unrelaxed systems — merging instability leads to the formation

of a giant, massive central galaxy early in the cluster history (Barnes 1985; Bode et al. 1994; Lima Neto & Baier 1997; Dubinski 1998; Garijo, Athanassoula, & Garcia-Gomez 1997; Athanassoula, Garijo, & Garcia-Gomez 2001). The mass distribution within the system greatly influences galaxy interaction and merger timescales. Within small systems removing mass from dark halos around individual galaxies and redistributing it throughout the cluster into a common halo results in lowering the galaxy merging rate (Bode et al. 1994; Athanassoula, Makino, & Bosina, 1997; see also Hickson 1997 for a summary of dynamical evolution of the dense compact groups). On the other hand, increasing the initial ICM or common halo mass while keeping the galaxy masses and structure unchanged raises the merging rate due to dynamical friction with the ICM. Galactic cannibalism of smaller galaxies by the massive central object may ensue for a Hubble time, resulting in a small increase in the mass of the latter (Dubinski 1998). The merger product residing at the group kinematic center can be identified with the first-ranked galaxy. Its formation history and properties (shape, surface brightness, and velocity dispersion) intimately reflect the initial galaxy distribution: anisotropic, aspherical initial conditions result in triaxial objects with anisotropic velocity dispersion, and principal axes that are aligned with the host cluster.

1.4 Objectives and Presentation of the Thesis

In this thesis we present an observational study — primarily through optical imaging — of galaxy properties within four X-ray luminous poor clusters at moderate redshifts ($0.08 < z < 0.25$). Our sample is small, so we perceive the work as a reasonable beginning into the systematic study of poor clusters beyond the nearby universe. Our approach will be to examine (i) the statistical properties of the galaxies, including their luminosity distribution, their stellar contents, spatial distributions, etc., and (ii) the brightest cluster galaxy in detail. We place these poor cluster members in context between those in dense rich clusters and the sparser loose groups and the field.

The arrangement of the rest of this thesis is as follows:

- Chapter 2 describes the selection and optical observations of the poor clusters. We select poor clusters as luminous, extended X-ray sources identified with galaxy overdensities that are noted as being optically poor in the EMSS Catalog of clusters of galaxies (Gioia & Luppino 1994). We give an account of the telescope and instruments that provided our observations of four poor clusters, and the analysis and photometric calibrations of the derived images. We report on the detection of faint objects on the CCD images and their separation into stars or galaxies, but postpone the galaxy catalogs to an appendix. We estimate the completeness of the detections, and accuracy of both the star-galaxy separation and photometry. Three of the EMSS clusters in our sample have been the subject of a few observations in the literature, some akin to ours. We will compare our results with the literature as we go along.
- What is the nature of the luminosity function in the poor clusters? Chapter 3 characterizes the distribution function of the cluster galaxies in luminosity. To cull cluster members from all the galaxies in the catalogs, we apply two independent methods: subtraction

of background galaxies using statistical counts in the literature, and using the tight color-magnitude relation of cluster galaxies which we derive in Chapter 4. We compare the number counts of galaxies in absolute magnitude of the four individual clusters, and then create a composite poor cluster luminosity function. We inquire into whether the “universal” nature, i.e., lack of environmental dependence, of the galaxy luminosity function is supported by our studies. We also estimate cluster richness defined by several authors and their correlations with X-ray properties.

- How do colors of galaxies in poor clusters compare with those in the field and rich clusters? In Chapter 4 we study the evolutionary properties, e.g., stellar content, of the cluster galaxies. We derive the relation between the optical magnitudes and colors of the galaxies, and show that a significant fraction of objects in the lines-of-sights to the various poor clusters fall within narrow ridges in the color-magnitude (CM) plane. We use this well-defined ridge to “identify” cluster members, to derive their luminosity functions in Chapter 3, and to deduce spatial segregation by galaxy luminosity or morphology, in Chapter 5. We estimate the fraction of bright galaxies that appear to be cluster members but have rest-frame colors bluer than those expected for early-type galaxies at the cluster redshift. We compare both the CM relation and the blue fraction with those in rich clusters.
- What is the morphology of the poor clusters? We provide optical–X-ray overlays of the sample poor clusters in Chapter 5. We provide the first-order quantitative information about the core and halo sizes of the poor clusters, and the spatial distribution of the galaxies within them. Besides these, we examine whether the galaxies show appreciable segregation in luminosity and morphology. We examine the orientation of the brightest cluster galaxy, the galaxy distribution and the X-ray emission.
- In Chapter 6, we shift focus from statistical descriptions of galaxies to the individual brightest cluster member (BCM) of the poor clusters, and ask: are the first-ranked galaxies in poor and rich clusters similar? We perform isophotal analysis of the BCM luminosity profile to derive the geometry and to look for deviations from ellipticity. We perform fits of the surface brightness profiles to the de Vaucouleurs law for elliptical galaxies, and search for the existence of the characteristic envelop of cD galaxies. We also seek signs of tidal interaction, dwarf satellite galaxies, etc.
- Finally, in Chapter 7, we summarize the results of this thesis, and indicate possible lines of future study of poor clusters. A collective bibliography of all the chapters, the catalogs of galaxies detected in the fields of the poor clusters, and two appendices follow the conclusions.

Chapter 2

Observations and Data Analysis

2.1 Avant-Propos

The motivation of this thesis is to explore the properties of galaxies in poor clusters at moderate distances and compare them with those in the field and rich clusters. These observations would contribute to the pool of information required for understanding galaxy evolution. The observing procedure involves imaging and photometry of faint galaxies over cluster-scale angular sizes. In this chapter, we describe the sample of X-ray emitting poor clusters of galaxies chosen for our study, the optical imaging observations we have acquired using the CCD camera at the Vainu Bappu Telescope, and the analyses performed on these data. Wherever necessary, we use Hubble constant $H_0 \equiv 50 \text{ km s}^{-1} \text{ Mpc}^{-1}$ and density parameter $q_0 = 0.5$, unless stated otherwise.

There are several good reasons for using optical observations for our purpose of studying normal galaxies in the not-too-distant universe. Normal galaxies are dominated by starlight, and emit much of their radiation in the visible band. An important and simple tool in revealing galaxy properties and evolution is the relative luminosity, or colors, over a wide range of wavelengths. Galaxy colors reveal the spectral energy distributions at a rudimentary level, and can shed light on the stellar composition of faint galaxies, and thus help probe their star-formation histories; the details, however, can be derived only from spectral lines.

At moderate distances ($z \sim 0.25$) the redshifted optical radiation of the galaxies still remains largely in the visible bands. Though galaxy evolution becomes evident even at $z \sim 0.2$ (e.g., Caldwell & Rose 1997), the objects are not so changed that local counterparts cannot be found. Therefore, comparison of colors of intermediate redshift galaxies and local ones does not lead to disastrous inconsistencies. Cosmological corrections to galaxy luminosity and surface brightness, and due to gravitational lensing are not of serious concern at moderate redshifts. The Earth's atmosphere is transparent to optical radiation and the dark sky does not contribute too high a background. Furthermore, optical detectors and observing techniques are very well developed, and standard image processing and analysis routines are firmly in place. For spatially resolved sources, optical images are useful in deriving image profiles (surface photometry), which provides information on the dynamics and dynamical histories of the galaxies. Color maps can provide important information about the distribution of both stellar populations in the galaxies as well as interstellar matter in the form of dust, ionized-Hydrogen regions, etc.

2.2 Sample Selection

In this section, we provide our definition of poor clusters, describe our sample and the caveats in its selection.

2.2.1 Poor Clusters : Operational Definition

As mentioned in Sec. 1.3.2, the very definition of a poor cluster is not unique; each definition, moreover, is riddled with its own ambiguities and exceptions. We have chosen poor clusters based on their X-ray emission and sparse galaxy population in optical images.

Our sample of poor clusters of galaxies is a small subset of the Extended Medium Sensitivity Survey (EMSS; Gioia et al. 1990) catalog of sources discovered serendipitously with the *Einstein* X-ray satellite in the 0.3 – 3.5keV energy band. The EMSS consists of over 800 high Galactic latitude ($|b| > 20^\circ$), bright X-ray emitters. Nearly 100% of the sources now have known optical counterparts. Active galactic nuclei dominate the extra-galactic component of this catalog, followed by clusters of galaxies. The EMSS cluster subsample (Gioia & Luppino 1994; henceforth GL94) consists of nearly 100 objects, whose X-ray properties are consistent with their being clusters of galaxies, and which are optically identified with galaxy over-densities initially on the Palomar Sky Charts and subsequently through CCD imaging. The X-ray luminosities of EMSS clusters, determined using a 6keV thermal spectrum, range over $3 \times 10^{43} \text{ erg s}^{-1} \leq L_x \leq 20 \times 10^{44} \text{ erg s}^{-1}$ (for $H_0 = 50 \text{ km/s/Mpc}$ and $q_0 = 0.5$). The cluster redshifts range over $0.05 \leq z \leq 0.85$, with median $z \approx 0.3$; GL94 quote redshifts for only the objects they identify as the brightest cluster galaxies. About 25% of the clusters are positionally co-incident with those in the catalog of Abell, Corwin and Olowin (1989) and 15% with those in the Zwicky et al. (1968) compilations. From inspection of deep CCD images taken as follow-up optical observations, GL94 provide comments about the optical appearance of the clusters and spectral properties of the putative brightest cluster members. GL94 note that 19 of these EMSS clusters appear to be “poor”, i.e., display morphologies and galaxy counts that are best described as (that) of poor clusters. *those*

We construct our sample of moderate-redshift poor clusters from among EMSS clusters that

1. show X-ray emission of luminosity $\geq 3 \times 10^{43} \text{ erg s}^{-1}$
2. have their X-ray centroid optically identified with galaxy over-densities
3. are noted by GL94 as being optically poor
4. are at redshifts $0.08 < z < 0.25$
5. lie north of declination $\delta \sim -30^\circ$.

We elaborate below on these selection criteria.

(1) If X-ray emission arises from the diffuse intra-cluster medium, then luminosities of the order of $10^{43} \text{ erg s}^{-1}$ usually correspond to the brightest galaxy groups (Ponman et al. 1996, Ledlow et al. 1996) and Abell richness 0 clusters (White, Jones & Forman 1997). As stated in the introduction,

the presence of extended X-ray emission suggests that these clusters are real, physical systems rather than chance superpositions of galaxies (but please see below). Some of the poor clusters are also spatially resolved in the *Einstein* images. More recent and higher resolution X-ray imaging using the ROSAT X-ray observatory (Oppenheim et al. 1997) have confirmed the extended nature of the high-energy emission of most of these clusters.

(2) Not always do the centroids of the cluster X-ray emission and the galaxy distribution coincide. It is quite often seen, though, that the peak of the X-ray emission rests on or near the first-ranked galaxy of the cluster, with a typical offset of < 30 arcsec. For the EMSS clusters, the accuracy of the X-ray positions is itself about 50 arcsec.

(3) Poor clusters, in our operational definition (Sec. 1.3.2), should have a galaxy population of at least 3 members but not exceed the Abell richness 1 criterion. It is worth noting that White et al. (1999) who created a catalog of poor groups from an objective search for galaxy over-densities, suggest that there is a continuity, even an overlap, in galaxy population from the poorest groups to Abell rich clusters. GL94 make richness estimates by visual inspection. Eye estimates of galaxy population, while not entirely reliable, are nevertheless useful descriptors, and can distinguish between rich and poor clusters. See Sec. 2.2.4 for an account of our preliminary, quantitative richness estimate of EMSS poor clusters using sky surveys, which shows that the poor clusters in our sample are usually less populated than Abell R=1 clusters at similar redshifts.

(4) The redshift criterion selects clusters at distances between 300–850 Mpc, with distance moduli $38.35 \leq DM \leq 40.24$ (for $H_0 = 50 \text{ km s}^{-1} \text{ Mpc}^{-1}$). Cluster diameters of about 2 Mpc would subtend angular sizes of 1000–450 arcsec, and the brightest cluster galaxies (50 kpc diameter) would span 24–11 arcsec over this distance range (as shown graphically in Appendix A). A redshift selection of $z < 0.25$ is also of practical importance because galaxy concentrations become increasingly harder to detect at higher redshifts, as evidenced by completeness limits of large-scale surveys.

(5) The final criterion for our sample selection, dictated by observational constraints, is that the clusters lie north of declination $\delta \sim -30^\circ$, so as to be accessible for imaging using the Vainu Bappu Telescope.

These precursory conditions lead to our selecting as “poor clusters” the sixteen EMSS objects listed in Table 2.1.

2.2.2 Other work done with the EMSS cluster sample

Whereas EMSS poor clusters have not so far been specifically explored, the most luminous, rich clusters from the EMSS cluster catalog have been used for a number of studies including:

- photometric properties of galaxies in X-ray clusters (Garilli et al. 1996), and evolution of galaxy populations in rich, distant clusters by the Canadian Network for Observational Cosmology (CNOC e.g., Yee et al. 1998)
- cluster kinematics, M/L ratios etc. (CNOC; e.g., Carlberg et al. 1997, 1998)
- cooling flows in high-redshift clusters (Donahue et al. 1992)

Table 2.1: Possible poor clusters in the EMSS catalog. The columns are (1) cluster name (2) X-ray luminosity (3) spectroscopic redshift and (4) apparent magnitude of the brightest cluster galaxy.

Cluster	L_X $10^{44} \text{erg s}^{-1}$	z	M_B
MS 0002.8+1556	1.64	0.116	16.0
MS 0043.3-2531	0.49	0.112	16.7
MS 0301.7+1516	0.33	0.083	16.9
MS 0433.9+0957	4.34	0.159	18.5
MS 0440.5+0204	4.01	0.190	17.0
MS 0735.6+7421	6.12	0.216	17.7
MS 1004.2+1238	0.93	0.166	17.7
MS 1050.7+4946	3.41	0.140	16.8
MS 1125.3+4324	0.76	0.181	18.5
MS 1219.9+7542	1.28	0.240	18.7
MS 1244.2+7114	3.84	0.225	17.5
MS 1306.7-0121	1.70	0.088	16.0
MS 1401.9+0437	0.88	0.230	18.5
MS 1409.9-0255	1.04	0.221	19.0
MS 1520.1+3002	0.79	0.117	18.5
MS 1910.5+6736	4.39	0.246	19.0

- evolution of X-ray luminosity and (Gioia et al. 1990; Henry et al. 1992) temperature functions of clusters (Donahue 1996; Donahue et al. 1998)
- cluster radio galaxies: structure, morphology and evolution with redshift (Stocke et al. 1999)
- gravitational lensing : giant luminous arcs (Gioia & Luppino 1994; Fort et al. 1992; Le Fevre et al. 1994; Gioia et al. 1998, Luppino et al. 1999) and weak-lensing (Luppino & Kaiser 1997)
- cosmological density parameter (Donahue et al. 1998)

2.2.3 Sample Selection: Caveats

Although X-ray selection minimizes the chances of spurious detection, the EMSS cluster subsample is not entirely free of selection biases. For one, the EMSS is not strictly a flux-limited sample (Donahue et al. 1992), and could be biased toward centrally-peaked surface-brightness profiles because its finding algorithm was geared toward point-sources. Sharp central profiles that signify cluster cooling flows are preferentially found in dynamically relaxed, old clusters (Fabian 1994), and not in evolving, dynamically young poor clusters. Donahue et al. (1992) argue that the EMSS does not miss non-cooling flow clusters; and the X-ray luminosity function of EMSS

clusters is similar to those derived both by later studies (e.g., Ebeling et al. 1997). So, if this bias is present, it is of little importance.

More importantly, recent optical and X-ray follow-up observations have shown that a few clusters are actually misclassified objects. For instance, long exposures using the ROSAT X-ray observatory have revealed that a few “clusters” appear to be point sources even at ROSAT’s higher resolution, and that their X-ray properties appear to be better described as originating from stars or AGN. Specifically, one of the poor clusters we observed (MS 1154.1 + 4255) has recently been identified with an AGN of BL Lac type (Rector et al. 1999). Though this object was in our sample list, and we have imaged it in multiple filters, we have excluded MS 1154.1 + 4255 from this thesis. Despite its classification errors, the EMSS cluster catalog remains one of the best sources for genuine clusters selected in X-ray, along with similar projects such as the Wide Angle ROSAT Pointed Survey (Scharf et al. 1997) and the Serendipitous High-Redshift Archival ROSAT Cluster survey (Romer et al. 2000), which are ongoing searches for galaxy clusters detected serendipitously in archival ROSAT observations.

Besides the very identification of clusters, another consideration is the estimates of their richness by eye. Visual typing of a cluster as “poor” involves subjective and nonphysical criteria, and can hardly be infallible. Some poor clusters may have had their population underestimated, while other clusters classified as “rich” could well be so due to superposition of two or more close groups. From imaging alone, it is not facile to derive reliable quantitative measurements of poor cluster populations. We should however keep in mind that even previous “objective” criteria have not been free of intrinsic biases.

We make no claims to completeness or homogeneity of our clusters, though we believe ours is a representative sample of X-ray luminous poor clusters of galaxies beyond the nearby universe. Table 2.2 presents the major properties of the four poor clusters that we study in this thesis.

Table 2.2: Cast of characters

Parameters	MS 0002.8 + 1556	MS 0301.7 + 1516	MS 0735.6 + 7421	MS 1306.7 – 0121
RA (J2000)	00:05:25.1	03:04:30.4	07:41:50.1	13:09:18.0
Dec (J2000)	16:13:24.09	15:27:53.0	74:14:01.36	-01:37:21.4
Redshift	0.116	0.083	0.216	0.088
l , degree	107.15	164.09	140.64	312.15
b , degree	-45.23	-36.56	29.44	60.93
L_X , 10^{44} erg s $^{-1}$	1.64	0.33	6.119	1.698
BCM m_v , mag	16.0	16.9	17.7	16.0

2.2.4 Preliminary Richness Estimates

Due to the effects of redshift, all but the nearest galaxies are identified more easily on red survey plates than on the blue. Identifying medium-redshift clusters is therefore profitable using red plates (near $\lambda 650$ nm). There is in general a “field” of galaxies, and superposed on this are the

clusters, which become conspicuous as count enhancements (above the statistical fluctuations) in the surface number density of galaxies. A bothersome source of contamination in a cluster catalog are the stars of the Milky Way itself. Even a moderately rich star field can not only camouflage the clusters but also make star-galaxy distinction quite precarious. How then, do we estimate the number of bona-fide cluster members?

Why m_3 and not m_1 or m_2 ?

Traditional measures of galaxy population for rich clusters include the Abell counts based on sampling a part of the luminosity function (LF). For this, one needs to estimate the magnitude m_3 , of the third brightest cluster galaxy. Then, Abell richness is defined as the count of galaxies in a $1.5h^{-1}$ Mpc radius of the cluster center, and which are within 2 magnitudes of m_3 , corrected for the field galaxy population projected into the same radius.

But such a number count cannot be directly applied to poor clusters. Since poor clusters are, by definition, ill-populated, and usually not compact, it is difficult to be sure of the third brightest member. Further, since they are unlikely to be as large as Abell clusters, it makes little sense to conduct a census of cluster galaxies within the same $1.5h^{-1}$ Mpc Abell radius. Instead, in our preliminary richness estimates, we adopt an Abell-like definition of richness: the number of galaxies, corrected for field contamination, inside a projected radius of $0.5h^{-1}$ Mpc of the brightest galaxy, and not fainter than 2 magnitudes of $(m_1+0.6)$, where m_1 is the magnitude of the brightest cluster member. The reason for choosing $(m_1+0.6)$ is that, assuming that the bright end of the LF of all clusters — rich or poor — is similar, m_3 is typically 0.6 magnitudes fainter than m_1 in red photometric bands (Abell et al. 1989).

To derive reliable quantitative measurements of cluster populations, we initially used the Automated Plate Measurement (APM) catalogs to count the galaxies in the fields of the poor clusters. We counted galaxies within $0.5h^{-1}$ Mpc of the brightest cluster galaxy and estimated the cluster population. We found that the galaxy counts could be upto 20% different between the blue and the red plates, due to uncertain star-galaxy separation. Later, we used the red plates of the Automated Plate Scanner catalogs (APS, Pennington et al. 1993) which are available online. The APS database of faint celestial objects is created from scans of the original Palomar Observatory Sky Survey plates. The catalogs contain information such as reliable neural-network classification of objects into stars or galaxies as well as approximate astrometric and photometric data.¹ We searched APS in an area of 25 arcmin around the poor cluster optical positions; this area is wide enough to completely encompass $0.5h^{-1}$ Mpc of the nearest cluster. (See Appendix A for a graphical presentation of the angular sizes described by $0.5h^{-1}$ Mpc at different redshifts.) From each resulting cluster catalog, we chose only galaxies with red magnitudes within two magnitudes of the respective $(m_1+0.6)$. We computed the angular size of $0.5h^{-1}$ Mpc at the cluster redshift, and then derived galaxy counts within a circle of this radius centered on the brightest cluster member (BCM). We estimated the field contamination by counting galaxies in a 3 arcmin annular region around the $0.5h^{-1}$ Mpc circle, and scaled these counts for the difference in areas of the circle and the annulus. We then derived the cluster population as the counts within the circle minus the area-scaled field counts.

For comparison, we performed the same analysis on several Abell clusters of richness class 0 or 1, with a single dominant galaxy (i.e. Bautz–Morgan type I or I-II clusters), spanning the redshift

¹We accessed the catalogs through the World Wide Web at <http://isis.spa.umn.edu>.

Table 2.3: Preliminary richness measurements (using the APS object catalog) for the poor clusters in our sample compared with those of Abell rich clusters. For MS0735 and Abell 520, the galaxy counts are from the APM survey and are not directly comparable to the other clusters.

EMSS Cluster	z	Pop.	Abell Cluster	z	Pop.
MS 0002.8 + 1556	0.116	8	Abell 2177	0.161	16
MS 0301.7 + 1516	0.083	1	Abell 1651	0.086	11
MS 0735.6 + 7421	0.216	3	Abell 0520	0.199	8
MS 1306.7 – 0121	0.088	5	Abell 2145	0.088	6

range of our poor cluster sample. We present the preliminary richness estimates in Table 2.3 which confirms that the EMSS poor clusters are without exception less populated than their Abell *richness 1* counterparts at similar redshifts. Strictly speaking, these richness measurements are *à posteriori* estimates.

2.3 Observations : Optical Imaging

Clear skies

I am eager to snare

Traveler photons

In this work, we use optical images obtained on both photometric and non-photometric nights close to new moon. The following section describes the telescope, filters and detector used in obtaining the observations.

2.3.1 Telescope: the Vainu Bappu Telescope

We acquired all optical imaging observations reported in this thesis at the prime focus of the 2.34 – m Vainu Bappu Telescope (VBT), at the Vainu Bappu Observatory (VBO) at Kavalur, India. The observatory (longitude 78° 8 E, latitude 12° 5 N, altitude 730m above sea level) is operated by the Indian Institute of Astrophysics, Bangalore, India. Besides the VBT, the VBO hosts a few smaller telescopes including a 1-m Ziess reflector. The best observing season for Kavalur is between December and April; the rest of the year is usually affected by the two Monsoons that bring rains to South India.

Since even the brightest galaxies within the clusters of galaxies in our sample are usually fainter than $m_v \geq 16.5$, we need to use at least moderate-sized telescopes to collect their small fluxes. The Vainu Bappu Telescope has a 2.34-m diameter mirror of focal ratios of $f/3.24$ and $f/13$ for the prime and Cassegrain foci respectively. For direct imaging observations at the prime focus, this configuration provides an image scale of 26 arcsec/mm, and a field of view of 10.5 arcmin \times 10.5 arcmin. (The Cassegrain mode is used for spectroscopic observations.) The seeing (measured as the full width at half-maximum (FWHM) of an unresolved source in a well-focused and tracked image) is typically 1.5 – 2.5 arcsec.

2.3.2 Filters: Broad-band B, V, R and I

Several sets of filters — both broad-band and narrow-band — are available for imaging at the VBT. Normally, observers at the VBO do not employ the near ultra-violet (U or u) filter due to the small short wavelength flux received at the ground at this low altitude site. We have employed the following filters in our observations: broad-band blue, visual, red and near infra-red (approximating the standard B, V, R and I photometric bands). Previous observations at intermediate and high redshifts (e.g., Butcher & Oemler 1984) indicate that rich cluster galaxy populations may be dominated by blue galaxies. Consequently, it is advisable to acquire observations in the B and V filters to sample the rest-frame blue spectral energy distributions of the faint galaxies. To maximize the wavelength range over which color information is derived, the R and I filters are useful.

The total exposure time in each filter depends on several factors: the intrinsic spectral energy distribution of the objects (faint blue galaxies are still relatively red objects compared to field stars), the quantum efficiency of the CCD detector (rather low in the very blue spectral region, fairly high around the V and peaking near the R and I bands), and the brightness of the night sky (low in B and V but increasing fast through R and I). We had to, therefore, choose appropriate integration times to give fairly uniform errors in the photometry in different filters. We made efforts to obtain observations in all bands on the same night; however we were not always successful in achieving this objective. In the span of 4-5 years over which we obtained observations, three sets of broad-band filters were available at the VBT, two sets of circular filters of 2-inch radii and another of 3-inch radii. The 2-inch filters are somewhat undersized to cover the entire field of view of the images, and give rise to vignetting in the corners of the CCD frame.

2.3.3 Detector: CCD

The light detector used at the VBT is based on the Charge-Coupled Device (CCD), which is widely used in astronomy. CCDs make ideal imaging devices because they provide numerical maps of the light intensity they record, have high quantum efficiency (better than 80%; compare with about 1% for the human eye), are sensitive to a wide spectral range from $\approx 100 - 1000$ nm, and are basically linear over an order of 10^4 in light intensity, thus allowing excellent photometry of even faint objects near bright ones. One disadvantage of CCDs compared to the older photographic detector is their small size. Another is the decline in the sensitivity in the blue region of the spectrum, which can, however, be compensated to some extent by application of special coatings. The counting of the charge in each pixel by an analog-to-digital converter, with a record of the pixel position constitutes a measurement of the original light intensity recorded by the array. The counts or Analog-to-Digital Units (ADUs) need to be turned back into number of electrons and finally to photons; the relation between ADUs and electrons, termed gain, is a characteristic parameter of the CCD chip. The amplifier read-out process also gives rise to electron noise, termed read-out noise. This extraneous source of counts, another parameter of the CCD chip, is equivalent to the photon noise associated with the detection of (gain \times read-noise) number of photons. Read-noise usually determines the minimum level of light that can be reliably measured by the CCD, thus influencing its dynamic range.

All our observations at the VBT used thinned, back-illuminated, 1024×1024 pixel format CCD chips from Tektronics Inc., USA. The bit saturation limit of the detectors is at 65,536 counts.

Table 2.4: CCD parameters

Properties	CCD#1	CCD#2	CCD#3
Period	1995Sep–1997Apr	1997May–1999Mar 2000Feb–2000Mar	1999Apr–2000Apr
Size of array (pixel ²)	1024×1024	1024×1024	1024×1024
Image Scale (arcsec pixel ⁻¹)	0.609	0.604	0.608
Quantum Efficiency (at 550nm)	60%	68%	70%
Gain (e ⁻ /ADU)	5.9	8.9	4.5
Read Noise (e ⁻)	8.0	9.8	9.1

The CCD image is a combination of the desired photons from the object(s) of interest, a background, and the systematics of the imaging system. The background consists of light from the foreground and background objects, zodiacal light, atmospheric emission, scattered light from the Moon or city lights. We will refer to these collectively as “sky”. The instrumental signature consists of both additive and multiplicative systematics that also require calibration. This *raw* CCD image, that maps the light distribution of the celestial object, can be written as:

$$\text{raw} = (\text{object} + \text{sky}) \times \text{CCD gain} \times \text{optical transmission} + \text{dark} + \text{bias.}$$

What about flat fielding effects?

The last two quantities are additive systematics present in the CCD. The bias level is a small positive voltage added to the measured signal from the CCD. The offset is added as it is not a good idea to have zero ADUs for zero photons, because the readnoise fluctuations could steer the counts unphysically below zero. Dark current is a background resulting from thermally created electrons in the CCD pixels, and increases proportional to the exposure time. CCDs are commonly cooled (usually employing liquid nitrogen) so that the dark current is negligible during the exposure time. The bias level, usually about 1-2% of the CCD saturation value, has to be subtracted during reduction of CCD data.

Multiplicative systematics cause variation in response across the CCD. They can occur because of intrinsic changes in the sensitivity of the pixels, varying sensitivity with wavelength, optical characteristics of the telescope and CCD detector such as vignetting, or dust on the CCD window or filters. The last is obviously unstable in time, and can never be completely corrected. The correction of multiplicative systematics that cause low-level noise in the images consists of the process of flat-fielding, which determines the pattern of response variation across the pixels. The simplest strategy to establish this calibration is the observation of a uniformly illuminated target. When normalized, the image of this flat target is a map of the relative efficiency of the array. Since the response of the CCD depends on wavelength, it is best to acquire flat-fields in all the filters used in observations. Then, scaling the actual object exposures (after bias-subtraction) by the flat-field frame in the particular filter removes the pixel response variations. Three common flat sources are the dark sky empty of any but the faintest objects, the twilight sky, and a uniformly

illuminated target within the telescope dome. A viable flat-fielding approach is to image the twilight sky, which is bright and uniform enough to give good signal for creating a flat field. However, there are two main drawbacks to this: the twilight sky is different in color from the dark sky, and usually contains brightness gradients over several tens of arcminutes.

2.3.4 Gainful Imaging: the Shift-and-Stare Technique

For imaging faint sources, only integrations longer than a few hours can ensure sufficient signal-to-noise ratios. However, there are low-level systematics that set limits to the longest integration times and thus the accuracy of the photometry: variations due to the weather (night sky, cloud drifts), etc. A way to circumvent this problem is to make good use of the highest efficiency, linear, stable CCD detector and configure the image acquisition and processing techniques to cancel the systematics.

We have used a variation on the conventional imaging technique, especially useful for fields containing faint objects that are much smaller than the angular size of the CCD. This is to take several (even several tens of) short (but sky-limited), well-guided exposures of the field, with successive exposures randomly offset with respect to each other. There must be sufficient overlap (say 80%) of the successive fields as well as a minimum offset that is larger than the angular size of the largest bright object in the image. The final size of the image is the common overlap area of all the frames. This set of unaligned images contains all the information about the celestial objects as well as the CCD systematics, in extricable form. Then, registering the flat-fielded frames and median combining them within each filter subset leads to final images that are more or less limited by sky (Poisson) noise. Residual noise in the background is ameliorated due to the smoothing of the CCD response on several pixels for the same point on the celestial object. The technique is effective in increasing the dynamic range of the CCD image.

2.3.5 Imaging Sequence at the VBT

During each observing run we acquired long exposures of the clusters of galaxies, short exposures of standard stars for photometric calibration, and flat-fields and bias frames for calibration of CCD systematics.

We scheduled the cluster observations so that the objects were always at small zenith angles, to minimize atmospheric extinction. Pre-1997, we usually imaged the clusters with long exposure times and only once per filter per night. For the rest of the observing runs, we applied the shift-and-stare technique. We took multiple exposures (at least three per filter) of the clusters, avoiding the saturation of any object in the frame. We moved the telescope between successive exposures, keeping a minimum overlap of about 75% of the region and a minimum offset close to the size of the brightest cluster galaxy. Typical exposures per frame were about 10 minutes. We made efforts to obtain cluster observations in all filters on the same night; however we were rarely successful in achieving this objective. Table 2.6 provides the journal of observations for the images we use in this thesis.

We also observed several standard stars to derive photometric zero-points and to transform in-

strumental magnitudes into Johnson B and V, and Kron-Cousins R and I photometric systems. We attempted standard star observations only if the skies were close to photometric quality. We chose the open cluster M67 and several Standard Area stars from Landolt (1992) for this exercise. The standard fields had between 3–8 stars located within a single field of view of the CCD, spanning a wide range in colors. Sandwiched between cluster observations, the standard star observations allow calculation of the photometric zero-points as well as the transformations from the instrumental magnitudes to the standard magnitudes.

For pre-processing the CCD images, we have chosen to use twilight flats. We acquired typically five frames of the twilight skies (both at dusk and dawn) in each filter. We chose flat-field exposure times (in the range of 1-5 seconds) so that the finite opening and closing times of CCD shutter do not produce spurious structure or non-uniform illumination. While taking flats, we pointed the telescope well away from the setting/rising Sun; we also kept it aimed not too far from the zenith. To ensure that adventitious bright stars in a frame do not illuminate the same pixel in subsequent ones, we moved the telescope tens of arcseconds away between successive flat-field exposures. However, if skies were either foggy or cloudy — thus possessing large, unpredictable brightness gradients — we omitted these observations.

At each run, we obtained several (6–8) bias frames once every few hours, to calibrate the additive systematics of the CCD, as well as to secure the identification of bad pixels on the chip. Since the CCD detector is well-cooled, and dark current is negligible, we did not spend time on acquiring dark frames.

2.4 Image Analysis

In this section, we describe how we obtain photometric information from the “raw” data which are in the form of an array of numbers read out from the CCD.

The data files from the CCD camera at the VBT are available in FITS format that is designed to provide a means for convenient exchange of astronomical data between installations with different hardware and internal data formats. We used the following standard software packages that work with FITS images to reduce and analyze our CCD data: the Image Reduction and Analysis Facility (IRAF)² for reduction of CCD data and photometry, and the Space Telescope Science Data Analysis System (STSDAS, available as an external package in IRAF) for fitting isophotes and determining galaxy brightness profiles. We employed the Faint Object Classification and Analysis System (FOCAS; Jarvis and Tyson 1981, Valdes 1982) for automatic detection, cataloging, and classification of objects as stars or galaxies. FOCAS works with an image format that can be created from FITS by IRAF. Appendix B presents some details of these packages.

CCD data processing consists of the following sequence:

1. extrication of the instrumental signatures of the telescope, filters and detector by bias-subtraction, followed by flat-fielding and cosmic-ray cleaning

²IRAF is distributed by the National Optical Astronomy Observatories, which are operated by the Association of Universities for Research in Astronomy, Inc., under cooperative agreement with the National Science Foundation.

2. registration of the individual cluster images to a common co-ordinate system - using astrometric information and then co-addition of these registered frames into deep images
3. detection of faint objects in the cluster frames and their subsequent classification as stars or galaxies employing the FOCAS package
4. object photometry and photometric calibration of the instrumental magnitudes to a standard system using standard star photometry
5. transformation of the standard magnitudes to the rest-frame of the galaxy by applying K- and evolutionary corrections.
6. derivation of color maps and surface brightness profiles of the brightest galaxies – we shall explain this in Chapter 6.

2.4.1 CCD Data Pre-Processing

From the raw image i.e., measured CCD pixel values, it is possible to derive the light distribution of the observed celestial object using:

$$(\text{object} + \text{sky}) = (\text{raw counts} - \text{bias}) / \text{flat}$$

where *bias* accounts for the additive systematics and *flat* accounts for the gain pattern of the pixels.

Bias Subtraction

Bias is measured as the counts per pixel read from the CCD for an exposure time of zero. Bias subtraction, then, involves determining the mean or median of the pixel values of a zero exposure CCD frame, and subtracting out this value from all other frames, including the flat-fields. For bias-subtraction of our CCD data, we combined typically 6–8 bias frames per night, to reduce the variations due to read-noise. For the CCDs used except during the 1999 April and 2000 February runs, we found that the bias images showed no gradient or any other non-uniformities. So, for these data sets, we bias-subtracted all frames using the median value of the bias-frame pixels (excluding the 10 edge rows and columns) as the bias value over each night. For the 1999 April and the 2000 February observations, where the bias frames showed repeatable, systematic patterns of the order of a few counts, we have subtracted the combined nightly bias frames themselves from all the other exposures.

All the CCDs we used showed very few cosmetic defects such as bad or hot pixels. We fixed the bad columns that are due to faulty registers by linear interpolation across the columns. We did not otherwise repair bad pixels or create bad pixel masks. Since we had planned our shift-and-stare observations so that such defects do not affect the observed objects, we would not be hampered by ignoring this step. Finally, the object detector and classifier routines (discussed in Sec. 2.4.3) are capable of discriminating against “noise” including bad pixels and columns, cosmic ray events, etc.

Flat-Fielding

In order to remove the pixel-to-pixel sensitivity variations, we performed flat-fielding. We median-combined the twilight flat-field frames within each filter. Prior to combining them, we scaled the individual frames by the mode of their pixel values to take into account the differences in signal-to-noise ratios. We found that the combined frames were clear of stars but retained the vignetting pattern. Then, we normalized the combined frames by the mean of the values in the unvignetted area of the flats to derive the final, master flat in each filter. We flat-fielded every bias-subtracted object frame using the master flat in the corresponding filter. Flat-fielding successfully removed the vignetting pattern to a large extent. The processed frames were fairly uniform, with residual sky-background inhomogeneities of $< 0.5\%$ over the full extent of each frame.

Cosmic-Ray Cleaning

We normally see about 10 cosmic ray events per minute registered on the CCD, and limited in size to 2–3 pixels. Where multiple exposures of the same object were available, we used the median filtering algorithm to reject these deviant measurements. In the cases where only single images were available (and while performing standard star photometry) we used tasks within IRAF to clean cosmic rays.

2.4.2 Image Registration and Co-Addition

We observed the poor clusters over a period of 4-5 years. For a given cluster, the galaxies in the different exposures will not be recorded on the same pixel because of the shift-and-stare technique of observation, as well as due to the small changes in the CCD Dewar orientation. So, the stack of such shifted images ought to be aligned before being combined into deeper images with better signal-to-noise ratios.

We registered the images for a given cluster field by identifying approximately 20 unsaturated stars (detectable in all four passbands and over a majority of the different nights) to be used as astrometric reference points. To improve the accuracy with which centroids of the stars can be computed, we first magnified all the images by a factor of two in both the x and y axes using a bicubic natural spline interpolator. We used the flux conserving option in the magnification process, since we are interested in performing photometry on the resulting registered images. As the stellar profiles are well sampled, there is no degradation of the image during the interpolation to the larger image.

We needed to relate positions of the stars on the images to their positions on the real sky, and set the relationship between pixel coordinates and sky coordinates i.e. the world coordinate system in the image headers. For the unsaturated stars, we identified the celestial co-ordinates (Right Ascension and Declination in J2000 equinox) from the US Naval Observatory's Precision Measuring Machine (PMM) Project database³. The PMM positions have relative accuracies of 0.1 arcsec and include stars from the Tycho astrometric catalog. We derived the centroids of the reference stars, then matched the celestial and pixel coordinates. Subsequently we computed the absolute astrometric solutions and updated the world coordinate system (WCS) header information for all the images.

³The USNO PMM database is online at <http://ftp.nofs.navy.mil/projects/pmm/index.html>.

We then estimated the sky of the individual images as the mode of the pixel values in annuli around 15–20 isolated stars, and subtracted this value from the images. The objects occupied less than half the area of the CCD, and we measured no systematic difference in the sky counts among the different regions of the CCD. Even if residual gradients exist, the FOCAS package is capable of handling these.

Next we created an artificial image whose dimensions were roughly as large as the combined area covered by all the cluster images, and assigned it a WCS centered on the brightest cluster galaxy optical position. We then computed the mean X and Y offsets and rotation of the reference stars of every frame relative to their locations in the fiducial image and averaged these to define the final values. Next, we geometrically remapped all image data for the cluster to match the fiducial coordinate system using a flux-conserving Lagrangian interpolation scheme to achieve registration at the subpixel level. Typical alignment accuracies in our equatorial coordinates are about 0.3 arcsec and at worst 0.6 arcsec. (This compares favorably with the CCD pixel scale of 0.61 arcsec.)

Once all frames of a given cluster were registered to a common coordinate system, we co-added the best independent exposures in each passband to produce four “deep” BVRI images. Generally, we made an effort to combine images only if the seeing was better than 2.5 arcsec, the signal-to-noise ratios similar, and if the number of common objects was at least 50%. Prior to combining, we scaled the individual images such that several of the stars common to them had the same counts within one FWHM. During the combining operation, we weighted the images by their exposure time. We further co-added these deep images to create an enlarged mosaic image of each cluster.

To restore the co-added images to their original scale, we then block summed them over two columns and lines. These final images served as the master frames that we would use for object detection. The mosaics improved upon the areal coverage of the single CCD field of view by about 2 arcmin for each cluster. There was no loss of resolution due to the combining operation. However, we sometimes noticed that certain parts of the mosaic which were formed by the combination of the fewest number of images did expectedly show sky noise of higher sigma than the rest of the frame. While this does affect the object detection limits using FOCAS, it is the trade-off for having a larger field of view. Occasionally, we had to edit the images to remove artefacts created by the interpolation and combining schemes near the constituent image borders.

2.4.3 Object Detection and Classification

Having reduced, aligned and combined the images of each cluster, we next had to assemble catalogs of the faint objects in the co-added images and extract object parameters such as positions, magnitudes, sizes and shapes. For this purpose, we used the FOCAS package, an automated detector and classifier, designed to work with objects in digital astronomical images. Since this is a crucial aspect of our analysis and was easily the most time-consuming, we shall devote considerable space to its description.

Object Detection

FOCAS assembles a catalog of faint objects in an image by searching for a minimum number of

contiguous pixels that are some sigma above the local sky background which it first determines from the image. An efficient scheme for object detections should extract the extended galaxies as well as the point-like stars, should not be prone to spurious detections, and ought to be free from major biases due to image scale or seeing. FOCAS requires input of three parameters that can be configured for optimal detection. We tuned these parameters in the following manner:

1. pixel detection threshold sigma = $4.5\text{--}5 \times$ the local sky noise
2. minimum pixel area or object size = $0.9 \times (\text{FWHM})^2$
3. spatial convolving filter = the FOCAS “built-in” filter

1. To detect the faintest and very low surface brightness objects, one may lower the threshold of detection, but at the cost of rising contamination by spurious objects, most of which will be the faintest objects in the catalog. FOCAS determines the background and its sigma by examining the first few lines of the image; it sets the sigma — and the associated detection value of some constant number of sigmas above the local sky — to be constant throughout the image though the background level may vary. As we were working with co-added BVRI images (composed of unequal numbers of individual frames of various filters), we had to experiment with a range of thresholds — in combination with the other two search parameters — for each cluster mosaic. In all cases, we managed best with thresholds of 4.5–5 times the local sky (rms) noise. We also detected objects 5 sigma below the background to remove dead pixels and other such holes in the CCD. The thresholds are deliberately conservative. We note here that the sigma of the sky background in the mosaicked images was not quite constant, and depended inversely on the number of individual frames that had gone into making the region of the mosaic. This means that the detection sensitivity is not entirely uniform over the field. However, within a 7 arcmin \times 7 arcmin area around the brightest cluster member, the variation in sigma was always within 1%, so this area is fairly completely detected.

2. The second detection parameter — the minimum number of pixels — is crucial for minimizing the number of false detections. Our choice was directed by the expected size of the cluster galaxies and the image seeing. A canonical galaxy size of 10 kpc projects angular diameters of about 7 arcsec and 3 arcsec for redshifts $z=0.075$ and $z=0.25$ respectively (as shown in Appendix A). Our image seeing was at best 1.5 arcsec in the mosaicked images, so the galaxies smaller than 10 kpc would be practically point-like. So, rather than fix an arbitrary constant detection area, we opted to fix the minimum object size to 0.8 times the area within the half-light radius of the image point spread function (PSF). For a 2-D Gaussian PSF, this translates to $0.9 \times (\text{FWHM})^2$; in our images $A_{\min} \approx 15$ pixels typically.

3. To assist the revealing of very faint objects which may be only a few percent of the sky intensity, FOCAS convolves the image with a 2-D weighting function, the detection filter, that assigns a value to a pixel by weighing it with its neighbors. If this spatial convolution filter has a profile similar to the object, then it maximizes the signal-to-noise ratio of the object detection. Obviously it is not possible to determine *à priori* the profiles of the galaxies to be detected! On account of this and the expectation that a large number of galaxies will be barely resolved in our

images, we have opted for the FOCAS “built-in” filter. This 5×5 grid is symmetric, as given below:

```

0 1 2 1 0
1 2 3 2 1
2 3 4 3 2
1 2 3 2 1
0 1 2 1 0

```

The efficacy of the filter depends on the PSF, which can create systematics in the number of galaxies detected.

The combination of threshold sigma, the minimum size, and detection filter determines the limits of the detection algorithm. Running the detector on the image produces a catalog that contains some minimal information about the objects in the field. Further steps evaluate more carefully the sky background, photometric data including three kinds of magnitudes (aperture, isophotal and total), radial moments and shape parameters such as ellipticity and position angle of the objects. Here the total magnitude is the flux within an area twice as large as that enclosed by the detection isophote. Subsequent steps involve the splitting of objects with merged isophotes, by progressively raising the detection isophote to see if the object splits into multiple components each of which satisfies the minimum area criterion to be declared a new object.

After putting our mosaic images through this sequence, we reviewed each resultant catalog by eye. We noted that the detector ran into problems in the following cases:

- near very bright stars, where it detects many spurious objects in the halos
- in picking out the tenuous, extended halos of the brightest cluster members
- in splitting objects: some FOCAS fails to split, some it fails to consolidate into larger objects.

We reviewed the catalogs by eye to verify the authenticity of objects. In all trouble spots such as those listed above, we edited the catalog to remove spurious objects near the bright objects, deleted erroneous splits, and restored some components into larger, composite objects. Of course, removal by hand of suspected objects in stellar halos may have the unwelcome side-effect of deletion of real, faint objects.

We will discuss in the forthcoming section the completeness of detection, in various passbands separately for each cluster. We would like to mention here that running the object detection algorithm on the deep mosaic makes it unnecessary to match catalogs from multiple passbands each with different detection isophotes, and consequently unequal incompleteness and contamination levels. Further, objects may be entirely undetected in a particular filter depending on their colors, or may be split into multiple objects; thus the deep image allows detection of objects with unusual colors. *We constructed the final catalog of faint objects with those that could be detected and photometered in at least two individual images among the four different filters.*

Though we detect objects in one combined image only, we measure their structural and photometric properties and classify them on the images combined *separately* in each passband. While measuring object magnitudes, FOCAS estimates the local sky using the mean of the background counts. But the mean can be raised due to faint objects in the sky aperture. Therefore, it is essential to correct for this error. One way to evaluate the bias is by the difference between the mode and the mean of the sky counts; the corrected sky is then the first estimate minus the bias.

Star-Galaxy Classification

The next step in cataloging the objects is to distinguish them into stars and galaxies. We classified objects with the standard FOCAS method and its built-in parameters, using the resolution classifier algorithm described in Valdes (1982b). We remind the reader that we performed the following analysis on a frame-by-frame basis, on not only the mosaic but also the combined images within individual filters. First, we determined the PSF in each image from a manually selected set of isolated, unsaturated stars. To assure ourselves that the PSF is not inappropriate, we inspected the PSF visually and compared it quickly with the compact, symmetric objects on the image. From this PSF, FOCAS creates a general template that is basically a scaled PSF with a second component that is narrower or broader. Two parameters describe the template:

1. *frac*, the fractional ratio between the stellar PSF and the second component and
2. *scale*, the scale difference of the second component.

Then, we used the FOCAS resolution classifier to find the *scale* and *frac* of the template that fits best the two-dimensional object image. We classified objects into “stars”, “galaxies”, “fuzzy stars” or “noise” in the three-dimensional parameter space of magnitude, *scale* and *frac*.

After running the classifier on the various combined images available for each cluster, we assigned a class to an object if it was classified by FOCAS as being of the same class in at least 50% of the images, and in at least 2 different filters. Therefore, the assignment of the class is unlikely to be dominated by the color of the object. We manually edited the catalog to put in the final object classification. We decided to include the (rare) “fuzzy stars” in our galaxy list to avoid missing objects which may show an active nucleus superimposed on an extended galactic host, or intervening galaxy.

As we mentioned in the previous section, we have checked by eye the authenticity of the detected objects. Likewise, we paid particular attention to manually checking object classification, which is increasingly unreliable at the faintest magnitudes. Here, though, we were helped by having multiple images to create several independent classifications for comparison. While visual inspection is definitely laborious and itself not entirely error-free, it is nonetheless a valuable step in faint object analysis. Through this procedure, we also made crude morphological classifications of the brighter few galaxies, into spheroid-like or disk-like.

2.4.4 Optical Photometry

We use aperture photometry of the galaxies in the poor clusters in the following chapters. We convert the CCD counts (in ADUs) registered by an object in a particular aperture to its instru-

mental magnitude, i.e., in terms of the actual photons received from it, using:

$$m = -2.5 \log_{10}(\text{counts in ADU/second}) + 25.$$

We performed aperture photometry of all objects (whose CCD pixel positions were derived by FOCAS) with the IRAF PHOT task, applying a centroiding algorithm to determine the position of the aperture center more accurately. We used a 3 arcsec radius circular aperture for the photometry, and a sky annulus ~ 5 arcsec wide and ~ 9 arcsec away. The 3 arcsec aperture was the best compromise between enclosing all the light from the object and minimizing errors due to varying focus, seeing or sky.

We then applied aperture corrections to correct the magnitudes measured within the 3 arcsec aperture to the 6.6 arcsec radius within which we computed the standard star magnitudes. We estimated the aperture corrections using nearly a dozen bright, isolated stars in the particular images.

We chose to transform our instrumental magnitudes to the standard Johnson-Morgan BV and Kron-Cousins $R_c I_c$ broadband systems, using the old Galactic cluster M67 for which many studies are available. We used standard stars from Selected Areas of Landolt (1992) for nightly zero-point calibrations of our observations. M67 (NGC 2682) is especially useful for standardization of CCD photometry since it has stars of a wide range in brightness and $(B - V)$ color index (-0.1 to $+1.3$) within a reasonably small area. It is most conveniently located for observers at the VBO, who benefit from its accessibility during the good observing season. Most of the calibrator stars we used are in the "Dipper Asterism" region in M67. We have used various sources (Eggen & Sandage 1964, Joner & Taylor 1990 and the unpublished updates of A. Porter) to compare our magnitudes with the standard ones. We reduced the standard star images in the normal manner for CCD images, with the same bias and flat-fields used for the galaxy cluster images. We derived instrumental magnitudes using circular apertures of radius 6.6 arcsec, with sky parameters being the same as used for the science images.

To determine the transformation co-efficients from our instrumental magnitudes to the standard system, we use the following equations:

$$\begin{aligned} (B - V) &= \alpha_{(b-v)} + \beta_{(b-v)}(b - v) \\ (V - R) &= \alpha_{(v-r)} + \beta_{(v-r)}(v - r) \\ (V - I) &= \alpha_{(v-i)} + \beta_{(v-i)}(v - i) \\ (R - I) &= \alpha_{(r-i)} + \beta_{(r-i)}(r - i) \\ (V - v) &= \alpha_{bv} + \beta_{bv}(B - V)_i \\ &= \alpha_{vr} + \beta_{vr}(V - R)_i \end{aligned}$$

where the capital letters denote magnitudes on the standard system, the small letters instrumental magnitudes and the subscripts "i" denote our "standardised" color indices.

In Table 2.6 we list the coefficients α and β and their standard deviations, derived from linear Chi-squares fits to the M67 data over the observing period. We see that the formal errors associated with the photometric transformation parameters are a few percent at most. At $V = 20$ mag,

Is this good enough?

we find that the total uncertainty in photometric calibration is about 0.07 mag. We made an independent check of the reliability of our photometry by matching our stellar locus with values for stellar colors from the literature. Though the match was not exact, it was within about 5%, which is satisfactory.

2.4.5 Galactic Extinction Correction

We used the values from the NASA/IPAC Extragalactic Database (NED) based on B-band extinctions derived by Schlegel et al. (1998) and converted to other bands assuming $R_V = 3.1$ according to the prescriptions in Cardelli et al. (1989). We list the computed extinction corrections in Table 2.5.

Table 2.5: Galactic extinction corrections

EMSS Cluster	b	A_B	A_V	A_R	A_I
MS 0002.8+1556	-45.23	–	0.16	0.13	–
MS 0301.7+1516	-36.56	0.72	0.55	0.45	0.33
MS 0735.6+7421	+29.44	0.10	0.08	0.06	0.04
MS 1306.7-0121	+60.93	0.12	0.09	0.08	0.06

Though the cluster MS0301 is at high Galactic latitude ($|b| > 35$ deg), the extinction towards it is anomalously high due to a “spur” of Galactic clouds along this longitude. The canonical value of $R_V = 3.1$ is probably not valid for this region, but lacking independent estimation of R_V , we continue to use it. For the other three clusters, the extinction correction is about 1.5 – 2 times the photometric errors at $V = 20$ mag.

2.5 Cluster Galaxy Catalogs

This section describes details of the object catalogs, and estimations of their completeness, efficiency of the star–galaxy discrimination and its associated errors.

Cluster	CCD area (arcmin ²)	Galaxies	Stars	Isophote (V mag arcsec ⁻²)
MS 0002.8+1556	10.2×10.2	361	183	26.5
MS 0301.7+1516	13.4×10.7	231	164	25.6
MS 0735.6+7421	10.2×9.3	242	177	26.1
MS 1306.7-0121	12.1×11.6	271	220	25.7

Table 2.6: Number of objects detected by FOCAS in each cluster image and their classification. The columns are: (1) cluster name, (2) area of the sky covered by the CCD image, (3) number classified as galaxies including “fuzzy” stars and (4) as stars. Note that the photometric depths are different in the different images, as is the completeness of detection.

Table 2.6 lists the number of detected objects, the break-up into stars, galaxies and other extended objects, and the detection threshold in mag arcsec⁻².

2.5.1 Individual Cluster Catalogs

Appendix A provides the photometric catalog of galaxies only. The columns are the position (right ascension and declination in J2000.0 co-ordinates), V magnitude, $(B - V)$, $(V - R)$ and $(R - I)$ colors in 6.6 arcsec apertures and corrected for Galactic extinction. As mentioned before, for objects in the line-of-sight of the cluster MS0002, we provide only V magnitudes and $(B - V)$ colors since we do not have usable I -band images of the cluster, and photometric calibrations in B are not reliable.

2.5.2 Completeness and Misclassifications

We need to estimate the object detection efficiency of FOCAS, i.e., the percent of all objects in an image that FOCAS catalogs. We also need to understand how well FOCAS classifies objects, or how often stellar objects are misclassified as nonstellar, and vice versa.

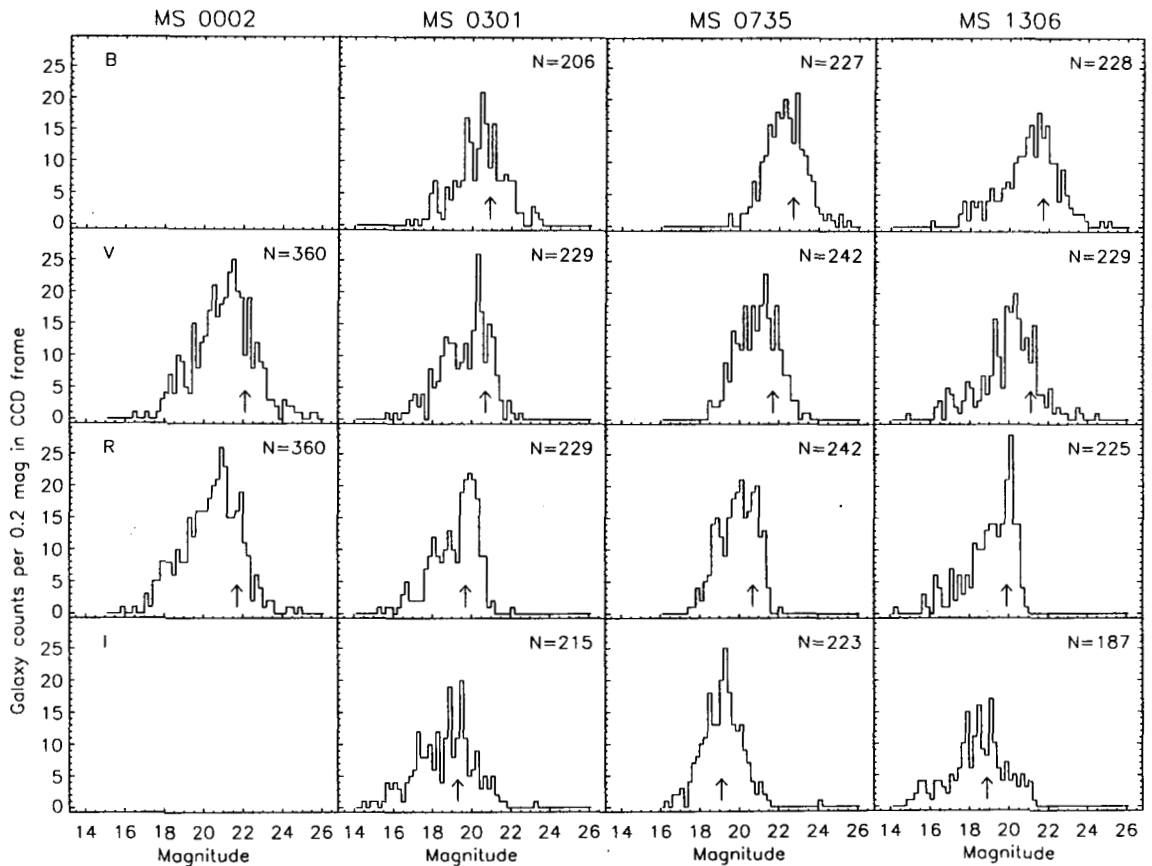


Figure 2.1: Galaxy counts in the CCD frames centered on the BCMS.

In the literature, there are different methods of determining the completeness of detection and reliability of classification of faint objects. These include addition of accurately simulated objects of known range of magnitude and morphology to the observed images, and creation of artificial data matching the real data. One processes these images in a manner similar to the original images, produces the catalog of objects, and then compares the output catalog with the input catalogs of

which is the second strategy?!

the artificial stars and galaxies. Then, it is straightforward to estimate the completeness and classification reliability of the software. However, the varying PSF among many of our CCD frames makes it difficult to accurately add similar artificial objects. Similarly, it is not straightforward to use entirely artificial data, since their parameters may not be matched exactly with our real data. A (third) strategy is to use the differential luminosity function of galaxies. Now, field galaxy counts in the literature (e.g., Tyson 1988) show monotonic increase (with steeper slopes in bluer bands) and appear to saturate at only $\approx B = 27$ mag. Therefore, a maxima in the histogram before such photometric depth implies the onset of statistical incompleteness in our sample.

We plot the frequency distribution of the galaxy number count within apparent magnitude bins of 0.2 mag, in Fig. 2.1. The relative number of objects rises linearly, until a turnover occurs between $V = 21.5$ and $V = 22.5$. We take the completeness limit (small arrows in the figures) of our data at 0.2 mag brighter than the peak of each histogram. These set the depth of our galaxy samples for further analysis.

Here we must bear in mind that object detection depends on seeing — if poor seeing blurs an extended object, its outer (very faint) isophotes would fall below the surface brightness threshold cutoff, rendering the object fainter and smaller, thus more difficult to detect (and more prone to misclassification as a star). We have attempted to avoid this problem by using only those images where the stellar profiles have full-width-at-half-maximum of < 2 arcsec (see also below). Crowding of objects is another pitfall; however, our poor clusters are not crowded fields (by their very nature). They are also at high Galactic latitude where stellar densities are not large. Therefore, crowding hardly contributes to uncertainties in completeness.

The assignment of stellar/non-stellar class to a detected object was on the basis of its receiving the same classification in at least 50% of the images in the different filters. The internal accuracy of the classifier — tested by comparing object classification in the multiple images — is rather dependent on the faintness of the object and on image seeing. Poor seeing will of course degrade the smaller extended objects into unresolved sources.

As Fig. 2.2 shows, in a plot of the logarithm of object area against the (extinction-corrected) V magnitude, stars and extended objects occupy two separate loci. Clearly, and expectedly, the apparent areas (radii) of bright galaxies are systematically larger than those of stars at the same apparent magnitude, while faint galaxies merge with stars. In fact, for seeing greater than the typical scale sizes of the objects, it is possible that objects of differing magnitudes would be smoothed to a similar size comparable to the seeing disk. The threshold of discrimination, which therefore depends crucially on the observed size of the objects, is roughly $V = 19.5$ after which the distinction is blurred. This magnitude expectedly corresponds to an object area of radius about the seeing disk.

However, FOCAS uses several parameters for bifurcation of objects (more than merely the locus in the area vs. magnitude) simultaneously (Valdes 1988), so Fig. 2.2 is merely an indication of the trend of the reliability of the classifier. For the brightest objects ($14 < m_V < 17$), there is virtual unanimity in the FOCAS classifications in the images in different filters. At $V \approx 20$ mag ($R \approx 19$ mag), where the surface number density of stars and galaxies are comparable, the fraction of objects that received conflicting classifications is $\sim 10\%$; this rises disappointingly to $\sim 30\%$

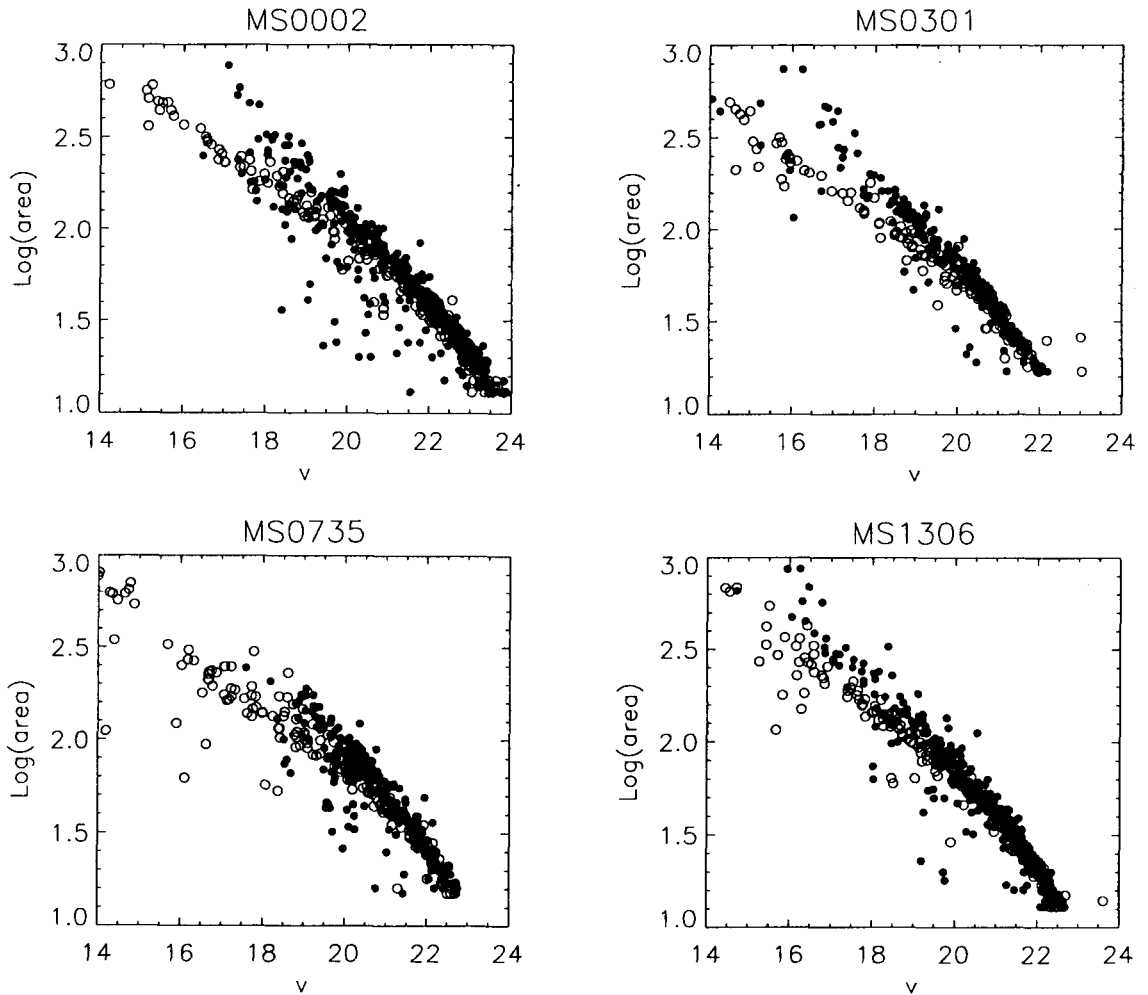


Figure 2.2: Star–galaxy separation plots for the EMSS poor cluster images. Stellar (open circles) and non-stellar objects (filled circles) occupy separate regions in the plot of logarithm of area vs. m_V , with stars having higher surface brightness than extended objects.

about 3 magnitudes fainter. Sometimes, FOCAS classified closely paired objects as galaxies; visual inspection usually clarified such discrepancies. In particular, visual inspection and object colors show that some 10% of galaxies fainter than 21.5 mag (close to the completeness limit) could be misclassified as stellar objects, while some stellar objects could well be QSOs. Adding the relevant contributions due to misclassification to the galaxy counts changes the overall faint number counts non-negligibly but without seriously improving the completeness levels. In fact, due to the relatively shallow number counts of stars (Bahcall & Soneira 1981) versus galaxies (e.g., Tyson 1988), the fractional stellar contamination actually decreases with increasing magnitude as shown in Fig. 2.3.

We have previously (Sec. 2.2.4) used the APS database for preliminary estimates of the richness of our sample clusters. We use the same as an external check of the reliability of our object classification. The APS star–galaxy discrimination is based on an automatic neural-network algorithm (Odewahn 1995), and is reliable to fainter than 20 mag. We find that, for all the clusters except MS0735 for which we could not access the APS database, there is agreement to

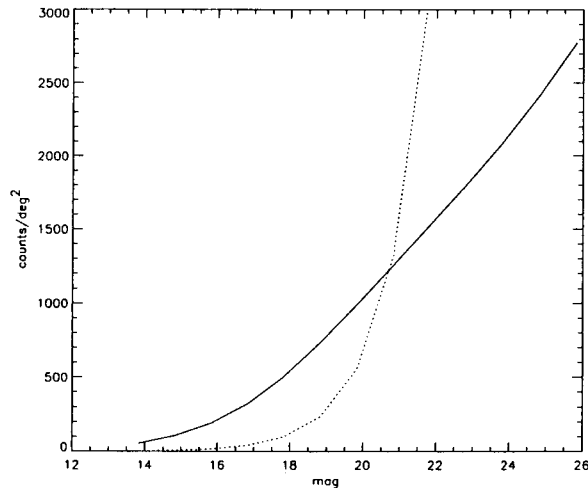


Figure 2.3: Number counts of stars and galaxies in the field of MS1306. The solid line is the prediction of the Bahcall & Soneira (1981) model of Galactic star counts, and the dotted line is the empirical ‘field galaxy’ count of Wilson et al. (1997), both in the V band. Notice that by $V \approx 20$ mag, galaxies begin to dominate over stars.

better than 92% between the classes assigned by FOCAS and the APS classifier. There were conflicting classifications usually for close pairs of objects or for those close to the CCD borders. In such cases, we re-examined our classification visually, and found that fewer than two objects needed to be reclassified in our catalogs.

We conclude that our detection algorithm and photometry are, within errors of $< 10\%$, complete to about $V = 21$ mag and our star–galaxy separation does not significantly contaminate the galaxy catalogs with stellar objects.

2.6 Discussion and Summary

We construct our sample of moderate-redshift ($0.08 < z < 0.25$) poor clusters from the X-ray selected EMSS cluster catalog of Gioia & Luppino (1994; GL94). These objects emit X-ray luminosities $L_X \geq 3 \times 10^{43} \text{ergs}^{-1}$, have their X-ray centroid optically identified with galaxy over-densities and are noted by GL94 as being optically poor. Our preliminary richness estimates indicate that these clusters would be similar to Abell clusters of richness class 0 or 1. We acquired optical CCD images of four poor clusters, and after pre-processing the data, detected the faint objects in the fields and separated them into stars and extended objects. We performed aperture photometry (corrected to ≈ 7 arcsec) transformed to the standard Johnson–Cousins’ B, V, R and I bandpasses. The galaxy catalogs are complete to about $V = 21$ mag, or $\approx M_V = -18$ in the rest-frame of the different clusters.

The literature does not contain redshifts for any but the brightest cluster galaxy in these fields. Therefore, we do not have any dynamical estimates of the clusters *a priori*. Nevertheless, from the empirical correlation between the cluster X-ray luminosity L_x and velocity dispersion σ_v (e.g., Edge & Stewart 1991; White et al. 1997), we may estimate the latter dynamical quantity. We

use the White et al. (1997) correlation: $\sigma_v = 6.97 \pm 0.19 L_{X;Einstein}^{0.15 \pm 0.01}$, to derive the cluster velocity dispersions of 580 km s^{-1} (for MS0301), 750 km s^{-1} (for MS1306 and MS0002), and 900 km s^{-1} (for MS0735).

In the chapters to follow, we shall study the statistical properties of the galaxies in the poor clusters, as well as the structure of the brightest galaxy in them.

Table 2.7: Coefficients of the photometric transformation equations 2.1.

Date	Setup	Index	α	stddev $_{\alpha}$	β	stddev $_{\beta}$
1996 March 11	CCD#1 Filters#1	$(B - V)$	0.821	0.003	1.461	0.015
		$(V - I_c)$	0.856	0.002	1.011	0.004
		$V_{(B-v)}$	-0.310	0.008	0.020	0.011
		$V_{(V-I)}$	-0.313	0.008	0.022	0.011
1996 April 22	CCD#1 Filters#1	$(B - V)$	0.892	0.008	1.439	0.025
		$(V - R_c)$	-0.122	0.006	0.996	0.015
		$V_{(B-v)}$	-1.589	0.009	0.024	0.014
		$V_{(V-R)}$	-1.592	0.010	0.048	0.028
1996 AVERAGE	CCD#1 Filters#1	$(B - V)$			1.439	0.025
		$V_{(B-v)}$			0.022	0.011
1997 March 07	CCD#2 Filters#2	$(B - V)$	-1.252	0.022	0.988	0.011
		$(V - R_c)$	-0.252	0.011	0.950	0.017
		$(V - I_c)$	-0.104	0.032	0.973	0.038
		$V_{(B-v)}$	-4.059	0.017	0.059	0.026
		$V_{(V-R)}$	-4.083	0.027	0.162	0.073
1997 March 08	CCD#2 Filters#2	$(B - V)$	-1.415	0.023	1.052	0.012
		$(V - R_c)$	-0.335	0.010	1.000	0.014
		$(R_c - I_c)$	0.134	0.005	1.003	0.016
		$(V - I_c)$	-0.223	0.013	1.025	0.013
		$V_{(B-v)}$	-4.047	0.028	0.015	0.030
		$V_{(V-R)}$	-4.062	0.015	0.032	0.015
1997 AVERAGE	CCD#2 Filters#2	$(B - V)$			1.020	0.012
		$(V - R_c)$			0.975	0.016
		$(V - I_c)$			1.000	0.020
		$V_{(B-v)}$			0.037	0.030
		$V_{(V-R)}$			0.097	0.070
1997 April 06	CCD#2 Filters#3	$(B - V)$	-1.268	0.007	0.976	0.004
		$(V - R_c)$	-0.529	0.011	1.080	0.013
		$V_{(B-v)}$	-4.354	0.007	0.071	0.009
		$V_{(V-R)}$	-4.373	0.009	0.182	0.022
1998 April 01	CCD#2 Filters#3	$(B - V)$	-0.330	0.005	0.967	0.005
		$(V - R_c)$	-0.960	0.022	1.081	0.019
		$(R_c - I_c)$	0.065	0.012	0.989	0.036
		$(V - I_c)$	-1.032	0.067	1.163	0.043
		$V_{(B-v)}$	-4.708	0.006	0.043	0.008
		$V_{(V-R)}$	-4.715	0.019	0.049	0.024
1999 April 11	CCD#3 Filters#3	$(B - V)$	-1.284	0.001	1.016	0.009
		$(V - R_c)$	-0.351	0.001	1.022	0.006
		$(R_c - I_c)$	0.124	0.002	0.893	0.005
		$(V - I_c)$	-0.205	0.002	0.957	0.010
		$V_{(B-v)}$	-3.312	0.018	0.073	0.042
		$V_{(V-R)}$	-3.309	0.016	0.036	0.020
2000 February 01	CCD#2 Filters#3	$(B - V)$	-1.318	0.030	0.999	0.014
		$(V - R_c)$	-0.514	0.016	1.045	0.017
		$(R_c - I_c)$	0.011	0.004	0.974	0.009
		$(V - I_c)$	-0.547	0.015	1.048	0.011
		$V_{(B-v)}$	-4.037	0.036	0.024	0.040
		$V_{(V-R)}$	-4.036	0.040	0.043	0.090
2000 March 03	CCD#2 Filters#3	$(B - V)$	-1.246	0.012	0.975	0.05
		$(V - R_c)$	-0.531	0.017	1.043	0.012
		$(R_c - I_c)$	-0.030	0.008	0.951	0.011
		$(V - I_c)$	-0.620	0.019	1.060	0.014
		$V_{(B-v)}$	-4.140	0.009	0.086	0.010

Table 2.8: The journal of cluster observations. The table shows the cluster name, filter, date, exposure time in seconds, and airmass.

Object	Filter	Date	Exposure (sec)	Airmass	
MS0002	V	1997 Oct 05	600	1.24	
			600	1.18	
			600	1.14	
			720	1.11	
			600	1.05	
	R	1997 Oct 05	600	1.04	
			600	1.04	
			600	1.06	
			600	1.08	
MS0301	B	1995 Dec 19	2700	1.05	
		2000 Feb 01	1800	1.07	
	V	1997 Oct 05	600	1.01	
		1998 Jan 22	600	1.04	
			600	1.06	
			600	1.08	
		1998 Dec 21	600	1.11	
			600	1.03	
			600	1.04	
	R	1995 Dec 19	1800	1.02	
		1997 Oct 05	600	1.01	
			600	1.02	
			600	1.03	
		1998 Jan 22	600	1.00	
			600	1.01	
			600	1.02	
	I	1995 Dec 19	1800	1.06	
	MS0735	B	2000 Jan 08	720	2.15
				720	2.13
900				2.12	
900				2.11	
900				2.11	
V		1997 Mar 07	1200	2.13	
			1200	2.18	
			1500	2.24	
R		1997 Mar 07	1200	2.34	
		1997 Mar 08	1200	2.11	
			1200	2.11	
I		1997 Mar 08	1200	2.12	
			1200	2.16	
			1200	2.21	
			1200	2.27	
MS1306	B	1996 Feb 16	2700	1.04	
	V	1996 Feb 16	2700	1.04	
	R	1996 Feb 16	900	1.03	
		1996 Feb 17	1800	1.03	
		1996 Apr 22	1200	1.13	
			900	1.22	
		1997 Apr 07	900	1.04	
			900	1.05	
		2000 Mar 05	900	1.20	
	I	1996 Feb 17	1800	1.04	

Chapter 3

Galaxy Luminosity Functions

The universe is wider than our views of it.

– Henry David Thoreau

3.1 Avant-Propos

Galaxies span more than six orders of magnitudes in their luminosity. The relative abundance distribution of galaxies within a given volume according to their brightness, termed the *luminosity function* (LF), stands in for the distribution of galaxy masses, and is thus a fundamental measure in extra-galactic astronomy and cosmology. The LF is important in understanding the global properties of galaxies, their formation, and evolution (see review by Binggeli, Sandage, & Tammann 1988, hereafter BST88). In optical bands,¹ the Schechter (1976) function provides a convenient analytic approximation to the (volume-limited) galaxy LF, $\phi(L)$. This is a combination of a power-law and an exponential function, parametrized as:

$$\phi(L) = \phi^* e^{-(L/L^*)} (L/L^*)^\alpha, \quad (3.1)$$

where L^* is a characteristic luminosity defining the transition or “break” between the exponential fall-off at bright luminosities and the power law of slope α at the faint end, and ϕ^* provides the overall normalization of the LF. Galaxies with luminosities $L > L^*$ are rare and have low space density. The power-law dependence with exponent α provides a galaxy dwarf-to-giant ratio, and determines the amount of mass in galaxies of low luminosity and mass. The integral of the LF, $\phi(L)$ over all luminosities is the (comoving) space density of galaxies. For “standard candles” the LF is simply $\phi(L) = \phi^* \delta(L - L_0)$. ?

The LF is a reflection of galaxy formation since galaxies are luminous tracers of the spectrum of the primordial density fluctuations. The evolution of galaxies in luminosity and number density — which then has an impact on the LF — occurs through both internal phenomena such as star formation and energy input from supernovae, and external i.e., environment-related, processes.

If the primeval galaxy mass function is a universal constant, and galaxies are outside the influence of their surroundings, and every subsequent evolutionary process retains the initial mass-to-light ratio, then it is not unreasonable to expect a “universal” present-day LF (e.g., Schechter 1976; Colless 1989). Few — if any — galaxies are isolated entities (see Sec. 1.1), so their properties including luminosity are subject to environmental effects and modifications throughout their

¹The literature contains estimations of the differential number distribution of galaxies over luminosities over virtually the entire spectrum, including the optical, far infra-red (Sanders & Mirabel 1996), radio continuum (e.g., Gavazzi & Contursi 1994). and neutral hydrogen (e.g., Schneider 1996).

lifetime. An important question in this context is whether it is the early environment (i.e., conditions at formation) or the current/recent environment (i.e., later influences) that plays the major role in determining galaxy luminosities and luminosity distributions, and to what extent. If it is only the early environment that matters, i.e., if the post-collapse dynamical mechanisms are not important in local clusters, i.e., if the LF is determined early in the cluster history, then there ought to be no strong correlation between the LF and dynamical properties of the cluster.

Most theories of cosmogony predict two distinct classes of galaxies: normal, bright galaxies and faint, diffuse dwarfs. The dwarf galaxies that populate the faint-end of the LF may be distinct from the set of giant galaxies in terms of scaling laws, dark matter content, and formation (Ferguson & Binggeli 1994). The standard model of biased galaxy formation (e.g., White et al. 1987) theorizes that (1) clusters of galaxies should be populated predominantly by bright galaxies, (2) the dwarf-to-giant ratio should be larger in the field than in clusters, flattening the cluster galaxy LF, and (3) cluster LF shapes should be correlated with their richness. Further, the “biased” giant galaxies concentrate toward the dense cluster cores while the fainter ones should preferentially occupy the sparse halos, thereby making the LF change with the cluster area surveyed.

The environmental mechanisms that alter galaxy luminosities post-collapse (see Sec. 1.2.2 for a general description of the usual suspects) have different relative influences on different parts of the LF. At the bright end of the LF, merging of the individuals into a more massive galaxy leads to a decrease in the normalization of ϕ^* ; most merger remnants have heightened luminosity for a few million years due to triggered star formation or even starburst, which brightens L^* . Tidal stripping due to galaxy-galaxy interactions or by the cluster tidal field, and ram-pressure stripping by the intracluster medium cause galaxies to become fainter. Since tidal stripping is more pronounced for brighter galaxies than for the less luminous ones, and increases with galaxy density, L^* should become fainter for denser clusters. Ram-pressure stripping is greatest for galaxies in the highest X-ray luminosity clusters, dominates at the cluster core, and is larger for galaxies on high-velocity (radial) orbits. This leads to a correlation of L^* with X-ray luminosity. Dynamical friction, whose timescale inversely proportional to galaxy mass and background medium density, applies brakes preferentially on the motion of the more massive galaxies that would merge into more massive conjugates. If luminosity is correlated with mass then this would result in fewer bright galaxies than faint ones, leading to fainter L^* in the more dynamically evolved clusters.

Dynamical friction, mergers, and tidal stripping together give rise to galactic cannibalism whose end product is an extremely luminous first-ranked galaxy along with a deficit of normal bright galaxies. As the cluster evolves, cannibalism results in the BCM (cD galaxy) growing in size and luminosity to populate the bright extremum of the LF, enlarging the deficit of bright galaxies and reducing M^* . Therefore, the contrast of the brightest cluster galaxies relative to the other bright galaxies (such as the second-ranked object) would correlate with the cluster dynamical state. The distribution of the average magnitudes of the first-ranked galaxies (0.5 mag brighter than those of the brightest normal galaxies) and its small dispersion support a scenario in which BCMs are a class of atypical galaxies created by “special” processes, and implies that BCMs cannot all be the statistical tail end of the bright-end of the (Schechter) luminosity function (Sandage 1976; Bhavsar 1989 and references therein). The deviation of the cD galaxies from the general LF is a

combination of formation mechanisms and late evolution.

Strong interactions can also lead to the creation of galaxies such as the faint tidal dwarf galaxies (with a median luminosity of $M_B = -14.2$; Duc & Mirabel 1998). Within small aggregates of low velocity dispersion, dwarf companions or satellites may coalesce with the bright parent galaxies, decreasing the faint-end contribution. Tidal stripping and galaxy harassment (Moore et al. 1996) tend to destroy the low-density faint galaxies. Infall of galaxies into clusters (e.g., some Virgo cluster spirals could have been accreted recently; Huchra 1985) would further alter the shape of the galaxy LF over the lifetime of the cluster.

Moreover, galaxies are vastly heterogeneous objects in terms of morphological type, star formation, surface brightness; further, they may have formed at different epoch and hence have different ages. The LFs for galaxies differentiated by morphological type appear distinct (BST88); even if LFs of galaxies of different Hubble types are individually invariant with the environment (Jerjen & Tammann 1997; Andreon 1998; but see Kashikawa et al. 1995), the morphology–density relation (Oemler 1974, Dressler 1980) which implies different relative abundances of spirals, ellipticals and dwarf galaxies in the field and clusters supplies an environment dependence to the total LF. Since the morphological types are correlated (albeit weakly) with colors, the LF is likely to be color-dependent (Marzke et al. 1994). Temporal evolution of galaxies is bound to change their luminosities and — if non-uniform — alter the global LF with epoch.

Galaxy LF may therefore behave differently in the field, galaxy groups and clusters. There are differences in galaxy densities even amongst clusters that may manifest themselves in global statistical properties of the galaxy luminosities. For instance, bright galaxies are more abundant in dense clusters (Garilli et al. 1999), consistent with biased galaxy formation. In contrast, the LF shows no evidence for variation with cluster richness (Colless 1989). The presence of an extreme object such as a cD galaxy at the bottom of the cluster potential seems to deplete dwarf galaxies and flatten the LF (Lopez-Cruz et al. 1997), indicating environmental effects on the faint-end slope of the cluster galaxy LF. Other studies, however, point to the ratio of dwarf to bright galaxies increasing with the richness of the environment (Ferguson & Sandage 1991; Phillips et al. 1998), opposite to that predicted from biased galaxy formation. Rich clusters display steeper LFs than their poor cousins (Valotto et al. 1997; but see Lopez-Cruz et al. 1997 who claim the opposite). Further, the spatial distributions of these low luminosity galaxies also varies with environment; cluster dwarfs may be spread out through the system, while in the field the dwarfs tend to be satellites of giants. X-ray luminous groups of galaxies have dwarf-to-giant ratios that are significantly larger than those of low X-ray luminosity groups (Zabludoff & Mulchaey 2000, here onwards ZM2000). The dwarf galaxies in X-ray luminous groups are clustered more closely than the giants, again opposite to the sense of biased galaxy formation (ZM2000).

Similarly, poor cluster LF determinations in the literature differ widely. Group galaxy LFs may be consistent with that of the field (Muriel et al. 1998), or may show a deficit of galaxies at intermediate luminosities (Hunsberger et al. 1998) or fainter (see review by Hickson 1997), or maybe similar to that of rich clusters (ZM2000). While the blue galaxy LF (Muriel et al. 1998) seems to turn over at the same luminosity as the field, the red galaxy LF (ZM2000) has a far brighter break than the field galaxy magnitude distribution. One reason may be a matter of the

definition of these “poor systems”. The different samples may represent a mixed bag of objects that are mutually different (see Sec. 1.3.2).

We observe that an uncomfortably large fraction of the results on galaxy luminosity functions are at variance with each other, testifying to the complexity of the theme. Studying a large numbers of clusters with a large range of characteristics — different richness, galaxy morphological fractions, and dynamical states — would help gauge the extent of environmental influence on bulk properties (such as the LF) of galaxy populations.

This chapter presents the luminosity distributions of the galaxies in our sample of poor clusters. Such a study has two main purposes: (1) to test for “universality” of the LF of the different poor clusters, and (2) to compare the galaxy LF in the EMSS poor clusters with those in the field and rich clusters, and thus study the influence of the environment on galaxy formation or in modifying the primordial LF through dynamical processes either during or after cluster collapse. The objective of this study is to determine an LF that reflects with reasonable fidelity the membership of a typical poor cluster, and not to compute how the general poor cluster population contributes to a global LF.

3.2 Analysis

Our catalogs of galaxies in the fields of the four EMSS poor clusters contain their positions, V magnitudes and colors. These provide the relevant data to construct luminosity functions. These are subject to photometric errors, detection completeness limits and uncertainties in the statistical background subtraction (as below). Since our I band data are not so deep nor so complete as the V and R filter images, we shall exclude them from the present analysis. Note also that for the cluster MS0002, we can estimate the LF only in V and R bands; the B -band data do not have good enough photometric calibration to be useful here.

In the following sections, we set forth the details of the various steps involved in construction of the LF.

3.2.1 Extraction of Cluster Galaxies

In studying cluster galaxies we need to “extract” them from the sum total of the objects projected into the same area of the sky (a great number of both fore- and back-ground galaxies, and perhaps a small number of misidentified stars).

Direct selection of cluster members is possible only with redshift and/or morphological information. Spectroscopic redshifts are lacking for all but the brightest cluster galaxy in our sample (and constructing spectrophotometric catalogs of the cluster galaxies would demand further huge amounts of observing time on large telescopes). Recent times have seen the development of a technique of using photometrically estimated redshifts to determine cluster membership. However, the accuracy with which photometric redshifts can be estimated is crucially dependent on the number of available colors and on the errors in photometry ($\delta z \approx 0.2$ at $z = 1$ for 0.1 mag errors in colors). This means that we cannot apply this technique for our clusters, of which the highest redshift one

is at $z = 0.216$. However, cluster galaxies tend to lie on a well-defined color–magnitude ridge line. So, we can use the color–magnitude relation to assign cluster membership, as done by Metcalfe et al. (1994), Lopez-Cruz et al. (1997), De Propris & Pritchet (1998), Moretti et al. (1999). Now, we have data in multiple filters and, as we show in Sec. 4.2, the color–magnitude diagrams for the clusters are reasonably well-determined. We can thus exploit galaxy colors and their closeness to the color–magnitude relation to identify cluster members; galaxies whose colors fall well away from the relation are interlopers. We assume all “sequence galaxies” are indeed cluster members, and that the sequence efficiently selects all probable cluster members. We construct LFs using this method to segregate cluster and non-cluster galaxies. However, since we lack independent confirmation of the efficacy and reliability of this method of “cleaning” clusters of the background, we will also apply another well-known method of correcting for contamination.

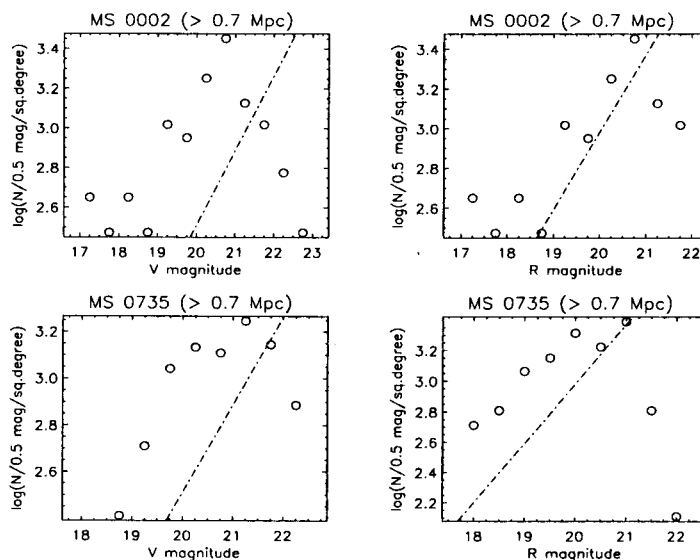


Figure 3.1: Galaxy counts at radii > 700 kpc from the centers of the poor clusters MS0002 and MS0735 to the largest circle covered by the CCD frame. The overplotted lines are the field galaxy counts of Wilson et al. (1997) in the V -band and Tyson (1988) in the R -band. The excess of galaxies over the predicted field counts (to the completeness limits) even so far away from the cluster centers in both cluster neighborhoods is obvious.

An alternative to acquiring a complete sample of spectroscopically confirmed members is to decontaminate the galaxy counts of contribution due to the field by applying a statistical background correction. To estimate the field or background density, one may use either counts defined locally in the lower-density regions around each cluster or a fixed, global estimate of galaxy density in the sky.

If the cluster images cover a wide field, as in photographic surveys, then it is possible to measure field counts around each cluster in a homogeneous fashion, by subtracting background counts from around the cluster region itself. Even when the detector field of view is small, (as in the Hubble Deep Field work), it may be possible to obtain flanking fields from where to establish the local field counts. Such a control sample and the object sample, having been obtained with the same instrumentation, would be directly comparable. Studies (e.g., Driver et al. 1998) have shown that the LF is robustly determined over the absolute magnitude range $-23 < M_R < -16$ using

subtraction of field number-counts provided: (a) the cluster has an Abell richness 1.5 or greater; (b) the redshift of the cluster lies in the range $0.1 < z < 0.3$ (c) the seeing is better than FWHM 1.25 arcsec, and (d) the photometric zero-points are accurate to within $\delta_m = +/ - 0.12$. If these conditions are not met (our data do not satisfy the first and third criteria), then the recovered luminosity distribution is unreliable. Using the local background would also allow contamination from the cosmic variance in projected galaxy counts and through gradients in galaxy densities from really large-scale structures.

The global method is based on empirical galaxy counts as a function of apparent magnitude from deep, large-area surveys of e.g., Tyson (1988), Metcalfe et al. (1995). Such counts are usually given as $\log N(m)$, where $N(m)$ is the number of galaxies brighter than apparent magnitude m . This method has its associated inaccuracies since assuming a global density would mean neglecting local inhomogenities. This deficiency contributes errors ranging from 25% (Dressler 1978) to 50% (Oemler 1974; Lugger 1986). Of course, these independent studies represent number counts using different filters or photometric systems, various definitions of galaxy magnitudes (fixed aperture, isophotal, total) and unequal angular coverage. Several doubts thus remain about the validity of a field correction based on a general $\log N(m)$ law (see BST88).

Background correction is especially difficult for poor clusters due to the meagre galaxy population and faintness of their density contrast against the background. Further, the number of background galaxies contaminating each cluster depends on its redshift. Short of obtaining velocity measurements for all galaxies in the region of the cluster, we have to take the cluster galaxy census after using one of the above options for background subtraction. It is possible to use an annular region far enough away from the cluster center only for MS0002 and MS0735, where the CCD images sample more than about 0.8-1.2 Mpc radii from the position of the brightest cluster member. However, we use the global background estimate throughout, to ensure that the measurements are uniform for all the clusters, and are not contaminated by other nearby systems in the CCD field. We derive an estimate of the cluster population using field galaxy counts from the literature.

We use the deep galaxy counts over high Galactic latitude fields performed by Tyson (1988) to “decontaminate” the cluster images in the B and R bands. The differential galaxy counts per magnitude at the galactic pole in the B_J and R bands found by Tyson follow the relations

$$\log N_B = 0.45 B_J - 6.55,$$

$$\log N_R = 0.39 R - 4.80.$$

We link Tyson’s isophotal (28 mag/arcsec²) photometry to the Johnson-Kron-Cousin system using the prescriptions of Fukugita et al. (1995). We use the field count estimates of Wilson et al. (1997) to derive the cluster galaxy counts in the V -band:

$$\log N_V = 0.377 V - 4.73.$$

In order to clean the cluster of interlopers, we determine the number of field galaxies in a given magnitude bin that are expected to be projected onto the cluster area (of $\pi \times 0.5 \text{ Mpc}^2$). While

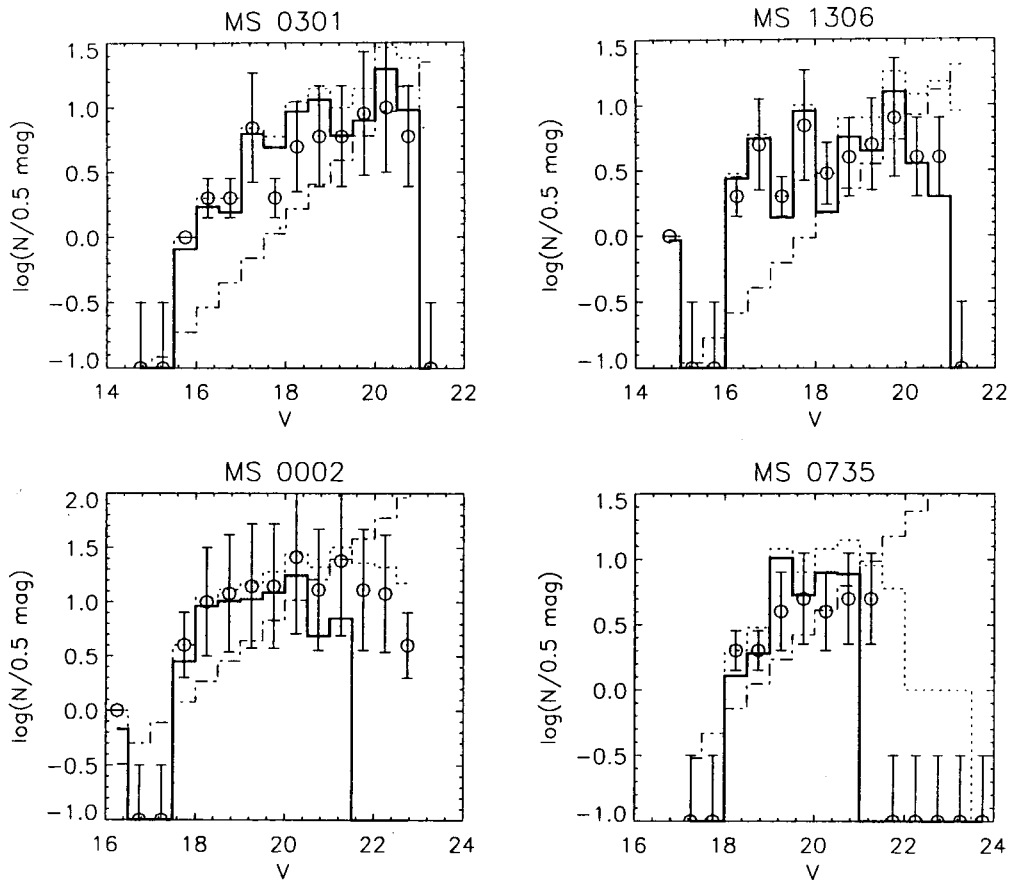


Figure 3.2: Generating the luminosity function from global background subtraction. The observed galaxy number counts in full CCD frame in the V -band (dotted lines) are corrected for the background that is estimated using the counts of Wilson et al. (1997; dot-dash lines). The corrected counts (solid lines), that shall later be transformed into absolute magnitudes, provide a luminosity function corrected statistically for the background. Superimposed as circles are the number counts of “sequence” galaxies with error bars assuming Poisson counts.

such a method estimates the non-cluster contamination in a statistical sense, it does not provide specific information on cluster membership for individual galaxies. Note that we use these background-corrected counts to provide an independent fiducial sample for comparison and not for the actual LF determination. We compare counts obtained through this technique with those using the color-magnitude relations, in Fig. 3.2. Agreement between the two exists at a level that is satisfactory, if not perfect.

3.2.2 Conversion to Rest-Frame Magnitudes

After selecting the sample of galaxies to be counted in the cluster LF, we must transform apparent magnitudes to rest-frame magnitudes through the distance modulus and other corrections. Because all cluster galaxies are virtually equidistant, their apparent magnitudes can directly give the luminosity function (to a certain limiting magnitude) after scaling by the distance modulus.

Our catalog contains galaxy magnitudes corrected for Galactic extinction but not internal absorp-

tion. There is some doubt that the extinction toward MS0301 may be patchy; however, we apply one value for the whole cluster. The relation between the apparent and absolute magnitudes of a galaxy is given by:

$$m - M = 5 \log(D_L) - 5 + K(z) + e(z),$$

where D_L is the luminosity distance (which depends on the cosmological parameters q_0 and H_0), $K(z)$ is the K-correction that accounts for the Doppler redshifting of the galaxy spectrum due to the expansion of the Universe, and the last term $e(z)$ is the evolutionary correction that measures the variation in luminosity (in units of magnitude) from the redshift of the galaxy to the present $z = 0$. We compute the distance modulus adopting (the long distance scale) $H_0 = 50 \text{ km s}^{-1} \text{ Mpc}^{-1}$ and $q_0 = 0.5$, and using the cluster redshifts listed by Gioia & Luppino (1994). This choice of cosmological parameters is not necessarily in accord with theoretical expectations or with modern observations, but follows most other studies of cluster galaxy LFs. If we had assumed $q_0 = 0$ then the transformed magnitudes (and inferred M^*) would be brighter by the amount of increase in the distance modulus: 0.13 mag at $z = 0.09$ and 0.20 mag at $z = 0.22$.

Table 3.1: K-corrections for elliptical galaxies from Poggianti (1997).

Cluster	z	V	$(B - V)$	$(V - R_C)$
MS0301	0.083	0.044	0.271	0.050
MS1306	0.088	0.047	0.289	0.051
MS0002	0.116	0.067	0.382	0.062
MS0735	0.216	0.223	0.551	0.195

The computation of K - and e - corrections is usually by means of spectrophotometric models of stellar populations assuming a galaxy formation redshift, initial mass function for the stars, and a star formation rate. Typically, the spectra of galaxies are not flat nor do all morphological types evolve in the same way, so $K + e$ -corrections are different for different galaxies. We shall study mostly the inner 0.5 Mpc areas of the clusters, where the high central densities make the morphological composition mainly elliptical/spheroidal, though there is bound to be a large dispersion. Therefore, and in keeping with common practice, we apply the corrections relevant to elliptical galaxies at our cluster redshifts. We shall also make the working assumption that evolution in the stellar component of the galaxies has a negligible effect (~ 0.1 mag at $V \sim 20$, of the order of our photometric errors). This is further justifiable by the tightness of the cluster color-magnitude relations and their similarity to that of the local Virgo cluster (see Sec. 4.2). We use the K-corrections for elliptical galaxies from spectro-evolutionary models of Poggianti (1997) and interpolate them to our required cluster redshifts. For any galaxy other than E/S0, the K-effect is smaller, so a small color correction would come into play; but at its largest, the correction is less than 0.15 mag at the highest redshift of our sample ($z=0.22$ for MS0735) if we use the relevant value for the bluest Sc-type spiral galaxies instead of the one for E/S0 morphological types. Table 3.1 contains the K-corrections we thus derive for the EMSS poor clusters.

3.2.3 Construction of the Individual Luminosity Functions

It is important to use homogeneous samples of galaxies over a well-specified range of absolute magnitudes when constructing the LFs since the different completeness levels of different clusters can have an important effect in determining the faint-end slope of the LF. Likewise, it is preferable to estimate the LFs within similar cluster radii, so as to avoid possible LF variations with distance.

We generate the LFs for galaxies in circular areas of diameter 0.5 Mpc for MS0301 and MS1306, and 0.7 Mpc for MS0002 and MS0735 centered on the BCM. This helps reduce the relative contamination by field objects by focusing on spatial regions that are most likely to be dominated by cluster members. Though such areas should be rather small for computation of the LF for rich clusters, they should be adequate for poor clusters whose core sizes is about 250 kpc (see Sec. 5.3.2).

We limit the LF exercise to galaxies brighter than $M_V = -18$ mag; fainter than this limit, incompleteness sets in (cf. Fig. 2.1). We shall see in Table 3.5 that this faint cut-off is ≈ 3 mag fainter than M^* for the Schechter function. Throughout this work, we deal with reasonably high surface-brightness galaxies; we are most unlikely to have included in our data set the diffuse low surface-brightness spirals or faint dwarf irregulars being found in increasing numbers in the nearby universe.

In constructing the LF of the individual clusters, we use sequence galaxies determined from the color-magnitude relation for early-type galaxies at the cluster redshift. Galaxies much redder or bluer than the sequence are likely to be back- or fore-ground objects, so we omit them in the generation of the LFs. We also determine the LF by decontaminating the cluster counts of non-members by statistical field correction. Field counts can be comparable with poor cluster galaxy counts even at $V \simeq 20$ mag. Figure 3.2 depicts the results of such field subtraction for the V -band. We bin the cluster galaxy sample in 0.5 mag bins in apparent magnitude in each passband. Next we transform the apparent magnitudes to absolute magnitudes, and directly use the distribution as the *nonparametric LFs*.

3.2.4 Estimation of Completeness

We wish to construct composite LFs (see Sec. 3.2.6) for the poor clusters. For this purpose, we must have knowledge of the luminosity (equivalently, magnitude) completeness limits for the individual clusters in various filters. We have evaluated these in Sec. 2.5.2, from which we may ascertain that LFs may be computed to faintness limits of $M_V \approx -18$ without being compromised by incompleteness errors. The galaxy counts for the cluster MS0735 are complete to only about a magnitude shallower than the other three clusters. We prefer to avoid “corrections for incompleteness” which would require different modeling for each cluster and would handicap us without a unique handle on the errors. This does mean that the luminosity range of the LF is limited and we miss the crucial dwarf galaxy populations; were we to observe the Local Group to the same absolute magnitude range, we would include only M31, the Milky Way, M33 (all spiral galaxies) and the Large Magellanic Cloud (an SdM-type satellite of the Milky Way). There is no trend in completeness among the B , V and R filters in which we shall construct the LF, i.e., the

data in the B and R filters are comparable in completeness to $M_V \approx -18$ assuming the colors of an elliptical galaxy at the appropriate redshift.

3.2.5 Errors in Construction of the Individual LFs

Much of the uncertainty reflected in computing the LF of poor clusters from imaging alone comes from the difficulties of separating cluster galaxies from those in the isolated field projected onto the clusters. The LF is subject to:

1. photometric errors,
2. systematics of star-galaxy discrimination,
3. uncertainties in background subtraction,
4. object crowding and surface brightness cut-offs.

Section 2.4.4 mentions that the photometric accuracy of our galaxy catalogs is about 0.07 magnitude at $V = 20$ mag. As we use 0.5 mag bins, the photometric errors should not greatly affect the determinations of the Schechter parameters below.

Sky noise in the images and poor seeing will blur the faintest objects and not only make them difficult to detect (and split from very close neighbors) but also give rise to errors in star-galaxy separation. In the brighter apparent magnitude range ($R < 20$ mag), though, essentially all objects are well resolved into stars or galaxies (extended objects), so the bright-end of the LF may be reasonably free of these errors. At fainter magnitudes, where both the photometry noise and misclassification probability rise, incompleteness also sets in. Further, high Galactic extinction and cosmological dimming of the surface brightness of galaxies even under the best observing conditions will preferentially remove faint sources from the catalogs. But at magnitudes fainter than $R=21$, galaxies are expected to dominate over the stars of the Milky Way.

For a statistically-corrected LF, the maximum error in its constructing — especially in determining the slope — arises from systematics in the field counts; additionally, an intrinsic (perhaps non-recoverable) contribution is due to field-to-field fluctuations in background counts which is not Poissonian given that clustering of galaxies exist to all magnitudes. This problem is aggravated for poor clusters by their very nature of being ill-populated. Even modest errors in background subtraction can have deleterious effects on poor cluster LFs as the expected fractional field contamination is worse for poor clusters than for their rich cousins, depending on the pertinent redshift.

We deal only with galaxies of high surface brightness; our detection isophotes do not permit inclusion of significant numbers of the low surface brightness galaxy population. Nevertheless, we find that the galaxies in the images span some 6 magnitudes in surface brightness, from the brightest cluster member to the faint, nearly unresolved galaxies. Our object detection and separation program (FOCAS) is efficient at deblending overlapping objects; there are fewer than six pairs per cluster whose projected separations are within 6 arcsec. Our photometry uses apertures of 3 arcsec calibrated to 6.6 arcsec using aperture corrections. The nearly-merged objects (that

are not always the brighter galaxies) have aperture photometry that may be contaminated due to the neighbors though not seriously (i.e., by more than 0.5 mag). We therefore believe that problems due to crowding — miscounting galaxies and photometric imprecision — are negligible within the poor cluster images, quite unlike in the case of rich cluster cores.

3.2.6 Construction of Composite Luminosity Functions

The number of galaxies counted in the individual luminosity function is (expectedly) small and is not quite conducive to being fit with a three-parameter analytical function such as the Schechter function. However, the total number of all galaxies in our sample of poor clusters allows an estimation of the mean shape of the LF particularly at the faint end. A comparison of LFs from poor cluster to poor cluster, and between the poor cluster and other environs helps determine whether galaxies participate in a universal LF or whether they are subject to environmental effects at formation and during their subsequent evolution.

The absolute magnitude limit to which galaxies are included in construction of the LF can influence their intercomparison as well as the parameters of the function fits, since evidence for a steep upturn could appear at different regions of the LF faint-end (Phillips et al. 1998). We must therefore choose the magnitude regions which are well within the completeness limits and are consistent with other work we choose for comparison. The nearest and most distant of our poor clusters differ by a distance modulus of 1.5 mag, so the absolute magnitude range of the LF will consequently suffer on account of the shallowness of the farthest cluster. We choose to use only galaxies brighter than $M_V = -18 + 5\log h_{50}$. In comparing the LFs among themselves and in Schechter functional fits, we exclude the first-ranked galaxies since they do not all appear to obey the statistics commensurate with the latter.

The most direct way to construct an unbinned composite LF is to accumulate the galaxies of all the clusters down to some limiting magnitude. Here we use only galaxies selected to be within the cluster color–magnitude “sequence”, i.e., whose cluster membership is highly probable. We then form an “unbinned composite LF” in two filters (V , R) from all four clusters through the union of the individual absolute magnitude data sets brighter than the completeness limits. While such a compilation changes the normalization of the LF, it does not alter the shape so long as the component LFs are similar. We use nonparametric tests to compare the individual LFs with the unbinned composite LF.

We also create “binned composite LFs” through weighted addition of the binned individual cluster LFs. We employ galaxy magnitude sets generated using two independent techniques of extraction of cluster members, i.e., through (i) closeness to the cluster color–magnitude relation and (ii) statistical background subtraction (as described in Sec. 3.2.1). We construct the binned composite LF within each filter by taking the weighted mean of all the individual cluster LFs to the completeness limits:

$$N(m_j) = \frac{1}{n_j} \sum_i N_i(m_j) w_i \quad (3.2)$$

where $N(m_j)$ is the galaxy count in the magnitude j th bin of the composite LF, n_j is the number of clusters with completeness limits fainter than the magnitude corresponding to the j th bin,

$N_i(m_j)$ is the number of galaxies in the j th magnitude bin of the i th cluster, and w_i , the weight of each cluster defined as the ratio of the number of galaxies brighter than $M_V = -18$ (within 0.5 Mpc of the cluster center for MS0301 and MS1306 and 0.7 Mpc for MS0002 and MS0735) to the sum total of galaxies with $M_V \leq -18$ in all four clusters. Again, the fainter magnitude bins will be determined by the cluster(s) with the brighter completeness limits. We then compute the errors on the composite LFs as:

$$\sigma_{N(m_j)} = \frac{1}{n_j} \sqrt{\sum_i N_i(m_j) w_i^2}. \quad (3.3)$$

Note that weighting by the total galaxy counts to $M_V = -18$ can distort the LF if there is a correlation between richness and the faint-end dwarf population (as suggested by Phillips et al. 1998). We apply parametric tests on the binned composite LFs.

3.2.7 Nonparametric Tests

We wish to test whether individual cluster luminosity distributions are drawn from a single parent distribution, or whether there are genuine variations amongst them. We need to determine also if the LFs are similar enough to justify their being combined into one composite LF. We can compare the cluster galaxy samples directly, or indirectly through the parameters of functional fits to the LFs. Such tests of hypotheses are classified into parametric and nonparametric methods, respectively. Parametric methods (see the next section) make assumptions about the underlying distribution from which sample populations are selected while nonparametric methods do not. With the objective of comparing individual cluster LFs among themselves and with the composite LF without making prior assumptions about the form of the LF, we use two nonparametric tests on the unbinned “sequence” galaxies.

The working (null) hypothesis we use in the tests is that the individual cluster galaxies (excluding the BCM) are all drawn from a universal LF. We first use the two-sided Kolmogorov–Smirnov (K-S) statistic to determine if pairs of individual cluster LFs from the same distribution. The K-S test falsifies the null hypothesis using the maximum deviation between the cumulative distribution of the data. We then employ the same test to test the null hypothesis that unbinned individual LFs are drawn from the unbinned composite LF. Small values (0.05 or 0.01) of the significance level of the K-S statistic indicate that the cumulative distribution function of the LFs (i.e., the integrated LFs) under comparison are significantly different. The K-S test is broadly sensitive to all variations between the samples under comparison. To supplement this test, we perform two other nonparametric comparisons of the unbinned LFs. We apply the Wilcoxon Rank-Sum test to test whether the individual cluster magnitude distribution have the same “location”, i.e., mean, against the hypothesis that they differ. A small value (0.05 or 0.01) of the computed probability indicates that the two samples have significantly different means, i.e., the magnitudes of one sample are on average brighter or fainter than those of the other. We next use the F-variance test to evaluate the probability that two galaxy populations have significantly different variances as indicated by a small value of the significance. The significance values take into account the sample sizes. These nonparametric tests are applicable to not only large data sets but also small samples such as the bright end of the poor cluster LF. Though the latter tests are individually somewhat

narrow in scope, they are both powerful and reliable (Wall 1996), and give us an indication of the detailed similarities of differences in the LFs. These tests do not account for uncertainties in the estimated magnitudes. However if the latter are the same for all the objects (that comprise a homogeneous photometric sample), then they should not affect the comparisons appreciably.

Here (and in the Chi-Square goodness of fit test below) it is important to remember that a successful test does not *prove* the proposed hypothesis, but a test that shows small probability of an occurrence does question the validity of the assumption.

3.2.8 Schechter Function Fits and Parametric Tests

In magnitude notation — as is the convention in optical astronomy — the Schechter function of Eq.3.1 becomes:

$$\phi(M)dM = 0.4\ln 10\phi^* 10^{-0.4(M-M^*)(\alpha+1)} \exp\{-10^{-0.4(M-M^*)}\}dM, \quad (3.4)$$

where M^* corresponds to L^* in absolute magnitudes. Observations must determine the three free parameters of Eq.3.4. ϕ^* varies by several orders of magnitude between rich clusters and the isolated field, M^* ($\equiv -2.5\log\frac{L^*}{L_\odot} + M_\odot$) is approximately -19.6 mag in the B -band, with $L^* \approx 10^{10}L_\odot$ (for $H_0 = 100\text{km s}^{-1}\text{Mpc}^{-1}$),² and the slope α ranges from approximately -0.7 (flat) to -1.6 (steep) from the field to the cores of rich clusters. (greater than -2 for the total luminosity $\int L\phi(L)dL$ to be finite) The fits usually performed do not measure the true spatial density ϕ^* , but instead the projected number density of galaxies within the cluster area. ?

But is it at all appropriate to model the poor cluster galaxy magnitude data using a Schechter function? While the Schechter function is motivated by a theoretical analysis of self-similar gravitational condensation in the early universe (Press & Schechter 1974), empirical determinations of the LF show both agreement with and deviations from it. For instance, the Schechter function appears to satisfactorily describe the galaxy LFs of the field (Loveday et al. 1992; Marzke et al. 1994; Lin et al. 1996), the Local Group (Pritchet & van den Bergh 1999) and other nearby groups (Muriel, Valotto & Lambas 1998), X-ray luminous poor groups (Zabludoff & Mulchaey 2000), and rich clusters (e.g., Lugger 1989).

However, individual subsets of the bright galaxies seem to typically describe an asymmetric Gaussian distribution (Ferguson & Sandage 1991) while faint ($M_B < -18$) galaxies show upturns from a “pure” Schechter form (e.g., Thompson & Gregory 1993; Trentham 1997), as do dim low surface-brightness galaxies (e.g., Impey et al. 1988). These complications imply that a simple Schechter function cannot fit all cluster LFs. For example, the Coma cluster, the nearby very rich cluster, exhibits an LF that is bimodal (Biviano et al. 1995) with a lack of $b \sim 17.5$ mag galaxies, i.e., at the luminosity where the separation between normal and early-type dwarf galaxies occurs. Indeed many galaxy systems appear to require combinations of a Gaussian (at the bright end) and a Schechter function, e.g., Hickson Compact Groups (Hunsberger et al. 1998), poor groups (Ferguson & Sandage 1991), rich Abell clusters (Wilson et al. 1997; Molinari et al. 1998), or multiple Schechter functions, e.g., Abell clusters with richness less than one (Lopez-Cruz et al. 1997).

²The Milky Way has a luminosity of roughly $0.5L^*$.

Despite conflicting antecedents, we shall proceed with fitting our data with the Schechter recipe for the empirical purpose of parametrizing our poor cluster galaxy LFs. We justify this on the basis of the following arguments: (i) we probe moderate depths of the LF. Since the bright-end of the LF is more or less similar for the different morphological types, the LF is — to a first approximation — independent of galaxy types for objects to the magnitude limits we study, and (ii) it is convenient for comparison of our LF with those in the literature which have largely adopted the Schechter model.

In the present study, we use χ^2 -minimization to fit the Schechter form to the composite LFs, with the errors computed from Eq.3.3. A limitation in the χ^2 -fitting technique is the loss of information due to binning the individual data points. However, methods such as the maximum likelihood analysis that use unbinned data require large samples for accurate estimates of the parameters, a desideratum our data do not satisfy. We do not perform the χ^2 -fitting analysis for the individual cluster LFs which are beset by small number statistics. Simulations (Lugger 1989) show that Schechter function fits to small samples result in large dispersions in the characteristic parameters (1.0 mag in M^* and 0.4 in α for 50 galaxies).

We then use the Chi-Square goodness-of-fit test to evaluate whether the observed poor cluster composite LFs and the field and rich cluster LFs follow a universal Schechter distribution. If the observed frequencies differ significantly from the expected frequencies, the χ^2 -test statistic will be large indicating the fit is poor. This situation requires the rejection of the hypothesis that the given observed frequencies are an accurate approximation to the expected frequency distribution.

3.3 Results

We construct both unbinned and binned luminosity functions for the cluster “sequence” galaxies in the four poor clusters using the absolute magnitudes and their frequency distribution. We use only the V - and R -band data for unbinned LFs, and B -, V - and R -band absolute magnitudes for the binned LFs. Fig. 3.2 shows that there is good agreement in the galaxy number counts derived using sequence galaxies and using a “global” background subtraction. Therefore, the sequence galaxy LF should be reasonably representative of the actual LF of the clusters.

As discussed above, the question of whether there is a “universal” LF translates to whether individual cluster galaxy luminosities are drawn from a single parent distribution or whether there are genuine variations with cluster richness, appearance and dynamical state, X-ray luminosity, etc. In view of this, we determine the cluster richness in Sec. 3.3.1, and the contrast between the first and second brightest galaxies of the clusters that we use as a measure of the cluster dynamical state (recall the description in the Avant-Propos to this chapter).

Then, using nonparametric tests, we perform direct comparisons of (i) the galaxy LFs of the individual clusters with each other, and (ii) the individual cluster LFs with the composite in Sec. 3.3.3. In Sec. 3.3.4 we report on Schechter function fits to the three binned composite LFs. Then we use parametric tests to compare the EMSS poor cluster galaxy LF parameters with those of the field, other poor systems and richer clusters. In all these statistical comparisons, we exclude the brightest cluster members which are thought to have “special”, i.e., non-statistical origins.

3.3.1 Cluster Richness

The “richness” of a system generally takes census of the member galaxies within some luminosity range and lying (in projection) within a well-defined metric radius of the cluster center.³ The richness estimates in the literature count (i) the total number of galaxies in a particular section of the LF, assuming a universal LF or (ii) brighter than a certain limiting magnitude of the cumulative (not necessarily universal) LF. The first two items below belong to the former category, and the third to the latter:

1. the Abell richness N_A : defined by Abell (1958), this represents the net galaxy count after field subtraction between m_3 and $m_3 + 2$ where $m_3 =$ magnitude of the third brightest galaxy, within one Abell radius. The Abell angular radius corresponds to a physical (metric) radius $r_A = 1.5 h^{-1}$ Mpc at the cluster redshift (usually estimated photometrically from the magnitude of the tenth brightest galaxy).
2. the Bahcall richness parameter $N_{0.5}$: Bahcall (1977, B77 now on) defined a like quantity that is better suited to measure the richness of poor clusters. $N_{0.5}$ is the average surface density of galaxies brighter than $m_3 + 2$ within the innermost circle of radius 0.5 Mpc (as against the 3 Mpc Abell prescription, for $H_0 = 50 \text{ km s}^{-1} \text{ Mpc}^{-1}$) around the cluster center after correction for the background.
3. the Allington-Smith et al. richness estimate $N_{0.5}^{-19}$: is the membership of the cluster to a fixed absolute magnitude limit of $M_V = -19$ within the same 0.5 Mpc radius, first proposed by Allington-Smith et al. (1993, AS93 hereafter), who studied poor groups surrounding radio galaxies.

The radius of 0.5 Mpc corresponds to the typical size of the X-ray emitting region for poor clusters. It also permits a compromise between the competing demands of good signal in cluster counts and minimizing the background uncertainty. Obviously, $N_{0.5}$ and $N_{0.5}^{-19}$ are in galaxies per $\pi \times 0.5^2 \text{ Mpc}^2$. An important concern in estimating N_A and $N_{0.5}$ is the identification of the third brightest galaxy: a misidentification could result in not sampling the same region of the LF. Bahcall (1980) also corrects for the third-ranked galaxy being fainter in the poor MKW/AWM clusters relative to rich clusters using a procedure that includes assuming a universal LF and calibrating the poor cluster m_3 with those of rich clusters. Figure 1 of Bahcall (1981) provides the correction factors (< 1) for the poor cluster counts. This calibration approximately halves the observed poor cluster galaxy counts. The potential errors with misidentification of the third most luminous member or differential luminosity changes within the cluster members do not arise for the AS93 richness estimate.

It is arguable whether one should use the Abell richness criterion for poor galaxy systems; we can neither make the assumptions of universality of the luminosity function nor extrapolate the galaxy counts to 1.5 Mpc using a particular galaxy surface density profile.

We calculate the various richness quantities using all galaxies within the cluster sequence (defined in Sec. 4.2) and within the required metric areas after identifying the brightest cluster galaxy

³The cluster richness thus measures the surface density of galaxies.

Table 3.2: Cluster richness estimates using “sequence” galaxies. Richness prescriptions are: Column 2 - Bahcall (1977); Col. 3 - Allington-Smith et al. (1993). The penultimate column is the V absolute magnitude of the third brightest cluster galaxy, and final column is ΔM_{12} which measures the luminosity contrast in magnitudes between the first- and second-ranked cluster galaxies in the V band.

Cluster	$N_{0.5}$	$N_{0.5}^{-19}$	M_3	ΔM_{12}
MS0301	30 ± 6	45 ± 7	-21.51	0.43
MS1306	18 ± 4	33 ± 6	-22.06	1.49
MS0002	30 ± 6	56 ± 8	-21.04	1.20
MS0735	22 ± 5	48 ± 8	-21.25	>0.37

with the cluster center. There are no obvious bright foreground galaxies which may contaminate the richness computations. In Table 3.2 we list the Bahcall richness values in Column (2), and the galaxy counts following the prescription of AS93 in Column (3). The formal errors are 1σ estimates assuming Poisson statistics which, realistically speaking, may underestimate the true errors due to the clustering of galaxies.

In comparison, the Bahcall richness N_0 is 11 for Virgo (an irregular cluster at $z=0.0033$), 15 for Centaurus (a $z=0.0113$ irregular poor cluster) as estimated by B77, and 40 for Coma (a rich, compact cluster at $z=0.023$). We see that the EMSS poor clusters are as populous as the Virgo cluster. Our clusters are about four times as rich as the poor groups of AS93 at similar redshifts (their mean $N_{0.5}^{-19} = 7.2 \pm 1.0$, with $-6.7 \pm 5.6 \leq N_{0.5} \leq 31.6 \pm 7.4$).

Note that a 0.5 Mpc aperture approaches the halo sizes (Sec. 5.3.2) of all our sample clusters but MS0735 for which it is roughly 60% of the total size. The specification of 0.5 Mpc depends on the assumed values of H_0 and (with small effect for our redshift range) q_0 . We use the same value of H_0 as B77 and AS93; however, we use $q_0 = 0.5$. Had we used $q_0 = 0.0$, the angular radius corresponding to 0.5 Mpc would decrease by about 5% at $z = 0.22$, decreasing the richness estimate by a few percent if $N \propto r$ as may be true for rich clusters. Since our error estimates (due largely to small number statistics and background contamination) are inevitably larger than a few percent, we do not worry about the effect of cosmological parameters on our counts.

For rich clusters, the estimated galaxy population and X-ray luminosity are correlated, though the intrinsic scatter in the relation is large. However, for poor systems with far fewer galaxies than big clusters, velocity dispersions of $\sigma < 500 \text{ km s}^{-1}$, and X-ray temperatures of $kT \approx 1 \text{ keV}$, there is little or no correlation between optical richness (i.e., the number of luminous galaxies) or total optical luminosity with the brightness of X-ray emission (e.g., Ebeling et al. 1994; Ponman et al. 1996).

In Fig. 3.3, we plot the Bahcall richness $N_{0.5}$ of the clusters against their *Einstein* X-ray luminosity. For comparison, we also show where selected Abell rich clusters and AMW/MKW poor clusters lie in such a plot. We use the richness measures of the Abell clusters from the NASA Extragalactic Database and for AMW/MKW clusters from Bahcall (1980), and the X-ray luminosities of these from the catalog of White et al. (1997).

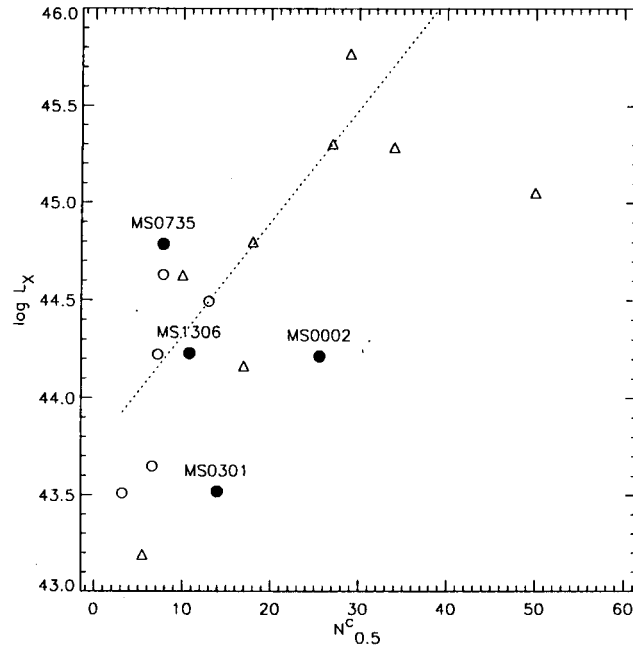


Figure 3.3: The correlation between *Einstein* X-ray luminosity and Bahcall counts for the EMSS poor clusters (labelled filled circles) compared with the same for Abell rich clusters (triangles) and AMW/MKW poor clusters (open circles). The dotted line is the linear regression fit $\log L_X = 43.741 + 0.058N_{0.5}^C$.

3.3.2 Binned Galaxy LFs for Individual Clusters

To first illustrate the shape of the magnitude distributions of the galaxies, we present the binned galaxy LFs for the four EMSS poor clusters in the B , V and R bands in Fig. 3.4. In these plots the ordinate is the number of galaxies within 0.5 Mpc of the BCM for MS0301 and MS1306 and 0.7 Mpc of the BCM for MS0002 and MS0735, per 0.5 mag bin in absolute magnitude, *including the BCM*. Filled circles and dotted lines depict the differential and integrated luminosity (magnitude) distributions, respectively. Dwarf galaxies, though likely to be numerous, are only just detectable in our work; these contribute a smaller fraction of the total cluster light depending on the slope of the LF.

In the $z \approx 0.085$ clusters MS0301 and MS1306 we see a differential LF somewhat flat in the magnitudes $M_V \approx -20 \pm 0.5$, and showing a peak immediately brightward. Further, in the LF of MS1306 there exists a large gap to the BCM at the bright end followed by a subsequent peak and dip in the fainter galaxy magnitude distribution. The cumulative distribution shows that the dip is not entirely an artifact. A similar feature appears in many rich clusters, e.g., the Coma cluster (Biviano et al. 1995) and in some of the Abell clusters (e.g., Gaidos 1997). The LFs of MS0735, the most distant of our sample clusters, reveal the onset of incompleteness fainter than $M_V = -19$, or about a magnitude brighter than the completeness limit for the other clusters. Therefore, the faintest two bins of our composite LFs shall exclude contributions from MS0735.

The dips etc mentioned here
could simply be due to
statistical fluctuations

The dips etc. mentioned here could
simply be

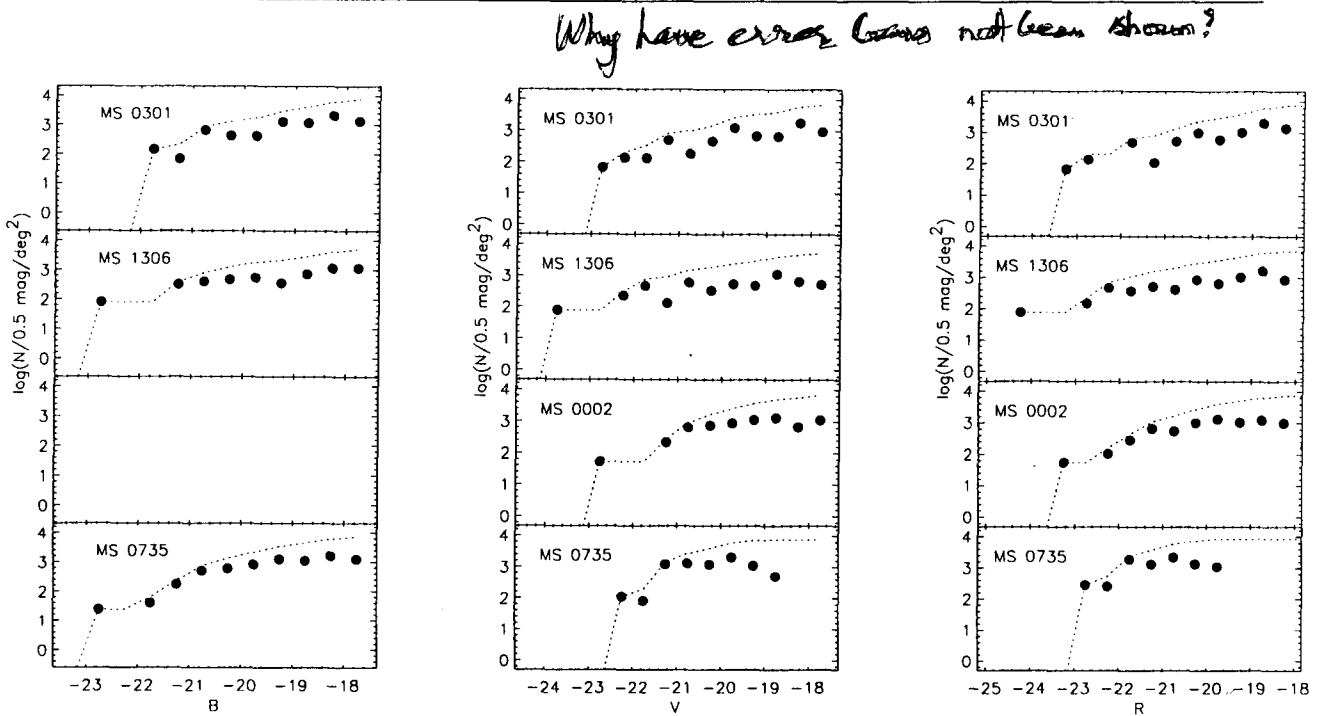


Figure 3.4: Binned luminosity functions of individual poor clusters constructed using cluster sequence galaxies. B, V, R -band LFs are in the left, center and right panels, respectively. The ordinate in each panel is the number of galaxies per 0.5 mag bin within the clustrocentric radii 0.5 Mpc for MS0301 and MS1306 and 0.7 Mpc for MS0002 and MS0735. The abscissa is the absolute magnitude. The solid circles represents the differential LF and the dotted line, the cumulative LF of each cluster including the BCM. Note that we do not estimate the B -band LF for MS0002 due to poor photometric calibration.

3.3.3 Direct Comparisons of Unbinned LFs

Never trust impressions, my boy, but concentrate yourself upon details.

– Sherlock Holmes

in ‘A Case of Identity’ by Arthur Conan Doyle

In this section we compare the unbinned “sequence” galaxy magnitude data of the individual cluster nonparametrically among themselves, using the two-sample Kolmogorov–Smirnov test. Then we compare the individual cluster LFs with the composite sequence galaxy LFs formed from all four clusters. Both comparisons exclude the brightest cluster galaxies.

Now models of cluster dynamical evolution predict (as discussed in the Avant-Propos to this chapter) variations in the bright end of the galaxy LF. We chose three magnitude cutoffs — brighter than $M = -21, -20, -19$ — to hunt for these variations; there is no *a priori* reason for selecting any one of these particular values. The fainter bounds include all of the galaxies participating in the brighter limit tests, so there is no unique determination of the differential variations with luminosity. Instead, the tests indicate at what bright-end turning point the clusters differ from each other.

Table 3.3 presents the results of the K-S tests for *the bright end of the LFs of each cluster compared with those of the other three clusters*. The tabulated values indicate the significance of the test,

Table 3.3: Significance of the Kolmogorov–Smirnov statistics of inter-comparisons between individual cluster LFs. Numbers in parenthesis indicate the populations of cluster 1 and cluster 2 within 0.5 Mpc for MS0301 and MS1306 and 0.7 Mpc for MS0002 and MS0735, brighter than the magnitude limit noted in the upper row.

Cluster 1	Cluster 2	K-S significance	K-S significance	K-S significance
V-band		$M_V \leq -21.0$	$M_V \leq -20.0$	$M_V \leq -19.0$
MS0301	MS1306	0.06 (11,10)	0.50 (18,21)	0.09 (45,33)
	MS0002	0.58 (11,04)	0.01 (18,26)	0.19 (45,57)
	MS0735	0.86 (11,09)	0.23 (18,26)	0.38 (45,48)
MS1306	MS0002	0.02 (10,04)	0.04 (21,26)	0.06 (33,57)
	MS0735	0.01 (10,09)	0.07 (21,26)	0.18 (33,48)
MS0002	MS0735	0.68 (04,09)	0.14 (26,26)	0.26 (57,48)
R-band		$M_R \leq -21.0$	$M_R \leq -20.0$	$M_R \leq -19.0$
MS0301	MS1306	0.32 (11,17)	0.28 (30,31)	0.24 (48,44)
	MS0002	0.05 (11,17)	0.44 (30,42)	0.41 (48,79)
	MS0735	0.86 (11,23)	0.07 (30,43)	0.01 (48,54)
MS1306	MS0002	0.03 (17,17)	0.09 (31,42)	0.09 (44,79)
	MS0735	0.02 (10,23)	0.17 (31,43)	0.29 (44,54)
MS0002	MS0735	0.10 (17,23)	0.14 (42,43)	0.01 (79,54)

with very small values (lower than 0.05) implying that it is unlikely for the two samples to be consistent. In parentheses are the numbers of galaxies in each restricted sample of the two clusters under comparison to the magnitude limit indicated.

For the most part, the K-S test validates the null hypothesis of the individual cluster galaxies being drawn from the same distribution. However, the K-S statistics of several inter-comparisons at the brightest ends ($M_V < -21$) show small values of the significance, indicating differences in the cumulative distribution functions of the galaxy magnitudes. The most obvious detailed differences exist between MS1306 and MS0002 brighter than $M = -21$ in both the V and R bands. In fact, the magnitude distribution of the galaxies brighter than $M_V = -21$ in MS1306 seems to be not quite consistent with those of any of the other clusters. Though both MS1306 and MS0002 have similar X-ray luminosities and nearly equal ΔM_{12} (see Table 3.2) signifying similar dynamical states in the cores, their content of galaxies whose luminosities are about a magnitude fainter than that of the brightest galaxy (m_1) are incompatible with each other. At such bright levels, completeness corrections are negligible and galaxy selection through the cluster sequence is secure. So, the variations are indeed real. It appears further that MS0002 has a sudden increase in galaxies of intermediate luminosity ($-21 < M_V < -20$). Note that the brightest part of the LF is very sparsely populated, so the differences are in part due to small number statistics. The V and

This could be the dominating effect.

R LFs of MS0735 at $M = -19$ display significant differences from the other clusters. However, we suspect that incompleteness has begun to hamper the comparisons in these instances.

In summary, the LFs appear similar overall, though they show statistically significant variations especially at the very bright end. Such differences are important because the giant, bright galaxies contribute the large part of the cluster luminosity, with the exact value depending on M^* .

Table 3.4: Non-parametric comparison of the composite LF with the individual poor cluster LFs in the same band. The LFs consist of cluster "sequence" galaxies excluding the BCM. The three results each are of the two-sided Kolmogorov-Smirnov (K-S), Wilcoxon (W) and F-variance (F) tests. The comparisons are for different magnitude limits, considering all galaxies brighter than the cut-off. Table 3.3 contains the population of the individual clusters brighter than the same cut-off values; the sum total of these is the population of the composite cluster LF.

		V band			
Faint limit	Test	MS0301	MS1306	MS0002	MS0735
-21.0	K-S	0.59	0.06	0.38	0.47
	W	0.33	0.06	0.23	0.24
	F	0.50	0.57	0.46	0.36
-20.0	K-S	0.19	0.15	0.08	0.94
	W	0.25	0.06	0.04	0.45
	F	0.24	0.36	0.02	0.36
-19.0	K-S	0.59	0.19	0.34	0.92
	W	0.30	0.04	0.07	0.24
	F	0.61	0.18	0.13	0.48
-18.0	K-S	0.45	0.46	0.30	0.02
	W	0.16	0.24	0.06	0.01
	F	0.57	0.09	0.10	0.12
		R band			
-21.0	K-S	0.63	0.09	0.09	0.81
	W	0.13	0.06	0.01	0.44
	F	0.99	0.38	0.10	0.51
-20.0	K-S	0.29	0.23	0.24	0.37
	W	0.15	0.16	0.13	0.13
	F	0.44	0.15	0.08	0.42
-19.0	K-S	0.44	0.37	0.22	0.02
	W	0.26	0.21	0.02	0.01
	F	0.92	0.10	0.12	0.39

The composite LF also contains the "tail" cluster which will weaken any differences.

If the individual cluster LFs are not grossly inconsistent with each other, we may expect that the composite LF constructed from combining the four individual LFs would represent the poor cluster LF reasonably well. Even considering Poisson statistics, the composite LF has twice the

signal-to-noise ratio of the individual cluster LFs. Note that in this section we compare the individual LFs among themselves and with the composite in the V and R bands only. In the next section (Sec. 3.3.4), we shall construct binned composite LFs additionally in the B band, assuming that the blue LFs of the four clusters are also similar following the behavior of the LFs in the other two bands.

Now we test the hypothesis that the individual cluster LFs are similar to the composite against the hypothesis that they differ at the 0.05 significance level. Table 3.4 lists the results for non-parametric comparisons of *the bright-end of the sequence galaxy LFs of each poor cluster with that of the composite in the same filter*. We recall that while the K-S test is broad in scope and tests the cumulative luminosity distribution, the Wilcoxon and F-variance statistics focus on the mean and spread of the distributions, respectively. Again, small values of the tabulated significance indicate that the samples are unlikely to be consistent. We discuss below the results for each of the four clusters.

MS0301: All three nonparametric tests indicate that the LFs of this cluster in both the V and R bands do not differ significantly from the composite LFs in the same bands for any magnitude cut-off.

MS1306: There is marginal evidence that the cluster LF between $M_V = -20$ and $M_V = -19$ is inconsistent with the composite function. The cluster galaxies are brighter on average than in the composite data. We recall that MS1306 shows a somewhat irregular differential LF (Fig. 3.4) with several dips.

MS0002: We see from the F-statistics that the intermediate luminosity ($M_V \approx -20$) members of MS0002 have a different spread in their magnitude distributions from the composite LF. The galaxies are also somewhat fainter on average than the composite distribution in this range. In the R band such a pattern occurs in the cluster galaxy LF for $M_R < -21$.

MS0735: Only for magnitude cut-offs to $M_V < -18$ or $M_R < -19$ are the significances small, implying differences in the LFs. We know that the LF of this cluster becomes incomplete at this turn-off, and may thus attribute the differences largely to systematics rather than intrinsic causes.

Thus there is no strong evidence that, over the range of $M^* - 1.5 < M < M^* + 2$, individual LFs of the EMSS poor clusters examined here are not all drawn from the same parent galaxy LF. In fact, the small numbers of very bright galaxies at the exponential end of the cluster LFs inhibit discrimination of subtle differences among themselves or with the composite LF via the nonparametric tests which themselves nevertheless provide reliable results for small samples.

3.3.4 Binned Composite LFs and Schechter Parameters

We present the Schechter fits to the B, V and R band composite luminosity functions of the EMSS poor clusters in Fig. 3.5; the error bars represent weighted errors estimated using Eq. 3.3. The figure shows the two independent LFs derived using “sequence” galaxies (filled circles) and by correcting for the background using counts from literature (open symbols). The binned composite LFs in each optical passband have about 10 data points each representing the weighted

average number of galaxies in the clusters. A total of ~ 300 galaxies of the four poor clusters in the magnitude range $-23 < M_V < -18$ comprise the composite LFs in each filter. The faint limit is ~ 1 mag brightward of the characteristic point where the transition from giant to dwarf galaxies takes place in the overall LF (Jerjen & Tammann 1997). The composite LFs are in all cases falling steeply in the brighter magnitudes and are relatively shallow at faint luminosities in the B and V bands, while the galaxy counts in the R band hint at a rise near the faint limits.

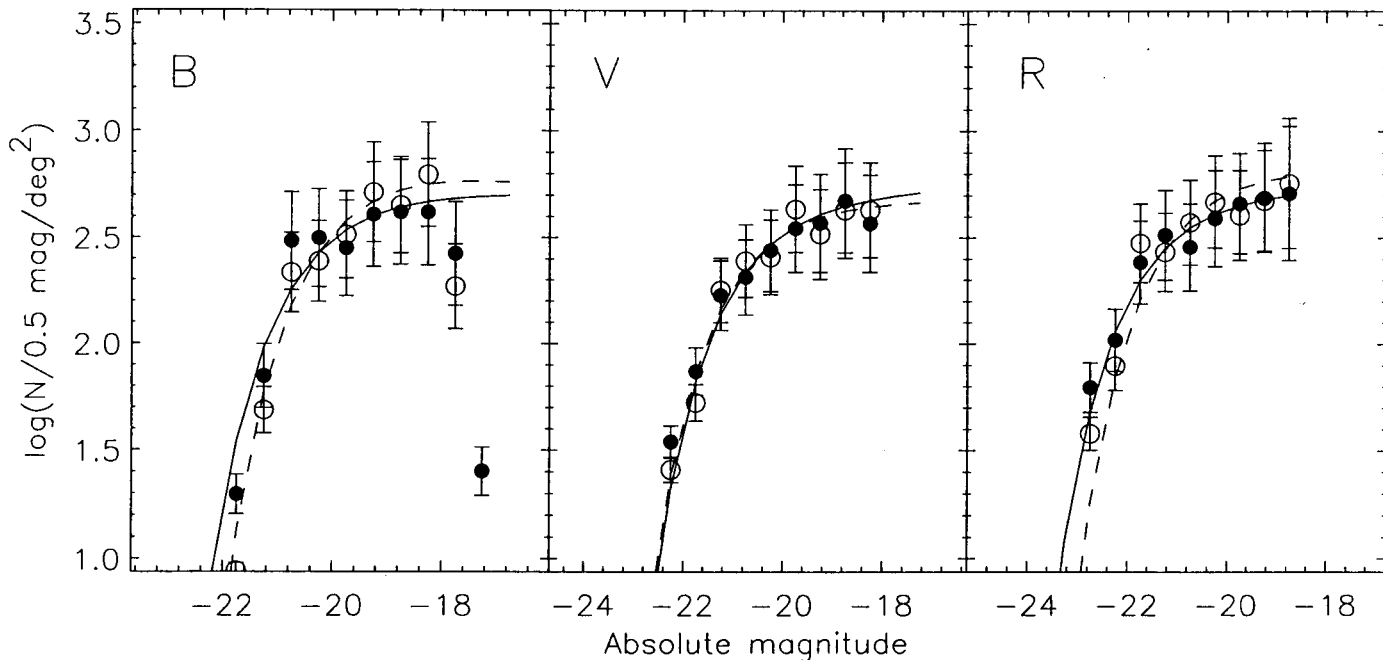


Figure 3.5: Binned composite LFs excluding the first-ranked cluster galaxies constructed using “sequence” galaxies (filled circles) and for the binned, magnitude data corrected for the background from field counts in the literature (open circles). The overplotted solid and dashed lines are the best-fit Schechter luminosity function fits for the sequence galaxies and background-corrected data respectively, with the parameters given in Table 3.3.4. The LFs are shown for the B , V and R filters.

Since the first-ranked cluster galaxies are unlikely to have all arisen from a statistical distribution function, we remove them from the individual catalogs prior to fitting the Schechter function. We perform Chi-square fits of the three-parameter Schechter function to the composite LFs in each photometric band. We list the resulting parameters M^* and α in Table 3.5. We do not use the ϕ estimate as it is meaningless in our case – we have scaled the cluster LFs to the same total number of galaxies while making the composite. The fitting accounted for errors on the galaxy counts but not in the galaxy magnitudes; the absolute photometric errors are less than about 0.1 mag for galaxies brighter than $M_V = -19$. The relative brightness of galaxies within the field are usually better determined to within about 0.05 mag. The errors quoted in the table on the Schechter parameters are the one standard error found in the χ^2 fitting.

Before discussing the values of the Schechter parameters, we mention that the reduced χ^2 is on average about 2 for the six composite LF fits. To attribute meaning to the χ^2 term is to presume

that the composite LFs fully represent the individual cluster LFs (see the discussion at the end of the chapter for more), and that the weighted (large) errors on the composite LF are entirely correct. In fact, the detailed differences between the magnitude distributions of the brightest galaxies in MS1306 and MS0002, and the dip seen especially in the sequence galaxies around $M_V = -20$ reduce the goodness-of-fit to the Schechter function. The large reduced χ^2 values may thus be too pessimistic in each case.

The composite binned magnitude data have slopes of the Schechter fit $\alpha \approx 1$ in all the passbands, implying a flat LF in each case. The differences between M^* estimates in the V and R photometric bands are close to the colors of early-type galaxies (e.g., Guiderdoni & Rocca-Volmerange 1988). This is not entirely surprising, as the bright cluster galaxies are usually of early morphological types that evince a tight color–magnitude relation (see Sec. 4.2). Recall also that we apply K-corrections appropriate to elliptical galaxies. The $(B - V)$ color difference in M^* of the sequence galaxy LFs is slightly bluer than expected for early-type galaxies. We notice that in the B -band, the Schechter function tends to underfit the more luminous galaxies which display a peak at $\approx M_B^* - 0.5$. We shall see later (Sec. 4.4) that there is indeed an excess of bright blue galaxies in the poor clusters.

Let us now consider if these do indeed provide the “true” picture of the luminosity distribution. Because we probe only a limited range of the luminosity function centered on L^* in our samples and fit the data to the Schechter function by least-squares after binning, an important concern is how well the Schechter parameters can be determined. We check whether arbitrariness in choosing the bins creates spurious results by rebinning the data in magnitude bins ± 0.25 of the original choice. Reassuringly, we obtain similar values (within 1.5σ) for all the characteristic parameters from the different best-fit solutions. The good agreements indicate that there is no substantial loss of information due to binning, and the Schechter parameters we derive are stable assuming the function represents the poor cluster galaxy LF perfectly. From Table 3.5, we see that M^* , the characteristic magnitudes for the Schechter fits, of the sequence and statistically-corrected LFs in a given passband are within one joint standard deviation of each other. Further, the M^*

Table 3.5: Best-fit Schechter parameters for the composite LFs of the sequence galaxies of the EMSS poor clusters in different bands, excluding the BCM. The data sets labelled “seq” and “stat” refer to the cluster color–magnitude sequence galaxies, and those applied with statistical background subtraction, respectively.

Waveband	Data set	Magnitude range	M^*	α
B	seq	$-22.0 \leq M_B \leq -18.5$	-20.66 ± 0.41	-0.99 ± 0.04
	stat	$-22.0 \leq M_B \leq -18.0$	-20.21 ± 0.25	-0.93 ± 0.04
V	seq	$-22.5 \leq M_V \leq -18.0$	-21.04 ± 0.26	-1.04 ± 0.04
	stat	$-22.5 \leq M_V \leq -18.0$	-21.06 ± 0.25	-1.00 ± 0.06
R	seq	$-23.0 \leq M_R \leq -18.5$	-21.83 ± 0.29	-1.02 ± 0.04
	stat	$-23.0 \leq M_R \leq -18.5$	-21.34 ± 0.37	-0.99 ± 0.04

values lie well away from the bright magnitude limits of the fits, implying the absence of any systematic errors due to the luminosity ranges chosen for the functional fits. Now, the composite LFs contain very few galaxies brighter than M^* ; clearly, it is the nature of the poor clusters and not any systematic error that places the bright end of the LF in the low signal regime.

As for the LF slopes, i.e., the α of the Schechter function fits, they appear – in all three passbands – to be virtually identical for both the “sequence” and the statistically-corrected galaxy magnitude distributions. Thus the consistency of both M^* and α of these independent LF data sets assures us that the LFs we determine are robust to the selection of cluster galaxies.

However, we must check if the choice of the bounds of the cluster color–magnitude “sequence” could exclude a part of the faint and blue population of presumably irregular galaxies in the cluster, thus artificially flattening the LF. For this we double the range of the color–magnitude “sequence”, go through the whole process of creating the weighted composite LF and fit the data using the Schechter function as before. We find that in the R passband, there is virtually no change in the slope for the new “sequence”; similarly, the new M_R^* is within one standard error of the previous value (see Table 3.5). In the V -band, the new characteristic magnitude remains similarly within one standard error of the earlier determination. The shape parameter α_V increases to -1.12 ± 0.03 , a marginally significant steepening compared to the earlier value. The composite sequence galaxy blue LF slope is therefore likely to be a little steeper (i.e., $\alpha \approx -1.1$) than we have found.

A similar situation holds for the LF generated by statistical field subtraction. Typically, the bright end of the luminosity distribution in a moderately distant cluster region represents galaxies physically associated with the cluster since the number of field galaxies is relatively low at those apparent magnitudes. But the low-luminosity end of the cluster LF corrected statistically for the field may be significantly contaminated by background (high-redshift) galaxies. In our case, though, we could be underestimating the LF slope due to the use of higher backgrounds (especially in the B and R bands, where the field galaxy counts of Tyson have been determined to much fainter isophotal levels of 28 mag arcsec $^{-2}$).

Further, the galaxies we count are mostly of high surface brightness. The inclusion of low surface brightness galaxies increases the faint-end slope (e.g., Sprayberry et al. 1997). The shape parameter α depends on the completeness limit in absolute magnitude of the galaxy sample (Trentham 1997). The bright giant galaxies that dominate our LFs individually have bounded LFs (Ferguson & Sandage 1991); together their sum should show flat slopes. The dwarf irregular and dwarf spheroidal galaxies — it is the latter that have a steep power-law distribution — are precisely those that our magnitude cut-offs do not accommodate. We believe, then, that the values of α we quote slightly ($\leq 10\%$) underestimate the true slope of the parent galaxy distribution particularly in the bluer bands.

3.3.5 LF over Different Cluster Radii

We may ask whether the LF varies locally, i.e., with differences in galaxy density between the cluster core and outskirts. In other words, do the galaxy magnitude distributions show radial

variations and are the fitted Schechter parameters sensitive to the extent of the cluster area over which galaxies are counted?

We first examine the unbinned LFs of the individual cluster sequence galaxies within 0.25 Mpc and the 0.5-0.7 Mpc radii considered in the previous section. The Wilcoxon and Kolmogorov-Smirnov non-parametric tests indicate that the sequence galaxy magnitudes (to $M_V = -18$) of the individual clusters within the small ($\pi 0.25^2 \text{Mpc}^2$) areas are fully consistent with being drawn from the same population as those in the 0.5-0.7 Mpc circles. We next remove the metric areal restrictions of 0.5 or 0.7 Mpc for sampling the galaxies and bring under consideration for each cluster the area covered by the biggest possible circle described on its CCD image (550 kpc for MS0301, 660 kpc for MS1306, 750 kpc for MS0002 and 1.1 Mpc for MS0735). Expectedly, the non-parametric comparisons show that there is no difference in the magnitude distributions when the areas < 100 kpc larger are included for MS0301, MS1306 and MS0002. The interesting point is that even for MS0735, the galaxy magnitude distributions within the original 0.7 Mpc are fully consistent with those in a much larger radius of 1.1 Mpc.

For the binned composite functions, we do not fit Schechter functions for the smaller 0.25 Mpc areas because of the very small number of galaxies there. We compare the Schechter fits obtained in the previous section for $r = 0.6 \pm 0.1$ Mpc with their counterparts for the largest-CCD-circle metric areas. We find that the general shape of the LF remains the same, with the counts in bright magnitude bins falling off rapidly and those in the faint bins showing a kind of plateau then sloping higher to fainter limits. The slopes of the Schechter function fit to the larger area sequence galaxy data become marginally flatter (by about 2σ in the B and V filters), and the characteristic magnitude becomes fainter (by about 0.1 mag) relative to the values in Table 3.5. We find a like response in the LFs computed for galaxies that have been corrected statistically for the field. The R data remain virtually unaffected, though.

One reason for the slight flattening of the background-corrected binned LF is that field counts computed statistically over the wider area increase rapidly, thus depopulating the fainter luminosity bins; the background counts are generally twice as large as the cluster counts within a 1 Mpc aperture. Moreover, we see in Sec. 5.4.1 that there are hints of luminosity segregation such that $M_V \approx -20$ galaxies have somewhat smaller characteristic separations (and are closer to the cluster center) than other galaxies. This could slightly skew the smaller region LF toward a brighter break magnitude. But coupled with the high Poisson noise (due to the small number of galaxies) in the bright magnitude bins, and of the intrinsic fluctuations in the background counts over the larger areas, the differences in M^* and α over the different cluster radial extents are not very significant.

In summary, there are no reasons to expect that the LF varies with cluster radius. Further, the Schechter function parameters of Table 3.5 are reasonably good representations of the EMSS poor cluster LF both within the restricted regions of 0.5 or 0.7 Mpc and over a much larger area that may include the cluster outskirts, with the possibility that α is slightly underestimated but by not more than ten percent.

3.3.6 Schechter Parameters: Comparison with Other Environments

probability: An erudite measure of ignorance. Being dimensionless, it is best used with a dimensional measure, especially a grain of salt.

– David Durand

To place the poor clusters in the general spectrum of clustering and to evaluate the manner in which this environment influences the behavior of galaxy luminosities, we compare the composite LFs — in particular, the Schechter function parameters — derived above for the EMSS poor clusters with those of the two extreme environments of the low density field and the high density cores of rich clusters as well as with those of other poorly populated galaxy aggregates.

We proceed on the basis that the Schechter function fitted to the composite LF in each band represents the poor cluster LF in the same color well. Problems arise when comparing luminosity functions derived using different colors and at different limiting magnitudes. For instance, short wavelength filters (e.g., B) may preferentially select galaxies with younger stellar populations at each magnitude than long wavelength filters (such as R). At the faintest levels, galaxies detected in one band might not even be present in the other due to variations in their intrinsic colors combined with K-dimming. The general practice while comparing LFs determined in different bands has been to assume a universal color for all galaxies, and transform the LF in one waveband to the other using the color of a particular morphological type from spectroevolutionary models. But galaxy colors vary by more than a magnitude between the early- and late-types (e.g., Guiderdoni & Rocca-Volmerange 1988). It is therefore advisable to compare luminosity functions determined in a particular band with others in the literature derived using the same filter.

The literature on parametrizing luminosity distributions often uses the Schechter function in combination with other functions such as the Gaussian. However, we fit only a single Schechter function, and therefore compare our work with published LFs that also use a single Schechter function. We find no suitable field LF in the V -band, but can use the V LF of both the Local Group and MKW/AWM poor clusters for comparison. Table 3.6 lists these other LFs compiled from the literature. We have scaled all the M^* values to $H_0 = 50 \text{ km s}^{-1} \text{ Mpc}^{-1}$ and $q_0 = 0.5$. From there we see that LFs of rich cluster galaxies (Gaidos 1997) have characteristic magnitudes brighter than those of the field (Lin et al. 1996) by approximately 0.9 mag in the red passband. Similarly, in the blue band, rich cluster galaxies (e.g., Valotto et al. 1997) have brighter M^* values than field galaxies (Folkes et al. 1999). The slope of the LF behaves differently, however. In the B -band it is nearly alike in the extremes of the field and the rich cluster, both of which show steeper LFs than the poor groups. In contrast, the R -band field LF is much less steep compared to the other environments. Note that the Schechter LF parameters determined even for rich clusters still lack concordance (e.g., Lugger 1986 vs. Gaidos 1997). The situation for poor systems is similarly complex as already discussed in the introduction to this chapter.

For quantitative comparison involving both the Schechter parameters α and M^* , we employ a one-sample χ^2 test in which we take the expected distribution to be the LF of the environs other than the EMSS poor clusters. We compare the observed composite binned LF with the distribution predicted by the best-fit Schechter function of the other environs (Table 3.6). The

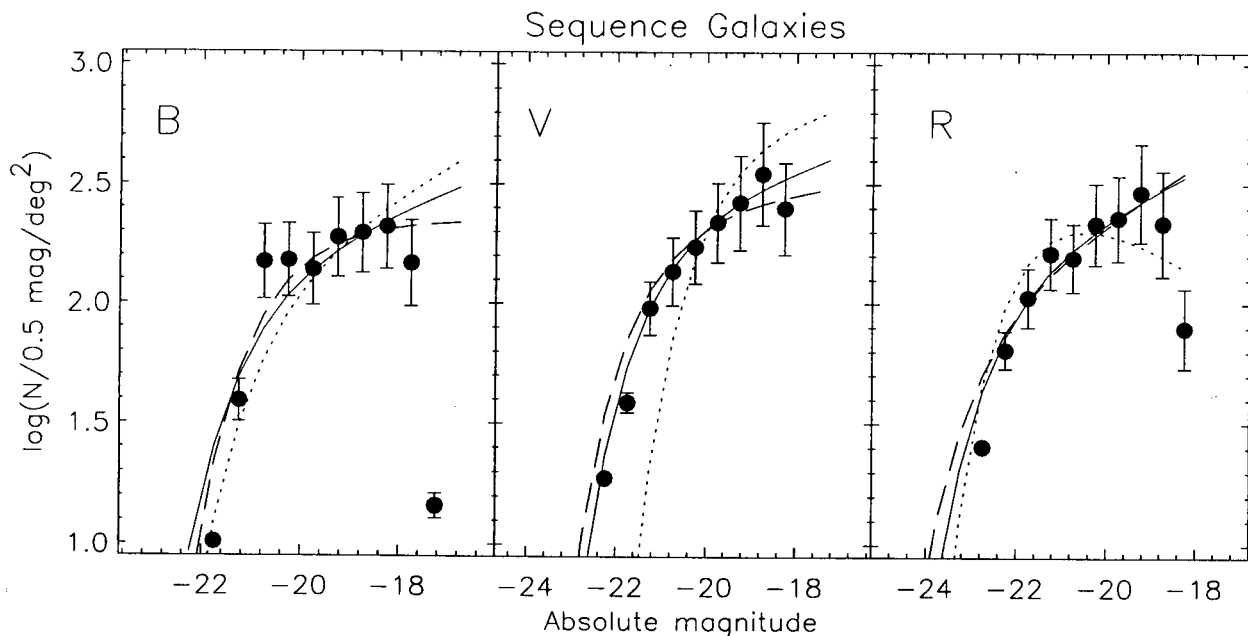


Figure 3.6: The left panel shows the EMSS poor cluster *B* band LF (filled circles) in comparison with those determined for the field by Folkes et al. (1999; dotted line), for poor groups by Muriel et al. (1998; dashed line), and rich clusters by Colless (1989; dot-dash line). The central column depicts the EMSS poor cluster LF in the *V* band (filled circles) overplotted with the LFs of the AMW/MKW cluster of Yamagata & Maehara (1986; dashed line), the Local Group determined by Pritchett & van den Bergh (1999; dotted line), and of the rich cluster Abell 665 ($z=0.18$) found by Wilson et al. (1997; dot-dash line). The right columns are the *R* band LF of our poor clusters (filled circles) compared with determinations in the same band of the LF for the field by Lin et al. (1996; dotted line), poor groups by Zabludoff & Mulchaey (2000; dashed line), and Abell rich clusters of Lugger (1989; dot-dash line). Table 3.5 and 3.6 list the Schechter parameters of the various LF estimations.

resulting χ^2 values are generally larger than unity per degree of freedom indicating that there are structures within the EMSS poor cluster LF not well-fitted by the Schechter function with parameters that describe the LFs of other environs.

The nearly flat blue composite LF of our poor clusters and its characteristic magnitude closely resemble those of the poor groups of Muriel et al. (1998). Neither are so steep as the field or rich clusters. The EMSS poor clusters also show a break between the bright giant galaxies and fainter ones at magnitudes significantly faintward of that of the rich clusters. This may mean that dwarf galaxies begin to contribute to the LF in rich clusters at brighter luminosities than in poorer systems. The χ^2 -test also shows that the EMSS poor cluster LF matches reasonably well with that of poor groups; it resembles least the rich cluster LF.

In the *V* band, the EMSS poor cluster LF slopes generally match those of the cD-dominated MKW/AWM poor clusters as well as that of the vastly different Local Group⁴. All of them show flat LFs of $\alpha \approx 1$. A major difference between the poor clusters (both the EMSS and MKW/AWM samples) and the Local Group is in the Schechter characteristic magnitude – the

⁴The dominant galaxies of the Local Group are spirals, not ellipticals or cD galaxies.

Table 3.6: Parameters for LF fits to a single Schechter function from the literature in different bands and environs.

Environs	Magnitude range	M^*	α	Reference
B-band				
Field	$M_B \leq -17.5$	-20.94 ± 0.1	-1.30 ± 0.2	Folkes et al. (1999)
Poor groups	$-23.2 \leq M_B \leq -17.2$	-20.84 ± 0.1	-1.00 ± 0.2	Muriel et al. (1998)
Rich clusters	$-22.5 \leq M_{bJ} \leq -19.0$	-21.54	-1.21	Colless (1989)
Rich clusters	$-22.5 \leq M_{bJ} \sim -18.0$	-21.23 ± 0.1	-1.4 ± 0.1	Valotto et al. (1997)
V-band				
Local Group	$-22.0 \leq M_V \leq -10.0$	-20.00 ± 0.1	-1.09 ± 0.1	Pritchett & van den Bergh (1999)
Poor clusters	$-23.0 \leq M_V \leq -17.0$	-21.57 ± 0.1	-1.07 ± 0.1	Yamagata & Maehara (1986)
Rich cluster	$-23.0 \leq M_V \leq -18.0$	-21.45	-1.17	(Abell 665) Wilson et al. (1997)
R-band				
Field	$-22.5 \leq M_R \leq -18.5$	-21.80 ± 0.1	-0.70 ± 0.1	Lin et al. (1996)
Poor groups	$-22.5 \leq M_R \leq -18.5$	-23.11 ± 0.1	-1.30 ± 0.1	Zabludoff & Mulchaey (2000)
Rich clusters	$M_R \leq -19.8$	-22.66 ± 0.66	-1.24 ± 0.22	Lugger (1986)
Rich clusters	$-24.9 \leq M_R \leq -18.9$	-22.63 ± 0.11	-1.09 ± 0.08	Gaidos (1997)

knee of the Schechter LF in the Local Group occurs a magnitude fainter than in the former. The EMSS poor cluster LF in the V filter is marginally flatter than that of the very rich X-ray luminous cluster Abell 665. Not surprisingly, the χ^2 -test rejects the hypothesis that our poor cluster galaxy magnitude distribution is statistically equivalent to that of the Local Group.

In the R -band, the EMSS poor cluster LF, though flat, is steeper than that of rarefied regions (Lin et al. 1996) but not so steep as the rich clusters. The flatness may be due to a significant “dip” in the LF seen around $M_R \sim -20.5$ that appears to be a general feature of the rich cluster LF (e.g., in the Coma cluster, Biviano et al. 1995). Unfortunately, the point at which the slope steepens in rich clusters ($M_R \sim -19$) is also the one where the completeness of our LF determination ends. Our R -band LF is quite different from its counterpart in X-ray luminous poor groups which show a far steeper faint-end and whose M^* is nearly 1.3 mag brighter. The χ^2 -test indicates that the Schechter parametrization of the EMSS poor cluster R -band LF is closest to that of rich clusters determined by Gaidos (1997).

3.4 Summary and Discussion

3.4.1 Is there a universal LF?

Observational studies have churned up various — often conflicting — results about the shape of the faint region of the luminosity distribution and the value of the characteristic luminosity across different galaxian environs, even among clusters of various morphologies, richness, X-ray luminosity and velocity dispersion. These lead to contradictory claims of the universality of the

luminosity distribution.

There have been two prongs to our analysis of the poor cluster luminosity functions here. First, we determined whether the individual poor cluster LFs are similar. The conclusion from Table 3.3 is that the individual LFs including all but the most luminous galaxies are statistically equivalent. Of course, with this small sample, one cannot discriminate finer differences without large statistical uncertainties. Indeed, most cluster studies (e.g., Schechter 1976; Dressler 1978; Luger 1986; Colless 1989) find the bright-end of the LF do appear similar in their general form. Combining the individual poor cluster LFs successfully forms a composite LF from which no individual cluster LF differs greatly (see Table 3.4). Further, the agreement between the individual galaxy magnitude distributions and the composite LF at various faintness limits implies that, if these clusters are indeed different, their galaxy luminosities nevertheless converge statistically and approach a hypothetical “poor cluster” LF.

Next we asked if the LFs are invariant across the environs from the sparse field, through poor systems, all the way to the dense rich clusters. As we saw in Sec. 3.3.6, LF measurements in different colors for the same environment have yielded different results for the Schechter function parameters. Bearing this in mind, our results are not inconsistent with the hypothesis that poor clusters have a flatter LF compared to rich clusters. Specifically, the EMSS poor cluster *B* and *V* LF match their counterparts for poor clusters but not those of either the field or rich cluster environment. In contrast, the *R* LF better matches the corresponding rich cluster LF than the poor group LF and is inconsistent with that of the much less dense fields environs.

Perhaps the variations in the LF slope in the literature may be artifacts of imposing a single Schechter function on the composite LF. The canonical Schechter LF — which glosses over differences in LFs of individual Hubble/spectral types, environments, and redshifts — is unlikely to be an adequate descriptor of the true galaxy luminosity distribution (BST88; Ferguson & Sandage 1991). Rather, the LF of each environment may best be parametrized using galaxy morphological types and surface-brightnesses. Further, the variations in M^* between environs may be on account of the strong correlation of the two Schechter parameters and may not be indicative of strong physical variations at the bright end.

However, even without recourse to parametric fits, there exist real differences in LF at the high galaxy density regime, i.e., between rich clusters, with several not showing the conspicuous upturn at the faint end created by increasing dwarf galaxy contributions (e.g., Phillipps et al. 1998). Either these clusters do not contain a similar and significant dwarf population or the dwarfs begin to appear only at fainter magnitudes (i.e., the dwarf-to-giant ratio is smaller). Deeper photometry may, in principle, help verify if our poor clusters too show dwarfs at much fainter luminosities that would steepen the LF.

Though the jury is still out, correlations of the LF (at least at intermediate luminosities) with cluster morphology and richness (e.g., Garilli et al. 1999) refute the claim of several studies (e.g., Colless 1989; Trentham 1998) for a universal LF.

3.4.2 Is the LF determined by Nature or Nurture?

Thus far there is no incontrovertible support for a luminosity function that is invariant with environment. But when do the variations set in? The differences in LF from field to clusters, between poor groups and rich clusters, and among clusters themselves, may be due either to biasing at galaxy formation (e.g., Dekel & Silk 1986) or to environmentally-sensitive differences in the strength of mechanisms that alter the LF.

Observations provide evidence both for and against the model of biased galaxy formation. In some rich clusters dwarf galaxies are less centrally clustered than the giants and form a significant halo around the cluster outskirts (Driver, Couch & Phillipps 1998). Moreover, richer and denser clusters may have a preponderance of giant galaxies relative to dwarfs (Valotto et al. 1997; Garilli et al. 1999). Both these vouch for biasing in the galaxy distribution. In contrast, poor groups in the nearby universe, dwarfs are more numerous (Ferguson & Sandage 1991) and more tightly clustered in center than giant galaxies, indicating anti-biasing at work at least at such small richness and high densities (Zabludoff & Mulchaey 2000).

In the poor clusters we examine there is no strong evidence for variations in the clustering scale — in either luminosity or color — of the member galaxies (Sec. 5.4). Luminosity segregation in terms of smaller characteristic radial separations for galaxies with $-21 < M_V < -20$ is however marginally evident in MS0301 and MS0002; this could have occurred through two-body relaxation over a Hubble time subsequent to violent relaxation in the cluster core (as we discuss in Sec. 5.6). Still, overall mass segregation is not important in our sample. As our areal coverage of these clusters is not incomplete, the LF or equivalently, the mass function, being similar in different cluster regions implies that spatial variations due to biased galaxy formation are not prominently noticeable in the poor cluster.

An implication of the flat LF in the poor clusters studied here is that dwarf galaxies are usually less abundant in poor systems relative to the more populated clusters. Can we infer the kind of dwarf galaxies that engender the variations? In the field, blue Magellanic-type irregular galaxies dominate the faint-end of the LF (e.g., Marzke et al. 1994) while in galaxy groups and clusters the dwarf spheroids contribute to the steep slope (e.g., Ferguson & Sandage 1991; Trentham 1997). The similarity of the EMSS poor cluster LFs across the wavelengths (B to R) implies that if dwarfs exist in these systems, they are unlikely to be very actively star-forming. Indeed, in dense environs, star-formation is preferentially suppressed in the fainter late-type spirals and irregulars compared to the bulge-dominated early-type galaxies (Balogh et al. 1996).

Our color-magnitude analysis (Sec. 4.2) shows no definitive support for luminosity evolution. The latter cannot then account for the inconsistency of M^* , i.e. the change-over from giant to dwarf galaxies, in the LFs of the EMSS poor clusters and other environments. Now assuming the form of the LF is universal at galaxy formation (though we argue against this), the comparison of LFs in different density environments should shed light on the differences between galaxy evolution in the field and clusters, and thus on some of the dynamical interactions occurring amongst non-isolated galaxies. The agents that affect the growth, interplay and ultimate evolution of galaxies — dynamical friction, mergers, multiple mergers, cannibalism, harassment, etc. — must modify the primeval LF.

The relaxation times for our sample of poor clusters are smaller than the Hubble time (Sec. 5.6). The quantity ΔM_{12} indicates our clusters are Bautz-Morgan Type I objects or in other words, dynamically mature clusters. (This class of clusters are also the most frequent and the brightest in X-ray selected catalogs.) Furthermore, the EMSS poor cluster velocity dispersions derived from the $L_X - \sigma$ correlations are somewhat high ($\approx 500 \text{ km s}^{-1}$, or between half or equal to those of rich clusters), resulting in lower merger rates for the galaxies. However, it is likely that though efficient merging is not occurring at the present in virialized clusters, it did take place at a very early stage in the system lifetime (Merritt 1984; Dubinski 1998).

But, the current sample of poor clusters are for the most part irregular, unrelaxed systems. A few galaxies may then show small relative velocities between themselves, which do allow slow two-body collisions leading to mergers to occur even at the present. Galaxy interactions and active mergers may then be prevalent in the clusters. Indeed, there are a number of bright ($M_V < -20$) blue galaxies in the EMSS clusters (Table 4.4.3); some show definite indications of collision with their neighbors. The interaction process may enhance star formation for a few million years, brightening the resultant galaxy and moving it from a fainter part of the LF to the brighter part for a small fraction of the Hubble time. Perhaps surprisingly, the optical luminosity function of compact groups of galaxies, which are expected to host the largest merger rates among all galaxian environments, shows little evidence for an interaction-induced luminosity enhancement relative to control samples (Sulentic and Rabaça 1994). The unenhanced luminosity functions may then be the result of a failure of interactions to induce star formation in these particularly dense environments, in keeping with the situation in rich clusters (Balogh et al. 1996).

The rarity of bright galaxies (reflected in the clusters being poor), and the flatness of the LF at luminosities of $-21 \leq M_V \leq -19$ indicate that the large, bright galaxies tended to merge. The large luminosity of the first-ranked cluster members — likely to be the products of such mergers — reflects their dynamical origin. For instance, the dips in the LF of MS1306 trace the depletion of bright galaxies through mergers that may have formed the body of the BCM. Thus as the cluster evolves dynamically, so does its galaxy LF. We cannot however claim any *conclusive* support of dynamical friction or galactic cannibalism in these clusters though ΔM_{12} is certainly one aspect in favor of the scenario. The remarkable homogeneity in the first-ranked galaxy magnitudes implies that such mergers must have been at early epochs, and later evolution must have been similar in the various objects (see discussion in Chapter 6).

All this also leads to the question of what reduces the cluster richness. The smaller richness of the EMSS poor clusters, i.e., with several bright ($m < m_3 + 2$) galaxies ‘missing’ from an otherwise rich cluster, is not readily explained as being solely due to mergers in either the early history of the cluster or in its recent past. An explanation that offers itself is that the EMSS poor clusters have smaller characteristic sizes than the Abell rich clusters (see Table 5.2), and so accommodate fewer galaxies than their larger thus richer counterparts. Indeed, such poor clusters appear to be smooth extensions of the clustering spectrum to lower galaxy population and mass from the rare rich clusters.

Many of our conclusions are not emphatic due to the limited range (to within $M^* + 3.5$, i.e., $0.05L^*$) over which we construct the LF, the low signal-to-noise ratio dictated by the small

number of galaxies in each magnitude bin, and the field contamination likely at faint luminosities due to lack of membership information. Further, faint galaxies — both reasonably luminous ones at large distances and dwarf galaxies in the local Universe — and low surface brightness galaxies may remain undetected due to the threshold isophotal value of surface brightness adopted in the detection algorithm. Since the seeing in our images is of the order of the scale sizes of the smaller galaxies, it further exacerbates the problem. We cannot therefore usefully relate the form of the LF to variations in galaxy formation or relative efficacy of post-formation dynamical influences between the different environs.

Our study would be more conclusive if data at much fainter magnitudes (2-3 mags below our current limit) were included. More insightful studies would additionally incorporate the galaxy morphological types and their surface brightness into building multivariate luminosity functions. It is essential to determine the luminosity distribution of poor clusters at all redshifts since these are likely to be found in increasing numbers at higher redshifts, i.e., larger lookback times, in hierarchical structure formation scenarios.

Chapter 4

Evolutionary State of the Cluster Galaxies

*From a fleeting glimpse [astronomers] reconstruct a whole history.
– Cecilia Payne-Gaposchkin*

4.1 Avant-Propos

Galaxies have been clearly evolving — as opposed to merely aging — with cosmic time, as traced by their morphological mix, colors or star formation rates, and interactions over a wide range of redshifts and across various environments. Now, galaxies are not isolated; most experience several collisions or tidal interactions that are strong enough to alter their structure and content. The galaxian environs decides how frequent galaxy interactions and mergers are, what fraction of galaxies are merger remnants, etc. A noticeable effect of the cluster environment is on galaxy colors: the mean galaxy colors are redder in the cluster centers than in the field. Tidal interaction, collisions, and mergers can induce star formation (Bushouse 1987, Kennicutt 1998) and enhance the possibility of nuclear activity, thus making the galaxies bluer. Contrary influences such as ram-pressure stripping of gas, galaxy harassment, even a huge starburst that consumes all the gas can quench star formation and drive galaxies toward red colors (see also Sec. 1.2.2). On the other hand, in isolated objects, continuous infall of gas from their surroundings may fuel star-formation throughout their lifetime.

Temporal evolution of galaxies can involve transformation of their morphologies, and changes in star formation activity, or equivalently, the stellar population content; this is not necessarily independent of the environment. The number of interacting and merging objects is significantly higher at large distances than among nearby galaxies, irrespective of environment. Though luminosities of galaxies do not evolve greatly below redshifts of about 0.5, their colors do vary, reflecting important episodes of star formation. In the high-redshift field, for instance, a large fraction of galaxies appear to be undergoing a strong episode of star formation, with many being bluer in their rest-frame than a typical local irregular galaxy. In cluster galaxies too star formation activity changes rapidly even at modest redshifts of $z \sim 0.2$ (e.g., Butcher & Oemler 1984). However, elliptical galaxies in particular — be they in the field or clusters — seem to evolve passively even up to $z = 1$ (Dickinson 1995). Further, the strength of star formation in cluster galaxies both at low and moderate redshifts is systematically smaller than that in field members for the same galaxy luminosity and morphology (e.g., Balogh et al. 1998).

If field and cluster galaxies do evolve along different paths, then the intermediate environs of poor

clusters could provide clues to the connection between the extreme environments, and illuminate how galaxy evolution depends on the density of the neighborhood. Even within a cluster, depending on the galaxy orbit, i.e., on the galaxy density and velocity dispersion, and on the density and temperature of the intracluster plasma, a given galaxy may find itself subject to varying forms and degrees of interaction as a function of time. Poor clusters, that have lower velocity dispersions than rich clusters but comparable X-ray luminosity, and higher galaxy densities than the field, provide an environment conducive to galaxy interactions different from both these extremes of galaxy density. The fraction of early-type galaxies in poor groups (less populated than the clusters we study in this thesis) varies from $\sim 25\%$ characteristic of the field to $\sim 55\%$ like that of rich clusters (Zabludoff & Mulchaey 1998). The early-type poor group members have similar star formation histories as their counterparts within substructures in rich clusters (Zabludoff & Mulchaey 1998). This probably points to galaxy-galaxy encounters, rather than the larger cluster environment and associated mechanisms like ram pressure stripping or galaxy harassment, as being the most influential mechanism in altering star formation histories and morphologies. Further, the fraction of blue galaxies in poor clusters remains virtually constant with redshift whereas for rich clusters, it decreases steadily from high- z to local objects (Allington-Smith et al. 1993). This may indicate that the morphology-environment relation must be of recent ($z < 0.25$) origin, and steepening rapidly with cosmic epoch.

This chapter presents color-magnitude and color-color analyses of the galaxies in our sample of poor clusters using the photometric catalog whose construction we reported in Chapter 2. We determine the correlation between the colors and luminosities of bright galaxies in the clusters. We then study the outliers from the bright-end of the color-magnitude relation, which are unexpectedly blue (i.e. star-forming), as well as very red (which could turn out to be objects far more distant than our clusters).

while others

some of

4.2 The Color-Magnitude Relation

In an overwhelming majority of clusters observed so far, the more luminous galaxies tend to have systematically redder colors. Since the luminous cluster members are usually of early morphological types, this reddening trend implies the existence of a color-magnitude relation (CMR) for early-type galaxies in clusters. The CMR is not only a tight correlation with small scatter but also is applicable to field ellipticals (Baum 1959; Kodama, Bower & Bell 1999) and to both E and S0 galaxies with the same slope and zero point (Visvanathan & Sandage 1977, VS77 hereafter). While the cluster disk galaxies also conform to a CMR, their color-luminosity relation is steeper and its scatter larger (Pierce & Tully 1992). The CMR exists with virtually similar characteristics in all clusters/groups at both low redshifts (e.g., VS77; Bower, Lucey, & Ellis 1992; Smail et al. 1998; Metevier, Romer, & Ulmer 2000) and high redshifts (e.g., Stanford, Eisenhardt, & Dickinson 1998, hereafter SED98; Ellis et al. 1997; Kodama et al. 1998; van Dokkum et al. 2000). The clusters, both regular and irregular, and with X-ray luminosities ranging over two orders of magnitude, exhibit no significant differences among themselves.

4.2.1 The Form and Causes of the Correlation

The existence of the early-type CMR in the field and in the cores of rich clusters, and its small dispersion suggest that the effect is not in response only to special conditions within clusters. The CMRs in the early-type and spiral galaxies may have different origins: the CMR for ellipticals may be due to variation in metal abundances with luminosity (see below) while that for disk galaxies may have to do with the mixture of different stellar populations and complex effects of dust. Nevertheless, the tightness of the CMR and its spectroscopic counterpart — the relation between the magnesium absorption line index and velocity dispersion — together relate the luminosity and mass of the galaxies to their stellar constitution and metal abundance.

The universality of the CMR lends itself to cosmological applications. It acts as a cosmological distance estimator (if galaxies evolve passively). The zero-point of the CMR at various redshifts provides information on the luminosity evolution of the early-type galaxies. Its small scatter indicates that the bulk of the stars in cluster ellipticals is coeval and constrains the epoch of elliptical galaxy formation to $z \approx 2$. The slope of the CMR sheds light on the *differential* behavior of galaxian photometric properties as a function of luminosity or, indirectly, galaxy mass. The slope finds explanation in two alternative interpretations:

- it reflects different mean stellar ages, with redder galaxies being older (e.g., Aragon-Salamanca et al. 1993)
- it is due to galaxy metallicity increasing with luminosity (Larson 1974; Arimoto & Yoshii 1987, AY87 hereafter; Ellis et al. 1997, SED98).

There are indications from its evolution with redshift that the CMR is primarily due to metallicity effects (e.g., SED98, Kodama et al. 1998) though the scatter indicating recent star formation in the presumably “coeval” galaxies may accommodate the varying age explanation (e.g., Worthey 1994). The luminosity–metallicity relation arises because more luminous (equivalently, more massive) galaxies have greater binding energies and can support star formation to completion; they can then retain more of the metal-enriched ejecta from their supernovae (see AY87 for a detailed exposition). If galaxies assemble in a hierarchical fashion rather than at a synchronized epoch, then the CMR could be due to massive ellipticals forming from the mergers of more massive disk systems that already obey a mass–metallicity relation (Kauffmann & Charlot 1998). Alternatively, if more luminous ellipticals are remnants of galaxy merging accompanied by very rapid star formation, then less gas stripping and a greater amount of metal enrichment occur, leading also to a tight CMR (Bekki & Shioya 1997).

4.2.2 Analysis

To examine the CMR in quantitative terms, we perform a linear fit to the $(B - V)$, $(V - R)$ and $(R - I)$ colors against V -band magnitudes. We restrict the fit to the inner 0.5 Mpc projected radius of the clusters to reduce the relative contamination by field objects and maximize the prominence of the CM sequence. We select early-type galaxies by elimination: through visual examination of individual bright galaxies, we exclude those which show signatures of disks or interactions.

This ensures, to a first approximation, that the finally selected set of objects is predominantly early-type, and makes clearer a red sequence in the cluster CMR. Further, spectro-evolutionary models predict that the early-type (E/S0) cluster galaxies at a given redshift are redder than similar objects at lower redshifts as well as all other morphological types of galaxies at the same distance or lower redshifts.¹ Therefore, the red sequence mostly represents the poor cluster early-type galaxies, with some probable contamination due to higher redshift late-type galaxies. The dispersions in the colors at a given magnitude seem to be of the order of the photometric errors. (Since we do not have membership information, we cannot rule out the outliers as being non-cluster galaxies.) For such a sample, the traditional Chi-square technique can result in a poor fit due to its sensitivity to outlying data points. Therefore, we compute the color-magnitude relation (CMR) for the brighter galaxies using a least absolute deviation (LAD) algorithm with recursive 3σ rejection. The LAD technique, which provides linear fits robust to the inclusion of outliers, turns out to be more appropriate in this instance.

We use galaxies in the magnitude range roughly between $M^* - 2.5$ and $M^* + 1.2$ in the LAD fit, where $M_V^* = -21.0$ for $H_0 = 50 \text{ km s}^{-1} \text{ Mpc}^{-1}$ (see Table 3.5). This is well within the average limiting magnitude of our sample (*cf.* Fig. 2.1), so incompleteness effects are minimal. The use of fixed apertures in determining the magnitudes of the galaxies can introduce a bias in the color-magnitude relation if there exist radial color gradients within the galaxies. For the brightest cluster member (BCM) of MS1306 we find that internal radial color variations cannot be neglected (Sec. 6.4.1). For this cluster, therefore, we have had to ignore the BCM while fitting the CMR; inclusion always created a sequence whose slope was much too large and with sign the opposite of those of the other clusters. We give uniform weights to all the data points, and run the fits through either three or four iterations. We always reached a final solution whose accuracy was within 1% in the absolute deviation. There are rather few galaxies (between 12–20 in each cluster) to result in a perfect fit. In each case, then, we check by eye to ensure that the fits are indeed good.

4.2.3 Results

Figures 4.1 and 4.2 present the K-corrected $(B - V)$ vs. V , $(V - R_C)$ vs. V , and $(R_C - I_C)$ vs. V color-magnitude diagrams for all the clusters in our sample (except for MS0002 for which we do not possess good photometric calibration in the B -band and can show only the $(V - R_C)$ vs. V diagram). Filled symbols represent galaxies within 0.5 Mpc (for MS0301 and MS1306) and 0.7 Mpc (for MS0002 and MS0735) of the brightest cluster galaxy, respectively. The solid lines in Figs. 4.1 and 4.2 represent the linear fits to the CMRs with parameters listed in Table 4.1. Dotted lines show the width of the sequence. Upward-arrows in the figure indicate the V magnitude of the faintest galaxies included in the linear fits of the CMR for each cluster. The superimposed dashed lines represent the correlation expected from the Virgo CMR of VS77 at the poor cluster redshift. We transform the original CMR of VS77 into the Johnson-Cousins system using the calibration

¹Since the morphology-density relation exists even in the field, the mere existence of a slight over-density of red galaxies does not a cluster locate. Despite this, the cluster red sequence, even if it has significant scatter, generally represents a distribution not found in the cumulative field that would span a large redshift range (Gladders & Yee 2000). One way to distinguish a genuine cluster from a clumpy field would be through its highly luminous and spatially extended X-ray emission.

in Sandage & Visvanathan (1978). The relations then read: $(B - V) = -0.0180 V + 1.043$ and $(V - R) = -0.0088 V + 0.944$.

Even though the data are field-contaminated at all magnitudes and colors, our poor clusters all manifest a distinct locus of galaxy colors in the color-magnitude diagram. The optical colors of the bright cluster galaxies form a sloping ridge such that the fainter galaxies are bluer, and are bounded by the red envelope. Early-type galaxies generally dominate the bright-end of the luminosity function and, if this locus is similar to the one in rich clusters, the bright, redder end of color-magnitude diagram corresponds to the region of passively-evolving elliptical galaxies. At the fainter magnitudes ($V > 22$ mag), the lack of very blue galaxies is due to incompleteness; therefore, the CMR will not be too well defined at the faintest luminosity bins of our clusters. The general appearance broadly resembles the CM diagrams of rich clusters both nearby and distant. (It would have been instructive to create such a diagram for field galaxies in the neighborhood of the poor clusters, to establish the cluster-member-only contribution to the CMR. But the limited size of our CCD images disallow such a project.)

Table 4.1 summarizes the parameter fits to the CMRs of the poor clusters. It lists for each CMR the range of galaxy V magnitudes considered in the linear fit, the zero-point color and the slope of the resulting line. The last column gives the mean absolute deviation for the data points in fitted color (which does not include systematic offsets in the photometry). Below, we shall examine each aspect of the CMR, *viz.*, its slope, zero-point, and scatter.

Table 4.1: The linear fits to the color-magnitude relations.

Cluster	V mag range	Color	Slope	Intercept	Deviation
MS0301	[-22.30,-19.30]	$(B - V)$	-0.137	2.907	0.14
		$(V - R_C)$	-0.023	0.745	0.03
		$(R_C - I_C)$	-0.030	1.313	0.41
MS1306	[-22.07,-18.67]	$(B - V)$	-0.053	1.787	0.08
		$(V - R_C)$	-0.011	0.794	0.04
		$(R_C - I_C)$	-0.046	1.590	0.07
MS0002	[-22.43,-18.63]	$(V - R_C)$	-0.017	0.917	0.03
MS0735	[-22.20,-19.84]	$(B - V)$	-0.012	1.015	0.15
		$(V - R_C)$	-0.027	1.234	0.07
		$(R_C - I_C)$	-0.019	0.971	0.04

The *slope* of the CMR is usually steeper in $(B - V)$ than in the other colors, suggesting that the $(B - V)$ colors are more sensitive to V luminosity than either the $(V - R_C)$ or $(R_C - I_C)$ colors. This is consistent with the pioneering work of VS77 that showed that the slope of the CMR is strongly wavelength-dependent, with maximum sensitivity near the 4000Å break. This further suggests that the slope of the number counts for galaxies to the same limiting magnitude is steeper at shorter wavelengths (see Chapter 3 for the cluster luminosity functions).

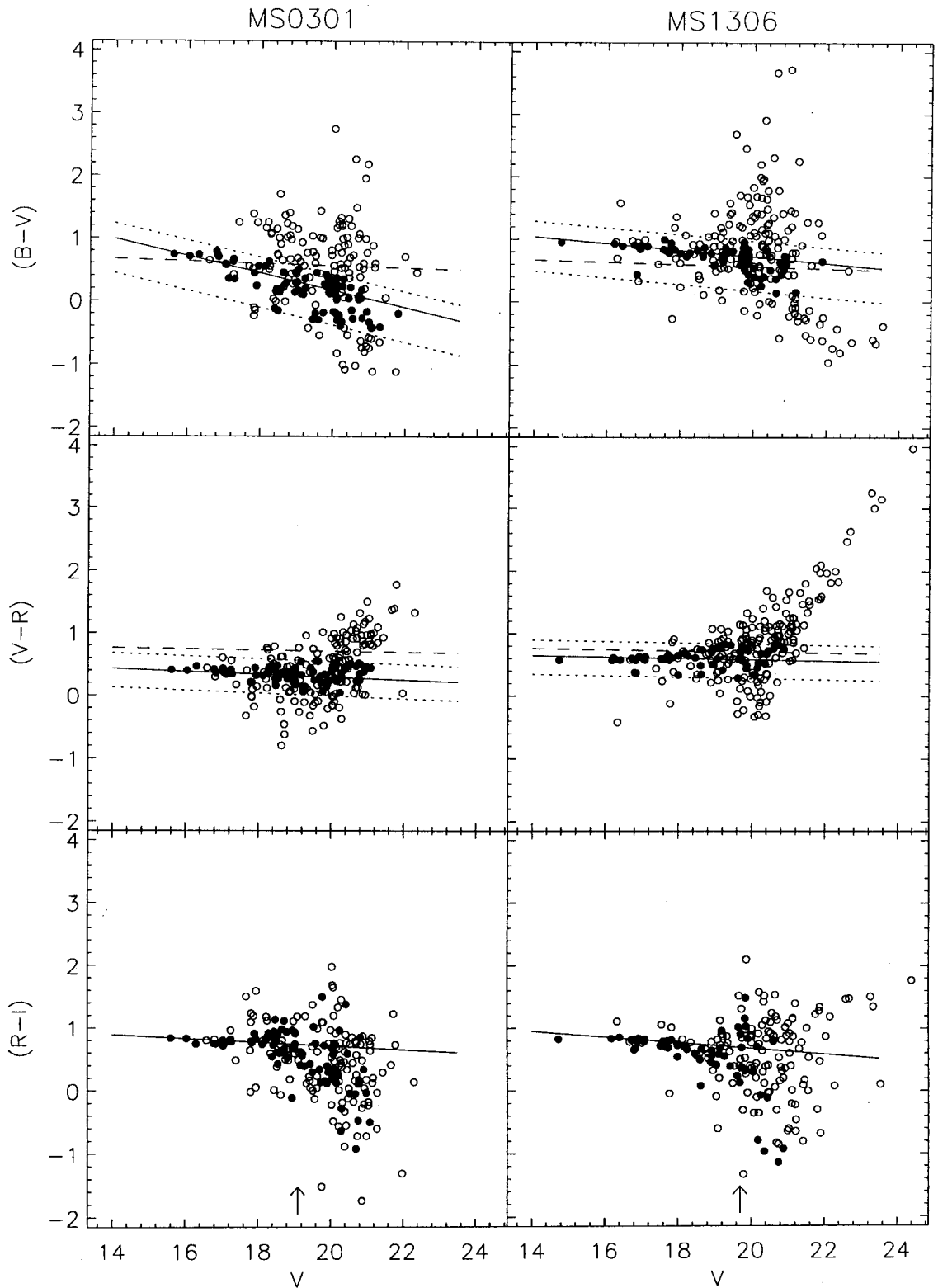


Figure 4.1: Color-magnitude diagrams, $(B - V)$ vs. V , $(V - R_C)$ vs. V , $(R_C - I_C)$ vs. V for galaxies within 0.5 Mpc of the center of MS0301 and MS1306. The solid line in each panel indicates the fit of a linear relation representing the locus of early-type galaxies in the clusters. Filled symbols represent galaxies within the $B - V$ “sequence” in the top panel, and within the $V - R$ “sequence” in the bottom two panels. See text for the definition of “sequence”. The arrows indicate the faintest V magnitude included in the fits. The dotted lines envelop the width of the color-magnitude sequence. The dashed lines represent the CMR expected from the Virgo cluster relation of Visvanathan & Sandage (1977) appropriately redshifted.

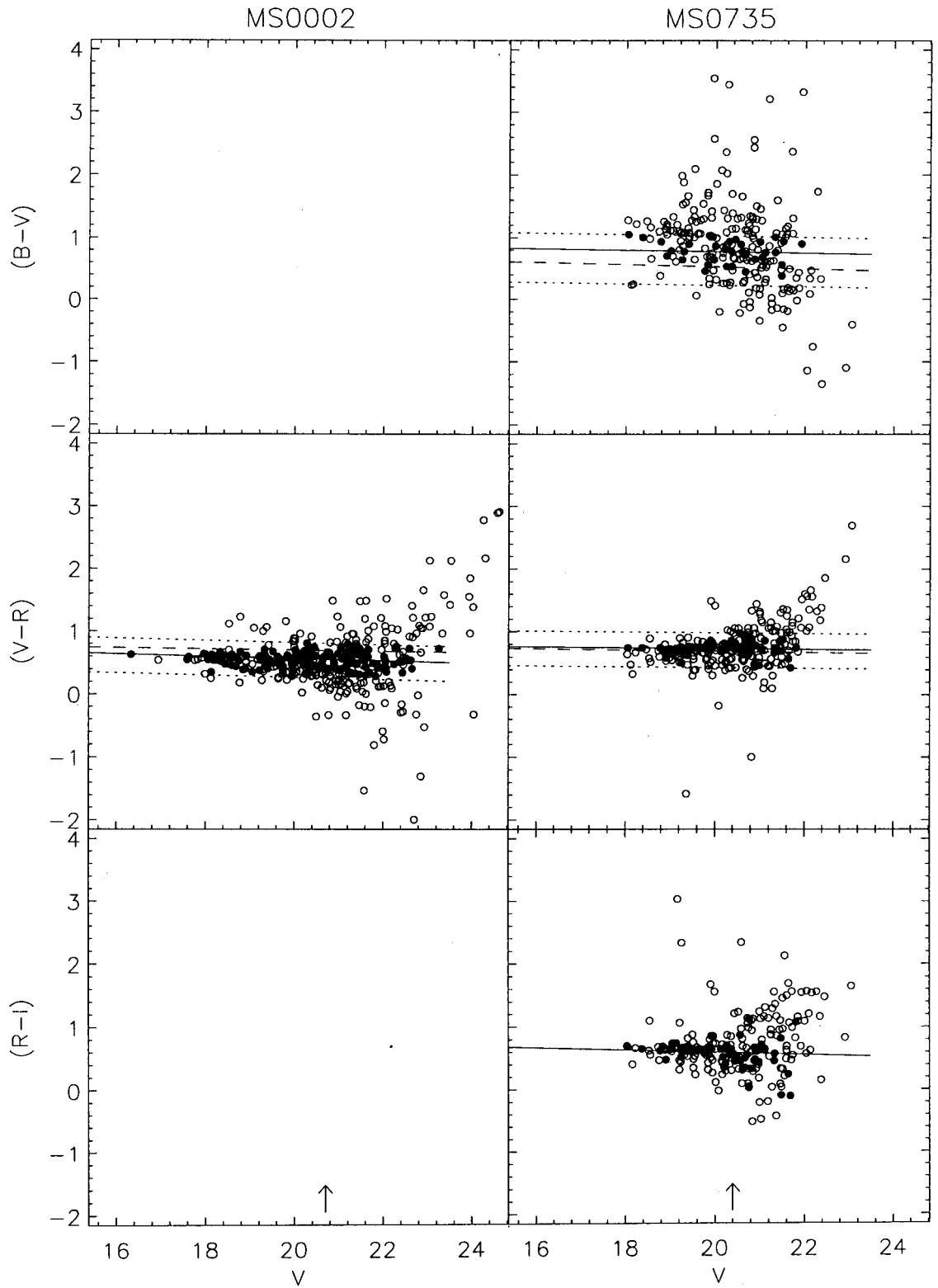


Figure 4.2: Color-magnitude diagrams, $(B - V)$ vs. V , $(V - R_C)$ vs. V , $(R_C - I_C)$ vs. V , for galaxies within 0.7 Mpc of the BCM in MS0002 and MS0735. Symbols as in Fig. 4.1.

Moreover, the slope (and scatter, see below) of the CMRs of the different poor clusters are roughly equal, and are comparable to that of Virgo and local rich clusters. This is clearly visible in Fig. 4.1 and Fig. 4.2 where all the $(B - V)$ vs. V and $(V - R_C)$ vs. V CMRs (but that of the $(B - V)$ vs. V correlation of MS0301) are parallel and nearly co-incident (see discussion about the zero-point below) with the fiducial Virgo linear relation whose corresponding slopes are -0.018 and -0.0087 (VS77, transformed by us into $(B - V)$ and $(V - R_C)$ using the relation in Visvanathan & Sandage 1978).

One expects that, unlike the situation in nearby rich clusters, early-type galaxies constitute not more than half of the galaxy population in poor clusters. Additionally, many galaxies in the lines-of-sight to our poor clusters also show signs of merging. Even these interacting systems appear to lie close to the CMR defined by the galaxies we determined to be free of disks at first glance, though most are slightly bluer by $0.07 + / - 0.02$ mag than the early-type sequence. Since there exists a strong trend of the slope and scatter of the CMR to vary with morphology, such that spiral galaxies have a steeper slope and larger scatter in their colors than the early-type galaxies, it is not quite surprising that the slopes we present are marginally steeper than those in rich clusters. In fact, in previous poor cluster CMR studies, just determining the CMR seems to have been exceedingly difficult if not actually impossible due to the paucity of early-type galaxies (e.g., Allington-Smith et al. 1993, AS93 henceforth). The robustness of the CMRs we present is particularly interesting since we have little membership or morphological information for the galaxies in the line-of-sight. Our results show that early-type/bright galaxies do indeed populate the centers of our X-ray luminous poor clusters in significant numbers and they resemble the E/S0 members of nearby rich clusters.

As we have stated, the formation and evolution of the population of massive (elliptical) galaxies remains a matter of lively debate. But let us now assume that all elliptical galaxies are equally old, and that the CMR is due to mean metallicities of galaxies varying as a function of galaxy luminosity or equivalently, galactic mass. Then we can apply the evolutionary model of AY87 to the CMR to determine the metallicity variations in the cluster galaxy population. Using the slopes for the $(V - R_C)$ color indices in Table 4.1, we find that, for every decade change in color, the metallicities of MS0301, MS1306, MS0002 and MS0735 vary as factors of 0.12, 0.06, 0.09 and 0.14, respectively. In other words, the metallicities of the poor cluster galaxies are consonant to within 10% over the luminosity range of roughly $M^* - 2$ to $M^* + 1.5$. Note that the $(B - V)$ CMR slope of MS0301 indicates a change in metal abundance of 0.6 per decade change in color; this high value perhaps evinces both the sensitivity of the bluer colors to mass and the contamination due to non-early-type galaxies in the cluster core. The order-of-magnitude variation in X-ray luminosities among the clusters does not appear, at this level of analysis, to make a difference in the mass-metallicity correlations of the cluster galaxies.

There are only small offsets ($< 2\sigma$) of the intercept of the CMRs of the poor clusters from that of the Virgo cluster (the exception is MS0301 for which the CMRs are offset by about 3σ). The co-incident of the color-magnitude relation predicted from that of the Virgo cluster confirms the lack of luminosity evolution in the early-type cluster galaxies over the modest redshifts ($0.083 \leq z \leq 0.216$) of our sample. Further, it shows that our photometry and adopted absolute magnitude normalizations are reasonably accurate.

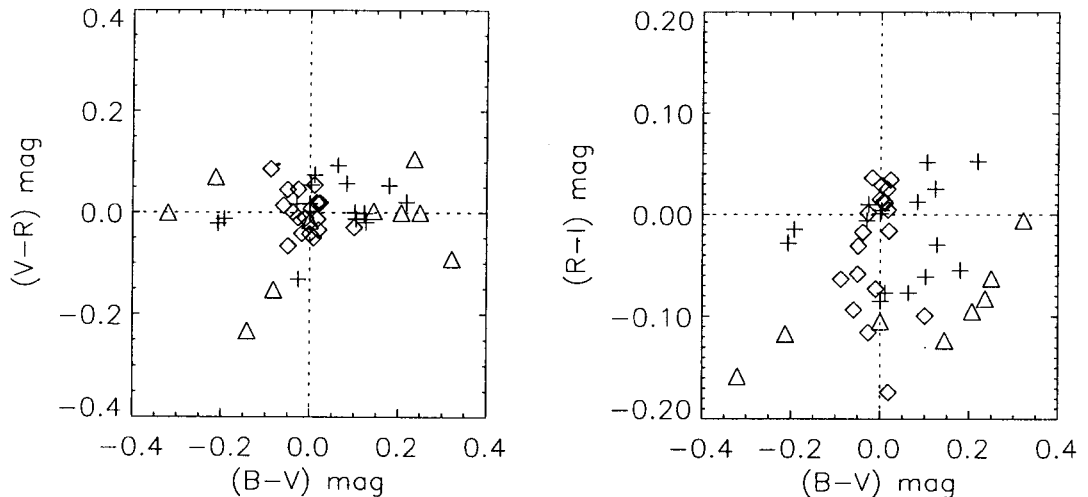


Figure 4.3: Color residual from the CMR for $(V-R)$ (left panel) and $(R-I)$ (right panel) against $(B-V)$, showing the correlation and intrinsic scatter about the color–magnitude relations for the poor cluster “sequence” galaxies with $M_V \leq -20$ mag. Crosses denote galaxies in MS0301, diamonds in MS1306 and triangles in MS0735.

Garilli et al. (1996, G96 henceforth) found the CMR of MS0301 to be redder by about 0.2 mag in $(g-r)$ than predicted from the Virgo relation. We find, on the contrary, that its $(V-R)$ vs. V correlation lies *bluward* of the latter. G96 claim that the difference of 0.2 mag between the expected normalization and the observed CMR, though of the order of the scatter in present-day bright cluster ellipticals, is well clear of their statistical errors. It is worth noting that G96 observed this cluster under seeing conditions of > 2 arcsec (their Table 2) and the color–magnitude diagrams they present for it contain only about twenty galaxies. Another subject of concern is with correcting the photometry in this cluster for Galactic extinction. Though MS0301 lies at high Galactic latitude, $(l, b) = (164, -37)$, the obscuration in its direction is anomalously large ($A_B = 0.72$ mag, Schlegel et al. 1998) due to a “spur” of Galactic clouds along this longitude. Now, G96 rule out any errors in their Galactic absorption corrections, derived from the N_H values of Stark et al. (1992). Yet another possible conclusion is that the canonical value of $R_V = 3.1$ is probably not valid for this spur region.

It is of interest to weigh the scatter in the CMRs relative to the photometric error to assess the presence of an intrinsic component to the scatter in each correlation, i.e., of a “cosmic dispersion” in the CM effect. The dispersions about our CMRs are similar to our photometric errors of about 0.07 mag at $V = 20$ mag, therefore we are at the limit of what we could expect with the accuracy of our observations for $(V-R)$ and $(R-I)$ indices. Accounting for the photometric errors leaves us with an excess scatter of typically 0.1 mag in $(B-V)$ which cannot be dismissed in this way. The $(B-V)$ excess could be due to an admixture of disk galaxies with the E/S0 galaxies (also seen as a slightly steeper CMR in MS0301) or a genuine scatter due to astrophysical reasons.

A simple demonstration of the presence of the intrinsic component in the scatter is to plot the color residuals about our CMRs against one another. Figure 4.3 shows residuals of $(B-V)$

against $(V - R)$ for galaxies with absolute magnitude $M_V \leq -20$ mag and within 0.5 Mpc of the cluster center. (This is possible for three clusters - MS0301, MS1306 and MS0735). A trend manifests itself; galaxies that lie on the blue side of the $(B - V)$ CMR do so also in $(V - R)$. While the $(R - I)$ vs. $(B - V)$ trend is weaker (and appears different for the different clusters), it nevertheless exists. Since the latter set of axes are independent, only an unfortunate coincidence of systematic errors, similar in the photometry of all the clusters, would produce such an effect. Due to the improbability of such an occurrence, we conclude that a part of the scatter in the CMR originates in real, physical differences in the colors of the CMR participants.

4.3 Cluster "Sequence" Galaxies

In the previous section, we have presented a study of the correlation between galaxy color and luminosity, derived for the population of presumed early-type galaxies. Here, we use two-color plots to address further questions about the nature of the cluster galaxies. While the interpretation of broadband colors is by no means either trivial or unique, galaxy colors are quite useful in exploring the nature of the objects. The colors, or crude spectral energy distribution of a galaxy, have contribution from not only the combined stellar population but also 'nebular' emission from interstellar gas, and possibly from a non-thermal central source, all of which may be attenuated by dust whose extinction depends strongly on wavelength. In general, it is not straightforward to disentangle color differences arising from redshift from intrinsic spectral differences. However, the tightness of the H-R Diagram which defines the stellar constituents of galaxies provides a useful diagnostic. Galaxies, which are composite stellar systems, are red or blue depending on whether they are dominated by correspondingly cool or hot stars.² The color positions occupied by galaxies at different cosmic distances shift according to the evolution of their stellar populations and the K-corrections. In any case, galaxies of different morphological types and distances lie on relatively well-defined and slightly different regions on a color-magnitude or color-color (CC) plot.

It is interesting to segregate the galaxies in different parts of the color-magnitude diagrams (see previous section) for such an analysis. We subdivide the galaxies in each cluster into three zones:

- a cluster "sequence" defined by the closeness to the CMRs and additional color constraints to be explained shortly,
- a "blue" zone with galaxies well blueward of the sequence, and
- a "red" region of galaxies far redder than sequence determined by the ridge-line of early-type galaxies.

Figures 4.4 and 4.5 display the distribution in color-color space of all the galaxies in the fields of our poor clusters. Solid and open circles plot galaxies which make up the "cluster sequence" (see

²Galaxy colors broadly indicate their morphologies, with blue galaxies tending to be of late Hubble types and red ones mostly comprising the E/S0 classes. This trend for colors to become bluer with later morphological types is somewhat weak, though, with dispersion of colors within each morphological class being comparable to that of the color differences between successive Hubble types.

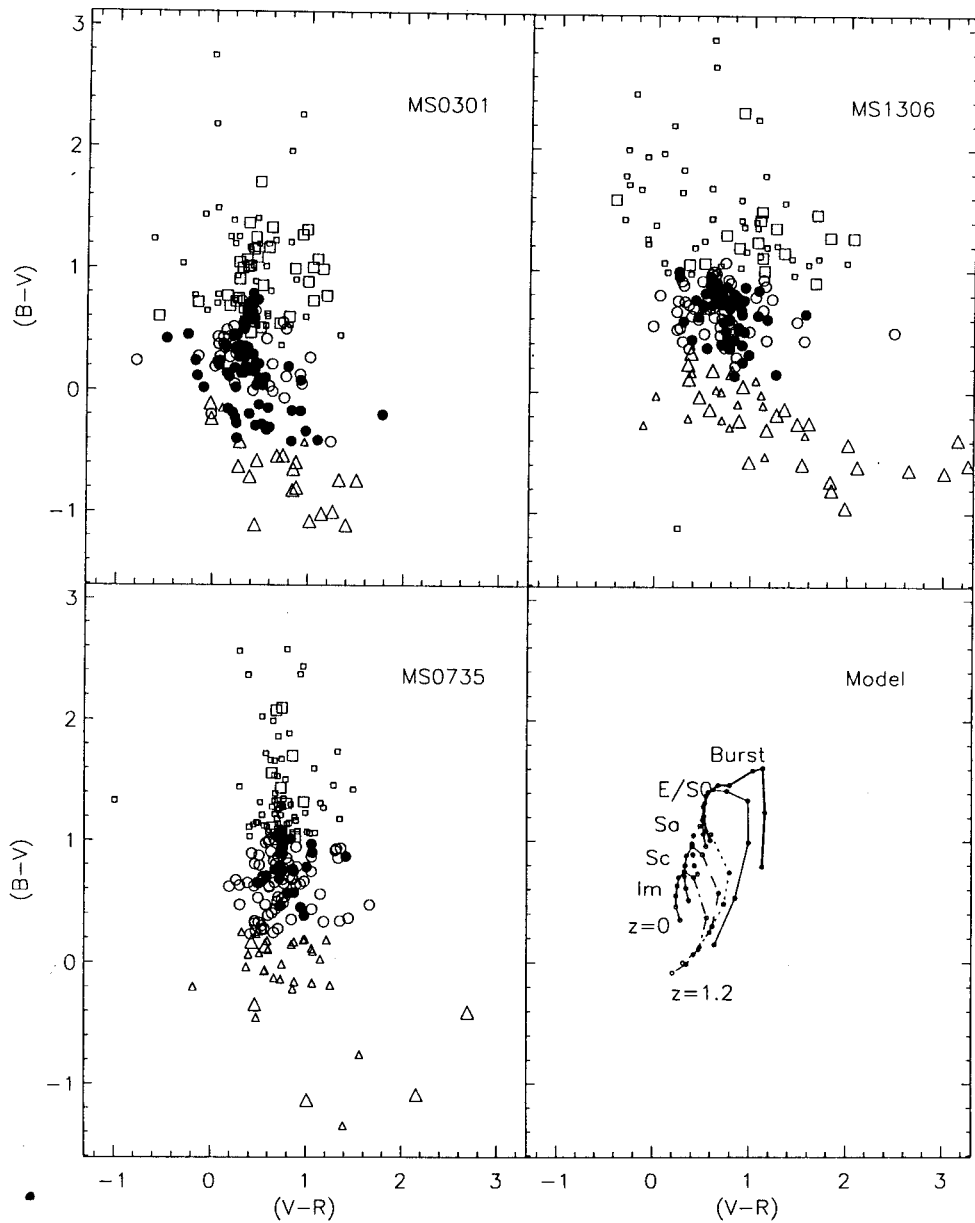


Figure 4.4: $(B - V)$ vs. $(V - R_C)$ color-color diagrams for the galaxies (to $M_V = -18$) in the EMSS fields. Solid and open circles: galaxies in the “cluster sequence” within and beyond 0.5 Mpc of the cluster center; large and small triangles: galaxies blueward of the sequence; and large and small squares: galaxies redward of the sequence, within and outside the projected 0.5 Mpc radius of the cluster, respectively. The bottom right panel shows galaxy colors predicted by the models of Guiderdoni & Rocca-Volmerange (1988) at redshifts of 0.00, 0.05, 0.10, 0.15, 0.20, 0.30, 0.40, 0.60, 0.80, 1.0 and 1.2 for the indicated morphological types.

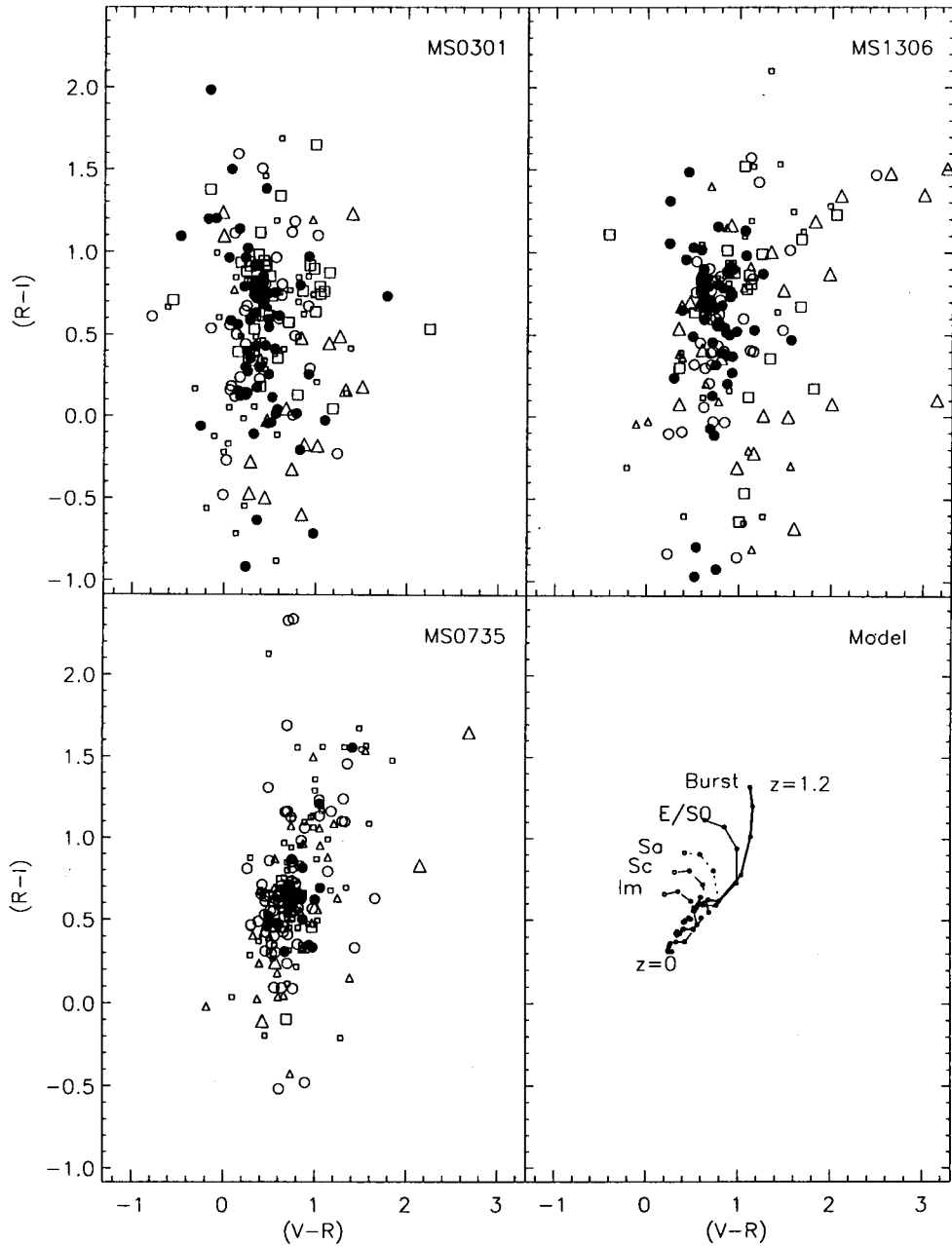


Figure 4.5: $(R_C - I_C)$ vs. $(V - R_C)$ color-color diagrams for the galaxies in the EMSS fields. Symbols as before.

below) within and beyond 0.5 Mpc of the cluster center, respectively. Large and small triangles represent galaxies blueward of the sequence, and large and small squares depict galaxies redward of the sequence, within and outside the projected 0.5 Mpc radius of the cluster.

In order to interpret the CC diagrams, we may use theoretical predictions of apparent magnitudes and colors for galaxies at various redshifts. The theoretical tool we use is an evolutionary synthesis model of spectrophotometric evolution by Guiderdoni & Rocca-Volmerange (1988). The model is able to compute the integrated spectrum of galaxies of different spectral (Hubble) types including both the contribution of the stellar component and the nebular emission in the galaxies. In the bottom right panels of the CC diagrams, we plot the synthetic color expected for different Hubble types between redshifts of $0 \leq z \leq 1.2$, in steps of roughly 0.1.

From both galaxy evolutionary models and the distribution of galaxy colors in the Virgo and Fornax clusters galaxies (Schroeder & Visvanathan 1996), we determine that almost all normal galaxies (to $M_V = -17$) distribute themselves within the color ranges $-0.55 \leq \Delta(B - V)_0 \leq 0.25$ and $-0.25 \leq \Delta(V - R)_0 \leq 0.25$, where the subscript '0' refers to the ridge line of the early-type cluster galaxies populating the CMR. Though there exists substantial dispersion of colors within each Hubble type at the same redshift, we consider the above a reasonable range of colors that the various galaxy types in a cluster would enclose. The color-magnitude relation can therefore sift out a "sequence" of the cluster galaxies from among all the detected objects. Such broadband color selection based on closeness to the cluster CMR can, in principle, act as a crude estimator of redshift and thus be a basic indicator of cluster membership.

In the CC diagrams of each poor cluster, we see a distinct clump of galaxies in the color ranges corresponding to the cluster sequence and within 0.5 Mpc of the cluster center (filled circles in the figure). Although there is a spread in the sequences, partly caused by the CMR (which is enhanced in the $(B - V)$ index), we are inclined to believe these regions correspond to galaxies belonging to the cluster, with the reddest being the cluster ellipticals. The model color tracks validate our assumption that these red clumps are indeed likely to be cluster members at the fiducial cluster redshifts. The somewhat inhomogeneous color distributions also straddle the range of colors occupied by all the Hubble types from E to Im, indicating that these EMSS poor clusters are populated by all morphological types. This is the case also with poor groups in the nearby universe, where the early-type fraction varies from 20% to 50% (Zabludoff & Mulchaey 1998).

If star formation in normal galaxies is governed by internal factors such as gas content and disk kinematics, it is not surprising that the tight CMR coexists with a significant scatter in the galaxian colors. The predominantly red bright galaxies in the core of the clusters — seen effectively in the CMR — indicate that most cluster members lack enough gas to actively form new stars. In fact, this could be a reflection of the predominance of early Hubble types in the cores of the poor clusters, similar to the situation in their rich counterparts. Apart from this, an important aspect to consider in the high-density regions of cluster cores is the expected high frequency of galaxy interactions and mergers. In particular, there may be blue ellipticals formed newly from mergers of gas-rich spirals. Though there are several galaxy pairs in each cluster, the interactions do not appear to have generated a corresponding number of starbursts to create

a significant population of very blue galaxies. We have, of course, no evidence that precludes a moderate enhancement in star formation in the recent past for these galaxies, through, for instance, starbursts in the nucleus or local (outer) regions. In fact, there is some support for the latter occurrence — the presence of morphological distortions in some blue galaxies on the cluster sequence. A more or less continuous process of low-level star formation that does not drastically alter the total content of the galaxies could also be occurring. In Sec. 4.4, we shall explore a few bright galaxies that appear to be cluster members but are too blue by more than 0.2 mag in $(B - V)$ to lie on the CMR (the putative “blue fraction”). We shall discover that most of these bluer objects are not objects of the highest luminosity, and are small sized galaxies usually located away from the densest cluster regions.

Our clusters all contain a centrally-located, very luminous galaxy each. Such first-ranked galaxies should participate frequently in mergers and receive the debris of tidally-disrupted cluster galaxies. This would serve to heighten the star formation and nuclear activity in these galaxies. We shall see in Sec. 6.4.1 that the brightest galaxy of MS1306 shows patchy star-formation and some evidence for dust in its central few kiloparsec, and perhaps shows accretion of low-mass stars in its outer regions, due to interactions with and subsequent coalescence of smaller neighbors into itself. The dominant member of MS0735 also shows the characteristic halo of cD galaxies. The brightest galaxies of the other two clusters do not evince any anomalies in their old stellar populations.

The general lack of galaxies showing exceptional star-formation activity or vestiges of recent mergers is a resounding feature of all dense, physical galaxy associations. Galaxies in Hickson Compact Groups and looser groups do not show any global enhancements in star formation activity or evidence for young merger remnants (e.g., Moles et al. 1994; Zepf & Whitmore 1991). Indeed, the star formation rate in group galaxies is depressed relative to that of the same Hubble type in the field (Iglesias-Paramo & Vilchez 1999; Allam et al. 1999). The deficiency is particularly evident in the late-type group galaxies; the strength of their emission lines (representing current star formation) is only one-half to one-third that of field galaxies of similar Hubble types. Perhaps tidal forces between galaxies are not so efficient in larger agglomerations or the intracluster medium may sweep away the interstellar gas through ram pressure, overall reducing the efficiency of star formation in these dense galaxy environments.

In MS0301, there are a few sequence galaxies that appear too red in $(V - R)$ compared to their $(B - V)$ colors. Their $(V - R)$ colors alone would place them at rather large redshifts, but their blue $(B - V)$ colors belie such a possibility. On the other hand, these objects could well be high-redshifts contaminants of the cluster sequence with the blue colors in $(B - V)$ being a result of emission in UV bands redshifted into the optical. Their brightness of $V \geq 20.5$ magnitudes seems to bolster this conclusion. In this case, the blanket K-corrections we have applied may be inappropriate for these objects, and their intrinsic colors different from what we quote.

Objects in the “blue zone” (triangles in Figs. 4.4 and 4.5) that are much bluer than the color ranges specified for the cluster sequence, are likely to be hot stars (misclassified as extended objects), foreground disk- and irregular galaxies, and quasars. Those galaxies much redder (squares in the figure) than the bright sequence ellipticals are in all likelihood exclusively field galaxies

at higher redshifts. The deficit of objects with extremely blue ($B - V$) colors is in part due to incompleteness in the B band. Foreground early-type disk galaxies (e.g. Sa or Sab spirals) could still lie in the bluer part of the cluster sequence, but due to their numbers in the field being relatively small, their adulteration of cluster galaxies should be negligible. Though foreground red galaxies do exist, they are likely to be very faint and do not contribute at the bright magnitudes we shall consider to calculate a blue fraction in the following section, except perhaps in the case of MS0735. As we can see from the color-color diagrams, compared with the model predictions, background spirals and foreground ellipticals do occupy somewhat different portions of the color-color space from the actual cluster galaxies. The color classes separate galaxies roughly on the basis of their recent levels of star formation. We shall have more to say about galaxies in the red zone in Sec. 4.5.

In summary, we use the locus of early-type galaxies in the color-magnitude diagrams to sift out cluster members from among the total set of galaxies in the region of the cluster, thus accounting for the 'contamination' from background galaxies. This is acceptable since most of the cluster population would not have greatly changed or been involved in strong star-forming activity within the redshifts we probe. Indeed, the CMR finds application in defining cluster populations in the recent literature (see, e.g., Biviano et al. 1995; Lopez-Cruz et al. 1997; de Propris & Pritchet 1998; Gladders & Yee 2000; Moretti et al. 2001). But a rigorous analysis of cluster galaxy populations requires reliable determination of cluster membership, Hubble types, and signatures of non-stellar activity. Strictly speaking, this requires spectroscopy which is difficult even at intermediate redshifts, when the background contamination becomes increasingly dominant.

4.4 Photometric Blue Galaxy Fraction

4.4.1 The Butcher-Oemler Effect

The universality of the cluster CMR makes it a powerful tool to trace *variations* of the galaxy population among clusters and over different redshifts. By identifying cluster objects whose colors are anomalously blue with respect to that of the expected narrow red locus, Butcher & Oemler (1978 and 1984, hereafter BO84) presented the first evidence of evolutionary phenomenon in cluster galaxies over the redshift range 0.003 (the Virgo cluster) to 0.54. BO84 and subsequent photometric studies (Couch & Newell 1984; Rakos & Schombert 1995; Lubin 1996; Margoniner & de Carvalho 2000) showed that the cores of compact clusters at $z > 0.2$ contain an excess of blue galaxies compared to the populations of local galaxy clusters which are almost homogeneously red. These changes imply a general decline in the star-formation rate in cluster galaxies since $z \approx 0.4$. Simple passive evolution of galaxies naturally leads to galaxies at higher redshifts ($z > 0.5$) being bluer, and deep galaxy counts suggest substantial evolution in the luminosities and colors of the bulk (especially the low-luminosity subset) of the galaxy population (e.g., Tyson 1988; Koo & Kron 1992). Nevertheless, the Butcher-Oemler result is surprising because of the rapidity with which the fraction of galaxies with blue colors increases from nearly zero at the present epoch to $\sim 40\%$ at modest redshifts of 0.5. Such extreme bluing of intermediate-redshift galaxies, and its apparent synchronization, indicates relatively recent star formation activity in

rich, dynamically old clusters, in contradiction to evolutionary model predictions and to the observed finespun color-magnitude relation of evolved (read early-type) galaxies which imply a long period of passive evolution.

Explanations for the putative “Butcher–Oemler effect” (BO effect) invoke virtually all environmental processes. Most cluster members classified as blue exhibit the morphology of normal disk or irregular galaxies (e.g., Dressler et al. 1994; Lubin et al. 1998), and their number counts in high- z clusters are similar to those of S0 galaxies within the cores of low- z clusters. Some blue members seem to be undergoing interactions and mergers with their neighbors (Lavery & Henry 1994; Oemler et al. 1997), and often exhibit features of “active” galaxies, or of young or intermediate-age stars superimposed on an older stellar population (Lavery & Henry 1986; Couch & Sharples 1987; Dressler & Gunn 1992; Poggianti et al. 1999). It is possible that the fraction of interacting and merging galaxies was higher at higher redshifts. Blue galaxies demonstrate a propensity to occur in the outer, less dense cluster regions (B084; Rakos, Odell, & Schombert 1997). One natural explanation of the BO effect is that at high-redshift, spiral galaxies fall into (sub-units of) young galaxy clusters and experience enhanced star formation induced by ram-pressure of the intracluster medium (Evrard 1990). The velocity dispersion of the subset of BO galaxies is usually higher than that of the cluster, supporting the above explanation. Blue cluster galaxies not only prevail in the outer cluster regions, but also prefer to reside within substructures in rich clusters (Caldwell & Rose 1997). When subcluster-subcluster mergers occur (more commonly at early epochs, i.e., high redshifts), they can create shocks in the ICM which could simultaneously induce starbursts in several galaxies (Kauffmann 1995; Bekki 1999). The blue galaxies, then, are at a phase of active star formation, after which they exhaust their gas supply perhaps due to ram-pressure stripping or cluster tidal fields (Rakos & Schombert 1995). Mechanisms such as cluster collapse (Larson, Tinsley, & Caldwell 1980) or galaxy harassment (Moore et al. 1996) may morphologically transform the depleted spirals into red S0s at low- z .

The corpus of studies suggests that redshift evolution is occurring in the star formation rate and stellar populations of cluster galaxies, in the morphologies of cluster galaxies, or both. But it is not clear if these different types of evolution are related phenomena. And several concerns about the validity of the BO effect remain. Are the samples affected by selection biases? Are rich clusters chosen for the BO studies at $z = 0$ and high- z the same type of objects? It appears that the BO clusters at low and intermediate distances may differ in their dynamical state (Newberry, Kirshner, & Boroson 1988) and X-ray luminosities (Andreon & Etori 1999). Selection of clusters in the optical bands while also looking for evolution in optical colors could certainly carry biases. An obvious way to circumvent such biases would be to use other criteria, such as X-ray luminosity or radio sources to select clusters for the BO effect determination. In a sample of massive clusters at $z = 0.22 - 0.28$ selected through their high X-ray luminosity, there appears to be only a small blue fraction, which does not increase with epoch in this small range of redshift (Smail et al. 1998). Further, the BO effect may be an environmental, as well as evolutionary, phenomenon. Among galaxy groups surrounding powerful radio galaxies, the nearby ones show a trend of redder galaxies to predominate in richer and denser environments (conforming to the morphology-density relation) whereas at $z \approx 0.4$, the blue galaxy fraction is independent of group richness (Allington-Smith et al. 1993). On the other hand, within Abell clusters, selected independently of richness,

morphology, or X-ray luminosity, the fraction of blue galaxies depends not only the cluster redshift but also on the richness, in the sense that, at a given redshift, f_b is systematically higher for poor clusters (Margoniner et al. 2001). Another concern is that over $0.18 < z < 0.55$, there appears to be no excess of cluster members compared to field galaxies at the same redshift that have unambiguously undergone starbursts within the last 1 Gyr (Balogh et al. 1999). So, the increase in cluster blue galaxy fraction with redshift may not be a strictly cluster-specific phenomenon.

Obviously, then, there is no consensus on the Butcher–Oemler effect. It is nevertheless an important feature of galaxy evolution, and a test of the connection between environment and evolution. In the following section, we compute the fraction of blue galaxies in our poor cluster sample and examine them in relation to other poor environs at similar redshifts. We also place them in the context of the Butcher–Oemler phenomenon.

4.4.2 Analysis

The selection criteria (BO84) to include galaxies in calculations of broadband blue fraction, f_b , are:

- the galaxies must be brighter than absolute magnitude $M_V = -20$ mag for $H_0 = 50$ km s⁻¹ Mpc⁻¹
- the measured color is $(B - V)$, K-corrected to the cluster rest-frame and corrected for the color-luminosity relation of E/S0 galaxies
- the host cluster must be compact and the galaxies must reside within a radius R_{30} that contains 30% of the total cluster population.

Then, those galaxies would qualify as “blue” whose $(B - V)$ colors are bluer by 0.2 mag than the peak of the cluster color distribution. The blue fraction, f_b , is then:

$$f_b = \frac{N_b}{N},$$

where N_b is the number of blue galaxies and N is the total census of the cluster to $M_V = -20$ mag, both corrected for background contamination. It should be noted that f_b is computed based only on the magnitudes and colors of the galaxies, without regard to the morphological classification.

While these criteria suit populous, orderly clusters well, they are not equally applicable to determining blue fractions in poor clusters. A typical poor cluster may be too sparse to even manifest a color–magnitude relation, and too irregular to compute R_{30} from its galaxy density profile.

For instance, in order to count the blue fraction within the same projected area as done by BO84, we need to establish the density profiles of our poor clusters. The structural analysis we perform on our sample (Chapter 5) indicates that the cluster profiles are not well-behaved, thus rendering difficult a proper definition of the BO radius of R_{30} . And our CCD images are $\sim 10' \times 10'$; thus we cannot be sure to have sampled the entire cluster, though we do believe that our clusters subtend only small angular areas on the sky. Now, the mean R_{30} of BO84 is about 0.7 Mpc (for $H_0 = 50$ km s⁻¹ Mpc⁻¹ and $q_0 = 0.1$) with fluctuations of about 30%. Here, in consideration of

the expected smaller sizes of our poor clusters, we adopt a fixed physical size of radius 0.5 Mpc (we assume $H_0 = 50 \text{ km s}^{-1} \text{ Mpc}^{-1}$ and $q_0 = 0.5$) within which to calculate f_b . The dependence of the conversion between angular and linear sizes on q_0 is not great at the redshifts we consider. If we use the BO84 choice of $q_0 = 0.1$, the projected angular size of 0.5 Mpc would decrease by less than 5% at $z = 0.2$.

We are able to match the magnitude and color selection criteria well. We select galaxies inside the 0.5 Mpc radius which, after K-correction, are brighter than the magnitude limit of $M_V = -20$ mag. We recall here that we do not apply color-dependent K-corrections, opting instead to use those of E galaxies for all extended objects in the cluster images. We then classify as “blue” those objects with rest-frame $(B - V)$ colors at least 0.2 mag bluer than the ridge of the early-type galaxies in the color-magnitude diagrams (Sec. 4.2).

Computation of f_b and its comparison between local and distant clusters require accurate foreground/background galaxy subtraction. Field contamination would tend to decrease f_b since field galaxies are in general bluer than the cluster core early-type population. As we cannot use spectroscopic redshifts to determine cluster membership, nor count the population of galaxies several Mpc away from the cluster centers (as did BO84), we use a statistical method to determine the number of field contaminants expected in the cluster images. In this section, we adopt an approach for field correction different from that of Chapter 3. Because the contrast of the poor clusters over the background is low, we can improve the accuracy of membership determination by restricting the color ranges of the cluster galaxies that can be counted as part of the cluster sequence or as “blue”. We constrain the color ranges to lie within the cluster “sequence” defined in an empirical fashion in the previous section. The sequence includes the range of colors occupied by disk and irregular galaxies which would most likely contribute to the BO effect. Therefore, we shall calculate N , N_b , and thus f_b , using only objects within these limits, which correspond to the bluest objects being not more than 0.55 mag deviant from the ridge-line of the early-type cluster galaxies.

Then, we compute the “blue fraction” (f_b), from the original definition of BO84, but within 0.5 Mpc of the poor cluster center. We estimate the error associated with f_b from counting statistics considering the quantity N to be Poissonian. Such propagation of errors is likely to be simplistic since it does not properly take into account the variations in background due to clustering of galaxies, nor the fact that N and N_b are perhaps correlated (Margoniner et al. 2001). However, with the data we have and the lack of independent estimation of the individual quantities, we have to consider the error estimation as acceptable to first order.

We would like to compare our results with those of Allington-Smith et al. (1993, or AS93), who determined the blue fractions for poor clusters surrounding radio galaxies. They used a V magnitude limit of -19 mag, and a fixed metric radius of 0.5 Mpc (for $q_0 = 0.0$). Therefore, we repeat our analysis above for a similar sample consisting of galaxies brighter than $M_V = -19$ mag.

4.4.3 Results

Table 4.4.3 lists the fractions of blue galaxies in our clusters, determined through the $\Delta(B - V)$ ($\Delta(V - R)$ for MS0002, see below) criterion. The first column is the cluster name, the second and third columns respectively list the cluster population and blue fraction for the magnitude limit of $V = -20$ mag prescribed by BO84, while the fourth and fifth column give the same quantities for a cut-off magnitude of $V = -19$ mag for comparison with the results of AS93.

Table 4.2: Cluster blue galaxy fractions.

Cluster	N_{20}	f_b^{-20}	N_{19}	f_b^{-19}
MS0301	18	0.05 ± 0.25	40	0.09 ± 0.18
MS1306	22	0.05 ± 0.21	34	0.13 ± 0.18
MS0002	14	0.12 ± 0.24	31	0.19 ± 0.17
MS0735	11	0.22 ± 0.33	22	0.16 ± 0.24

The number of galaxies brighter than $M_V = -20$ mag and $M_V = -19$ mag within the core region of 0.5 Mpc are typically less than 20 and around 30, respectively. Errors are large due to the limited galaxy populations in the cluster cores. (Note also, that due to the existence of a CMR, and type-dependent K-corrections, a blue galaxy with a given observed magnitude is in reality fainter than a red galaxy of the same brightness.)

The fact that f_b to a cut-off of $M_V = -19$ is a few percent larger than (though within errors, due to small number statistics) the corresponding fraction limited to one magnitude brighter tells us that blue BO galaxies are faint but not too much fainter than their fellow poor cluster members. Visual inspection leads to classifying a majority of the blue galaxies as disk (50%), perhaps late-type, galaxies. A few also show clear signatures of interactions (12%), but this does not seem to be a one-to-one effect, with only one member of a pair being classified blue. There seem to be irregular galaxies (12%) also among the blue members; we cannot state confidently if these are peculiar due to mergers. Our resolution and seeing do not permit us to say anything concrete about the rest.

If the zero-point of the CMR corresponds to the E-type galaxies, then the $\Delta(B - V) = -0.2$ cut-off falls between Sab and Sbc types of the compilation of galaxy colors by Fukugita, Shimasaku & Ichikawa (1995). Since we have the advantage of multiple colors through our photometry, we may check if the objects we determine to be blue through the $(B - V)$ index would appear blue through any other available CMRs and color indices, specifically if they correspond to disk galaxy colors. Position in the color-color plots are also crude clues to galaxy morphology. So, let us now apply our BO analysis to the $(V - R)$ color. In the previous section, we determined that the CMRs of our clusters in the $(B - V)$ and $(V - R)$ indices matched those of the Virgo cluster. We can therefore transform the $\Delta(B - V) = -0.2$ criterion for blue galaxies into one through $(V - R_C)$ using the relation between these colors for galaxies (of morphological types E to Sc) in the nearby Virgo and Fornax poor clusters. We determine that the 0.2 mag criterion in $(B - V)$ color translates to $(V - R_C)$ colors at least 0.11 bluer than the locus of the early-type galaxies in

the respective color–magnitude diagrams. (We recall that for MS0002, we have determined the f_b through the $(V - R)$ color index, since we do not have reliable photometry in the B band for this cluster.) We find that $> 60\%$ of galaxies classified as blue in $(B - V)$ show up as blue in $(V - R)$ as well. These are mostly the bright disks and interacting galaxies.

Overall, from both colors (referring to star formation) and morphologies, we may state that the blue galaxies in the EMSS poor clusters are similar to those in richer, distant clusters. We are therefore probing the same phenomenon within the vastly different environments.

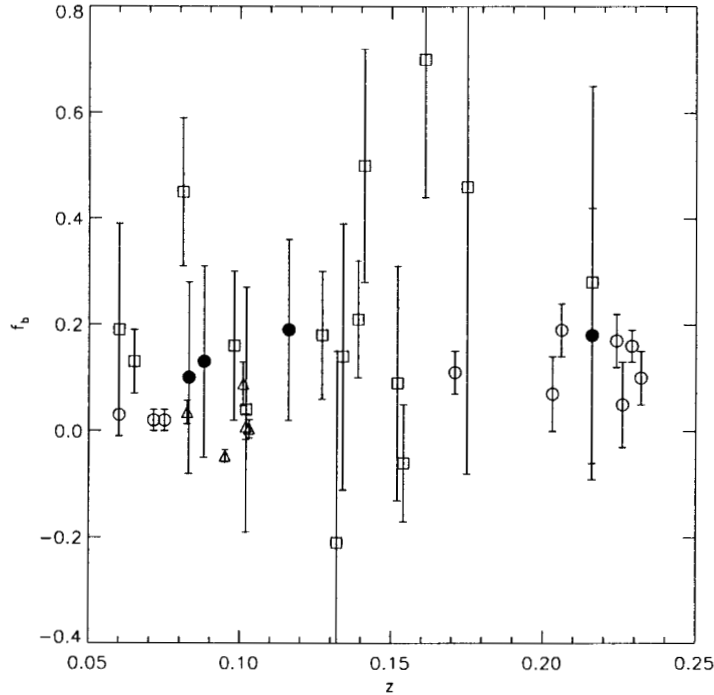


Figure 4.6: The blue fractions in our poor clusters (filled circles), in the poor groups around radio galaxies (squares) studied by Allington-Smith et al. (1993), and in Abell richness 0 clusters (triangles) from the work of Margoniner & de Carvalho (2000). Also shown are f_b values from the pioneering work of Butcher & Oemler (1984) for compact, rich clusters (open circles).

The smallness of the blue fractions are consistent with the minimal evolution expected over the redshift range $z < 0.25$. In order to explore if the blue fraction values of our poor clusters adhere to those for similar systems in the literature, we plot in Fig. 4.6 f_b to $M_V = -19$ mag for the poor clusters in our sample (filled circles), for poor groups around powerful radio sources (open squares) from AS93, and for the five Abell Richness 0 clusters (open triangles), among the 48 observed by Margoniner & de Carvalho (2000, MdC00 henceforth). We overplot on these the blue fractions from the original rich cluster sample of BO84 (open circles). We plot the actual data points (especially for the BO84 points, instead of their “guiding line”) chiefly to depict the real, large scatter associated with f_b at each redshift, and to show that the error bars are usually large, and particularly so for the poor groups.

AS93 provide blue fractions, as already stated, to the cut-off magnitude of $M_V = -19$ mag within the same metric radius we use. So, our estimations of f_b are directly comparable. However,

MdC00 computed f_b in the magnitude range $M^* - 1$ and $M^* + 3$ (where $M^* = -20.91$ assuming $h = 0.75$), using $(g - r)$ color indices; their f_b is larger than that of BO84 (i.e., to magnitude $M_V = -20$ mag) by 0.13 on average. It is not clear if there is a direct relationship between the estimates of MdC00 and ours. Overall, despite our large error bars, our data lie in the same range as that of these two studies. All of the above values of f_b are typically 0.05 larger than those calculated for rich, compact clusters by BO84 (open circles in Fig. 4.6) at similar redshifts.

We conclude that galaxies within not-too-distant X-ray luminous poor cluster are experiencing mildly enhanced star formation with respect to compact, rich cluster members, and are similar in this respect to objects in poor groups and Abell richness 0 clusters. This finds support in the recent study of Margoniner et al. (2001) who established that f_b is systematically higher for poor clusters than for rich clusters at the same redshifts, though the rate of redshift evolution is approximately similar for all richness classes.

But could the fraction of blue galaxies in these poor clusters be influenced by a selection effect - of using clusters that are strong X-ray emitters? Now, the blue fraction in the cores of clusters at $z = 0.22 - 0.28$ selected on the basis of their similar X-ray luminosities (Smail et al. 1998) and simple, regular morphologies, is $< 10\%$; therefore, the classical BO effect is not present in them. Though our selection of poor clusters is also through their being strong X-ray emitters, our f_b values are larger and more scattered than such X-ray bright rich clusters. The X-ray morphologies of the poor clusters in this study are more or less regular; in particular, there is no evidence of strong substructure or bimodality in the high-energy emission. So, we can rule out large-scale shocks caused by merging (sub)clusters as the cause of the blue galaxy phenomenon in these poor clusters. However, in a small sample of clusters with binary X-ray structure at redshifts of $z = 0.1 - 0.2$, the number of blue galaxies is indeed enhanced with respect to rich clusters with relaxed morphologies (Wang et al. 1997; Metevier et al. 2000).

Could it be that the X-ray luminous clusters of Smail et al. are not part of the same class of objects as those of the BO84 work? Indeed, this was the objection raised by Andreon & Ettori (1999) about the original BO84 work itself. Further, rich, X-ray luminous clusters from the EMSS sample (of various X-ray structures) at $0.18 < z < 0.55$ show a significant Butcher-Oemler effect, but only when radii larger than about 2.3 Mpc are considered (Ellingson et al. 2001). While the cores of these rich EMSS clusters contain evolved composite stellar populations, the objects close to and outside the virial radius are similar to coeval field galaxies. If we similarly check for dependence of f_b on angular sizes, i.e., at different radial distances from the cluster center, we determine that the fraction of blue galaxies does increase by nearly a factor of 1.6 when we include the region 0.7 Mpc (or 200 kpc further than we have thus far considered) of the cluster centers for MS0002 and MS0735. This further supports the idea that BO galaxies tend to avoid the very cores of their clusters. Galaxy groups and small clusters are correlated with rich clusters and, in hierarchical models, fall into clusters in greater numbers at intermediate redshifts than at present. The foray of subclusters into the larger structures, and of field galaxies into these subclusters, at high/intermediate redshifts may still induce the BO effect. A restatement of the BO effect in this perspective is one of a decline over time in the infall rate of field galaxies, leading to smaller number of starbursting cluster members at low redshifts.

A number of blue galaxies in our poor clusters are distorted or irregular; but most are likely to be normal luminous disk galaxies. It could well be that the poor cluster environment, where ram-pressure sweeping is less effective than in rich clusters, allows massive disk galaxies to sustain star formation for a long time aided further by the infall of gas from the intra-cluster medium.

Now, we find that a small number of the blue galaxies are interacting, consonant with dense environments hosting a greater number of pairs and small galaxy families than the field. This provides another scenario for the BO phenomenon, especially valid in poor clusters that do not foster high internal tides or show substantial substructure to perturb galaxies into bursting into star formation. Perhaps the processes governing the Butcher–Oemler effect are more susceptible to galaxy-galaxy interactions than to any large-scale influence. Now, there are early-type spectroscopic counterparts of the blue galaxies, E+A galaxies (Dressler & Gunn 1992), initially identified in distant clusters, that contain young/intermediate-age stellar populations superposed on the more evolved elliptical population. However, it turns out that these E+A galaxies exist also in the local universe, largely as pairs with many showing tidal features, in both field and cluster environs (Zabludoff et al. 1996). Further, dusty starbursts are twice as common in the field (at similar redshifts) as in X-ray luminous clusters (Balogh et al. 1999). Therefore the presence of E+A galaxies in distant clusters or very blue galaxies in the outer regions of clusters do not provide clinching evidence uniquely for the effects of cluster environment on galaxy evolution. The properties and evolution of such galaxies may reflect the typical behavior of galaxies in pairs rather than the global influence of clusters on the star formation history of galaxies.

Clearly, the BO effect is a complex phenomenon, and may have some or all of the above mechanisms at work. Perhaps a detailed analysis of the phenomenon including a study of the cluster perturbations and galaxy interactions in a large sample of clusters spanning all richnesses and redshifts may lead to a confident answer.

4.5 Red Galaxies

As we have mentioned previously, almost all normal galaxies occupy the color range $-0.55 \leq \Delta(B - V)_0 \leq 0.25$ and $-0.30 \leq \Delta(V - R)_0 \leq 0.25$. Just as one may estimate the fraction of blue galaxies using the tightness of the color–magnitude relation, one may also check for the presence of unexpectedly red galaxies in the lines-of-sight to clusters of galaxies. Garilli et al. (1996; or G96) used the CMR to study galaxy populations in clusters over $0.05 \leq z \leq 0.25$. While they found no signs of evolution in the blue fraction, they noted the presence of a rather large number ($\sim 7\%$ of the total population) of red galaxies, with both $(g - r)$ and $(r - i)$ colors (in the Thuan-Gunn bands) at least 0.3^m redder than the early-type sequence. Most of these are compatible with being field galaxies at redshifts of 0.3–0.5. However, a significant fraction (upto 25%) of these “field” galaxies have $(r - i)$ color indices indicating they may be at $z > 0.7$, but their $(g - r) \sim 1.2$ colors are not red enough for them to be so distant. G96 suggest that the anomaly of the spectral energy distributions may arise due to emission in the bands above $0.7 - 0.8\mu\text{m}$. Such a population of galaxies would be important for both number counts and in testing galaxy evolution models. Therefore, we use a similar methodology as G96 to search for a red galaxy population in our sample, with both $(B - V)$ and $(V - R_C)$ colors at least 0.3 mag

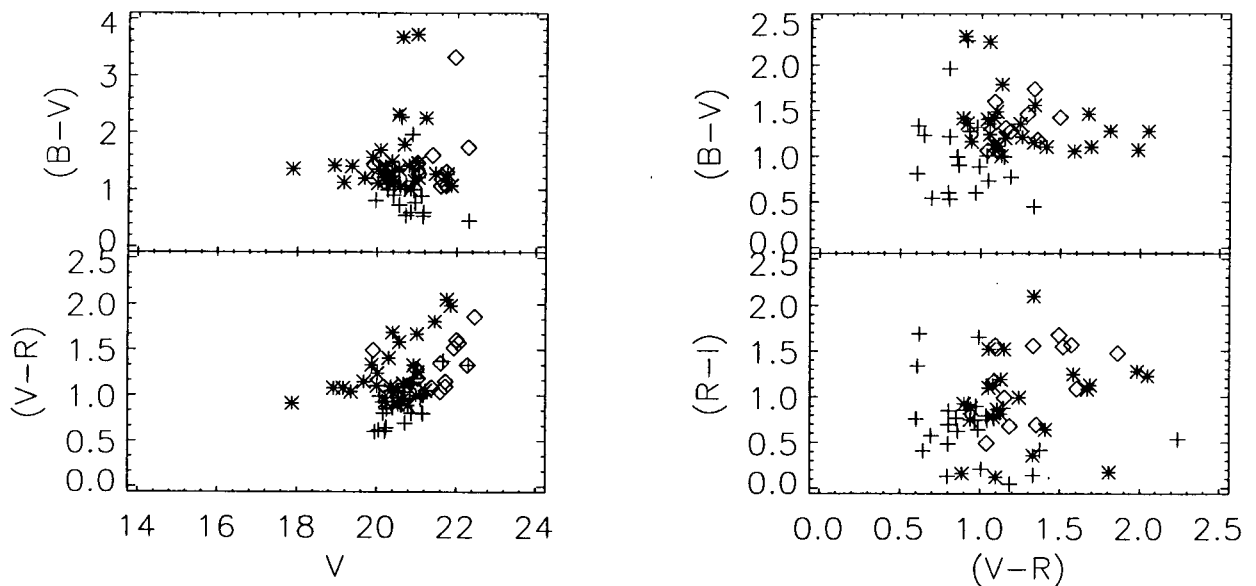


Figure 4.7: Red galaxies in the EMSS fields.

redder than the early-type sequence. Note that in this case, we do not translate the $(g-r)$, $(r-i)$ criteria into the corresponding $(B-V)$, $(V-R)$ values, being inclined to believe that the same interval picks us background galaxies with equal effectiveness in both photometric systems.

In the color-magnitude diagrams of the poor clusters, we have seen that an extended tail of faint red objects exists. The nature of these objects becomes apparent in Fig. 4.7, where we have replotted the color-magnitude and color-color diagrams for them. Most of these objects have the colors of high-redshift field galaxies. They must be intrinsically quite luminous to appear at the magnitudes we probe. We determine, further, that most of the objects lie at metric distances of > 700 kpc from the cluster center (which we identify with the position of the brightest cluster galaxy). Of course, the number of background galaxies contaminating each cluster depends on its redshift. Further, similar to the findings of G96, we discover a subset of red galaxies that are extremely red in $(R-I)$ but have $(B-V)$ and $(V-R)$ colors too blue and thus are incompatible with the former color to be at high-redshifts. The color distributions of these objects are much broader than the errors of typical measurements. These objects account for about 10% of the total red galaxy population, and are mostly faint, with $V \approx 20$ mag. The possibility that these reddest objects are stars misclassified as galaxies is not large; within our CCD fields (though all are at high Galactic latitudes), it is unlikely that we include so many faint red (M-type) stars. We therefore attribute the surprisingly red $(R-I)$ colors of these objects to their unusual spectral energy distributions, with emission in the redshifted I band.

Metcalf et al. (1994), Aragon-Salamanca et al. (1993) and others have found similar cluster galaxies identified through extremely red optical-near-infrared colors. Put together, these results suggest that the “anomalous” red galaxies are not exactly uncommon, and deserve closer attention. It would be most worthwhile to determine the redshifts of these objects, and study their

spectral line characteristics. These will prove necessary to connect the evolution of these galaxies with the nature of their local counterparts.

4.6 Discussion and Conclusions

The existence of a linear locus in the color-magnitude diagram, a main characteristic of the cluster early-type galaxy population, is clearly visible in the EMSS poor clusters. Further, the poor cluster CMRs have slope and scatter unchanged with respect to local clusters such as Virgo, within the observational errors.

Let us use the mutual consistency of the CMRs of our poor clusters with those of Virgo, and by extension, those of higher redshift clusters, to establish constraints on galaxy formation and evolution. By considering the color evolution of galaxies after star formation ceases, Bower, Kodama & Terlevich (1998) showed that the scatter of the CMR constrains the spread in age that is allowed for the bulk of the stellar population; the cluster galaxies must be coeval to within 4 Gyr. The breadth of the color distribution could imply significant scatter in the star-formation histories of the galaxies, assuming the effect of field galaxy contamination at these magnitudes is small. (The field contamination depends on the richness of the clusters, and becomes rather large especially among fainter, likely late-type, galaxies.) Following this analysis, an unambiguous conclusion from the smallness of the scatter in the CMR and near constancy of its slope over the admittedly modest redshift range of our poor cluster sample is that the bulk of the stars in these cluster early-type galaxies is coeval and has perhaps formed at $z > 2 - 3$.

There is evidence for a substantial fraction of poor cluster galaxies bluer than can be ascribed to the existence of a CMR and in excess of predictions of passive evolution. The blue fraction is higher than in rich clusters at similar redshifts. However, the overall redness and tightness of the cluster sequence in the color-color plots, and the smallness of the blue fraction indicate that within the poor cluster cores, the dense environment appears to suppress star formation and support galaxies of mostly early Hubble types. This is true even of a cluster like MS0301 which appears to contain a large fraction of disk galaxies.

Interestingly, early-type galaxies in low-density environments possess a substantial intermediate-age population of stars that is considerably reduced or altogether lacking in the dense cluster ellipticals (Rose et al. 1994). Perhaps, early-type galaxies in cluster cores have experienced a truncated star formation and chemical enrichment history compared to their counterparts in lower-density regions because of ram-pressure evaporation of interstellar gas, or ran out of molecular gas due to a massive starburst when the gas-rich galaxy plunged into the cluster environment for the first time. Or the truncation of star formation in cluster galaxies may be largely gradual, due to long-term exhaustion of gas in the galactic disks (Balogh et al. 1999). It is still uncertain whether environmental differences outweigh the intrinsic dispersion between local galaxies.

Many key issues in galaxy evolution remain open, and require a well-understood sample of galaxy clusters of all richness and at a wide range of redshift to be resolved. Ultimately, such studies would help constrain galaxy formation in the context of large scale structure formation, and provide tools for the determination of cosmological constants.

Chapter 5

Cluster Morphology

*In the summer evening
Where is my star
hidden in the Milky Way?
- Issa Kobayashi*

5.1 Avant-Propos

The appearance of clusters of galaxies indicates to some extent their physical properties. There is evidence that optical morphology, the presence of a dominant D or cD galaxy in the cluster center, and X-ray emission of the clusters correlate with their richness and dynamical states (e.g., Bahcall 1980, Forman & Jones 1984), and influence the ratio of dwarf galaxies to bright ones (Lopez-Cruz 1997). Cluster structures reflect, to some extent, their galaxy content — dense environments like cluster cores are populated almost solely by elliptical and S0 galaxies, whereas the less extreme environments of the cluster peripheries host spiral and irregular galaxies (Oemler 1974, Dressler 1980). Further, regular clusters which show spherical symmetry and high central concentration of galaxies contain predominantly E and S0 galaxies, whereas irregular clusters which are amorphous and less dense contain galaxies of all types, including appreciable numbers of late-type spirals and irregulars. Rich, regular clusters also turn out to be strong X-ray emitters more frequently than irregular clusters (Forman & Jones 1982).

It is interesting to ask whether poor clusters that contain fewer galaxies than their rich counterparts are gravitationally bound systems instead of chance projections of galaxies, and how their morphologies and X-ray emission compare with those of rich clusters.

Clusters of galaxies are neither isolated nor static. Galaxies from the neighboring field continuously fall into them, and complex interactions within and between clusters modify their structures all through their lifetime. One of the indicators of the dynamical status of a cluster is the degree of regularity of the galaxy and gas distributions. A large fraction of clusters do not show a smooth morphology; they contain within themselves several clumps in the distribution of their galaxy population and X-ray emitting gas. Such substructure suggests that the cluster is in its dynamical youth and has not reached the state of virialization. Further, if cluster galaxies experience the effects of dynamical friction, they can approach energy equipartition in such a way that the bright galaxies stay closer to the cluster center while the smaller, fainter ones spread themselves out over larger volumes. Other anisotropies in the cluster galaxy distribution include the preferential alignment of the bright cluster galaxies with the host cluster (e.g., the work of Lambas, Peebles and collaborators), and clusters themselves being aligned with neighboring clusters (Flin

1987). Since the universe is expected to be homogeneous and isotropic on the largest scales, these preferred alignments are clues to cosmic structure formation mechanisms. Structures formed by gravitational collapse of small fluctuations in an expanding universe. The type of dominant dark matter determines the initial form of the fluctuation spectrum. Structure may have formed from fragmentation of very large (supercluster-scale) regions into smaller regions (for hot dark matter) or from the hierarchical coalescence of small sub-units into successively large structures. The different nature of these scenarios lead to observable differences in the clustering properties of the universe, and in properties of galaxy clusters such as density profiles, the amount of substructure, and orientation effects among member galaxies and larger scale structures. Thus, morphology tells us not only about the shape and dynamical state of clusters but also reveals interesting details about cosmogony.

This chapter presents analyses related to the morphology of the four EMSS poor clusters of galaxies we have imaged with the VBT. We study the cluster morphology at various levels: qualitatively by visual assessment and through a simple comparison of the optical image with the contours of X-ray emission; and in a quantitative manner using maps of the projected galaxy distribution. We look at the spatial arrangement of the galaxies as a function of their colors to evaluate the radial trend of morphology. We check if the clustering properties of the cluster galaxies depends on their brightness by estimating the amount of luminosity segregation. We then discuss the alignment effect wherein the brightest cluster member points in the same direction as the distribution of cluster galaxies.

5.2 Visual and X-Ray Morphologies

Inspection by eye leads to a first qualitative description of the cluster morphologies. Assuming spatial homogeneity of field galaxies, the general concentration of galaxies around a bright galaxy is a clue about the location of a cluster. The clusters in our sample are all bright at X-ray wavelengths, a selection criterion. X-ray observations provide information on the intracluster gas, which, since it is gravitationally confined, traces the cluster mass distribution or gravitational potential (Sarazin 1988). X-ray images, then, allow one to study the distribution of both baryons and dark matter. In fact, as already stated, the hot gas in galaxy systems such as groups or clusters accounts for more mass than is found in the visible galaxies. By piecing together the optical and X-ray data, it may be possible to arrive at a better understanding of the morphologies of the clusters.

In Figs. 5.1, 5.2, 5.3 and 5.4, we present the optical/X-ray images of the poor clusters (PCs). The VBT optical mosaic images of the poor clusters cover different angular fields, all corresponding to metric sizes of at least 1.0 Mpc at the cluster redshifts. Table 5.1 lists their important parameters. We note here that the brightest cluster member (BCM) is not always centered in the mosaics. The X-ray data are from the data archives of the ROSAT X-ray satellite observatory position sensitive proportional counter (PSPC) in the energy range 0.1–2.4 keV. The PSPC (energy-dependent) PSF has a mean FWHM of about 2 arcmin, and increases dramatically as a function of off-axis angle over the two degree field-of-view, from 20 arcsec at the center to 4 arcmin at the edges. None of our PCs are too far from the PSPC center, though MS0301 has a PSPC rib shadowing it

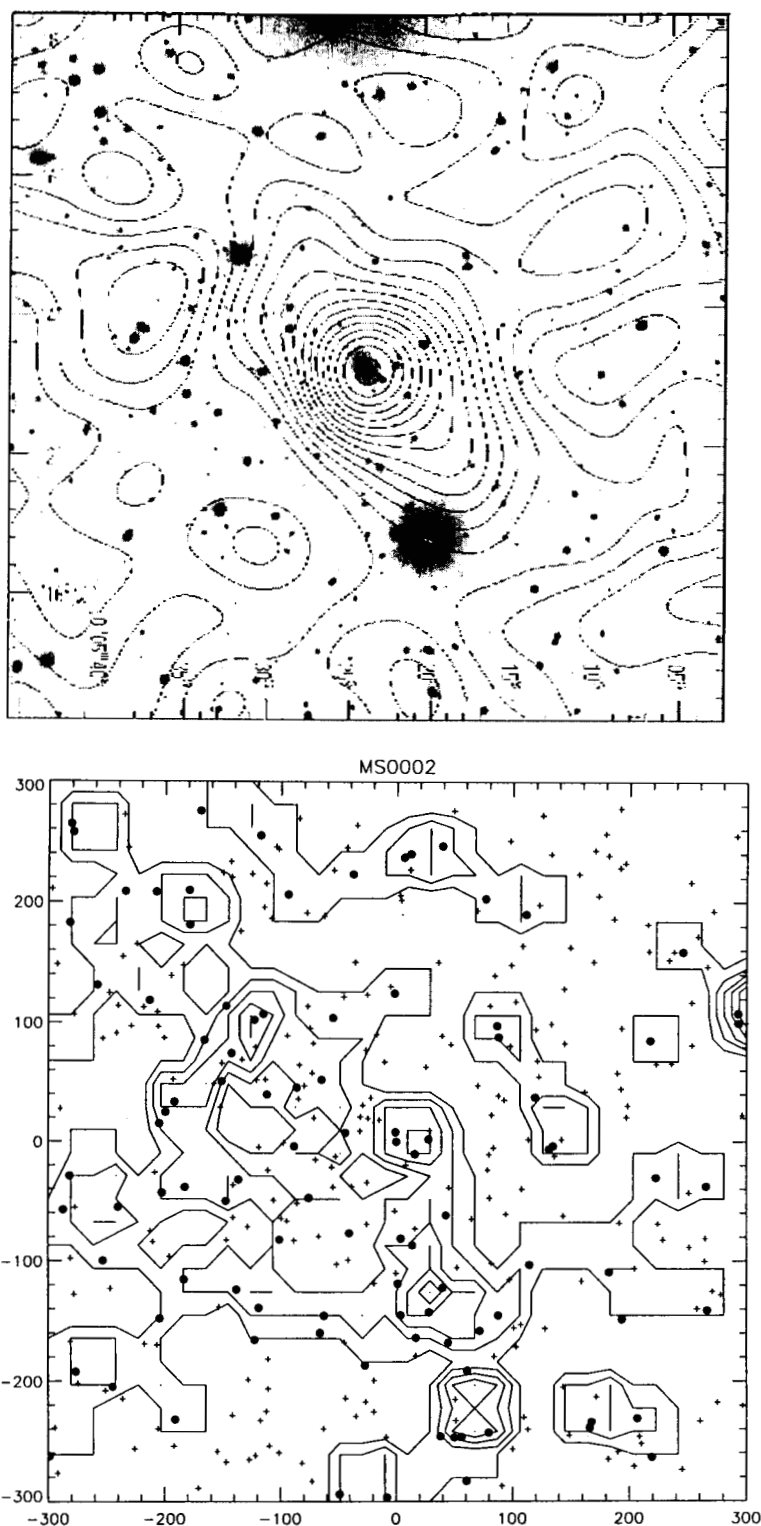


Figure 5.1: Top panel: Gray-scale optical CCD image of MS 0002.8+1556 overlaid with ROSAT-PSPC X-ray emission iso-contours. The axes are sky co-ordinates in the epoch J2000. Bottom panel: Isopleths of the galaxy distribution in the cluster region, from counting galaxies in 20×20 arcsec bins and smoothing over an area of 1 arcmin^2 . The brightest cluster galaxy is at the center, and the axes are in terms of distance in arcsec from it. North is at the top and east to the left in both panels.

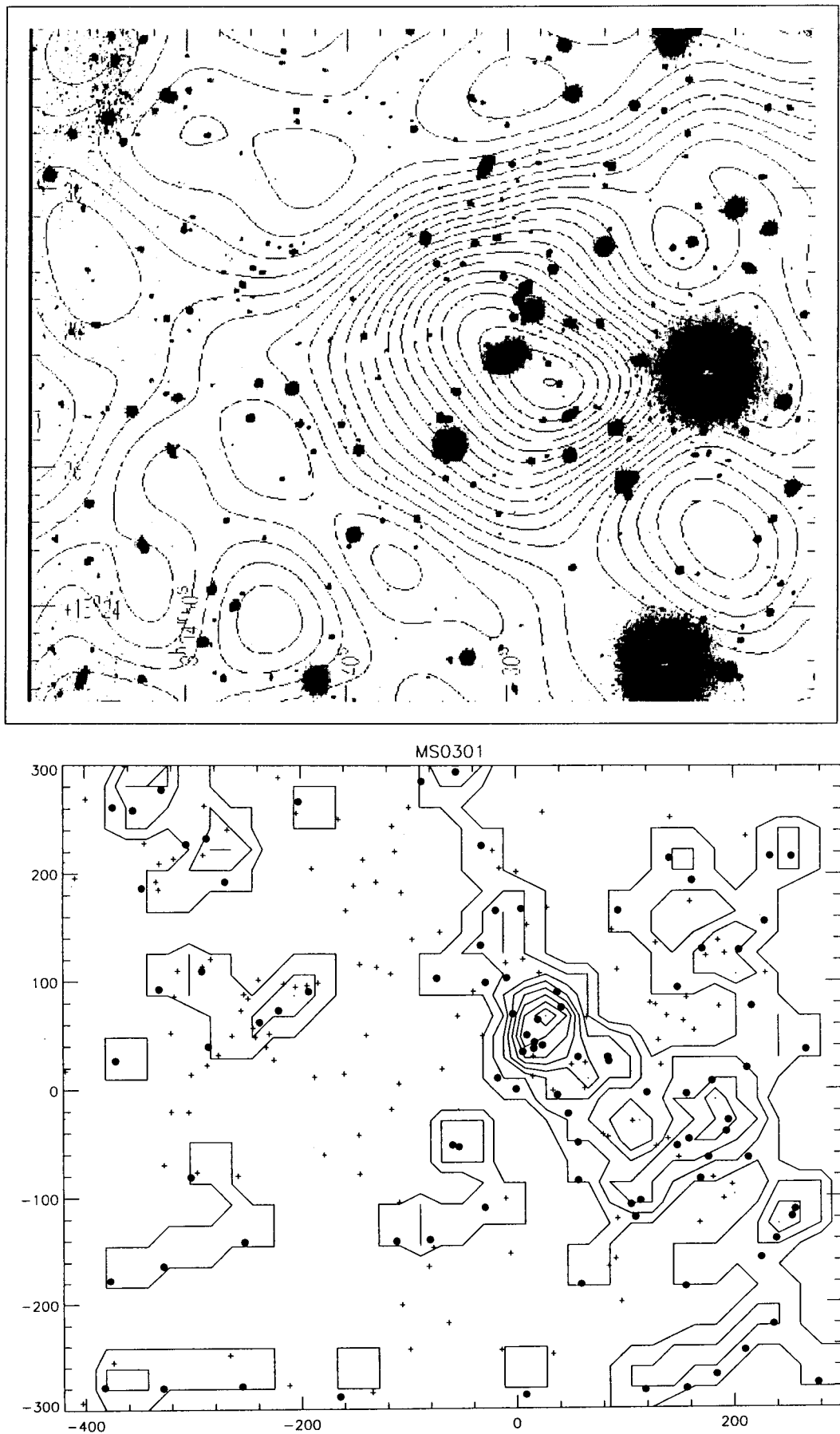


Figure 5.2: Optical and X-ray morphology of MS 0301.7+1516. Axes, gray-scale images and contours as before.

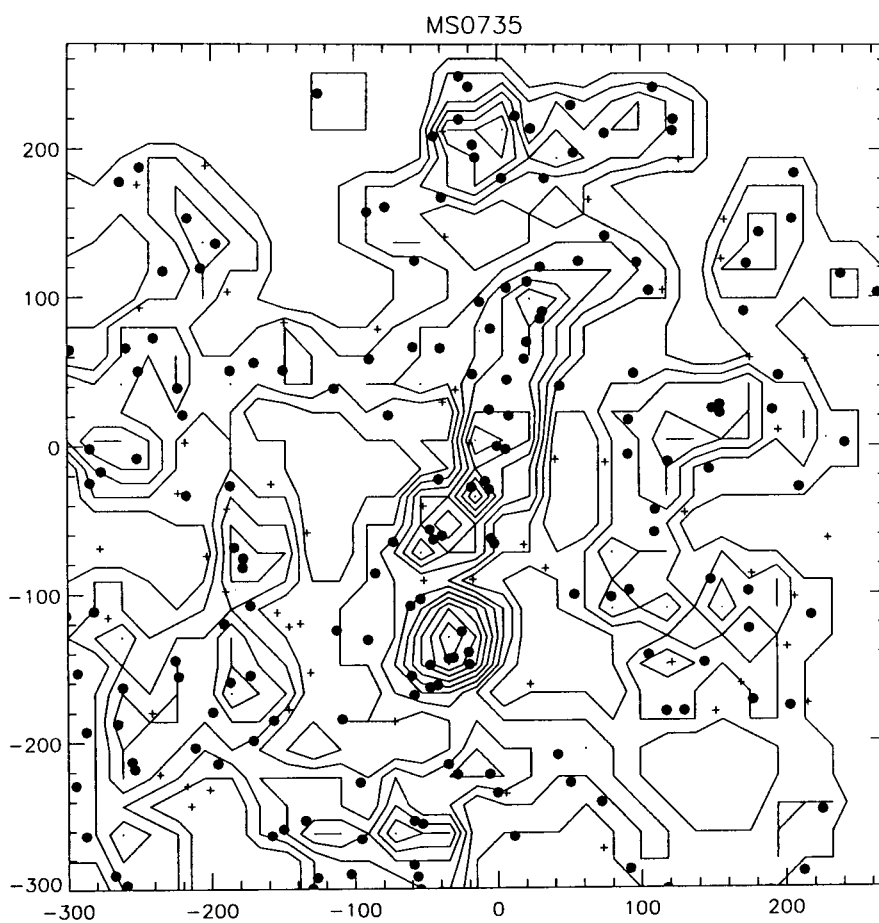
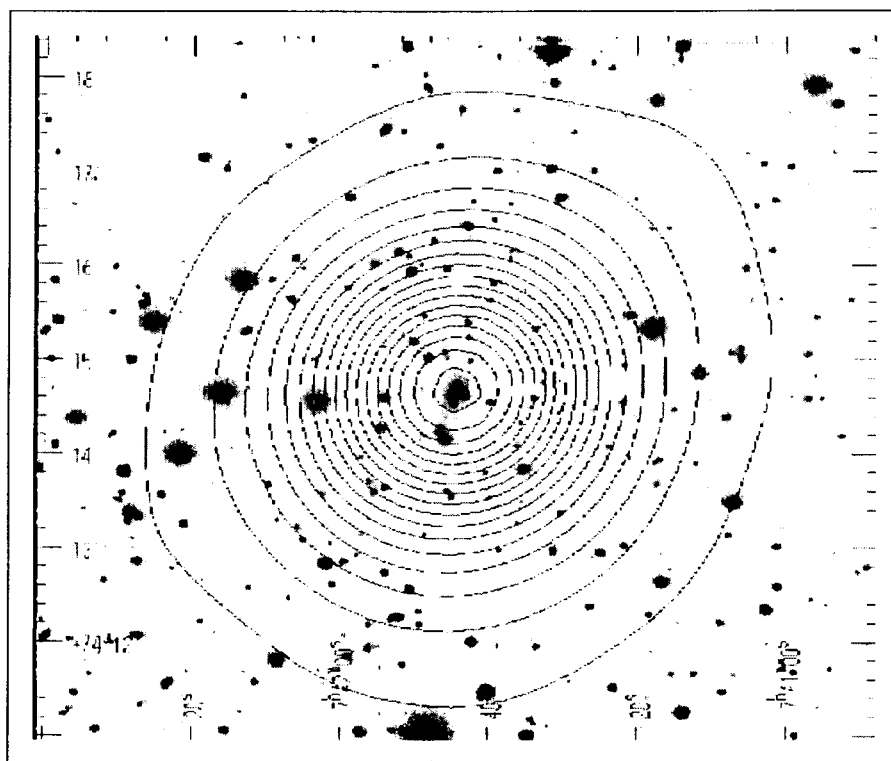


Figure 5.3: Optical and X-ray morphology of MS 0735.6+7421. Axes, gray-scale images and contours as before.

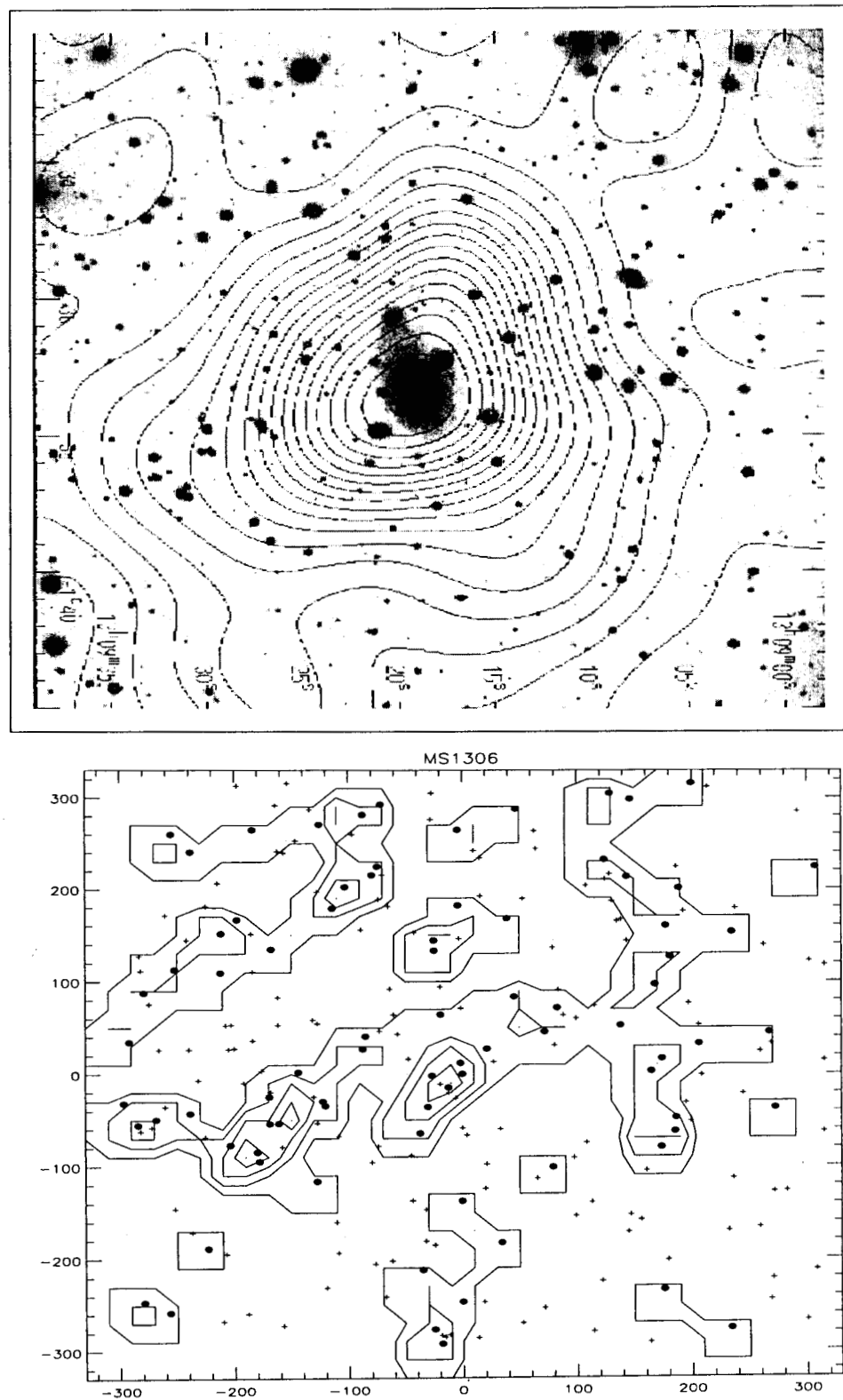


Figure 5.4: Optical and X-ray morphology of MS 1306.7-0121. Axes, gray-scale images and contours as before.

immediately to its North, and one (MS0735) has been the subject of pointed observations.

The overlays show contour plots of (uncalibrated) broad-band ROSAT image data superposed on our optical CCD frames (see Chap. 2) after accurate alignment of the co-ordinate frames. We generated isointensity contour maps by extracting the photons in the total energy band (0.2–2.5 keV band) and convolved the images with a $\sigma = 75$ arcsec Gaussian profile. We applied no sky- or detector background subtraction.

All four PCs show a visible concentration of galaxies around the BCM. As mentioned in Chapter 3, we are limited by the lack of a local estimate of the galaxy background, which would account for any presence of large-scale structures, of foreground clusters and groups, and of local variations in background counts. The X-ray emission is extended, centrally peaked and in all cases but that of MS0301, there is evident coincidence between the BCM and the X-ray centroid to within a few arcseconds i.e., within the positional errors of the X-ray data. While not entirely circular in projection, the high-energy emission is more or less azimuthally symmetric in the clusters with $L_x > 10^{43}$ erg s $^{-1}$. This near-circularity implies that the clusters are not too far from being dynamically relaxed. We do not ourselves perform much detailed analysis of the X-ray structures of the clusters but for a rudimentary estimation of the X-ray position angle.

Table 5.1: Optical mosaic images of the clusters

Cluster	Image Size		Metric Scale kpc/arcmin	Metric Size Mpc 2
	pixels,	sq. arcmin		
MS 0002.8 + 1556	1017×1017,	10.2×10.2	166.9	1.7×1.7
MS 0301.7 + 1516	1321×1051,	13.4×10.7	125.9	1.2×1.0
MS 0735.6 + 7421	1020×931,	10.2×9.3	267.2	2.7×2.5
MS 1306.7 – 0121	1185×1137,	12.1×11.6	132.4	1.2×1.1

Some specific classification schemes for the optical morphology of rich clusters include the Bautz-Morgan (BM; Bautz & Morgan 1970) system, and the Rood-Sastry (RS; Rood & Sastry 1971) system. The BM scheme classifies clusters based on relative contrast (i.e., dominance in luminosity and size) of the brightest cluster member over the other cluster members, ranging from type I to III in decreasing order of BCM dominance. Type I clusters contain a single, centrally-located dominant (cD) galaxy (e.g., Abell 2199); at the other end, type III clusters contain no galaxy that dominates over all others (e.g., Hercules); in between are type II whose brightest members are intermediate in appearance between cD and normal giant ellipticals (e.g., Coma), and further intermediate types I-II and II-III. The RS system distinguishes clusters depending on the distribution of the ten brightest members, in classes cD, binary, core, line, flat, and irregular. Both classes seem to be independent of cluster richness but are sensitive to the central cluster density (BM I clusters are denser than BM III clusters). The classification systems may give rise to systematic errors due to the distance of the clusters (the large envelopes of the cD galaxies may be dimmed due to K-corrections) and misidentification of the brightest galaxies due to projection effects. While the second scheme is not quite suitable to classify poor clusters owing to its requirement of the first ten bright galaxies, the first scheme may be useful in revealing morphological features of systems less populous than rich clusters. Therefore, we determine the

BM types of our four poor clusters below, by studying the brightest 3–4 galaxies and using the ΔM_{12} determinations quoted in Table 3.2.

We now proceed to descriptions of the individual clusters.

MS0301 is noted by Gioia & Luppino (1994, GL94 from here on) as being ‘a poor, irregular nearby cluster’. It appears in the VBT optical images as a sparse system with an irregular spatial distribution of galaxies whose brightest member is an elliptical. We estimate it as being BM type either II-III. West of the BCM, the presence of a very bright star affects the galaxy counts. The image also shows an additional clump of faint galaxies about 4 arcmin east and slightly north of the BCM. We speculate that this faint system is a distant cluster of galaxies, not related in any way to MS0301. MS0301 has a filamentary grouping of bright galaxies visible in the vicinity of its dominant member. Classification by eye of some of the brighter galaxies leads to the conclusion that the cluster is dominated by disk systems. The X-ray contours indicate that the structure of the hot gas is far from simple and symmetric. As we have previously mentioned, the X-ray data for this cluster are of rather low signal-to-noise, and are hampered by the PSPC rib occurring to its immediate north. The peak of the X-ray emission, as already mentioned, does not coincide with the BCM optical position. The projected separation between the optical position of the dominant galaxy and the host cluster X-ray centroid is about 1 arcmin (≈ 120 kpc). This is similar to the famous case of the galaxy group around NGC 2300, where the extended X-ray emission is not centered on any particular galaxy and is offset from the elliptical NGC 2300 by several arcminutes. The X-ray structure shows an almost one-to-one correspondence with the galaxy isopleths (see the next section). Perhaps the individual large galaxies within the cluster contribute to the high-energy emission, making it patchy, as in several MKW/AWM poor clusters (Kriss et al. 1983; Price et al. 1991). It is also possible that the high-energy emission is associated with a shock front created by the infall of smaller groups into the cluster, as in the case of Stephan’s Quintet (Sulentic et al. 1995). However, due to the low X-ray flux and irregular morphology, we cannot rule out the possibility of unresolved point sources (e.g. bright cluster galaxies, foreground sources such as weak AGN) being confused with the cluster emission. This could also explain the weakness of the X-ray emission itself. The low X-ray luminosity is in conformity with the trend of spiral-rich clusters being irregularly shaped, with no central concentration. But if the gas is all associated with the ICM, and if it traces the gravitational potential, then this implies that the cluster is unrelaxed and is probably in the process of being assembled by the agglomeration of smaller units.

MS1306 is at a redshift ($z = 0.088$) similar to that of MS0301 ($z = 0.083$) but its dominant galaxy is about a magnitude brighter, and obtains a BM classification of Type II for the cluster. GL94 note that it is a ‘poor cluster with a dominant central galaxy.’ The X-ray emission of the clusters is likely to be spatially resolved; it is close to being azimuthally symmetric with no prominent substructure. MS1306 shows an extended core of about eight bright galaxies within 50 arcsec of the nominal X-ray centroid quoted by GL94, which nearly coincides with the BCM position. The BCM, a giant elliptical much larger than the BCM of MS0301, shows obvious signs of interacting with one (possibly two) of its neighbors. In turn, the smaller neighbors are distorted by interactions with the BCM. The probability of a fortuitous coincidence of so many bright galaxies in such a small region corresponding to a linear diameter of less than 100 kpc is

low. We therefore expect that this galaxy configuration is a real physical association.

MS0002 is, in the description of Zwicky, an open cluster in optical images. Its elliptical BCM is more than a magnitude brighter than the second brightest cluster galaxy and makes the cluster BM type II. Oppenheimer et al. (1997) have recently identified it with the Abell cluster A2703 (of richness class 0), using the X-ray position in their EXSS catalog and the remeasured optical position of the BCM of A2703 (Paturel et al. 2000); the latter coincides with the BCM of MS0002. The PSPC X-ray contours are elongated but nearly featureless, indicating that the intergalactic gas is in a relaxed state. Indeed, both the X-ray gas and the optical major axis of the BCM are elongated in roughly the same direction (see Sec. 5.5). However, Jones & Forman (1999) also presented contour plots of the X-ray emission of A2703,¹ and classified the cluster morphology as “complex”, or containing substructure. Such morphologies, could, according to the authors, imply that the cluster is still undergoing subcluster mergers. Jones & Forman did not, however, derive the gas-density profile or estimate quantities such as the core radius for this cluster.

The optical morphology of MS0735 is that of a moderately poor cluster with a large cD galaxy (GL94). The Zwicky catalog labels it a medium compact, “very distant” cluster (but its spectroscopic redshift qualifies it to be one distance class farther, or “extremely distant”). The presence of the cD renders the cluster BM type I, though the contrast of the cD galaxy with respect to the second brightest member is not large (see Table 3.2). However, due to its redshift not being low enough for us to detect the full extent of the cD envelop, we could be significantly underestimating the total magnitude of the BCM. The first impression derived from its X-ray image is that the cluster gas is regular and extended, with no significant departures from symmetry. Donahue & Stocke (1995) analysed PSPC as well as the ROSAT High-Resolution Imager data (at 5 arcsec resolution). Through a detailed morphological analysis, they found the cluster to be symmetric and elliptical, with a core radius of 230 ± 40 kpc, and containing no significant structure on scales of 20-230 arcsec (1 arcsec is ≈ 4.5 kpc at the cluster $z = 0.216$). This probably indicates that the cluster has suffered no recent disturbances and is more or less relaxed on its large scales. Donahue & Stocke determined the cluster luminosity in 0.2–2.5 keV band to be $L_x = 6.1 \times 10^{44} \text{ergs}^{-1}$, and computed a gas temperature of $T_x \approx 2.4$ keV (significantly lower than expected from the empirical correlation between L_x and T_x (e.g. Edge & Stewart 1991). They further concluded that the cluster contained a central (Gaussian) source of Gaussian width 30 ± 3 kpc superposed on the extended emission, and located on the dominant central galaxy. This, together with the lower X-ray temperature, points to a putative cooling flow in this distant object similar to those seen in nearby clusters. Donahue & Stocke estimated a cooling flow mass deposition rate of $\approx 125 M_\odot \text{yr}^{-1}$. In more recent work using multi-resolution analysis, Pierre & Starck (1998) detected an additional very elongated core with evidence of two maxima, confined within the cD envelop. They also determined the position angle of the cluster core to be -30 deg and declared it close to that of the cD galaxy (-21 deg by their reckoning, -18.5 ± 1.8 deg according to this study). Donahue & Stocke show, however, that the position angle goes from about 10 deg at the very center to about -40 deg at a radius of ≈ 90 kpc, again climbs to 10 deg at roughly 350 kpc and twists gradually back to about -30 deg at 600 kpc and remains almost

¹Jones & Forman did not identify A2703 with MS0002, but the co-ordinates of the X-ray data of A2703 and the optical position of the BCM of MS0002 match to within the positional accuracy of the *Einstein* detection.

constant from there outward to 1 Mpc. The ellipticity of the X-ray emission, in contrast, is almost constant through the entire cluster outward of 50 kpc from the BCM. Such complex variation in the position angle implies that processes other than self-similar gravitational collapse are at work. For instance, the intracluster gas may be dense enough to cool; indeed, the cooling flow could extend to a few hundred kiloparsec. Therefore, the X-ray isocontours of MS0735 do not simply trace the gravitational potential. The cD galaxy turns out to be a special radio source as well (see Chapter 6).

Thus, our poor cluster sample is heterogeneous in its optical and high-energy appearance, and one (MS0735) presents evidence of a cooling flow in its center. Indeed, there is a considerable range in the observed X-ray morphologies of the whole class of poor clusters (including small groups of galaxies). X-ray luminous ($L_X > 10^{42}$ erg s $^{-1}$) but poorly populated galaxy systems tend to exhibit somewhat regular morphologies, with X-ray emission peaking on the most luminous (early-type) galaxy, and often extending well beyond the optical extent of the cluster (e.g., Mulchaey & Zabludoff 1998). They share these characteristics with rich clusters containing cD galaxies (e.g., Allen et al. 1995). In contrast, low-luminosity X-ray groups (to which class MS0301 may belong) tend to be irregular, and have their X-ray emission not centered on any one particular galaxy (e.g., Mahdavi et al. 2000). This dichotomy of morphologies with X-ray strengths may indicate the differences in the nature of the X-ray emitting gas in the two types of poor galaxy systems. The observed diffuse high-temperature emission in X-ray luminous poor clusters may originate from a true intra-cluster medium confined by the global potential while that of lower luminosity systems may involve contributions from the global medium as well as from intra-cluster gas gravitationally bound to individual massive galaxies, and activity in cluster members. These could have additional contributions from shock heating by collisions between galaxies and substructures.

5.3 Spatial Distribution of Galaxies

To place the above qualitative statements regarding cluster morphology on a firmer — quantitative — footing, the data necessary are the galaxy positions and magnitudes available in our catalogs. In this section, we perform 2-D cell counts and evaluate the areal density of galaxies in our cluster sample. We also attempt to identify possible substructure in the optical galaxy surface distribution and the X-ray contours, and look for correlations between the two. Had we *a priori* information about which galaxies belonged to the cluster, we could perform a quantitative analysis of the morphology without worrying about background contamination. As it is, we make an *ad hoc* assumption that the large-scale distribution of field galaxies is uniform and any non-uniformity is due to the cluster.

5.3.1 Galaxy Isoleths

A straight-forward quantitative analysis is to impose a rectangular grid over the entire cluster image and count the number of galaxies per box of fixed angular or metric width within it. If galaxies are located at random on the sky, such 2D cell counts would have a width expected

from a simple Poisson distribution. Any width larger than that of the Poisson counts implies galaxy clustering. Then, contours of constant projected surface density of galaxies, measured in galaxies arcmin⁻², constitute the cluster isopleths.

To construct the isopleths for our poor clusters, we use square cells of size 20×20 arcsec² (that correspond to different metric areas for the different clusters). We then smooth the isopleths over a 1×1 arcmin² region to ameliorate the effects of discreteness in galaxy counts. We present the isopleths of the clusters in Figs. 5.1, 5.2, 5.3 and 5.4, along with their optical/X-ray images to provide a direct comparison between the contours of galaxy and cluster gas distributions. Our contours being limited to galaxies brighter than $M_V = -18$ mag obviously do not count the dwarf galaxies; undoubtedly there are several tens, if not hundreds, of faint cluster members, analogous to the dwarf spheroidal companions of our Galaxy or the Virgo cluster. But, if — as we believe — these are not seriously affected by luminosity segregation, they are unlikely to alter the appearance or major structural parameters of the cluster.

From the smoothed isopleths we identify peaks in the spatial distribution. Using the idea that galaxies close to the BCM have a higher probability of being cluster members, we can take the centroid of the peak of the galaxy density around the BCM as the cluster center. In all these clusters except MS0735, the barycenter lies virtually on the BCM itself. MS0735 is similar to the case of the X-ray rich cluster Cl 1358+6245 (which also features in the EMSS catalog) where the galaxy isodensity contours are displaced ≈ 125 kpc south and ≈ 10 kpc east of the cD galaxy.

Nearly all of our clusters appear to have indications of substructure in their galaxy distribution. Though the signal-to-noise in the isopleths is compromised by the paucity of galaxies (not to mention the lack of cluster membership information), the appearance of substructure is in concordance with other studies. Such substructure in the galaxy distribution implies that the geometrical center of the cluster need not be physically meaningful. We find significant correlations between the optical isopleths and X-ray morphological features, including the centers, which indicate that these are perhaps identifiable with the dynamical state of the clusters. The optical galaxy positional data indicate distinct structure (like groups of galaxies) near the cluster cores. Although these could be due to projection effects (for we lack radial velocities for the galaxies), our data do not permit us to rule out weak X-ray emission emanating from such galaxy groups, causing patchiness in the X-ray appearance. A large fraction of the hot gas in poor clusters may not be primordial, owing their creation to ejections from cluster galaxies (Kriss et al. 1983; Ikebe et al. 1992) by galactic wind. The clusters appear, in general, to be rounder in the X-ray than in the galaxy isodensity contours.

The largely irregular nature of the clusters reflects that of the Virgo cluster (the archetypal poor cluster) whose primary characteristic is the overall irregularity with no one well-defined center and bright ellipticals such as M87 and M86 being the centers of secondary subclusters (Binggeli et al. 1987). The Virgo subclusters seem to be in a state of merging as evidenced by the kinematics and the X-ray properties of the cluster. Many, if not most, rich clusters show similar features at a closer look. Whether clusters are “regular” and “relaxed” (e.g., the Coma cluster) or “irregular”, they appear to be aggregates of subunits which have merged or are in the process of merging; many bear witness to the coincidence of optical and X-ray substructures. In short, the EMSS

poor clusters are similar in large-scale morphology to Abell rich clusters.

5.3.2 Structural Parameters

The dependence of galaxy density with radius in a cluster provides information on cluster dynamics and state of equilibrium. A simple description of the cluster density profile is through a three-parameter function of the observed (i.e., projected) galaxy number counts:

$$\sigma(r) = \sigma_0 f(r, R_c, R_h),$$

where $\sigma(r)$ is the projected galaxy density profile, σ_0 is the central density, R_c is the core radius (a central scale length, defined by $\sigma(R_c) = \sigma_0/2$, and R_h the halo size (a cutoff radius important at large distances from the cluster center and a measure of its limiting extent). In all regular rich clusters, the observed density profile falls off smoothly from a high central density to a low-density tail at the outer regions ≈ 3 Mpc from the center. Commonly-used fitting functions for these profiles in the literature are those given by Hubble (1936), Zwicky (1957), de Vaucouleurs (1960, with only two parameters), and King (1972). All of them assume that the clusters exhibit radial symmetry and are dynamically relaxed systems.

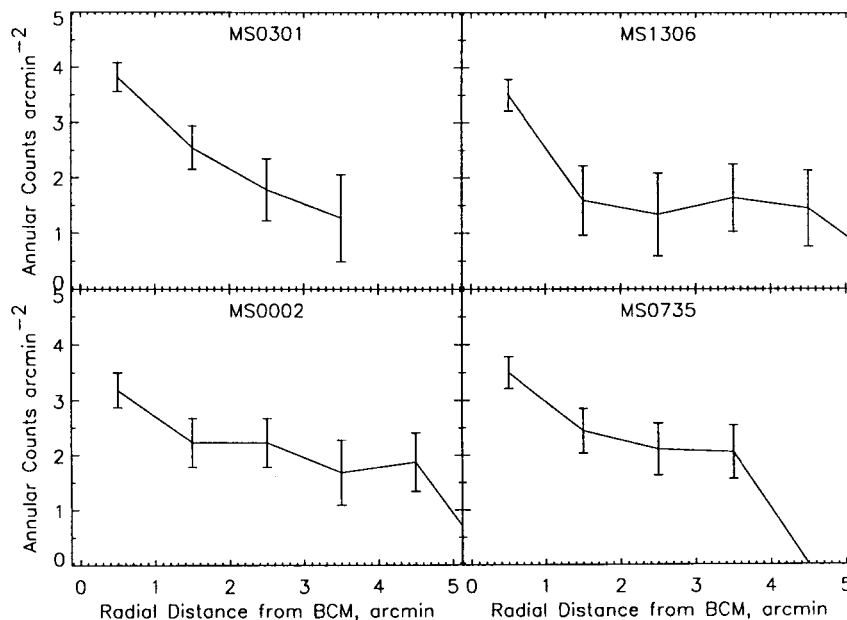


Figure 5.5: Galaxy counts in annuli centered on the BCMs with Poissonian error bars.

There is actually little justification in modeling our poor clusters as spherically symmetric systems in equilibrium. As we have noted in Sec. 5.3.1, the systems mostly appear ragged and far from tidy and symmetric. There are pockets of substructure i.e., local enhancement in projected galaxy counts. In Fig. 5.5, we plot the radial surface density profile of the galaxy distribution in the EMSS poor clusters. Though cluster galaxy counts broadly decrease with radius, they do not seem to match any well-defined profile. The inner 2 arcmin (250–450 kpc) regions of the clusters seem to contain the largest deviations from symmetry. A quick estimate, using the isopleths, of

the azimuthal dependence of galaxy counts around the cluster center (identified with the location of the BCM) further rules out symmetry from being a tenable assumption.

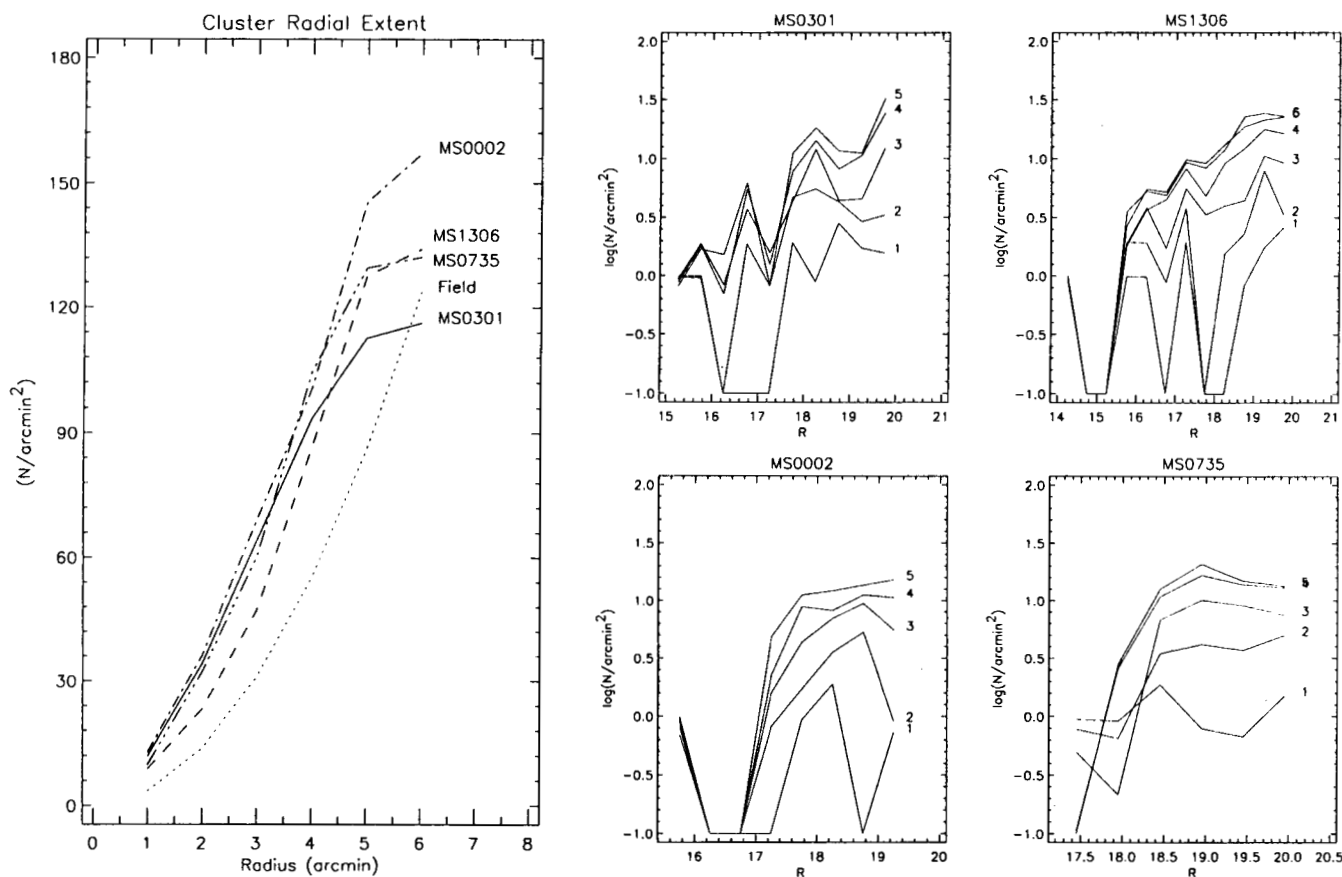


Figure 5.6: Radial extent of the poor clusters. Left panel: through the “curve of growth” method. Middle and right panels: using the method of Yamagata & Maehara (1986).

It is difficult to accurately determine the density profiles of even rich clusters at the outermost regions because of the low galaxy density and considerable uncertainties in the (largely inhomogeneous) background. There is virtually no determination of the “edge” of any cluster; the total “size” of a cluster is then a matter of definition. A standing example of the complexities in estimating cluster sizes due to different assumptions about field contamination around a cluster is of our nearest, most extensively-studied rich cluster, Coma ($z = 0.023$). Using both galaxy density and velocity profiles, different studies have arrived at discrepant results from 4 to > 10 Mpc for its size.

To estimate the expanse of clusters of galaxies, a common procedure is to construct an azimuthally-averaged profile of the surface distribution of the galaxies; the cluster size is then the radial distance at which the galaxy surface density falls to the background value. For most rich clusters, the galaxy density is several orders of magnitude higher than the field, so their radial profile has high signal-to-noise. Even so, different authors have obtained very different core radii for the same cluster (see Sarazin 1988). The situation for poor clusters is — not unexpectedly — different because their central density contrast is only a few times that of the field. Poor systems

individually occupy smaller regions than their rich counterparts and are quite often not virialized. As we have seen above, our poor clusters lack strong central concentrations. The present sample does not therefore lend itself gladly to computation of any “azimuthally-averaged” parameter.

As an alternative, we may borrow a procedure from aperture photometry to estimate how extended our clusters are. We apply the method in the following way: using the position of the BCM as the cluster center, we count the number of galaxies in R-magnitude steps of $\Delta m_R = 1.0$ beginning with the BCM magnitude and within circles increasing in radius from 1 to 6 arcmin (the latter is a little larger than allowed by the typical field of view of our CCD images). We estimate the field correction using the faint galaxy counts of Tyson (1988)² for the same circular areas. We then correct the observed counts at each radius for the background, thus estimating the contribution due to the cluster. The radius where the total cluster galaxy count falls to what is predicted for the field determines the cluster “boundary” or extension. The left panel of Fig. 5.6 presents the curves of growth for the cluster galaxy counts (corrected for background) relative to that expected from the field, at different radial distances from the BCM.

One other unconventional way of measuring the radial extent is that proposed by Yamagata & Maehara (1986, YM86 henceforth) for MKW/AWM poor clusters. This consists of determining the maximum radius where the cumulative galaxy count (to different magnitude limits) shows an appreciable excess over the field value. This is in fact the generalization of the curve of growth method, and is equivalent to determining the luminosity function for a range of radial distances from the cluster center, until the total galaxy count saturates. We perform a similar analysis; and plot the resulting curves in the second and third columns of Fig. 5.6.

From Fig. 5.6, we conclude that all our poor clusters extend to at least 5-6 arcmin, or the edge of the CCD frame. The galaxy density is significantly higher than that expected from the field counts of Tyson, especially within the central 3-4 arcminutes; outward of this, galaxy counts saturate largely due to incomplete coverage of the cluster in the optical images. Figure 5.6 confirms the trend in Fig. 5.5 for the largest deviations from symmetry to occur within about 2 arcmin of the cluster barycenter (defined to coincide with the BCM location). We see that the galaxies populating the brighter region of the luminosity function congregate within the cluster cores ($r < 2$ arcmin) while faint galaxies increase in number toward the outer regions (see Sec. 5.4.1).

Though we ourselves do not provide detailed analyses of the diffuse X-ray emission from the poor clusters, we use results from the Einstein Extended Sources Survey (EXSS; Oppenheimer et al. 1997) to determine if the PCs are indeed spatially extended in X-ray. Whereas the original EMSS source detection algorithm was most sensitive to finding point sources, the EXSS searched for diffuse sources using four circular apertures with radii of 1.25, 2.35, 4.20 and 6.10 arcmin. The progression of signal-to-noise in the various apertures help ascertain which of the detections are truly extended and which of the four aperture sizes best approximates each detection. Signal-to-noise should increase until the limiting radius of the source beyond which it should drop rapidly. We would then be able to compare the X-ray extension to the optical and determine whether the distribution of galaxies and hot gas extend to the same radius.

²We convert Tyson’s R-magnitudes to the Cousins passband with the aid of Fukugita et al. (1995).

The cluster MS0301 is not in the EXSS catalog. We can conceive of two possible reasons for its exclusion: its signal-to-noise in all the EXSS apertures is less than the threshold of 2.5σ or it is too close to the *Einstein* IPC rib. The EXSS extent of MS1306 is 6.1 arcmin (807.6 kpc), which is already as extended as the largest aperture covered by the EXSS. The actual size of both the galaxy distribution and the spread of the intracluster medium for MS1306 are therefore likely to be a little larger than 800 kpc (though we determine a halo size of about 600 kpc through an independent method below). MS0002 is also an extended X-ray emitter with an EXSS size of 4.2 arcmin corresponding to ≈ 700 kpc at the cluster distance. MS0735 is also excluded from the EXSS catalog; we are unable to establish the reason for the same. However, Donahue & Stocke (1995) who performed a detailed spatial analysis of the X-ray emission of MS0735, derived a core radius of 234 ± 40 kpc for the X-ray emitting gas which goes out to > 1 Mpc (see their figure 3). The presence of large-scale X-ray emission reinforces the idea that the poor clusters are genuine, bound systems.

In place of using detailed radial galaxy counts to determine cluster angular sizes, we use another alternative approach based on relative positions of cluster galaxies (Hickson 1977, henceforth H77) that lets us deduce both cluster size and structure. We can apply the method without resorting to binning of data or assuming a given center of the galaxy system. It consists of using the pixel or sky coordinates to construct all possible separation vectors $\vec{r}_{ij} = \vec{r}_i - \vec{r}_j$, measured in angular units. The separations preserve many structural properties of the galaxy distribution but do not contain any direct reference to absolute features such as spatial center nor require any assumptions of symmetry or regularity of structure. The pair-wise separations, $r_{ij} = |\vec{r}_{ij}|$, can thus illuminate the consequences of ambient density on galaxian properties.

We may define two characteristic distances from the (projected) separations of the galaxies:

$$\theta_c \equiv \left\{ [2/(N^2 - N)] \sum_{i>j} |r_i - r_j|^{-1} \right\}^{-1}, \quad (5.1)$$

$$\theta_h \equiv [2/(N^2 - N)] \sum_{i>j} |r_i - r_j|, \quad (5.2)$$

where N is the number of galaxies within a designated area, and r_i the position vector of the i th galaxy. Obviously, there will be $nC_2 = (N^2 - N)/2$ values of the pair-wise separations to compute. Writing the above statistical measures as generalized t-means following Capelato et al. (1980), we have:

$$\lambda_t = \left[\frac{1}{N_p} \sum_{i>j} r_{ij}^t \right]^{1/t}, \quad (5.3)$$

where t is a real number and N_p is the total number of galaxy pairs.

Since $\theta_c = \lambda_{-1}$ is a harmonic mean, it is sensitive to small separations; hence it evaluates a “core” size. $\theta_h = \lambda_1$ evaluates large-scale variations, and behaves as a “halo” size that parametrizes the overall galaxy distribution and can be considered the size of the cluster itself. Note that this

halo size is not necessarily the same as those derived from fits to the King or other functional forms of the surface density of galaxies. We can derive the corresponding core and halo metric sizes by correctly scaling θ_c and θ_h to the cluster redshift using the data in Table 5.1. Note that these core and halo sizes are not directly comparable to the ones in literature that are derived from fits to models such as the King or other isothermal functions. From the core and halo sizes, one may define a “concentration factor” following Austin & Peach (1974) and H77, $C \equiv \theta_h/\theta_c$, which is a measure of the core-halo separation. The presence of inhomogeneities (or pronounced substructures) may affect the values of $\lambda_{t<0}$.

Another interesting parameter definable from the t-means is λ_{-2} that measures the degree of “clumpiness” (H77):

$$K \equiv \frac{1}{\theta_c} \left\{ [2/(N^2 - N)] \sum_{i>j} |r_i - r_j|^{-2} \right\}^{-1/2}. \quad (5.4)$$

Now, to compute the separation vectors and length scales of the clusters, and interpret the means correctly, cluster membership information for galaxies is essential. It is easy to provide operational definitions of the field correction but hard to implement it. Clumpiness and the very diffuse extension of faint galaxies compared to bright galaxies are additional complications. In particular, one must account for the increasing fractional contamination due to non-cluster interlopers at fainter magnitudes. Normally, calculation of the core radius is more secure than halo size as it is less affected by the outer, sparser regions of the cluster where faint field galaxy contamination is likely to be higher. Consequently, the concentration factor is more sensitive to the error in halo radius than in core size.

A complete removal of non-cluster galaxies is not possible with our data as mentioned several times previously. But all is not lost since the division of our sample into “sequence”, “blue” and “red” (in Sec. 4.3) enables us to enhance the contrast of the cluster members over the background, and thus examine the cluster galaxy projected separations. If we further limit our analysis to reasonably bright magnitudes where the compromising effects of incompleteness and field galaxy interlopers are small, our results will be of better significance.

Table 5.2: Values of the core and halo sizes, the concentration factor and clumpiness parameter for the sequence galaxies computed within the largest circle enclosed by the CCD frame. Column 1 is the cluster name and Column 2, its redshift.

Cluster	z	θ_c , Mpc	θ_h , Mpc	C	K	N_{-19}	Diameter, Mpc
MS0301	0.083	0.20	0.34	1.66	0.63	30	1.00
MS1306	0.088	0.38	0.58	1.55	0.58	49	1.46
MS0002	0.160	0.44	0.68	1.56	0.58	70	1.67
MS0735	0.216	0.60	0.93	1.54	0.66	51	2.14

We therefore calculate the desired length scales, θ_c and θ_h , for our clusters using “sequence” galaxies brighter than rest-frame magnitude $M_V = -19$ within the largest circle enclosed by our

CCD images centered on the BCM. and list them in Table 5.2. In this table, we provide core and halo sizes (in Mpc) in columns (2) and (3) and concentration factors in column (4). Column (5) contains the values derived for the clumpiness parameter. We list the number of sequences galaxies counted in column (6) and in column (7), the diameter of the largest circle within which we perform the counts.

There is a clear trend between cluster angular size and redshift; this is a presentation of the Hubble law which is nearly linear over this redshift range. We compare our parameters with the mean values determined by H77 (Column (All) of his Table 3) for rich clusters at $0.021 \leq z < 0.10$. About one quarter of the clusters in the sample of H77 possess a cD galaxy as the dominant member. We find, not surprisingly, that the core and halo values for our poor clusters are typically one third and one quarter of the corresponding sizes (1.17 and 2.23 Mpc) for Abell clusters. The calculated sizes are also well within the diameter of the largest possible circle enclosed by our CCD images; thus, it appears that the smaller sizes of our poor clusters are not merely artefacts of the limited field of view of observations. The core size of MS0735 is a factor of ~ 2.5 larger than the core of the X-ray emission and six times as large as the cooling flow radius determined by Donahue & Stocke (1995). Small X-ray core radii (50–100 kpc) derived from fits to isothermal models appear common in rich clusters (e.g., Durret et al. 1994, but see Jones & Forman 1992, who compute much larger values) where the core radius of the galaxy distribution derived from the King function fits is close to 0.25 Mpc (Bahcall 1975, Girardi et al. 1995). This suggests that the distribution laws for the galaxies and gas (and dark matter) are different from that predicted by hydrostatic isothermal equilibrium in many clusters (see Baier et al. 1996), implying that most galaxy clusters are more complex than generally accepted.

The concentration factor C of our clusters is smaller than the average (1.90) determined by H77. The reason for this is simple: though the cores of rich clusters are larger than those of poor clusters, they contain a smaller fraction of the cluster population. This means that the halos of rich clusters are correspondingly larger. We find also that C is smallest for MS0735 with the central cD; this conforms to the results of H77 who found that Rood-Sastry type cD and L clusters show low values of concentration parameters with also small values of their associated dispersion compared to other cluster morphological types. Alongside the lack of central condensation in the poor cluster galaxy distribution, the smallness of θ_c values compared to the cluster X-ray extensions (determined from the EXSS catalog) also indicates that the poor cluster galaxies are more concentrated than the diffuse intracluster gas distributions. Such concentration could be due to small-scale correlations such as pairing of galaxies, in the galaxy distribution. Subgroupings in galaxy distributions toward the cluster barycenter could also reduce the core size.

Such substructure does indeed present itself in the isopleths; the irregular aspects of the cluster suggest it. Without a dynamical study, though, we cannot determine if the subgroups form a bound system within the clusters or if the clusters are still expanding with the Hubble flow and when they will condense from it. The clumpiness parameter turns out to be of similar amplitude as that in rich clusters, once the difference in core radii are taken into account. The clumpiness parameter, K of Equation 5.4, goes as \sqrt{N} . If the location of galaxies in the cluster is a Poisson process, K measures the breadth of fluctuations in galaxy density over the cluster mean normalized by the core size θ_c , and thus is a useful measure of the scale of subclustering.

From Table 5.2, we see that substructures in our clusters are about half their respective core sizes. The clumpiness is mildly larger for MS0301 and MS0735, caused presumably by the structures seen in the isopleths near the BCMs. There is no reason to believe that the *reasons* for the clumpiness are the same in both clusters. As already mentioned, the clumps seen in the isopleths of MS0301 coincide with the substructures (admittedly noisy) in X-ray emission. In contrast, the high-energy map of MS0735 is smooth on large scales, while the galaxian isodensity contours evince two condensations toward the south-east of the BCM (almost along its optical major axis).

We prefer to use our halo size and concentration factor results prudently, since they are likely to suffer from having been determined over the small luminosity interval of about 4 magnitudes brighter than $M_V = -19$ (*cf.* Sec. 5.4.1). It is essential to acquire multi-object spectroscopy of the poor clusters to determine fully their structure and sizes among other important quantities.

5.4 Galaxy Segregation

The density profiles of galaxies separated into E, S0 and S morphological types demonstrate that in regular clusters with strong central concentration, the projected density of late type galaxies decreases non-linearly toward the center and is consistent with a zero space density of spirals and irregulars in the core (Oemler 1974, Dressler 1980). Such a trend of early-type galaxies to be found in denser regions such as the cluster cores and for spirals to be more common in sparse regions goes by the name of morphology-density relation or morphological segregation (see Sec. 1.2.3 for more). Clustering strength is another among many properties of galaxies that are correlated with their morphology. In particular, early-type galaxies tending to cluster on smaller angular scales than later types (as in, e.g., the Pisces-Perseus supercluster, Giovanelli et al. 1986).

Now, if early-type galaxies are on the average brighter than late-type galaxies (see review by Roberts & Haynes 1994), then galaxies that are more strongly clustered are brighter than those less clustered, leading to luminosity segregation. Luminosity segregation results in brighter galaxies tending to be found in denser regions such as the cluster cores and faint galaxies being more common in regions that are not so dense. A consequence of such segregations is that the core radii of clusters can change significantly with the limiting magnitude of the sample: larger core radii result from deeper samples as in, for instance, the Coma cluster (Quintana 1979). But observational evidence for this effect remains uncertain and controversial, with some studies claiming to see segregation with the most luminous galaxies being closer to the cluster centers (e.g., Capelato et al. 1980; Dominguez-Tenreiro & del Pozo-Sanz 1988; Yepes et al. 1991; Adami, Biviano, & Mazure 1998 and references therein) with significantly lower velocity dispersions (Rood et al. 1972), and others refuting such claims (e.g., Einasto 1991). Luminosity and color segregation appear in both nearby clusters e.g., Coma (Capelato et al. 1980) and more distant ones (Thompson 1976; Mellier et al. 1988), as well as in poor galaxy systems (Hickson 1980). Further, the brightest few galaxies of a cluster appear to have velocities lower than the cluster average and tend to be preferentially located in the cluster centers (Biviano et al. 1992).

Such luminosity segregation, if the dark matter distribution is well-defined and if galaxies are homologous, presumably represents a real mass segregation. The fact that it is usually the

brightest few galaxies that show segregation suggests that the dynamical status of these galaxies is different from that of the rest of the members. The interpretation of segregation effects recall the “nature *vs.* nurture” problem of galaxies. Mass segregation may be a result of either primordial effects i.e., due to more massive galaxies forming at high peaks in the primordial density field (e.g., Kaiser 1984) or environmental effects such as dynamical evolution during the cluster relaxation phase and/or dynamical friction over a Hubble time. If, after a first phase of violent relaxation, a slow two-body relaxation occurs within the clusters, leading to equipartition, the multi-mass cluster presents mass segregation with more massive objects being concentrated toward the cluster center. Or dynamical friction can preferentially slow down massive galaxies, causing them to fall closer to the cluster core, circularize their orbits and enhance their merger rates (Mamon 1992). In the case of morphological segregation, the fundamental parameter determining it remains elusive — it could be the local galaxy density (Dressler 1980, Postman & Geller 1984) or ‘global’ cluster properties such as the distance from the cluster center (Whitmore, Gilmore, & Jones 1993 and references therein).

Usually, studies of segregation effects employ the galaxy angular two-point correlation function or radial distribution over various magnitude ranges. Alternatively, we may look for segregation effects using two quantities suggested by Capelato et al. (1980):

- the average distance of galaxies within a magnitude or color bin from the cluster center and
- the distance of each galaxy from all other of the same absolute magnitude or color.

The first case generates a characteristic length defined by the generalized t -means, given the distances r_i of galaxies from the cluster center, as:

$$\langle r \rangle_t \equiv \left[\frac{1}{N_g} \sum_i r_i^t \right]^{1/t}, \quad (5.5)$$

where N_g is the number of galaxies in the cluster. For our poor clusters, we designate the cluster center to coincide with the location of the brightest cluster member (BCM). The second item corresponds to the mutual separation vectors defined in Eqn. 5.3, which may be used to estimate the “halo” and “core” sizes defined by Hickson (1977), set out in Eqns. 5.1 and 5.2. The intergalactic separation calculated for each galaxy from all others is more suited to analyzing poor clusters since it does not depend on the number of galaxies or the choice of cluster center or the smoothness of the galaxy distribution.

The catalog of magnitudes, colors and positional information of the galaxies in our poor cluster fields provide the required data to study galaxy segregation. These data constitute a complete sample for $M_V \approx -18.5$ for each poor cluster. Usually, colors of galaxies are more amenable to determination than their morphologies. Since morphologies and colors are correlated, (as are velocity dispersions and colors), we may speak of color segregation being equivalent to morphological segregation to first order.

In order to detect segregation confidently, one must first remove the perturbing effects of field galaxies. Now, a uniformly distributed field has a higher characteristic separation than a clustered region, resulting in an artificial enhancement of the overall moments of the separation vectors.

Note that field galaxies have an intrinsically weaker clustering amplitude than cluster members. Literature contains references to two (irreconcilable) scenarios of field contamination on luminosity segregation: that the field *masks* real segregation (Dominguez-Tenreiro & del Pozo-Sanz 1988) and that failure to correct for the field *produces* spurious segregation due to increase in scale sizes at fainter magnitudes through a higher proportion of field over cluster galaxies (Metcalf, Godwin, & Peach 1994). Of course, we do not have velocity information to sift out the interlopers from cluster galaxies. However, the division of our galaxy sample in each cluster into three zones in the color-color plots in Sec. 4.3 helps enhance the contrast of the cluster “sequence” members over the background, thus nulling to some extent the contamination by non-cluster interlopers. It also helps us examine the distribution of probable cluster members in comparison with “blue” galaxies composed mainly of late-type galaxies in the field and some cluster irregulars, and “red” galaxies which should almost exclusively contain background (high-redshift) objects.

We study *differential* luminosity and color segregation by studying the variations of the projected characteristic length scales (1) for subsamples of “sequence” galaxies in different magnitude bins and (2) for galaxies separated into the three different color zones mentioned above. We choose a magnitude interval of $\Delta m = 1$ mag, which is large enough to be free of systematics due to photometric errors and ensures that a reasonable level of mass segregation can be observed. We shall say that a set of galaxies is segregated in luminosity or color for a given magnitude or color range, respectively, if the values of the core and halo length-scales are smaller than those of any other set.

5.4.1 Luminosity Segregation

Table 5.3: Intergalactic separations for different magnitude ranges computed within 0.5 Mpc of the BCM.

Cluster	Absolute Magnitude Range	λ_{-1} kpc	λ_1 kpc	$\langle r \rangle$ kpc
MS 0301.7 + 1516	$M_V < -21$	199	363	230
	$-21 \leq M_V < -20$	194	489	171
	$-20 \leq M_V < -19$	163	303	244
	$-19 \leq M_V < -18$	206	405	185
MS 1306.7 - 0121	$M_V < -21$	294	510	249
	$-21 \leq M_V < -20$	250	561	265
	$-20 \leq M_V < -19$	434	677	282
	$-19 \leq M_V < -18$	270	610	212
MS 0002.8 + 1556	$M_V < -21$	391	766	407
	$-21 \leq M_V < -20$	454	712	211
	$-20 \leq M_V < -19$	438	705	422
	$-19 \leq M_V < -18$	461	728	335
MS 0735.6 + 7421	$M_V < -21$	516	1006	392
	$-21 \leq M_V < -20$	586	984	603
	$-20 \leq M_V < -19$	576	970	472

We divide the sequence galaxies brighter than $M_V = -18$ mag into four groups by increasing

magnitude. We choose a magnitude interval of $\Delta m = 1$ mag till $M_V = -21$ and include in the last bin all galaxies brighter than $M_V = -21$. Note that this system of binning accomodates a different number of galaxies in each bin. We calculate the length scales λ_t and $\langle r \rangle_t$ fot $t = 1$ and $t = -1$. Table 5.3 gives these values. Similar to the results of the halo and core sizes (Sec. 5.3.2), we find that the scale sizes are much smaller than those of rich clusters such as Coma ($\lambda_{-1} \sim 1$ Mpc, Capelato et al. 1980).

The small differences seen between $\lambda_{\pm 1}$ and $\langle r \rangle_t$ are consistent with the reasonably small values of the clumpiness parameter derived in the previous section. The erratic behavior of these parameters for galaxies fainter than $M_V = -21$ mag indicates that this is a threshold luminosity below which luminosity segregation effects are likely to be very weak or non-existent.

When we apply the first method of comparing radial distances from cluster center, we see that, on average, fainter galaxies are more distant from the cluster center than their brighter cousins. We find feeble evidence that the galaxies with absolute magnitude $-21 \leq M_V < -20$ congregate more strongly to the center in the clusters MS0301 and MS0002. In MS0735, the opposite situation occurs along with the brightest four galaxies showing the smallest radial separations from the BCM that presumably defines the center of the cluster potential well. Typically in rich clusters dominated by cD galaxies, only the brightest few galaxies show luminosity segregation (Oemler 1974). In MS1306 however, galaxies with $-20 \leq M_V < -19$ are the most spread out of all, indicating anti-segregation. Thus the analysis using the second quantitative description of intergalactic separations also illuminates the presence of weak luminosity segregation.

The fact that the luminosity segregation responds marginally more strongly to cluster-centric distance rather than to local environment suggests that its dominant driver is the global (dynamic) potential of the cluster. It is possible though, that we are detecting a genuine spatial segregation but one which is superposed on field-contamination at the faintest luminosities. Therefore, we consider the above evidence as being only tentatively in favor of luminosity segregation.

5.4.2 Color Segregation

Table 5.4 provides the estimates of the characteristic length scales for galaxies in the different color zones. Figure 5.7 shows the projected spatial distribution of the three subsets — sequence, blue, and red — in the field of each poor cluster. Down to the limiting magnitudes of the galaxy datasets, the galaxy distributions within each subset are highly asymmetric. This supports our conclusion from Fig. 5.5 that azimuthal symmetry is in general not a valid assumption for poor clusters.

The macroscopic color distributions also show that the surface density of the brighter sequence galaxies is larger closer to the cluster center, as already noted while discussing luminosity segregation.

We see from above that blue galaxies i.e., those with signs of recent or ongoing star-formation, dominate in the outer parts of the cluster. We recall that while the color selection does indeed discriminate against non-cluster galaxies being included into the sequence, the blue zone may still contain some late-type cluster members. Then, this result sits well with our previous discussion of

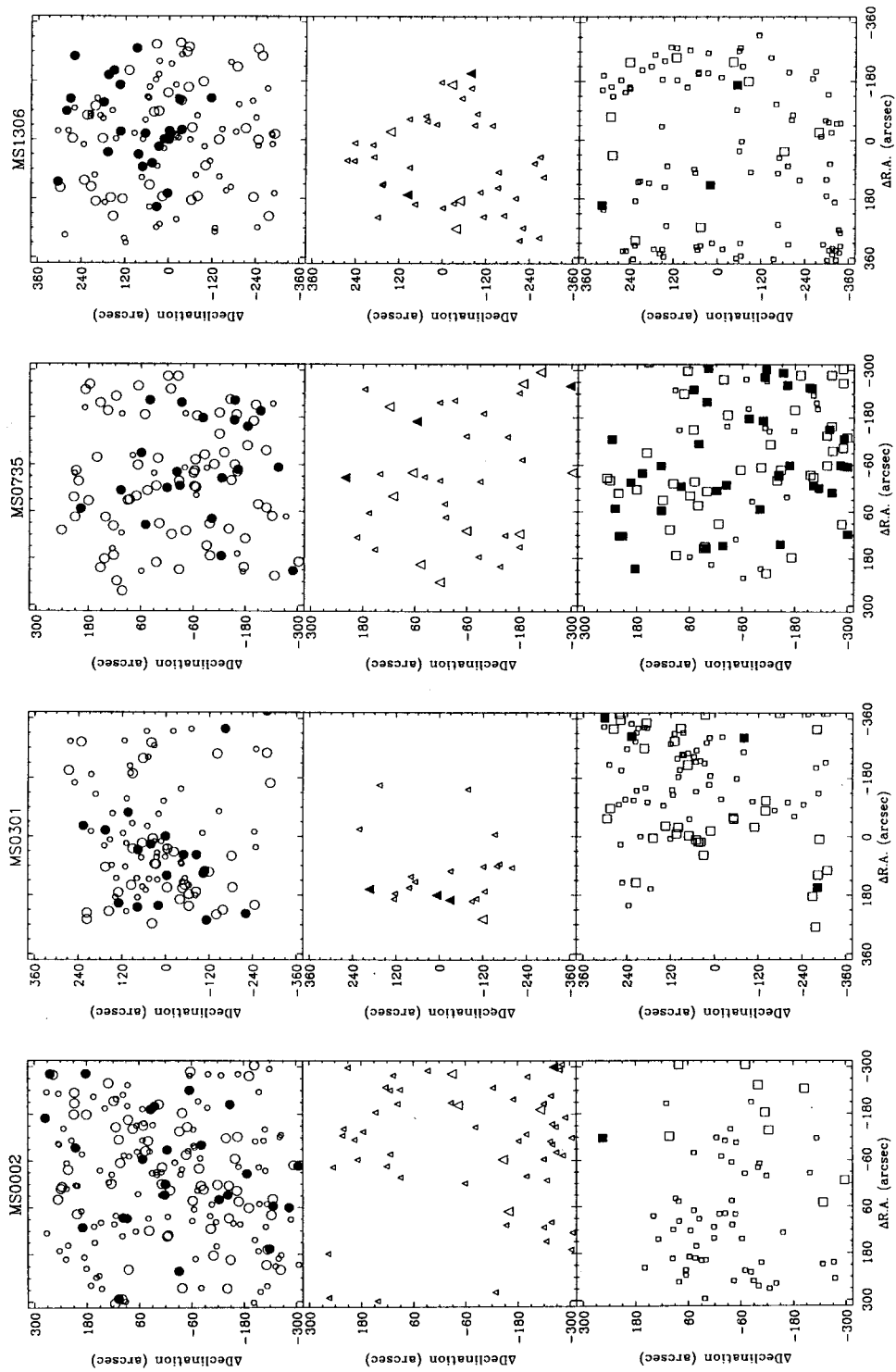


Figure 5.7: The distribution on the sky of galaxies in the three color zones defined in Sec. 4.3; top panel “sequence”, middle “blue”, and bottom “red” galaxies. Galaxies shown by filled symbols are brighter than absolute magnitude $M_V = -20.5$, large open symbols are in the range $-20.5 < M_V \leq -19$, and small open symbols are fainter than $M_V = -19$.

Table 5.4: Intergalactic separations and mean radial distances for galaxies brighter than $M_V = -18$ in different color zones (using the $B - V$ color-magnitude relation) and within the largest circle enclosed by the CCD.

Cluster	Color Zone	λ_{-1} kpc	λ_1 kpc	$\langle r \rangle_{-1}$ kpc
MS 0301.7 + 1516	Sequence	214	353	213±181
	Blue	121	261	385±900
	Red	201	359	187±149
MS 1306.7 - 0121	Sequence	369	586	239±123
	Blue	377	651	326±304
	Red	370	674	492±574
MS 0002.8 + 1556	Sequence	453	701	319±132
	Blue	329	819	605±175
	Red	493	833	404±301
MS 0735.6 + 7421	Sequence	604	944	500±316
	Blue	737	1103	579±388
	Red	581	973	411±102

the Butcher-Oemler (BO) effect in the clusters, and the frequent occurrence of the BO participants in the cluster outskirts (Butcher & Oemler 1984; Dressler et al. 1994; Oemler et al. 1997). Early-type galaxies which populate the red zones appear to cluster more strongly than the blue or late-type galaxies. Nevertheless, they appear to be as much or more spread out in the cluster fields than the blue galaxies. In the field of MS0735, there seem to be remarkably many red galaxies which appear to overlap the cluster sequence members. These show a similar degree of aggregation as the sequence objects. One possible interpretation of this is to hypothesize a second cluster along the line of sight to MS0735, and at a slightly higher redshift. If such is indeed the case, we may be detecting the late-type population of the background cluster (due to the K-correction being that of MS0735). As always, since we use only colors, with the attendant uncertainties of morphological typing, we may speak of early- or late-types simply based on whether the galaxies are red or blue in a particular pair of color indices.

Overall, the evidence for morphological segregation is subtle and not very tractable to our analysis. We emphasize that what we have presented here represents the situation for the four EMSS poor clusters only, and does not presume to be either conclusive or meaningfully applicable to all clusters. However, these results may be regarded as possible directions for further investigation.

5.5 Alignment Effect

If the Cosmological Principle is valid, the properties and distribution of galaxies and large-scale structures must be random. Signatures of systematic coherence such as the oft-cited morphology-density relation of galaxies direct attention to questions of whether systematic properties are inborn or if they are a result of galaxian environments and evolution. Alignments in the galaxy orientations comprise another coherent effect that must be fit into the galaxy formation puzzle.

Literature on the “alignment effect” has the following protagonists: (1) cluster galaxies, mostly

the bright ones and most prominently, the BCM; and (2) clusters themselves. At the spatial scales of a few tens of megaparsec, clusters appear to be weakly collimated with their neighbors (Binggeli 1982; Struble & Peebles 1985; Tully 1986; Flin 1987; Plionis 1994, but see Martin et al. 1995 for a refutation; Chambers et al. 2000), constructing elongated superclusters that may percolate into larger-scale structures. Groups of galaxies also tend to align themselves with neighbors on scale extending to $\sim 30 - 60$ Mpc (West 1994). Within clusters themselves, mildly non-random effects exist in the member galaxy orientations (e.g. Rood & Sastry 1972; Thompson 1976; Lambas, Groth, & Peebles 1988). Further, ellipticals sometimes tend to align in parallel with their host clusters while disk galaxies tend to be either parallel or perpendicular to the principal axis of the cluster (e.g., Adams, Strom, & Strom 1980). The most persuasive indication of alignment involves the dominant galaxy of clusters, in particular the cD galaxies. The cD optical major axis is closely aligned with that of the galaxy distribution in the parent rich cluster (Sastry 1968; Carter & Metcalfe 1980, Binggeli 1982; Struble & Peebles 1985), the diffuse emission from the intracluster gas (Sarazin et al. 1995; Allen et al. 1995), and is co-directional with the nearest neighbor cluster (Rhee, van Haarlem, & Katgert 1992) out to 20 Mpc (West 1994). Further, the BCM major axis is oriented along the line connecting the two brightest member galaxies (Struble 1990); the effect is stronger than the alignment caused by the ellipticity of clusters (Trevese, Cirimele, & Flin 1992). However, the second brightest member is itself not aligned with the parent cluster; this supports the unique status of the BCM as the product of 'special' formation processes. Further, this alignment effect operates even in poor clusters (Mulchaey & Zabludoff 1998; Fuller, West, & Bridges 1999) indicating that the processes responsible for the coherent effect operate independently of system richness.

If the gas giving rise to the observed X-ray emission from clusters is in hydrostatic equilibrium, it is a good tracer of the cluster potential, and thus the position angle of X-ray isocontours point along the distribution of baryons in the cluster. It is not entirely certain that the alignment represents a primordial effect; dynamical evolution or tidal forces could create the effect. Since large objects such as galaxy systems evolve slowly with time, they provide the fossil record (to use a phrase from Bahcall 1988) of the history of formation of galaxies and cosmic structures, which must be reconciled with the minute temperature fluctuations in the cosmic background radiation. The type of dominant dark matter determines the initial form of the fluctuation spectrum from which structure formed by gravitational collapse. In general, large-scale alignments require power on large scales in the initial fluctuation spectrum, arguing for structure formation from large to small scales (Zeldovich 1970; and much subsequent work) based on hot dark matter. However, alignments are possible on protocluster scales in the context of cold dark matter theory too, if the mass profiles and mass-to-light ratios of clusters are universal (e.g., West et al. 1991). Since it is not the intention of the present work to test the above theories (and since quality evidence through measurements of fluctuations in the cosmic background has kept researcher busy), we simply summarise that alignment studies are important tools to test structure formation theories which posit gravitational instability acting on Gaussian perturbations giving rise to cosmic structure.

We examine the following sets of orientations for alignments among themselves:

- the major axis of the BCM

- the vector between the BCM and the second brightest galaxy
- isopleth of galaxies
- the inclination of the X-ray emission.

Table 5.5: Position angles of the BCM, the angle between the BCM and the second brightest galaxy, the position angles of the extended X-ray emission and the galaxy isopleths. All angles are in degrees North through East.

Cluster	ϕ_{BCM}	ϕ_{12}	$\phi_{isopleth}$	ϕ_{X-ray}
MS 0301.7 + 1516	-74 ± 4	-32	$+39 \pm 10$	$+68 \pm 10$
MS 1306.7 - 0121	$+10 \pm 2$	-83	-64 ± 01	-45 ± 08
MS 0002.8 + 1556	$+31 \pm 4$	+91	$+42 \pm 06$	$+49 \pm 08$
MS 0735.6 + 7421	-18 ± 2	+168	-16 ± 02	-15 ± 09

We determine geometrical parameters including the position angle of the BCM, ϕ_{BCM} in Sec. 6.3; we see there that there is hardly any isophotal twisting, so the position angle is securely derived. We identify the second brightest cluster member and compute the angle ϕ_{12} of the great circle containing it from the meridian containing the BCM. To estimate the position angles (ϕ) of the isopleths and X-ray emission, we fit ellipses to the isopleths and to the light distribution of the intracluster medium using the method of Sec. 6.2. The reliability of ϕ derived from an ellipse fit depends on the ellipticity of the isopleths and X-ray emission (for round distributions, ϕ is not a meaningful quantity), the signal-to-noise ratio, and whether there is any isophotal twisting. A greater problem with this study is, of course, the severely limited number of cluster galaxies creating large errors in the statistics. This makes reliable determination of the position angle of the isopleths rather difficult. The incompleteness at magnitudes $m_V > 21$ and noncluster interlopers (due to lack of membership information) exacerbate the problem.

Despite the difficulties, it is possible to use projected galaxy positions, assuming field galaxies have a homogeneous distribution, to determine cluster position angles. We restrict determination of the orientations of the isopleths to galaxies brighter than $M_V = -18$ and to the X-ray emission within 0.7 Mpc of the BCM. These are, of course, much larger radii than that of the BCM itself. To check how robust our determination of the isopleth position angle is, we estimate it for a subset of the galaxies, those in the “sequence” of the color-color diagram (Sec. 4.3) of each cluster. A comparison of Figs. 5.1, 5.2, 5.3, 5.4, and 5.7 is instructive to gauge differences in distributions of the two sets of galaxies. We find that for all clusters except MS0002, the sequence $\phi_{isopleth}$ is similar to that determined using all $M_V < -18$ galaxies within the errors. For MS0002, however, $\phi_{isopleth}$ for the “sequence” galaxies is 30 ± 6 deg, or $\approx 1.5\sigma$ westward of the isopleths determined using all galaxies. Keeping these in mind, we look for alignments among the various entities.

As we have mentioned in Sec. 5.2, the position angle of the X-ray isocontours of MS0735 changes with radius in a sinusoidal fashion. The position angle should not change with radius if only self-similar processes such as gravitational collapse are important. Thus the emission does not directly trace the cluster gravitational potential, and attests to the cooling of the gas within the inner 200 kpc or so. Outside the cooling radius of the ICM, however, one may expect that the

behavior of the position angle is mostly controlled by the cluster potential. So, the ϕ_{X-ray} we quote for this cluster is for the outer regions. Typically, the position angles derived using the X-ray maps have errors of about 10 degrees.

Table 5.5 lists the position angles of the major axis of the BCM in column (2), the angle on the sky between the BCM and the second brightest cluster galaxy (ϕ_{12}) in column (3), the long axis of the isopleths of the galaxy distribution, $\phi_{isopleth}$, in column (4), and that of the X-ray emission (ϕ_{X-ray}) in column (5). All angles are in the sense north through east. Among these, the position angle of the BCM is the most accurately determined.

In all our poor clusters, there seems to be no preference for the line connecting the first and second brightest cluster galaxies to participate in the alignment effect with either the BCM, or the galaxy isopleths or the X-ray emission from the ICM.

In MS0301, all four position angles are essentially different, suggesting a complete lack of alignment among the BCM, the galaxy distribution and the intracluster gas. This is not unexpected, considering the disordered appearance of the cluster as traced by galaxy positions and discrete sources possibly contributing to the X-ray luminosity. The BCM of MS1306, the most luminous among our sample, is oriented to within 20 deg in the direction of the isopleths but is pointed nearly 40 deg to the east of the X-ray emission. We may argue here that the cluster X-ray emission is somewhat disordered, and the ellipticity and position angle vary spasmodically, thus masking any possible alignment. Or we may choose the other viewpoint to say that, as in the inner regions of MS0735, the X-ray emission may deviate from hydrostatic equilibrium and thus does not faithfully follow the gravitational contours of the cluster. In contrast, for MS0002 and MS0735, the optical major axis of the BCM, the isocontours of the galaxy distribution and the X-ray emission (from the intra-cluster hot gas which, outside the cooling radius, traces the cluster gravitational potential) are clearly elongated in approximately the same direction.

The collimation of the BCM major axis with the galaxy distribution in the parent cluster follows the statistical behavior of BCMs in rich clusters (Sastry 1968; Carter & Metcalfe 1980, Binggeli 1982; Struble & Peebles 1985). The alignment of the BCM with the diffuse emission from intracluster gas also resembles that seen in rich clusters containing cD galaxies (see, e.g., Rhee et al. 1992; Sarazin et al. 1995; Allen et al. 1995), and in poor groups with $\sigma < 500 \text{ km s}^{-1}$ and $L_X \approx 10^{41} - 10^{42} \text{ erg s}^{-1}$ (Mulchaey & Zabludoff 1998). It is tempting to speculate we have detected the alignment "effect". We believe the alignments are not artefacts of our analysis; in fact, the probability that two (conceivably three) of four X-ray selected clusters should randomly show the effect is rather small. Since we deal with such a small sample, we do not perform statistical analyses of the distributions of the differences of the various position angles, and cannot therefore quantify the significance of the alignments.

This similarity between our X-ray luminous poor clusters, much poorer groups, and cD clusters offers support to the insensitivity of the alignment effects to system richness. These alignments further suggest that the formation and/or evolution of the central galaxy is linked to the shape of the global cluster potential.

Now, the major axes of groups (West 1989) and clusters (Binggeli 1982) of galaxies within superclusters exhibit a strong tendency to orient themselves along similar directions, thus creating a

supercluster “axis”. The possibility of such collimation arising fortuitously is $< 1\%$. In our own sample, we can look for such alignment for one cluster. MS0002 (now identified with A2703) and six other Abell clusters — A1, A43, A93, and probably A79, A84 and A2678 — all at redshifts of $0.09 \leq z \leq 0.12$ comprise a supercluster of dimension ≈ 80 Mpc (for $H_0 = 50 \text{ km s}^{-1} \text{ Mpc}^{-1}$; Batuski et al. 1985). We found, through a NED search for Abell clusters within 300 arcmin of MS0002, that the richness 1 cluster A2705 could also be part of this supercluster. So, we can apply a modification of Binggeli’s (1982) test consisting of comparing the cluster position angle and the orientation of its BCM with the direction to its nearest neighbors in the supercluster. The orientation of MS0002 vis-a-vis Abell 2705 (at $z = 0.1147$) is 102 deg and with respect to Abell 1 ($z = 0.1249$) is 87 deg. While the lines joining these clusters to MS0002 are inclined by more than 60 deg away from the BCM, they are within ~ 10 deg of the line joining the BCM and the second brightest galaxy of MS0002.

5.6 Summary and Discussions

It is a capital mistake to theorize before one has data. Insensibly one begins to twist facts to suit theories, instead of theories to suit facts.

– Sherlock Holmes (Sir Arthur Conan Doyle)

There exist a number of strong correlations between the optical, radio and X-ray properties of clusters of galaxies. However, if the cluster morphology is related to its degree of dynamical evolution, the correlations may be affected. The X-ray luminosity, temperature, and optical velocity dispersion relations may depend significantly on differences in cluster cooling flow mass-deposition rates, which create differences in the density profiles (White, Jones, & Forman 1997).

We may now address the issue of whether the poor clusters are bound systems. Our poor clusters are similar to rich clusters in terms of a significant number of faint galaxies in the cluster “sequence”, their central concentration, the coincidence of the position of the BCM and extended X-ray emission, and reasonable coincidence of X-ray and galaxy density isocontours. From the velocity dispersions (computed from the $L_X - \sigma$ correlations in Chapter 2) and their halo sizes (Table 5.2), we compute that the crossing times are ≈ 400 million years for MS0301 and MS1306 and ≈ 600 million years for MS0002 and MS0735. Such short crossing times (≤ 0.05 of a Hubble time) suggest that they are likely to be bound systems, and that the *cores* are perhaps close to being virialized.

The lack of a clear galaxy density profile for the poor clusters could be due to both poor statistics as well as internal dynamics. If genuine, the non-uniform radial profiles demonstrate that violent relaxation is probably not as efficient in these poor systems as in their rich counterparts. The substructures found (admittedly at weak significance, not much larger than that expected from random fluctuations) attest perhaps to these structures still collapsing for the first time, or to secondary infall into the clusters of small groups from the surrounding larger-scale structures.

Optical and X-ray studies (Geller & Beers 1982; Dressler & Shectman 1988; Slezak et al. 1994; Pierre & Starck 1997; Jones & Forman 1999) suggest that over 40% of rich clusters exhibit

substructure in their galaxy distribution (both in position and velocity space) and in their intra-cluster medium. It is also arguable whether the distributions of galaxies, gas, and dark matter in the clusters are similar; the subclustering seen in the galaxy distribution is not prominent in X-ray. Many, if not most, poor as well as rich clusters of galaxies are thus likely to be out of dynamical and hydrostatic equilibrium.

The implication is that the clusters, both rich and poor, are either young systems being formed in an inhomogeneous fashion by the continual formation and amalgamation of subcondensations, and/or are regions of complex, violent interactions that drive them out of equilibrium.

Dynamical friction, implicated in the formation of cD galaxies, segregates the most massive galaxies toward the cluster center. But it may not be very effective in poor clusters, where the two-body relaxation time can be greater than the age of the Universe. Let us assume that luminosity segregation is tantamount to mass segregation if all galaxies carry a certain mass-to-light ratio. After virialization, the galaxy cluster undergoes dynamical evolution with no radial mass segregation. However, during encounters of cluster members which may lead to merging, energy exchange leads to decay of the orbits of relatively massive cluster members through dynamical friction. These bright galaxies thus arrive at the cluster center thus showing mass segregation. Near the cluster center, the tidal forces due to the cluster are weak, but there are increased chances for the slow-moving bright galaxies to be cannibalized by the dominant galaxy. As a consequence, the dominant galaxy grows at the expense of its bright neighbors; this process results in a decrease of luminosity segregation in the center. This would explain why we see MS1306 with a bright, compact core embedded in a sparse structure. similar to the situation in compact groups.

Alignment effects are important and meaningful if the geometric axes reflect the cluster or galaxy dynamics. For instance, the shapes of elliptical galaxies arise from their velocity anisotropy, which is set into the stellar orbits once the dissipative galaxy formation is complete. In an analogous manner, if the intrinsic shapes of clusters — rich or poor — are related to their formation process, then it is likely that they inherit characteristics such as ellipticity and position angle from the progenitor large-scale structure. Tidal effects or torques after formation are unlikely to perturb the shapes and dynamical axes significantly. Then, the alignment can be traced back to the collapse of the cluster along the filament present in the cosmological initial conditions (Merritt 1985; Dubinski 1998).

We shall argue in Sec. 6.6 that the BCMs in these poor clusters are indeed likely to be results of galaxy interactions and consequent mergers. The high galaxy density and low velocity dispersions of poor clusters make them hospitable to such multiple mergers. To recall the simulations of Dubinski: the central galaxy forms via galaxy-galaxy mergers early in the lifetime of the poor cluster, and the BCM which does not suffer significant recent dynamical evolution, remains at rest in the center of the cluster potential. Such mergers will not occur in a haphazard fashion, but rather will proceed in an organized manner along preferred axes which may trace the large-scale anisotropies in the primordial density field. This gives them a tendency to be aligned with the major axis of their parent cluster and the galaxy distribution on much larger scales.

We have seen that the static properties of poor clusters — *viz.*, the positions, magnitudes (or

luminosities), and colors (or crude morphological types) of the member galaxies — have strong correlations, and permit inference of cluster dynamical evolution and even shed light on the formation of cosmic structures. To determine the actual mass distribution, one requires the map of the cluster dark matter, which is best derived using gravitational lensing (see Mellier 1999). None of our poor clusters show evidence of lensing in our CCD images; MS0735 does not exhibit lensing even in images obtained with much better seeing (Luppino et al. 1999).

Our evidence for substructure in poor clusters, for galaxy segregation in luminosity or morphology, and of galaxy alignment are far from definitive. However, there is reason to believe that substructure and alignment effects occur in our poor clusters just as they do in the richer systems, and thus are independent of cluster richness. Poor clusters, which occupy the intermediate regime in density-enhancement, are about ten times as numerous as rich systems. They can therefore serve as very useful tools in mapping the relief of the universe and in distinguishing structure formation scenarios. To separate systematic properties of clusters of galaxies from those peculiar to only a few, it is desirable to assemble a large dataset of spectroscopic redshifts to construct samples of confirmed cluster members.

Chapter 6

The Brightest Cluster Galaxies

In Nature's infinite book of secrecy

A little I can read.

– William Shakespeare

6.1 Avant-Propos

Many clusters of galaxies (including all in the present study) contain one or two remarkably luminous, gigantic elliptical galaxies near their centers which far outshine all the others. These brightest cluster members (BCMs) also turn out to be the most luminous ($\sim 10L_*$) and most massive ($10^{12-13}M_\odot$) galaxies in the universe. Cosmologically important, BCMs serve as “standard candles” due to their being bright and large and remarkably homogeneous despite each galaxy having experienced a complex formation history (see below). The dispersion in their luminosity is only about 30% of the average compared with six orders in luminosity over which normal ellipticals range. Hoessel et al. (1980) have used BCMs as distance indicators to anchor the bright end of the Hubble diagram, while Postman & Lauer (1995) have employed them to map the nearby large-scale galaxy velocity field. Bender et al. (1998) have explored the possibility of using BCMs as “standard rods” to calculate the deceleration parameter of the universe’s expansion. If most galaxy mergers occur in deep potential wells, and if BCMs - presumably formed from multiple mergers - can be thought of as tracing these uncommon depths, then they mark important structure formation processes.

$$\mu(R) = \mu(0) + \text{const. } R^{1/4}$$

Though BCMs are at first glance like normal elliptical galaxies (Es), with radial light profiles described approximately by the de Vaucouleurs surface brightness law, $\mu(r) \propto r^{1/4}$ (de Vaucouleurs 1953), they form a distinct class, with enlarged characteristic radii and shallower profiles (Schombert 1986, Graham et al. 1996). Actually, BCMs comprise a heterogeneous family in appearance. Many are simply super-luminous, giant ellipticals whose profile follows the de Vaucouleurs law, some are “D galaxies” which have somewhat shallower light profiles than Es, and some others are “cD galaxies” with a colossal elliptical body surrounded by an extended halo of light that can be traced out to several hundred kiloparsec (Oemler 1976; Schombert 1987). There is a suggestion that the slope of the BCM luminosity profile is correlated with its environment in the sense of scale length increasing with increasing cluster galaxian density (Garilli et al. 1997). BCMs may have multiple or complex nuclei, and distinct faint satellite companions, or they can consist of two comparably bright elliptical components, or resemble a nest of galaxies. The components of the BCM usually display velocity dispersions of about $300 - 400 \text{ km s}^{-1}$, close to the internal velocity dispersion of the dominant parent galaxy, implying that they are probably

bound to it.

The colors of many first-ranked galaxies generally redden toward their centers, in a manner similar to that of bright Es (Mackie et al. 1990). The magnitude of the color gradients are consistent with these galaxies being formed or enhanced by merger events. However, 25% of BCMs in X-ray-selected clusters evince young or intermediate-age stellar populations in their centers (Crawford et al. 1999). On the other hand, there seems to be great homogeneity in the strength of the CO stellar absorption feature of BCMs (James & Mobasher 2000), which could be the result of greater stellar age, or more uniform history of star formation in BCMs than in other ellipticals.

The BCM is frequently located at the local density maximum (Beers & Geller 1983), and at the dynamical center or bottom of the cluster potential well. X-ray emission from the tenuous, hot intra-cluster medium (ICM) is usually centered on the dominant galaxy (Jones & Forman 1984), which then preferentially collects the gas from a possible cooling flow and enhances its mass by $10 - 100 M_{\odot} \text{ yr}^{-1}$. The intrinsic luminosity of the BCM in Abell clusters is related to the X-ray luminosity and temperature of its host cluster (e.g., Schombert 1987). Additionally, there is an inverse correlation between the cooling time of the ICM and the radio luminosity of the cluster cD galaxy (Bagchi & Kapahi 1994), which in turn depends on the local galaxy density. Thus it appears that the BCM is responsive to the overall cluster properties, and evolves in tandem with its global neighborhood.

Now, BCMs in different environments appear to evolve differently: those at the centers of clusters with high X-ray luminosity are brighter and show smaller scatter than their counterparts in clusters with lower X-ray luminosity (Burke et al. 2000). Further, within low-mass clusters, there are suggestions that BCMs are growing by accretion and mergers of nearby galaxies even at $0 < z < 1$ (Aragon-Salamanca et al. 1998), which should add younger stellar populations to the first-ranked galaxy and thus reduce their homogeneity.

While there is a substantial corpus of work on rich cluster BCMs, there is little in the nature of an unbiased observational exploration of poor cluster BCMs in the literature. Among the latter are Thuan & Romanishin (1981; TR81 hereafter) who determined the luminosity profiles of dominant galaxies in poor clusters. TR81's surface photometry indicates that poor cluster BCMs show elliptical bodies similar to those of their rich cluster counterparts and normal ellipticals, but lacking giant haloes, probably fail to become genuine cD galaxies. Yamagata & Maehara (1986) concluded that the total luminosity of the first ranked galaxies of poor clusters is closely related to the amount of hot intracluster gas and total visible mass in the systems. Thus, poor cluster BCMs are akin to rich cluster dominant galaxies. Bridges & Hanes (1994) detected a globular cluster system in the cooling flow poor cluster MKW 4, with a specific frequency typical for an average elliptical. Fuller et al. (1999) found that poor cluster BCMs exhibit a strong propensity to be aligned with the principal axes of their host clusters as well as with the surrounding distribution of nearby ($\leq 20h^{-1}$ Mpc) more massive clusters. The last is very similar to the behavior of their counterparts in the rich Abell clusters. (Interestingly, the objects in all these studies are the brightest galaxies of AWM and MKW poor clusters *selected on the basis of the presence of distinctive D- or cD-like galaxies*, as mentioned in Sec. 1.3.2.)

The "nature *vs.* nurture" question is valid here as well: have BCMs reached their present status

in the course of their evolution or did they inherit their size and luminosity from exceptional conditions at birth or at least early in the cluster history? The realization that at least 60% of the BCMs of rich and poor clusters are more luminous than expected from a statistical formation process necessitates invoking a special creation process for (at least two-thirds of) these objects (Sandage 1976; Bhavsar 1989). There are indeed various theories for the origin of BCMs, especially that of the big and bright cD galaxies. Some approaches treat both the elliptical core and diffuse halo as having similar formation mechanisms, others explain the origins of these two components separately. The genesis theories have invoked virtually every galaxy-environment interaction mechanism described in Chapter 1. Briefly, these include galactic cannibalism to make up the body and tidal destruction of dwarf galaxies to create the stellar halo (Richstone 1976; Ostriker & Tremaine 1975), multiple galaxy mergers during the collapse and formation of the cluster core (Merritt 1985) and halo formation from gas condensing through X-ray cooling flows (Fabian 1994). However, each of these theories have their shortcomings. Lack of incontrovertible evidence for young stars in BCMs and their small dispersion in colors refute the cooling flow scenario; dynamical friction timescales are too long (by about twice) and velocity dispersions are too high for BCM formation via frequent galaxy merging; and galactic cannibalism is too inefficient in virialized clusters for much mass and luminosity to accumulate in the cluster core. Any theory of BCM formation must finally account for the homogeneity in BCM photometric properties.

There are several important theoretical ideas specifically regarding poor cluster BCMs. Bode et al. (1994) simulated isolated clusters of 50 galaxies, similar to present-day poor clusters. A dominant galaxy forms from the merging due to enhanced encounter rates among the cluster members; almost all subsequent mergers involve the cannibalism by the centrally-located BCM, but these contribute weakly to the growth of the BCM luminosity. Garijo et al. (1997) have averred that under a variety of initial conditions, merging instability within poor clusters leads to the formation of a giant central galaxy. Galaxies in spherical virialised galaxy systems collapse to relatively round and isotropic BCMs, while aspherical initial conditions give rise to triaxial objects. N-body simulations of poor clusters by Lima Nieto et al. (1997) showed that a massive galaxy with cD characteristics is always formed within 100 kpc of the cluster centre. They showed further that with increasing mass of the intra-cluster medium, the merging rate rises due to the dynamical friction of the galaxies with the ICM. Dubinski (1998) proposed a suite of N-Body simulations that posits the formation of the main body of the BCM through rapid galaxy merging during the initial collapse of the cluster along a filament. The merger product may then accrete its smaller neighbors and build up a cD-like halo.

In this chapter, we shift focus from the ensemble properties of the galaxies in our poor clusters to their individual brightest cluster members. In our CCD images three of these BCMs are sufficiently well-resolved (covering approximately 2000 pixels) to allow their structural analysis. For the BCMs of the three clusters, MS0002, MS0301 and MS1306, we obtain surface photometry in multiple filters. We model the galaxy isophotes as ellipses over a large range of galactocentric distances. From the surface photometry, we determine the radial variation of the surface brightness, ellipticity, and position angle. We also compute the Fourier coefficients of the higher order deviations from ellipticity to look for structural irregularities. We model the brightness profiles of the galaxies with the de Vaucouleurs law. We then look for 1-D color gradients as

diagnostics for radial variations in stellar populations. Additionally, we create two-dimensional color maps to pick out irregular structures superposed over the galaxian surface, which could be due to interstellar matter.

Two of the dominant galaxies in the present study (those of MS0002 and MS0301) are in common with the BCM sample of Garilli et al. (1997, hereafter G97). This allows us to also evaluate the external accuracy of our profile analysis. The fourth BCM, that of MS0735, is unfortunately too small in our images to allow detailed study; it is of great interest as it harbors an unusual radio source. We can make only a brief mention of this object, as its long-wavelength exploration is beyond the scope of this thesis. We also perform a comparison of the first-ranked galaxies in our clusters with normal ellipticals and cD galaxies in rich clusters.

6.2 Techniques: Isophotal Analysis and Color Maps

Bright galaxies not classified as irregular or peculiar, when projected onto the sky, exhibit isophotes that can be approximated by ellipses. Quantitative analysis of the structure of regular galaxies involves modeling their isophotes as ellipses described by parameters including the “centers”, mean intensity, ellipticity, and position angle, as a function of radius. Further, one may also decompose the elliptical isophotes into a Fourier series. The high (> 2) order Fourier components indicate deviations from true elliptical structure of the isophotes. Carter (1978) has provided the algorithmic foundations of such analysis.

6.2.1 Pre-Processing

For this work, we crop regions of about 2 arcmin along each axis of the aligned CCD images centered on the BCM. The frames have north to the top and east to the left. The cropped regions cleanly include the BCMs and several of the neighboring galaxies.

In Chapter 2, we have described how we prepared the CCD images for object detection and photometry. For very accurate surface photometric analyses, we ought to subtract from the galaxy a two-dimensional sky background to eliminate any systematic sky variations across the CCD frame. Due to practical considerations, however, we remove a constant, average sky level. We determine this background correction from the mode of the intensities of about fifteen circular regions of the CCD images uncontaminated by objects. This correction carries its own dispersion; the variance in sky level is about 0.8% over each CCD frame. This is the limit to the uniformity or flatness of the background, thus to the derived profile at the faint, outermost isophotes of the galaxies. We do not perform any deconvolution of the data, since the final images are generally created by co-adding images that may have non-similar PSF shape.

6.2.2 Photometric Calibration

The photometric calibrations come from our 11-pixel (6.7 arcsec) circular aperture magnitudes tied to the Johnson-Cousins' standard system, and are accurate to within 0.1 mag in every filter. In the innermost few arcseconds of the profiles, seeing changes could cause photometric

variations of up to $\approx 0.^m1 \text{ arcsec}^{-2}$. The standard magnitudes we quoted in Chapter 2 include corrections for Galactic extinction, estimated from Schlegel et al. (1998). To further convert these magnitudes to the rest frame of the galaxy, we must apply the appropriate K-corrections and evolutionary corrections for elliptical galaxies at the redshifts of these BCMs. We derive these from the spectro-evolutionary models of Poggianti (1997), as explained in Chapter 4. We used the corrections to a normal elliptical galaxy, assuming that the star formation history and evolution of a giant elliptical is not radically different from that of the former. Moreover, the lack of evidence of any major merger in progress (see below) and the small look-back times to the redshifts of our sample clusters are small enough that significant stellar evolution would not have occurred. We have tabulated these photometric corrections earlier in Table 3.1. We also account for a factor of $(1+z)^{-4}$ decrement in surface brightness due to cosmological effects.

6.2.3 Ellipse Fitting

Since BCMs appear structureless at first glance, and resemble elliptical galaxies, the methodology for structural analysis of BCMs is similar to the well-established procedures for surface photometry of elliptical galaxies.

We use the standard package STSDAS layered onto IRAF to interactively fit ellipses to the isophotes of the galaxies. The tasks in the package measure the galaxy images using the method of Jedrzejewski (1987).

Our procedure includes masking of superposed non-galaxy light sources such as stars, and remnant cosmic-ray events, and excluding these from the ellipse fit. We are careful to delete regions substantially larger than the visible extent of the stars. Further we flag the brighter 30% of the pixels to stay clear of very faint stars or spurious features we might have missed masking.

After removing the interfering objects, we proceed to fitting the isophotes with ellipses. The main outputs of this fitting include the azimuthally-averaged parameters of the best fit ellipses to the isophotes — the intensity and the geometric parameters (the X and Y center co-ordinates, ellipticity and position angle) — over the radial extent of the galaxy.

STSDAS uses the definition of ellipticity as $e = 1 - \text{minor axis}/\text{major axis}$, which relates with the visual “flattening” of an ellipse rather than the canonical eccentricity. The position angle is in degrees counterclockwise from the +y axis, which in our work corresponds to an angle defined north through east.

STSDAS also outputs the higher-order harmonic content of the data points on the isophote, fitted by the following function:

$$y = y_0 + A_n \times \sin(n \times E) + B_n \times \cos(n \times E),$$

with $n = 3$ and $n = 4$, and E being the eccentric anomaly. The amplitudes A3, B3, A4, B4, normalized by the semi-major axis length and local intensity gradient, measure the isophote’s deviations from perfect ellipticity (see below for further details).

Initially we keep all the geometrical parameters variable while finding the best fit ellipse at each

semi-major axis length. But at large radii, i.e., low surface brightness regions, the small radial gradient can introduce large errors and output meaningless values for the ellipse parameters. So for isophotes more than 15 arcseconds from the center of the galaxy, we hold the center co-ordinates fixed at the previous best fit; the wander in ellipse centroids is usually much less than 1 arcsec till such radius, except for MS1306 (see below). We increment the semi-major axis by 10% for successive ellipses. This helps maintain a nearly constant signal-to-noise ratio in the azimuthally averaged intensities by compensating through a larger number of pixels for the decline in surface brightness with radius. We terminate the task when the isophotal intensity falls to below a few percent of the sky level.

From the parameters of the fitted ellipses in the various filters, we determine the geometry of the isophotes, the surface brightness profiles, and the color gradients of the BCMs.

6.2.4 Residual and Color Maps

From the fitted ellipses, we can construct a (noiseless) photometric model image of the elliptical galaxy based on its isophotal parameters of brightness, position angle and ellipticity. Then, subtracting the model from the original and smoothing the subtracted image results in a “residual map”. If the galaxy is deploying its stellar light quietly, the residual should be only sky and noise. However, if there are significantly strong patterns in the resultant image, they are signals of diskiness of the galaxies, or fine-structures, or non-uniform ISM. If the residues can be attributed to ISM/dust, then the residual map is essentially a map of optical depth, and can be thought of as an “extinction map” as well. Such a procedure works best when the ISM signal is strong, i.e., when the disturbance over the simple elliptical model is obvious in the direct image itself.

A more sensitive way of detecting ISM using broadband multi-filter imaging is through a color map i.e., by taking the ratio of images in two filters. This is the logical extension of finding the galaxian color using aperture magnitudes in different filters, and is analogous to obtaining the galaxy color at every individual pixel. The method can unearth subtle (often small-scale) color changes over the entire galaxy, indicative of dust, shells, disks etc. One can use either the two direct images or one direct image and a model of the galaxy in one of the filters (usually the longer wavelength one). The latter method works better due to the noise being present in only one image, and results in the removal of a smoothed background provided by the longer wavelength image from the shorter wavelength one. The color maps can reveal features differing by about 0.05 mag over their surroundings, depending on the signal-to-noise of the individual images. Note that absolute photometry is not essential to this analysis. But a caveat here is that photometry on results derived using the smoothed images is fraught with uncertainties, since the flux is usually not conserved in the smoothing. Of course, variations in seeing between filters would also contribute spurious features in the nuclear regions.

From interpolation of the geometric parameters derived from isophote fitting, we build a model image in the V and R bands for each BCM (except for MS0002, for which we construct only the R-band model). Then, we generate a color map thus:

$$C(x, y) = -2.5 \log(N_{\lambda_1}/N_{\lambda_2}),$$

where N_{λ_1} and N_{λ_2} are the sky-subtracted counts per second at pixel (x, y) in the higher-wavelength (B or V) and lower-wavelength (V or R) filter images, respectively.

6.2.5 Errors in Isophotal Analyses

Several technical and image reduction constraints come into play during the detailed study of elliptical galaxy shapes. Errors in the fitting process are themselves small, and are defined by the local scatter of the point.

The principal contributions to the error budget, besides those in photometric calibration, include:

- in the central regions: seeing effects that circularize the elliptical cores consequently leading to underestimates of the ellipticity, randomize the position angle, and flatten the central brightness distribution. This last also results in the flux being diverted to intermediate radii. The fits in the innermost regions are incidentally not too good due to the small number of pixels available for fitting the profile. Another problem is the possibility of saturation of the very bright central regions. Fortunately, we are not worried by this error.
- at the faint outer regions: residual non-flatness of the “sky” background due to imperfect flat-fielding and vignetting, and due to Poissonian fluctuations, which contribute inaccuracies at levels of a few percent of the night sky luminosity.

The shape and size of the image are also affected by telescope focus, and guiding errors which may change from one exposure to the next. Further errors come in due to overlapping galaxy halos and scattered light which are minimized though by the masking of visible superposed objects and by not including the higher-count pixels in the fits.

For these reasons, we derive the overall ellipse parameters and model the galaxian surface brightness outside 5 arcsec from the center and until the isophotal surface brightness falls to 24.5 mag. However, in the case of MS1306 we derive the profile fits from an inner radius of 8 arcsec in all bands, and only till a surface brightness level of 23.6 mag. Interior to this 8 arcsec radius, the de Vaucouleurs $r^{1/4}$ law does not fit the observed data points well. The individual values of all these ranges can be read off from Table 6.3.4 in the next section. Figure 6.1 displays the V-filter images of the three BCs we analyze here. Overplotted on each are the isophotes corresponding to the ranges mentioned above.

In the following section, we discuss our results on the geometrical parameters of the ellipse fits, as well as the fitting of a de Vaucouleurs profile to the radial surface brightness distribution. We also perform detailed surface photometric studies to uncover subtle deviations from symmetries and presence of dust in the inter-stellar medium of the galaxies.

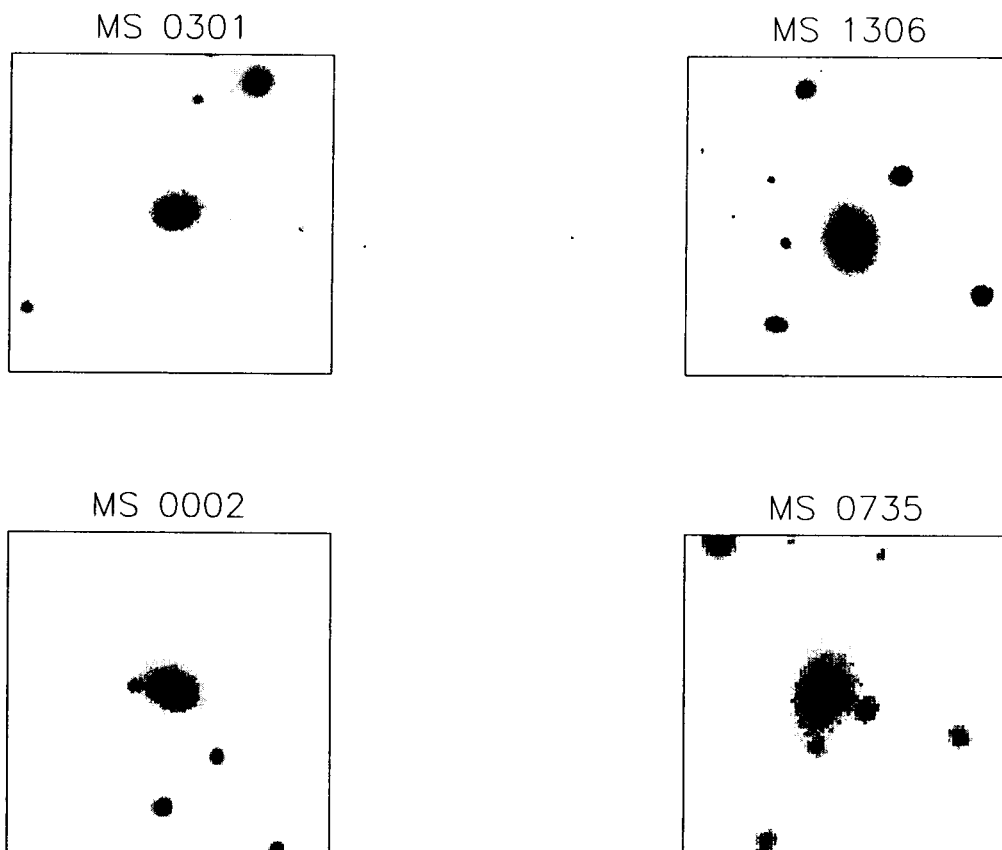


Figure 6.1: Images of the BCMs, with North at the top and East to the left. The images of brightest galaxies of MS0002, MS0301 and MS1306 are in the V-band, while MS0735 is in I-band. Metric areas covered by the stamps are about 200 kpc for the BCMs of MS0002, MS0301 and MS0735, and 300 kpc for MS1306.

6.3 Morphological and Structural Parameters

6.3.1 Visual Morphology

Visual inspection of the brightest galaxies of the clusters here shows that they are undoubtedly early-type galaxies. All the BCMs have several faint companions seen in projection. But there ends the resemblance. While the BCMs of MS0002, MS0735 and MS1306 are large and clearly dominant over their neighbors, their counterpart in MS0301 is not particularly impressive, appearing like an ordinary elliptical.

The dominant galaxy of MS1306 is surrounded by a diffuse envelop, has superposed on its core a dwarf galaxy, and shows clear tidal interactions with one, possibly two of its neighbors. There is a clearly visible tidal bridge that links this BCM with its small neighbor to the north by north east. There is also a hint of a distension of its tidal companion to the west. There are also small stellar groupings mostly within the corona of this BCM that we identify as dwarf galaxies.

The first-ranked galaxy in MS0735 is evidently a cD galaxy, with its halo enclosing at least two small galaxies. There is weak indication that the cD halo is asymmetric with respect to the major axis of the main body of the galaxy. For this BCM, unfortunately, we can provide only visual morphology due to its small size in the images, though we do perform a cursory ellipse-fitting analysis to derive its ellipticity and position angle. Therefore we shall exclude it from subsequent discussions of surface photometry.

6.3.2 Isophotal Geometry

The actual 3-D shape of an undisturbed galaxy seen in projection as elliptical could be either spheroidal or triaxial (i.e., with the three axes being of different lengths). When a purely elliptical galaxy is projected onto the sky, its isophotes are simple, symmetric, coaxial ellipses and the semi-major axis will retain the same direction irrespective of the galaxy inclination (Mihalas & Binney 1981). However, if the galaxy is triaxial in the sense that it has three orthogonal planes of symmetry, the position angles of its isophotes will depend not only on its orientation with respect to the line of sight but also on its axis ratios. Then (if the line of sight is not through one of the principal axes) the isophotes will appear (from the same vantage point) to have changing axial ratios (i.e., varying ellipticity) and will show a continuous, definite pattern of twists (for more on the topic, see Kormendy 1982). Another possible origin of position angle rotation is gravitational interaction; tidal forces disturb the galaxy in an asymmetric fashion and also cause isophotes to deviate from pure ellipses. Inclination effects could play a role in the shape variation, though physical causes such as triaxiality or gravitational interactions are most probable causes for the disturbances in ellipticity. The behavior of ellipse parameters in different wavebands is an indicator of dust, since in the presence of dust, the bluer band will be more affected than the red one, consequently distorting the bluer isophotes more than their corresponding red ones. Ellipses provide a reasonably good fit to the isophotes of all three BCMs under consideration here. As we shall see from the analysis of the Fourier components of the residuals to the fit, the isophotes do not deviate significantly from ellipses over most of the galaxy.

In Table 6.1 we list the mean ellipticity, ϵ and the position angle, ϕ of the major axis at the effective radius in each band for the three BCMs. Position angle are positive north through east. We also tabulate the gradients of the ellipticity and position angle (per kiloparsec) computed over the fitted isophotes between 5 arcsec from the center and the chosen faintest outer isophotes. In Fig. 6.2 we present the profiles of ellipticity and position angle in three passbands (B, V and R) for the BCMs (except for MS0002, which we study in only two (V and R) bands). For the figures that follow, the solid lines represent the V band profiles, the long dashed lines, the R band, and dashed-dotted lines, the B band.

Ellipse Centroids

The isophotes for the first-ranked galaxies of MS0002 and MS0003 are virtually concentric, with the pixel co-ordinates of the centroid moving barely 0.5 pixel (0.3 arcsec) within the inner 15 arcsec (after which we hold them fixed for the rest of the isophote fitting). The centring errors are typically less than 0.1 pixel.

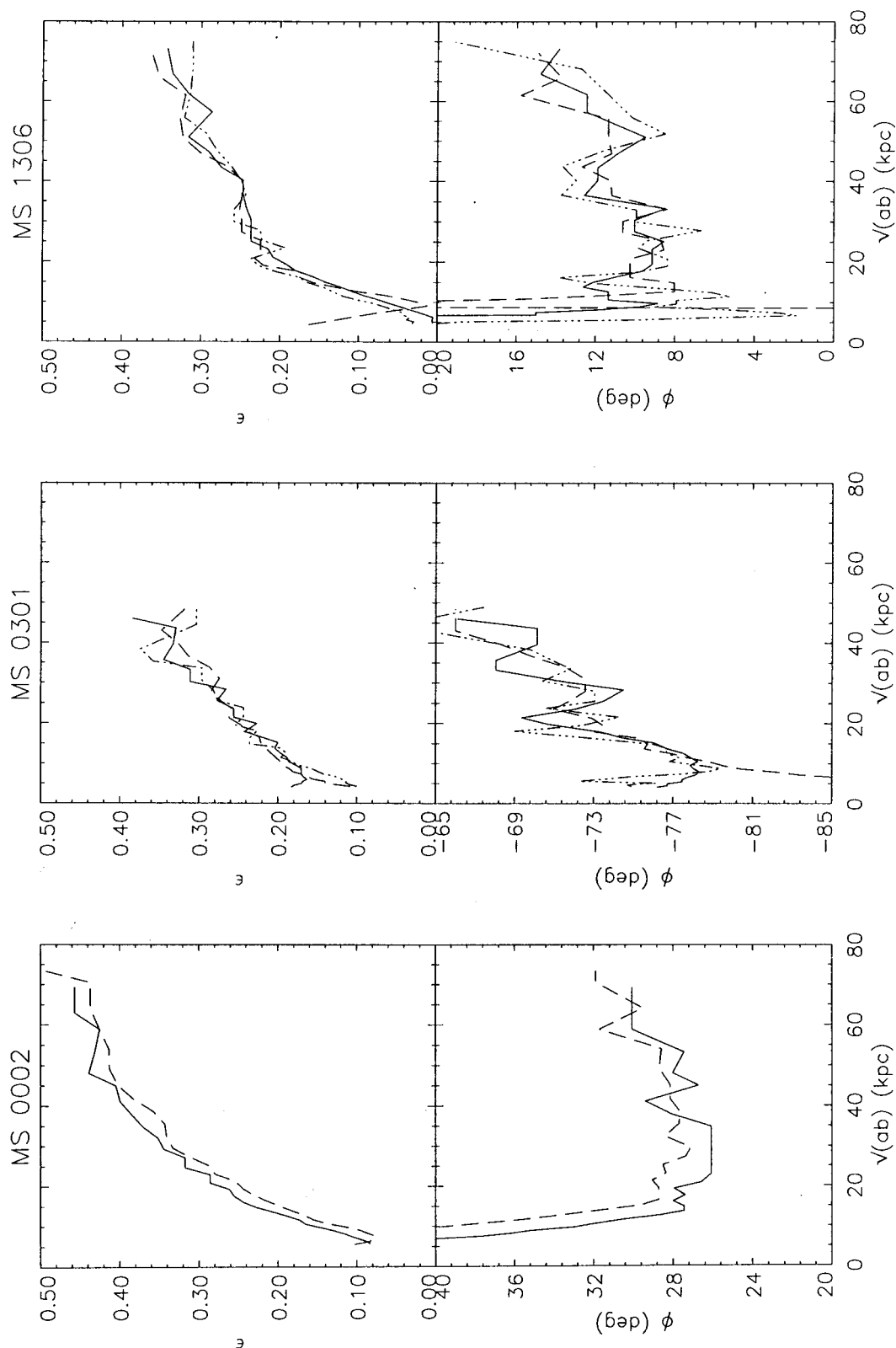


Figure 6.2: Profiles of Ellipticity and Position Angle (measure N through E) for the BCMs. The abscissa is the equivalent radius of the best-fit isophote, defined as $r = \sqrt{ab}$ where a and b are the semi-major and semi-minor axis length, respectively. The solid lines represent V band profiles, the long dashed lines are of R band, and dashed-dotted lines, the B band.

For MS1306 however, the center exhibits a wander in position largely along the minor axis of about 1.2 arcsec (the seeing is itself about 1.9 arcsec). Jedrejewski (1987) suggests that if there is a region of very diffuse emission on one side of the frame, it would show up as a shift in the centers of the outer isophotes with respect to the inner ones. The center shifts would generally influence neither the ellipticity nor position angles to first order. We notice that this is indeed the case for MS1306, from the R-band residual map (see below) which shows a not inconsequential excess in a major-axis sector about 12 arcsec (26 kpc) north of the center.

Object	Filter	ϵ	$\Delta\epsilon \text{ kpc}^{-1}$	ϕ , deg	$\Delta\phi \text{ kpc}^{-1}$
MS 0002	V	0.36	0.007	27.1	-0.01
	R	0.32	0.006	28.0	-0.05
MS 0301	B	0.27	0.006	-70.2	0.54
	V	0.24	0.006	-73.6	0.36
	R	0.23	0.004	-75.7	0.32
MS 1306	B	0.32	0.006	10.1	0.05
	V	0.25	0.005	10.5	-0.01
	R	0.24	0.005	06.0	1.06

Table 6.1: Isophote Geometrical Parameters. Ellipticity and Position Angles derived from linear fits at the effective radii given in Table 6.3.4.

Ellipticity

In all objects, the ellipticity of the isophotes clearly increases, i.e., the BCMs flatten at increasing galactocentric distance. At small radii the typical ellipticity is < 0.2 , which increases almost monotonically to > 0.3 at 40 kpc along the major axis. The rms error in ellipticity has a mean of 0.006 which rises to 0.01 at the innermost and outermost isophotes. Only for MS1306 is there a slight plateau between 25 and 40 kpc. We also see that ϵ remains nearly the same across the filters, i.e., across a wide range of wavelengths, again except in the case of MS1306, where the R-band ϵ is marginally lower than that of the two other filters.

The rate of change of ellipticity with radius, or ellipticity gradient $\Delta\epsilon \text{ kpc}^{-1}$, are remarkably similar across all filters of the individual galaxies, as well as among the three BCMs.

In comparison with G97, our derived ellipticities appear to be a few percent higher for MS0002 and 5% lower for MS0301, which may be attributable to variations in seeing, though both of our data sets have stellar FWHM close to 2 arcsec. However, the ellipticity gradients compare very well (MS0002: ours = 0.004 and G97 = 0.003, and for MS0301: ours = 0.0036 versus G97 = 0.003, within the ranges of radii that they use).

Other observations (e.g., Schombert 1986) also demonstrate that the ellipticity of BCM rises sharply with radius. Few, if any, BCMs exhibit any noticeable decrease in ellipticity with increasing

radius. In an extensive study of surface brightness profiles of elliptical galaxies, Franx et al. (1989) have cautioned that at radii as large as five times the seeing FWHM, seeing can affect the ellipticity at the 10 percent level and smear the position angles by several degrees. Therefore, it is not unlikely that the gradient of ellipticity is a little lower than what we derive.

Position Angles

The inclination of the major axis of the BCMs of MS0002 and MS1306 remain almost constant, and close to north-east, within the rms error of about 1 degree. For MS0301, though the overall ϕ is $\approx -75^\circ$, it appears to change jerkily by about 8° between isophotal radii of 20 and 40 kpc. In the blue band, some part of the discontinuous change can be attributed to the lower signal-to-noise ratio of the image. We shall have more to say about the behavior of ϕ in conjunction with the higher-order Fourier terms, in the next section.

Comparing the derived position angles with G97 who measure inclination in the E-W direction, we find that the match is within 1 degree. However, for MS0002 G97 find a PA gradient of $0^\circ.6 \text{ kpc}^{-1}$ whereas we derive, in the same range of radii, $0^\circ.01 \text{ kpc}^{-1}$. We attribute the difference to the isophotes in the radial range of 30-40 kpc. Figure 1 in G97 indicates that the PAs of MS0002 twist by about 10 degree in this range, whereas we find a much smaller twist of ≈ 1 degree. Note that the rms error in deriving PAs is never larger than 1 degree in our work.

Our BCMs are likely to be ellipsoidal since the semi-major axis seems to retain roughly the same direction through the run of the radial distance. But, this smooth behavior of ϕ does not entirely rule out triaxiality. Franx (1988) shows that there exists a class of triaxial models (mainly axisymmetric) that have changing axial ratios, hence changing ellipticities, but show no twist in projection. This could well be happening in the BCM of MS1306, whose isophotes exhibit considerable higher-order deviations from ellipticity.

We have seen in Sec. 5.5 that the BCMs of MS0002 and MS0735 are oriented in similar directions as the cluster X-ray isocontours and galaxy isopleths. Along with the flattening of the fainter isophotes, this could indicate that the BCM outer regions are dynamically coupled to the elongated host cluster.

6.3.3 Deviations from Elliptical Structure

Now, are the BCMs always perfectly elliptical, or do they show distortions? Deviations from elliptical isophotes and other such structural anomalies in an elliptical galaxy could be evidence of bars or weak disks or dust absorption features. These could have their origins in a recent merger or interaction or internal gravitational instability. Simulations show that “fine structure” is an inherently transient phenomenon: when two galaxies collide, their structures can retain vestiges of the interaction for only a few hundred million years. When they actually merge, the remnants settle down to becoming “normal” elliptical galaxies over about a billion years (for an excellent exposition on this, see Schweizer 1998). But there are three quasi-stable (i.e., long-lived) morphologies possible for an elliptical merger product: “pure” elliptical isophotes, “boxy” isophotes, and “disky” isophotes. Disky isophotes mean that the galaxy has excess light along

the major and minor axis directions, making the object's isophotes pointed much like an edge-on disk galaxy. Boxy isophotes mean that the galaxy has a light deficit along the major and minor axes, making its isophotal shape somewhat rectangular.

Observationally, the higher-orders (3 and 4) terms of the harmonic expansion of the ellipse fits to the isophotes are pertinent in detection of deviations from pure ellipticity; the third- and fourth-order coefficients are zero for perfect ellipses. Positive $\sin 3\theta$ (called A3) and $\cos 3\theta$ (or B3) testify to "egg-shaped" or "heart-shaped" isophotes respectively. The 4θ components indicate deviations at even higher spatial frequencies. Nonzero $\cos 4\theta$ (termed B4) is unambiguously indicative of fine structure: $B4 < 0$ and $B4 > 0$ imply boxy and disky structures respectively. Differences in these terms between filters are useful indicators of dust in the galaxy; non-zero 3θ or 4θ terms are often found in galaxies at radii with known dust features.

Figure 6.3 presents the A3 (or $\sin 3\theta$) and B3 ($\cos 3\theta$) component plots, and the A4 ($\sin 4\theta$) and B4 ($\cos 4\theta$) components of the deviations from pure ellipticity. The uncertainties come from the rms scatter of the intensities along the fitted ellipse.

Traditionally, only the B4 term has been considered important in determining the character of the deviations from ellipticity. However, Franx et al. (1989) emphasize that the signs of the $\cos(4\phi)$ and $\sin(4\phi)$ terms are determined by the phase of these fourth-order residuals with respect to the apparent major axis, and projection effects can produce phase shifts of the residual harmonics. So, instead of using the A4 and B4 components separately, it would be better to study the *amplitudes* of the residual terms,

$$R_n = \sqrt{A_n^2 + B_n^2}.$$

So, in Fig. 6.3 we also plot the quadrature-added amplitudes of the third- and fourth-order residuals for the BCMs.

All the BCMs have isophotes fairly well fit by ellipses, as already stated, but show small third- and fourth-order deviations (usually less than 0.2% at most measured radii). Though small, these higher-order deviations appear to be real; they exist in the images in different filters at similar galactocentric distances. Indeed it is not uncommon for elliptical and cD galaxies to display nonzero 3θ and 4θ terms; the typical values are of the order of 1% (see e.g., Franx et al. 1989).

For MS0002, there is some signature of the B3 component of the galaxy being positive about 20 kpc, implying an egg-shaped isophotal structure. The B4 component, though, is not significantly different from zero here. But at 40 kpc from the center, this galaxy exhibits fairly negative A3 and B3 terms and a positive A4 term. The quadrature-added amplitudes of the 3θ and 4θ harmonics are insignificant at the 20 kpc radius, but are both 3% between 40–60 kpc. These higher-order deviations show up in both V and R filters. The position angle (ϕ) of the isophote also shows a small but unmistakable jump at the 40 and 60 kpc regions. Since the color profile (see below) shows a 0.1 mag blueing at the same radius, we can rule out dust as the contributor to this behavior.

Both the 3θ and 4θ components of the profile for MS0301 are rather noisy. It is therefore impossible to decide whether there are real variations within the 2% level that the components straddle. However, at the 30 kpc isophote, the 3θ total amplitudes are about 3% in the B and V

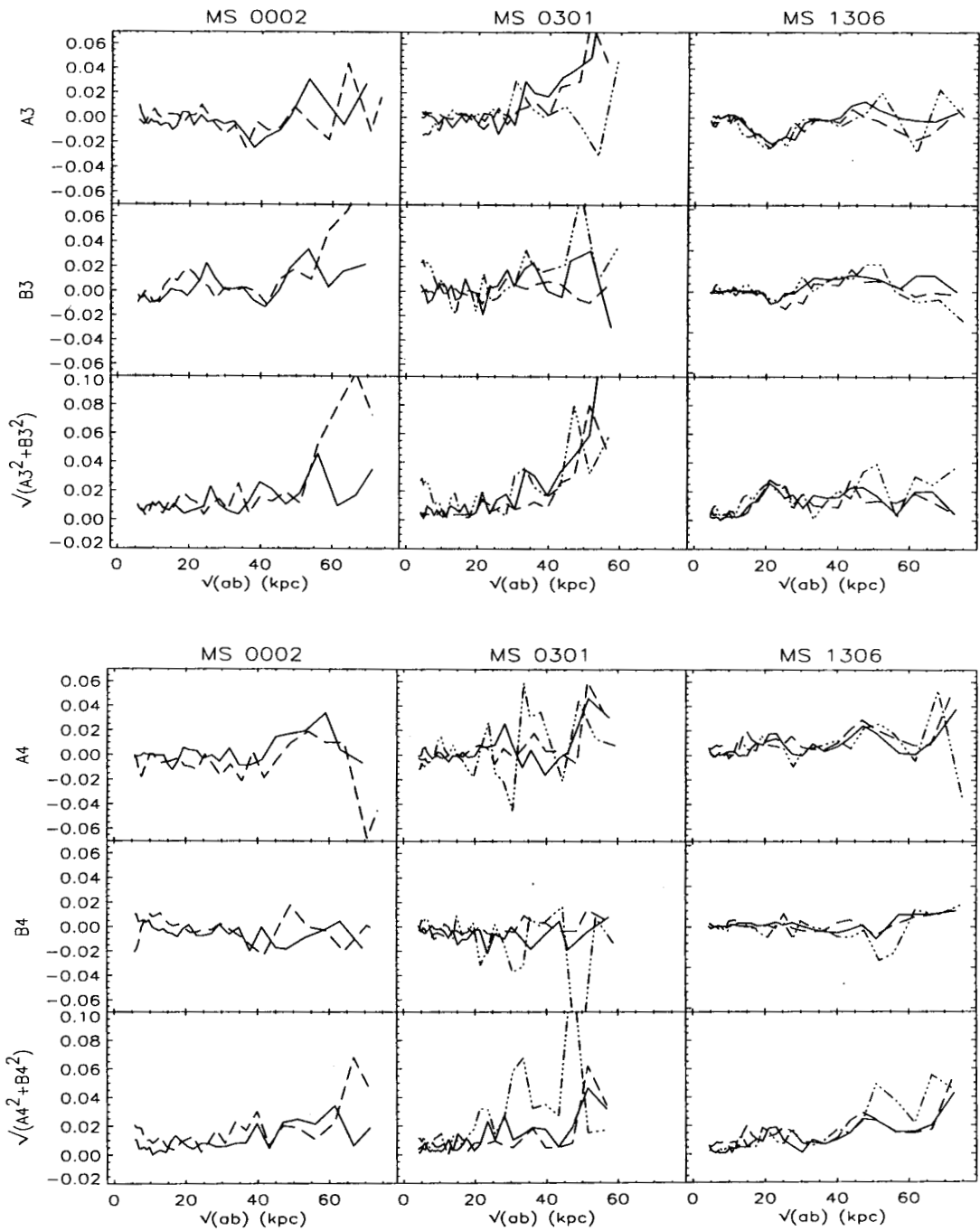


Figure 6.3: Profiles of third- and fourth-order deviations from ellipticity. The abscissa is $r = \sqrt{(ab)}$, the geometric mean of the semi-major and semi-minor axis length. Solid line - V, dashed line - R, dash-dotted line - B band.

filters, indicating that the distortions here have a three-fold symmetry. Usually, the $\text{Cos}3\theta$ term reflects perturbations due to dust absorption; then, the strongest signal should be in the blue bands. This is not the case here, since both the B- and V-band higher-order terms seem to follow each other in both magnitude and direction. We also notice that ϕ changes unevenly in this region and the galaxian colors become marginally bluer. We do not consider the considerable deviations at > 40 kpc to be reliable, since they are at more than twice the effective radius (derived in Sec. 6.3.4) of the BCM.

Since the dominant galaxies of MS0002 and MS0301 show neither obvious signs of tidal interactions nor the present of dust in the color maps, it is possible that the higher-order deviations from pure ellipticity represent nonelliptical stellar distributions, perhaps embedded faint disk-like components. We need better signal-to-noise to decide whether there is an extra (disk) component superposed upon the elliptical body at large radii. These may represent remnants of not-too-recent interactions with the neighbors which created a disk of material in the outer regions of the BCM.

It is clear from Figs. 6.3 that the BCM of MS1306 shows deviations from pure ellipticity near 20 kpc from the center and outside of the 30 kpc isophote. The changes are rather smooth, unlike that of the counterpart in MS0301, and are seen in both the individual 3θ and 4θ components as well as their corresponding quadrature sums. The inner distortion suggests that this galaxy is somewhat ovoid but otherwise not boxy. The presence of individually positive 3θ and A4 harmonic components in the outer regions — in fact, located around the characteristic radius of the galaxy — suggests that the galaxy has complex deviations from the basic elliptical structure. The total amplitudes of these harmonics further support this picture. We recall that this BCM also shows a plateau in its ellipticity gradient around the 25-40 kpc region. However, there is not much evidence of similar isophotal irregularities of the innermost regions which, as we shall discover subsequently, contain patchy dust. The amplitudes of the 3θ and 4θ terms are themselves small and somewhat uncertain, as can be seen from the scatter of neighboring values. This emphasises the need to consider the total amplitudes of these terms, to account for phase changes and to improve the reliability of the analysis. If we consider the usual interpretation of positive fourth-order harmonics, we must conclude that the elliptical MS1306 has an additional disk component at large distances from the core. However, as we shall see, the parent body becomes *redder* outwards, making a disk unlikely, unless it happens to be composed only of very low-mass stars. These distortions of the outer regions could then be due to the visible interactions of the BCM with one (perhaps two) of its small (spiral) companions or as the result of acquisition of low-luminosity galaxies. Since this galaxy does not show any large PA twists either, we may conclude that if it is not entirely ellipsoidal, it may however be mildly triaxial.

G97 claim that the BCMs in common with ours show no significant corruscations in their isophotes; however they also mention that their analysis is sensitive only to strong ($> 5\%$) signals of deviations from ellipticity. In fact, poor seeing and low signal-to-noise ratios could erase the signatures of fine structures, so it is not untenable to suggest that the detected higher harmonics are usually the lower limits. For the BCM of MS1306, which shows the clearest evidence for fine structure, it would be very useful to derive harmonic residuals beyond fourth order. However, we are limited by the lack of adequate signal-to-noise in our images, and opt out of extending the

analysis to higher harmonic terms.

6.3.4 Surface Brightness Profiles

The average brightness along the isophotes describes the luminosity distribution in the galaxy, which presumably indicates the mass distribution if the mass-to-light ratio is well-behaved. Empirical laws, such as those formulated de Vaucouleurs (1953) and Freeman (1970), provide adequate descriptions of the radial brightness distributions of the bulge and disk components of galaxies, respectively. (The stellar halo is normally considered too discontinuous in the visible stars and star clusters to lend itself to surface photometry.) The de Vaucouleurs law for elliptical galaxies is applicable to the main body of the BCMs. Parametrically, this “ $r^{1/4}$ law” is:

$$\mu(r) = \mu_e + 8.33 \left(\frac{r}{r_e} \right)^{1/4},$$

with r_e the scale or effective radius enclosing half of the total galaxian luminosity, and μ_e the surface brightness along the isophote with radius r_e . One restriction of the $r^{1/4}$ law is that it has only two free parameters, scaling for length and surface brightness; the profile shape is fixed. There are other fitting functions, such as the Hubble-Oemler law (Oemler 1976) and the dynamics-based King law (King 1966) which are also convenient representations of the early-type galaxy profiles. Graham et al. (1996) found that Abell cluster BCM surface brightness profiles are better modeled by a “generalized de Vaucouleurs law”, or $R^{1/n}$ law, where n is a free parameter, with larger BCMs having larger values of n . But TR81 have demonstrated that the structure of giant elliptical galaxies in poor clusters are well fitted by the r to the $1/4$ power law over a range of more than nine magnitudes.

Recent Hubble Space Telescope studies have found that the nuclear regions of ellipticals (some of which are the brightest cluster members) can be characterized as “cores”, i.e., surface brightness profiles which flatten in the central regions, and “power-law” profiles. Our sample does not have seeing so good as to study the very central regions, so we focus on the global behavior of the larger main body. An active galactic nucleus (AGN) may well be present in the BCM. In terms of galaxy profiles, the AGN contributes a point-source at the center of the galaxy. But if the seeing is not excellent, the PSF can redistribute the AGN contribution to larger radii and weaken the central peakedness.

We perform the fits of the de Vaucouleurs law to the surface brightness versus radius data points using linear least-squares approximation including errors in both co-ordinates. For MS0301 and MS1306, we perform the fits for all four filters (B, V, R and I) in which we have imaged the clusters. For MS0002, we analyse surface brightness profiles only in V and R passbands. We take the errors in surface brightness as the rms deviation in intensity along the isophote, while for the radius, we assume a (generous) uniform 1% error in the computed radius. We have, as explained earlier, restricted the range of radii to exclude those seriously affected by errors due to seeing or sky subtraction.

In Fig. 6.4 we plot the rest-frame surface brightness (in magnitudes arcsec⁻²) as a function of $r^{1/4}$ (in kpc^{1/4}), where $r = (ab)^{1/2} = a(1 - \epsilon)^{1/2}$, the geometric mean of the semimajor and semiminor axes. Overplotted on the data points are the best fitting de Vaucouleurs law profiles. Obviously,

in the $r^{1/4}$ co-ordinate frame, the fit is a straight line. Table 6.3.4 presents the final parameters of the fits within the reliable radial ranges.

The BCMs of MS0002 and MS0301 show brightness profiles that fall off as the $r^{1/4}$ law in the characteristic manner of luminous Es. This is true for all the filters in which we derive the profiles. The small deviations from ellipticity as shown by the 3θ and 4θ harmonic components do not appear to affect the global profile. As the dominant contribution to the luminosity of the BCMs is from their stars, the apparently elliptical structure of the galaxies is a clue that the distribution of stellar densities and dynamics across their breadth can be described by elliptical models.

For MS1306, though, the de Vaucouleurs law is hardly an excellent representation of the BCM luminosity profile, particularly in the inner regions. We choose, therefore, to fit only points outside 8 arcsec of the center with the $r^{1/4}$ shape. The profiles are somewhat different in the different filters: the B band data points are rather more consistent with the standard law than those of the R filter. The extrapolated profile provides evidence for a central (inside of 5 kiloparsec) excess in both the R and I filters. It could be that the > 1.5 arcsec seeing disk has smeared the probable point source into relative non-prominence in all the filters. There is a feature in the surface brightness profile between $r \sim 6 - 15$ kpc which falls below the projected $r^{1/4}$ shape. This annulus then leads to a 10 kpc region which shows the contrary - a slight excess of emission. On the other hand, though this BCM displays a halo to the eye, the outer isophotes are consistent with being simple extensions of the $r^{1/4}$ law. Matthews, Morgan, and Schmidt (1964), who first identified cD galaxies as a separate class of objects, defined them as “supergiant” galaxies having an elliptical-like nucleus surrounded by an extensive envelope. The good fits to the fitting function imply no envelope of surface brightness fainter than 25 mag in blue which is characteristic of the supergiant cD galaxies (Oemler 1976). So, by the conventional definition, the first-ranked member of MS1306 is not a genuine cD galaxy since it lacks the additional halo.

Could we have over-subtracted the sky, thus depleting the light content of the halo of the brightest galaxy in MS1306? That seems unlikely, since we have estimated the sky from regions fairly far away from the BCM. We shall see in Sec. 6.4.1 that this first-ranked galaxy is also unusual in terms of becoming redder with increasing galactocentric distance. It is then not surprising that the red profile of the brightest galaxy of MS1306 is most the deviant from that of an “ordinary” elliptical galaxy.

It is important to note that the final fit parameters depend on the galaxy region included in the fit. In the inner region, there are more points in the profile which are also influenced by seeing variations. In the outermost regions, the uncertainties in the background subtraction are a significant fraction of the isophote level, so the modeled profile may be a little above or below the observed data points. For instance, for MS1306, if we fit the R-band luminosity profile excluding only the inner 5 arcsec region, which we have said does not appear to follow the $r^{1/4}$ law, we derive a μ_e of 22.23 (nearly half a magnitude fainter compared to the one derived excluding a larger inner region of 8 arcsec) and an r_e of 44.3 kpc (or nearly 20% larger compared the earlier value). This is undoubtedly a reflection of the radial changes in color (see next section) that are present in the BCM. In such cases, the derived r_e will not be a genuine half-light radius but will merely describe the slope of the luminosity fall-off within the range of the linear fit.

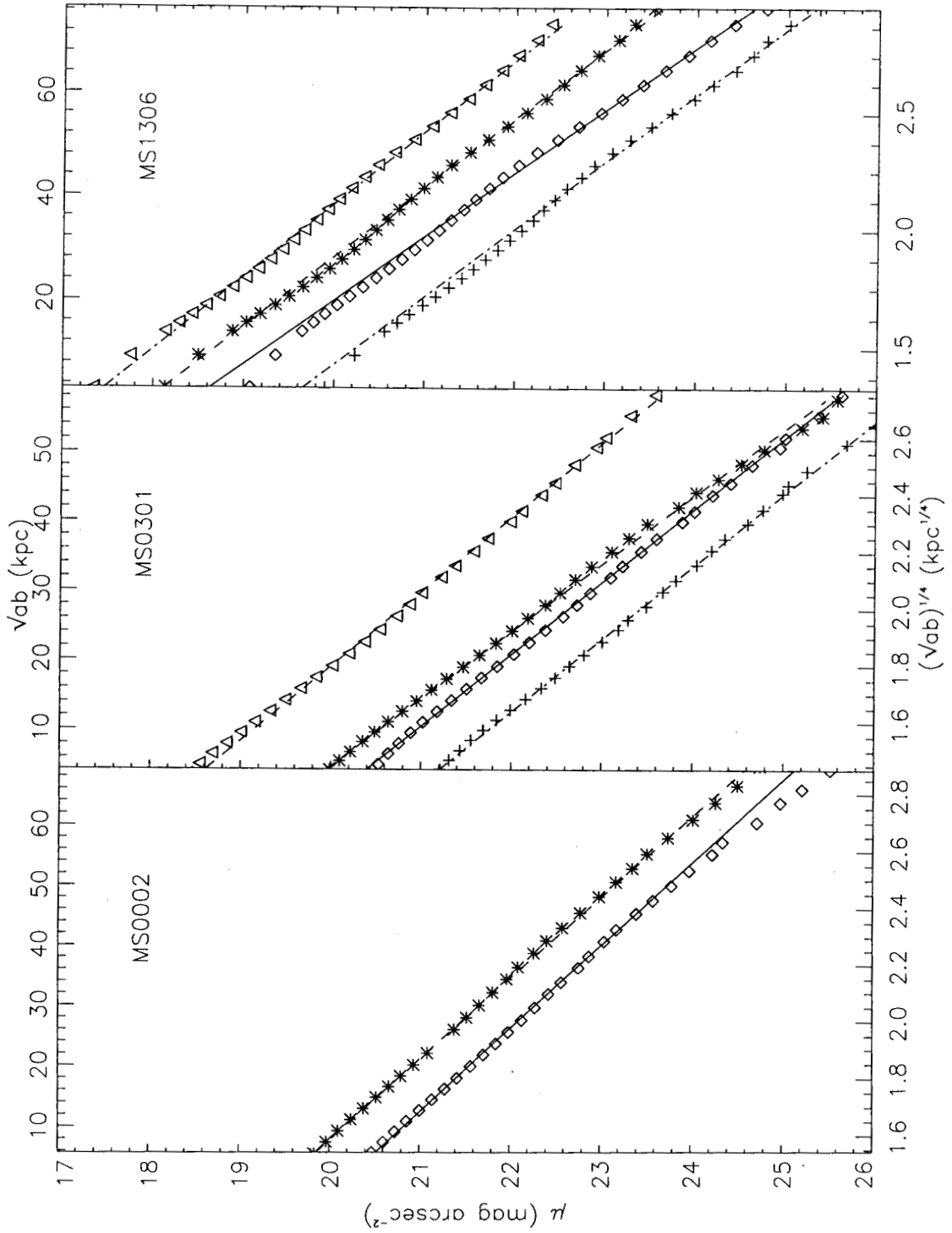


Figure 6.4: Surface Brightness profiles for the three BCs. The abscissae are the fourth root of the equivalent radius defined as $r = \sqrt{(ab)}$ where a and b are the semi-major and semi-minor axis length, respectively. Pluses, diamonds, asterisks and triangles represent the B , V , R and I band profiles, respectively. The overplotted lines are the best fit de Vaucouleurs laws, whose parameters are listed in Table 6.3.4.

Object	Filter	Fit region (kpc)	μ_e , mag	r_e , kpc
MS 0002	V	14 – 53	23.54 ± 0.25	34.5 ± 1.3
	R	14 – 71	22.94 ± 0.21	31.8 ± 1.1
MS 0301	B	10 – 22	23.92 ± 0.38	20.6 ± 1.6
	V	10 – 33	23.08 ± 0.20	20.0 ± 0.8
	R	10 – 40	22.25 ± 0.19	15.4 ± 0.8
	I	10 – 36	21.49 ± 0.20	22.9 ± 2.2
MS 1306	B	18 – 48	23.36 ± 0.30	33.2 ± 2.4
	V	18 – 62	22.06 ± 0.25	26.2 ± 2.4
	R	18 – 62	21.87 ± 0.26	37.1 ± 2.3
	I	17 – 52	21.50 ± 0.26	43.9 ± 2.3

Table 6.2: Fit parameters for the de Vaucouleurs law.

We note that, no matter what ranges we use to derive the linear fit to the $r^{1/4}$ law, the outer isophotes of the BCM of MS1306 do not show the excess corresponding to a cD-like halo. This is in keeping with the trend of BCMs in the poor MKW and AWM clusters which are well fit by the de Vaucouleurs law over nine magnitudes, and are devoid of an additional envelope that is the cD characteristic (TR81). But our profile fitting not being reliable fainter than V-band surface brightness of 24.5 magnitude may contribute in some way for non-detection of the envelop; a majority of cD galaxies in rich clusters have halos that become dominant usually beyond $\mu_V = 25$ magnitude.

Despite the above caveats, we find that the de Vaucouleurs parameters we derive agree reasonably well with those of G97 within the radial ranges they use. For MS0002 and MS0301, the r_e we obtain are 28.3 ± 2.2 and 16.2 ± 2.5 kpc, while G97 quote 36.7 kpc and 21.1 kpc respectively. Similarly, our values for μ_e for MS0002 and MS0301 are 22.7 ± 0.2 and 22.35 ± 0.3 , in modest agreement with those of G97, i.e., 23.43 ± 0.1 and 23.09 ± 0.1 mag arcsec $^{-2}$ in the Gunn r band. (The Gunn r band in G97 is approximately 0.4 mag fainter than the Kron-Cousins R band of our work.) Some of the difference is attributable to the method of sky subtraction and sky-error measurements especially important in the outer isophotes. If we have overestimated the value of sky and thus truncated some of the outer low surface brightness regions, we could underestimate the characteristic radii.

We next consider the relation between the quantities that the de Vaucouleurs law provides: the effective surface brightness and radius. We shall use this correspondence to test whether our poor cluster BCMs are similar to normal Es or if they show any influences of their special place at the centers of thinly populated clusters. Kormendy (1977) discovered that normal ellipticals define a tight linear relationship between surface brightness and effective radius in the optical wavelength

regime. This “Kormendy relationship”, expressed as:

$$\mu_{e,B} = 3.28 \log r_e + 19.45; \quad \mu_{e,V} = 3.28 \log r_e + 18.79,$$

where μ is in mag arcsec^{-2} and r_e is in kiloparsec, shows a dispersion of only $0.38 B \text{ mag arcsec}^{-2}$.

The structural parameters of the brightest galaxies of MS0002 and MS0301 conform to the very high end of the Kormendy relation to reasonably high accuracies. In a similar vein, Thuan & Romanishin (1981; TR81) found that structural parameters characterizing only the central part (i.e. excluding the envelope component in the case of rich clusters) of first brightest galaxies in both poor (AWM and MKW) and rich (Abell) clusters follow the brightward extrapolation of the Kormendy relation, and thereby smoothly extend properties exhibited by normal ellipticals. They showed further that brighter galaxies are on average more diffuse i.e., have larger r_e , and exhibit brighter μ_e (of about 1.4 mag) than normal ellipticals, though with large scatter. The latter is evidently applicable in the case of MS1306 in particular. While the Kormendy relation leads one to expect a central surface brightness of $\mu_{e,V} = 23.4 \text{ mag arcsec}^{-2}$, the galaxy turns out to be brighter by 1.3 mag than predicted for its r_e .

Normal elliptical galaxies actually follow a family of bivariate scaling relations that puts them on a two-dimensional “fundamental plane” (FP), of which the Kormendy relation is but one projection. The FP includes dynamical, structural and metallicity indicators of elliptical galaxies. De Carvalho & Djorgovski (1992; DD) established that while both cluster and field ellipticals obey the FP, cluster ellipticals are more homogeneous than field members, in the sense of showing tighter correlations between measures of luminosity, radius, surface brightness, and stellar population indicators. We shall employ their bivariate fits using $(B - V)$ colors as the second parameter in the effective radius–mean surface brightness relation, in order to check if our BCMs lie on the FP. Note that DD used the mean surface brightness within the effective radius, not μ_e itself. We have, therefore, estimated the former for our BCMs, as well, except for MS0002 for which we have not photometered $(B - V)$ colors. We apply the DD solutions for the clusters and field galaxies of the “7S” dataset; these represent field and rich cluster ellipticals.

We find that, for their measured $\mu_{e,V}$ and $r_{e,V}$ the BCMs of MS0301 and MS1306 would be too blue by about 0.25 mag in $(B - V)$ (well over the observational error) for the field galaxy solutions. The brightest member of MS1306 has the right $(B - V)$ color (within errors) for its $\mu_{e,V}$ and $r_{e,V}$ on applying the cluster correlation, while MS0301 would be marginally bluer. (Note that we use 11-pixel aperture magnitudes, and the BCM of MS1306 becomes redder with increasing galactocentric distance.)

Since BCMs are physically different from normal ellipticals, having experienced complex dynamical processes specific to their location near or at the bottom of the cluster potential well, it is indeed not surprising that our poor cluster BCMs do not at all fit the FP solution for field galaxies, while their properties are more or less similar to ellipticals in rich clusters. What is unexpected, however, is that the first-ranked member of MS1306, while not falling on the Kormendy relation, appears on the bivariate relations relating color to the $\mu_e - r_e$ fits.

6.4 Stellar Populations and Interstellar Matter

Besides measuring the shape of the BCMs, we address another important issue of the distributions of their stellar populations and metallicity. By comparing the luminosity profiles in different filters, we can derive the color and therefore information about the types of stars that contribute to the observed luminosity. Such multi-passband surface photometry is also useful in the detection of the inter-stellar medium (ISM) including (asymmetrically distributed) dust. Radial color distributions provide us with information not only about the stellar properties but also of the dynamical history of the system, i.e., whether the galaxy has formed through dissipational collapse or has undergone tidal interactions.

Akin to the color–magnitude relationship of the early-type galaxies in clusters such that more luminous galaxies are redder (Sandage & Visvanathan 1978, see also Chapter 5), individual galaxies are also redder at smaller radii i.e., in their bright central regions and generally bluer at larger galactocentric distances.

There are two scenarios for the origins of color gradients:

- variation in age of the stellar populations
- metallicity gradient (Faber 1977).

Both models reproduce the average color gradient seen in nearby ellipticals, creating an age - metallicity degeneracy. But they predict significantly different gradients at redshifts larger than ~ 0.3 , with the deviation increasing with increasing redshift. Derived by comparing models of the origin of color gradients with elliptical galaxies observed in the Hubble Deep Field, and in high- z clusters, the currently favored scenario is one in which the color gradients originate not in the age variations but in the metallicity gradient of the stars (e.g., Tamura et al. 2000, Saglia et al. 2000). On the other hand, the combined analysis of metal-sensitive and age-sensitive line indices (i.e., Mg_2 and $H\beta$, respectively) indicates a combination of both age and metallicity variations (e.g., Mehlert et al. 2000). Other factors like dust (Goudfrooij & de Jong 1995, Wise & Silva 1996) and localized star forming regions can also affect the color gradient. The effect of dust and star formation are complementary; dust tends to redden the galaxy whereas young stars lead to its blueing.

6.4.1 Color Gradients

The comparison of effective radii (derived from the de Vaucouleurs law fits) in different filters enables description of large scale trends in the distribution of galaxian color. It also provides a way of determining if the BCM shows dust or patchy star-formation, both of which would affect the brightness profiles as a function of wavelength.

Another informative, quantitative expression for the radial change in color of a galaxy is :

$$\frac{\Delta(m_{\lambda 1} - m_{\lambda 2})}{\Delta(\log r)},$$

where $m_{\lambda 1}$ and $m_{\lambda 2}$ represent the magnitudes in the two filters. This color change per decade in radius is usually well-behaved, can be computed from linear fits to the color profile. A negative gradient indicates that the galaxy is reddish outward.

For the brightest cluster members we next construct the radial profiles of the color indices ($B - V$), ($B - R$), ($V - R$) and ($R - I$) using the derived surface brightness profiles in the individual filters. As before, for MS0002 we perform the analysis only in the V and R filters. We then determine the logarithmic color gradient, $\Delta C / \Delta \log r$ from linear fits to the colors as a function of the logarithm of the radial distance, accounting for errors due to seeing differences in the two filters. Unequal seeing may result in spurious color gradients in the innermost ($r \leq 3$ arcsec) galaxy regions. We compute the effect of seeing on the determination of the radial color variation using the prescription of Sparks (1988) who studied the effect of unequal seeing disks on the measurement of color gradients in $r^{1/4}$ galaxies. For the outer faint isophotes, the systematics of background subtraction are the dominant contributors to the error budget. But since the sky subtraction errors are likely to be in the same direction in both filters, the errors in determining the color and color gradients in the outer parts of the galaxies are likely to be much less than those in the individual profile measurements. We chose, conservatively, to perform the linear fit over the points over the radial ranges free from the strongest seeing effects and where the isophotes in the bluer filter fell to 24.5 mag in surface brightness, and not on the basis of any scale lengths of the galaxies. In these ranges the straight line is visibly a reasonable descriptor of the changes in color, though the linear fits are not excellent, with the reduced chi-square values being on average 2-5.

While this analysis works well for the BCMs of MS0002 and MS0301, it provides a somewhat incomplete description of MS1306, whose first-ranked member is clearly differentiated into three regimes of color changes: the inner-most 10 kpc region (where the color gradients are dominated by seeing effects) shows a blueing with radial distance, then there is a region of a few kpc which has a negligible color gradient, followed by the large outer regions which are definitely reddening with galactocentric distance.

The characteristic radii of the dominant galaxies of MS0002 and of MS0301 are very similar in all the filters; the small variations are quite consistent with seeing differences among the various frames. This is an indication that color gradients are largely absent in these galaxies.

In contrast, for the BCM of MS1306 the scale lengths in the different filters are different, in the sense that $r_{e,V} < r_{e,B} < r_{e,R} < r_{e,I}$. This clearly indicates that its profile is most concentrated in the V band. (Incidentally, the V -band image has the worst seeing of the lot, with the V FWHM nearly 0.3 arcsec broader than those in the other filters.)

In Table 6.3 we list the color gradients we derive along with the range over which we have performed the linear fits. Negative values reflect colors becoming bluer with increasing galactocentric distances. Figure 6.5 presents the color profiles for the BCM sample; the ordinates are the logarithm of the galactic radius in kiloparsec and the abscissa are the various colors.

The color profiles, while noisy, become bluer more or less regularly with radius. For MS0002 and MS0301, the magnitudes of the color gradient are of the order of the errors on the color profile due to seeing variations. The color profiles of MS0301 display no strong variation in slope, while

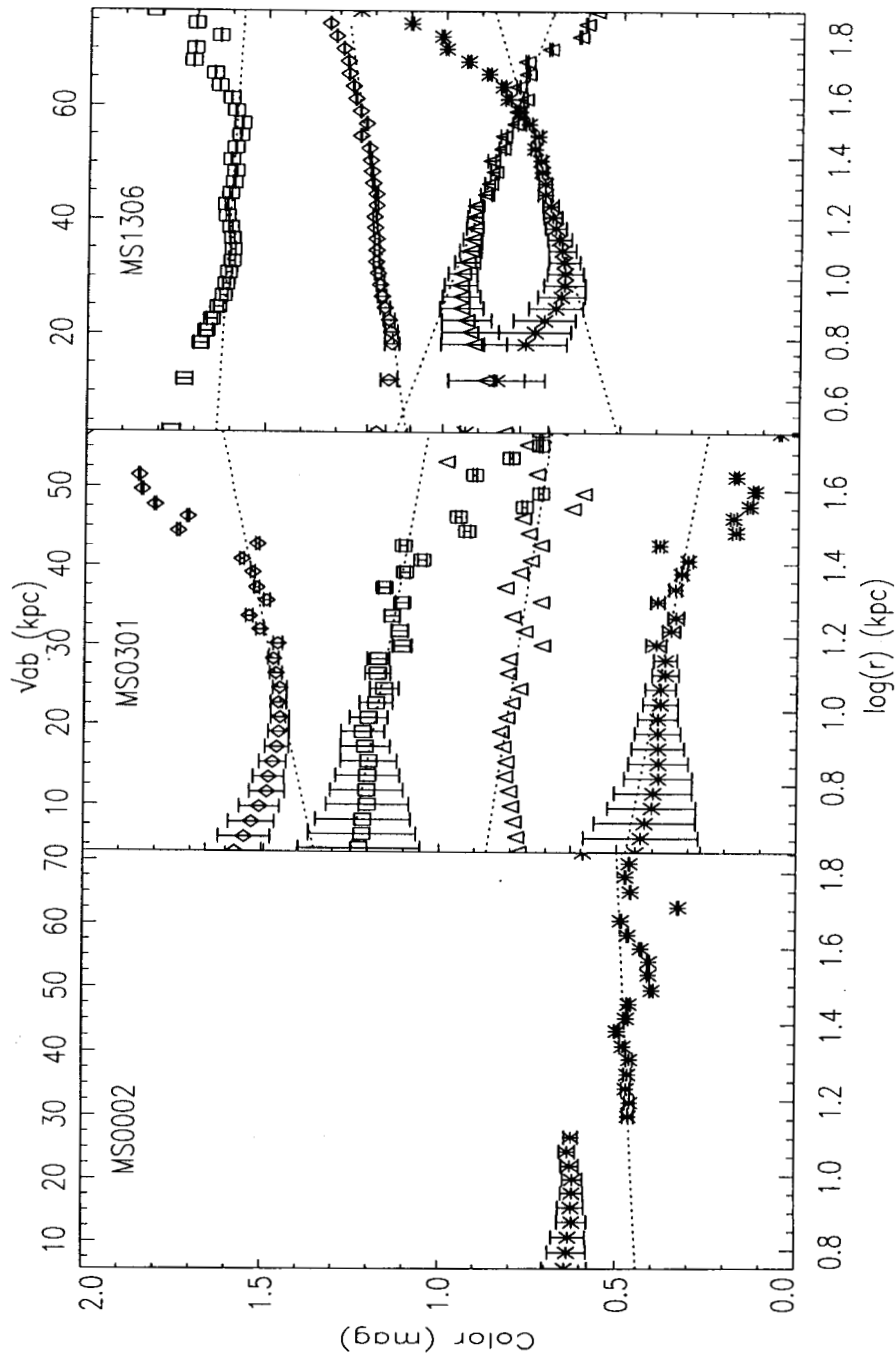


Figure 6.5: Color profiles for the three BCs. The abscissa is the logarithm of the equivalent radius, $r = \sqrt{ab}$. The ordinates are the colors (B-V), (V-R), (B-R) and (R-I) in magnitudes, plotted with triangles, asterisks, squares and diamonds, respectively. The (R-I) profile for MS1306 has been shifted by +0.3 mag to ease visual comparison. Error bars correspond to the color gradients caused due to seeing differences in the concerned filters, calculated according to the prescription of Sparks (1988). Each overplotted line is the best fitting straight line to the corresponding color profile.

Object	Filters	Color mag	Range kpc	$\frac{\Delta C}{\Delta \log r}$ mag $\log(\text{kpc})^{-1}$
MS 0002	V-R	0.69	14-26	0.05 ± 0.04
MS 0301	B-V	1.01	8-26	-0.16 ± 0.08
	V-R	0.46		-0.18 ± 0.06
	B-R	1.47		-0.18 ± 0.04
	R-I	0.88		0.17 ± 0.10
MS 1306	B-V	1.24	11-28	-0.31 ± 0.03
	V-R	0.62		0.26 ± 0.04
	B-R	1.86		-0.05 ± 0.01
	R-I	0.89		0.13 ± 0.01

Table 6.3: Color gradients of the BCMs given as change in color (in units of magnitude) per interval of one decade in the logarithm of the semimajor axis. A negative gradient indicates that the galaxy is bluer outward.

that of MS0002 is somewhat ill-fitted by a straight line, showing several step-like changes along the length of the galaxy.

G97 concluded from their multi-color surface photometry of the above galaxies that their color gradients were consistent with almost no change in color over the entire galaxian areas, as against showing the small gradients we derive. G97 accounted for spurious color differences due to erroneous background corrections but did not include seeing corrections. A quick look at their Figure 4 shows that even in their data, MS0002 shows the non-smooth variation in colors that we report above.

The $(B - V)$ gradients of MS0002 and MS0301 compare well with those derived for rich cluster cD galaxies by Schombert (1988) and Mackie et al. (1990), while the $(B - R)$ slopes are not different from that of the brightest E galaxies in the core of the Virgo cluster (Cohen 1986). Indeed, Andreon et al. (1995) have suggested that in a sample of optical and X-ray selected clusters, the richness of the environment does not strongly influence the color gradients. We assume that small color gradients can be produced by metallicity gradients within old stellar populations, particularly since there is no evidence for the presence of dust or non-thermal emission in either of the above BCMs. Then we derive metallicity gradients from the $(V-R)$ color changes of ≈ 0.2 dex per radial decade for the BCMs of MS0002 and MS0301, applying the model of Arimoto & Yoshii (1987; AY87) which calculates broad-band color-metallicity correlations.

Again, an obvious anomaly with regard to both the magnitude and direction of the color gradients is MS1306. At intermediate galactocentric distances, in the $(V - R)$ and $(R - I)$ color indices, it shows a blueward gradient with *decreasing* radius, in contrast to the other two BCMs. In the central few kiloparsec, and the outermost regions, though, the galaxy once more becomes predominantly red, as already stated. The bumps and dips in the gradients are larger than

caused by differences in the seeing half-radii between the filters, and are likely to reflect true variations in the optical spectral indices of the galaxy. If one considers the annulus of blueing, it corresponds to the galactocentric distances at which the ellipticity remains nearly constant and where the third- and fourth-order Fourier components of deviations from pure ellipticity are significant (see Sec. 6.3.3), implying a possible superposed disk of material. To check on possible emission-line contribution to the regions close to the center of the brightest galaxy of MS1306, we refit the gradients to radii outside of the central 10 arcsec. We find no significant change in the behavior of the color gradients, with and the inflections in the profiles remaining at about 30 and 50 kpc.

It is interesting to compare the BCM of MS1306 with another poor cluster first-ranked galaxy which also shows reddening of the outer regions (but is nowhere blueing). The cluster, 1E 1111.9 – 3754, which is X-ray luminous but optically poor, is similar to those in our sample, and is at a redshift $z = 0.1312$. Maccagni et al. (1988) reported multi-band optical surface photometry that showed the BCM of this poor cluster as having the structure of a normal elliptical galaxy in the main body. But beyond 100 kpc in the R filter and beyond 50–80 kpc in the I band, it is surrounded by a very red halo with $(R - I) \approx 1$ mag that contributes luminosity in excess of the $r^{1/4}$ law. This BCM is also extremely bright, with its absolute magnitude $M_V = -25.2$ making it comparable to the rich cluster cD galaxies. Further, it is located at the center of the potential well of a cluster whose velocity dispersion ($\sigma \approx 1220 \text{ km s}^{-1}$) is similar to that of rich clusters. Maccagni et al. suggested that this giant galaxy must have formed during or even before the cluster itself collapsed, going by the color of the envelop. They suggested that the halo may contain a large fraction of cool AGB stars, and ruled out contribution from low-mass stars which may have had their origins in deposition from a cooling flow. Johnstone & Fabian (1989) disagreed with the latter conclusion, and proposed that the extended red halo may well be explained by a population of low-mass ($M \leq 0.2 M_\odot$) stars. Joy et al. (1995) resolved this conflict by showing that near infra-red surface brightness profiles showed no evidence of extended halos, arguing against low-mass star accretion.¹ Two other galaxies are known to display such large red gradients outwards. Both are cD galaxies of rich clusters (A3284, Molinari et al. 1995; and PKS 0745 – 191, Mackie et al. 1990) that harbor massive cooling flows.

The central galaxy of MS1306 shows no optical emission lines (GL94) and its $H\alpha$ luminosity is less than $6.7 \times 10^{40} \text{ erg s}^{-1}$ (Donahue et al. 1992). Then, going by the strong correlation of $H\alpha$ luminosity and the mass accretion rate determined from X-ray surface brightness data, it does not lie in the core of a strong cooling flow, and so is not similar to the BCMs above. Our own data unfortunately do not permit unambiguous explanation for the physical cause of the red outer regions of this BCM. If the color gradients owe themselves to changes in the ages of stellar populations then the center and outermost regions must be older than the intermediate regions. If, in contrast, metallicity gradients within old stellar populations may be implicated, then the red regions must be more metal rich than the middle blue one by about 1.35 per decade in galactocentric distance, as per the predictions of the chemical enrichment models of AY87. It may also be that the radial color distribution is revealing the presence of substructures with

¹However, none of these studies considered the reddening as being driven by either metallicity changes or large scale dust distributions.

different composite stellar populations in the galaxy.

6.4.2 Presence of Dust and Fine Structure

Many ellipticals exhibit non-symmetric features such as shells (Forbes & Thomson 1992), ripples, plumes, etc. (Seitzer & Schweizer 1992). Far from being free of an interstellar medium as originally supposed, a majority of luminous ellipticals and first-ranked cluster galaxies contain significant amounts of dust (van Dokkum and Franx 1995, Goudfrooij et al. 1994); and gas whose temperature ranges all the way from a few tens to 10^6 K (e.g., Knapp et al. 1985, Fabbiano et al. 1992). Interestingly, the spatial distribution and kinematics of the stars, gas and dust do not show strong coupling in these galaxies, pointing to perhaps different origins and evolution in time.

Extending the analysis of color gradients (which are azimuthally-averaged color changes) to measuring color at every pixel results in a color map of the galaxy. We may use extinction maps and color maps to uncover the presence of dust and fine structure. If neither are present, the statistics of the color maps should be the same over the galaxy and over the “sky” i.e., the regions unoccupied by any detected objects. The color maps highlight high spatial frequency (relative to the local length scale of the galaxy) disturbances, if any, which may be identified with regions affected by dust or intense star formation depending on whether they are red or blue, respectively. We recall here that dust extinction is influenced by viewing geometry.

The residual maps, obtained by subtraction of the best-fit model with purely elliptical isophotes from the direct image, show no marked features for any of the BCMs in our sample in any of the filters. So, there is no indication for significant variation in optical depth over the entire surface of the galaxies. As we have mentioned, such an exercise is optimal for galaxies which show obvious signatures of the inter-stellar medium or of dust in the direct images themselves.

Similarly, for the BCMs of MS0002 and MS0301, even the color maps, more sensitive locators of inhomogenieties, do not display any features with good signal-to-noise over the sky. It appears, then, that the embedded disks implied by the Fourier components of deviations from ellipticity are hard to detect as coherent structures. If the disks are face-on, for instance, they could produce only weak signals in both the residual and color maps.

As mentioned before while speaking of the shift in isophotal centers, the BCM of MS1306 shows evidence of a dust patch close to its center. In Fig. 6.6, we reproduce part of the $(V - R)$ color map, that of the central region of the BCM of MS1306. The darker regions represent the redder areas, hence the more extinguished regions within the BCM. (Though it would have been better to provide $(B - R)$ color map analyses, we chose to use $(V - R)$ since the signal-to-noise is rather a lot better.) There is a patch - extending faintly to a ring - of reddening seen in the figure as the darkened region covering an oval about 3 arcsec across. Note that the 1-pixel wide ring feature at the very center is an artefact of seeing differences between the two filters and of the unreliability of ellipse fitting within one PSF of the galaxy center. The broader dark region near and around it, though, is no artefact, and is presumably dusty and cooler than its surroundings. The swathe of extinction happens to be located in the reddened center of the galaxy that also shows deviations (particularly in the R-band) from the $r^{1/4}$ law.

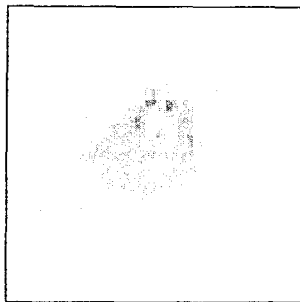


Figure 6.6: Color map that shows the presence of dust in the central few (≈ 5) kiloparsec of the BCM of MS1306. While the thin ring structure is likely to be an artefact of seeing and cessation of modeling in the innermost regions of the galaxy, there is no mistaking the region of higher extinction surrounding it.

We compute the reddening within a circular region of radius 3 pixels (or 1.8 arcsec), comparable to the seeing disk. We then compare this with the color differences in closely neighboring areas (assumed dust-free) along the same isophote (to avoid the effect of the appreciable radial color gradient). We find that (with arbitrary zero-point) the “dust-free” regions around the center range in $(V - R)$ from 0.59 to 0.65 mag with individual photometric errors of about 0.06 mag, and have a mean color of $(V - R) = 0.63$ and standard deviation of 0.03. The areas occupied by dust span a $(V - R)$ range of 0.78 – 0.88, with a mean of 0.84 mag and pixel-to-pixel rms of 0.04.

It is well known that the Galactic extinction is correlated with the column density of HI gas (e.g., Burstein & Heiles 1982). The relation between the reddening and the column density of absorbing gas (which then provides an estimate of the associated gas mass) for our Galaxy is:

$$N(H) = 5.8 \times 10^{21} E(B - V) \text{ atom cm}^{-2}.$$

Assuming that the gas and dust of the BCM of MS1306 obey the Galactic extinction law, the selective extinction or color excess of $(V - R) \approx 0.21$ mag translates into $(B - V)$ of 0.275, using the conversion from Cardelli et al. (1989) assuming $R_V = 3.1$. Then, the column density of neutral gas of is $1.6 \times 10^{21} \text{ atom cm}^{-2}$. This is a lower limit to the gas column density if we assume that the extinction is due to the dust in the foreground of the stars. In order to convert the selective extinction into gas and dust masses, we need to determine the surface area of extinction, and make an assumption regarding the gas-to-dust ratio. Since the optical dust signal is not too strong to estimate the full surface area it occupies, and since we do not have an independent estimate of total extinction in each filter, we prefer not to extrapolate the column density into total gas/dust masses.

An interesting question that arises here is how the dust has survived despite being surrounded by hot X-ray emitting plasma of the intra-cluster medium. Many recent studies have found indications for an external origin of dust in ellipticals, since the kinematics of stars and gas and dust are decoupled from each other (e.g., van Dokkum & Franx 1995, Bertola et al. 1988). If this is true of the BCM of MS1306 as well, then it augurs well for a scenario in which the dust is generated from evaporation of cool clouds associated with a gas- and dust-rich dwarf galaxy the BCM captured.

6.5 Further about Individual Galaxies

6.5.1 Dwarf Galaxies of MS 1306.7-0121

The most luminous galaxy of MS1306 displays about eight compact objects in its diffuse outer regions. These objects, which FOCAS classifies as “non-stellar”, show no symmetry in their spatial distribution. The density of objects of similar magnitude over the rest of the CCD frame is only one half of what we find over the BCM outer extremities. Table 6.4 presents the photometric parameters of some of these objects which we could reliably photometer. The ($V - R$) colors of the majority of them are close to that of the outermost regions of the BCM.

RA (J2000)	Dec (J2000)	V mag	(V-R) mag
13:09:20.7	-1:36:59.3	21.9040	0.98
13:09:20.4	-1:37:32.7	21.6180	0.72
13:09:20.0	-1:37:35.9	21.0860	1.02
13:09:19.9	-1:37:41.8	22.4140	1.87
13:09:19.6	-1:37:48.5	21.5650	0.44

Table 6.4: Properties of the candidate dwarf galaxies around MS1306.

What are these objects: globular clusters (GCs) or companion dwarf galaxies?

In the BCM of Virgo, M87 ($z = 0.0044$), GCs become detectable at $V \approx 20$ mag. Since MS1306 is twenty times more distant, or 6.4 mag fainter, we should start seeing M87-like GCs only more than five magnitudes above where we do detect them. Are these objects then GCs a hundred times more luminous than their cousins in M87? That is quite unlikely. For instance, Bridges and Hanes (1994) discovered a GC system around another poor cluster BCM (that of MKW 4 at $z = 0.02$) and concluded that its luminosity function is similar to that of the GCs around the Virgo giant ellipticals scaled appropriately in distance. Furthermore, GC spatial distribution is usually centrally concentrated.

So, by the process of elimination, we shall conclude that the compact objects around the most luminous member of MS1306 are likely to be dwarf galaxies. Additionally, the sizes of the faint objects ring more true if they are dwarf companions than if they are GCs. Let us proceed assuming they are physically associated with the bright central galaxy. From this arises an interesting question regarding their origin: have they been created from mass transfer during gas-rich interactions/mergers in which the galaxy was involved (as in the case of the ‘Antennae galaxies’)? Perhaps they are seen in the outer halo of the BCM rather than in the main body as a result of outer regions being most strongly affected by tides. What are the prospects of these dwarfs? Will they be cannibalized by the dominant galaxy creating a cD halo to it? We need deeper images with better seeing to respond to these questions.

6.5.2 The VSSS in MS 0735.6+7421

The brightest cluster galaxies, due to their location at the dynamical center of their host cluster, receive the tidal debris from galaxy interactions as well as the deposit ($10\text{--}100 M_{\odot}$ per year) due to any cooling flow. Even a small fraction of this accreted matter could be enough to fuel nuclear activity in the BCMs, which then appear as powerful radio sources. The hot, diffuse ICM could confine the radio plasma (jets and lobes) ejected by their central engines. If the ICM confines the radio ejecta for sufficiently long periods (a few 10^9 years), radiative losses by synchrotron and inverse-Compton effect would preferentially remove the higher-energy photons of the radio emission, and greatly steepen the radio spectrum.² Such very steep spectrum sources (VSSS) would then be “relic” radio objects, where the central engines have long since ceased their activity, leaving the lobes to age by radiative losses. Interestingly, the steepest spectrum radio sources (with $\alpha < -1.3$) are rare, typically comprising only 0.5% of a complete low frequency sample. A large fraction of these can be identified with very high-redshift galaxies (e.g., de Breuck et al. 2000) or (for $\alpha < -1.6$) Galactic pulsars. X-ray emitting VSSS are almost always associated with galaxy clusters. Evidently then, low- z cluster VSSS are among the rarest phenomena.

The BCM of the cluster MS0735 in our sample hosts one such VSSS. Slingo (1974) first associated a steep-spectrum radio source, 4C +74.13, from the Fourth Cambridge Catalog of radio sources with the cD galaxy of the Zwicky cluster Zw 0735.7+7421. This particular cluster is in the EMSS catalog of GL94 bearing the name MS 0735.6+7421. The cluster is one of the most luminous EMSS sources, with 0.2-2.5 keV luminosity $L_x = 6.1 \times 10^{44} \text{ erg s}^{-1}$ and gas temperature of $T_x \approx 2.4$ keV (significantly lower than expected from the empirical correlation between L_x and T_x (e.g. Edge & Stewart 1991). The evidence points to the cluster containing a cooling flow with a mass deposition rate of $\approx 125 M_{\odot} \text{ yr}^{-1}$ (Donahue & Stocke 1995). The BCM has strong, extended $H\alpha$ emission as well as low-ionization emission lines with $[\text{OII}]\lambda 3727 > [\text{OIII}]\lambda 5007$ emission (Donahue, Stocke & Gioia 1992), all attesting to the presence of a cooling flow.

We collate fluxes at various radio frequencies and compute the two-point spectral indices $\alpha(\nu_1, \nu_2)$ over a frequency range of several decades. We also estimate the rest-frame radio luminosity (at the observed frequency) using the formula given in Weedman (1981). We list these in Table 6.5.

Radio maps of 4C +74.13 from the Westerbork Northern Sky Survey (WENSS; Rengelink et al. 1997) at a wavelength of 92 cm (327 MHz) and from the NRAO/VLA Sky Survey (NVSS; Condon et al. 1998) at 20 cm (1.4 GHz) show quite different morphologies. The angular resolutions of the two surveys are slightly different, though; 45 arcsec for NVSS images and about 10 arcsec worse for WENSS. We depict the WENSS and NVSS radio contours over our optical image in Fig. 6.7. While the low frequency radio morphology of this VSSS is distinctly double (i.e., two components arranged in a “peanut” form), the NVSS appearance is not, showing a barely resolved single component.

²The two-point spectral index between two frequencies (ν_1, ν_2) is $\alpha = \log_{10}(\frac{s_1}{s_2}) / \log_{10}(\frac{\nu_1}{\nu_2})$ where s_1 and s_2 are the flux densities at the respective frequencies.

Frequency MHz	Flux Jy	Spectral Index	Luminosity $\log P \text{ W s}^{-1}$	Reference
38	45.80	-1.84	28.08	Hales et al. (1995)
151	3.61	-2.05	27.99	Hales et al. (1991)
232	1.5	-1.77	26.58	Zhang et al. (1997)
325	0.827	-2.46	26.39	Rengelink et al. (1997)
1400	0.0227	-1.8	24.77	Condon et al. (1998)
5000	0.0023		22.93	GL94

Table 6.5: Radio fluxes and spectral indices of the very steep spectrum source 4C +74.13.

6.6 Discussion

According to theories of structure formation, luminous galaxies are built up within dark matter halos in a hierarchical fashion, with small galaxies forming first, and merging into progressively more massive objects. While the details of the structure formation processes and merging history of the dark matter depend on the assumed cosmology, there is no contention on the basic premise of merging and hierarchical structure formation. In poor clusters, the low crossing time and reasonably high galaxy densities dictate that galaxy-galaxy and galaxy-cluster interactions alter both the structure and stellar content of the member galaxies, and tidal interactions could disrupt entire galaxies. Complementarily, such a cluster environment is also home to the most massive and luminous galaxies in the universe. The tenuous but all pervasive hot intra-cluster gas could also alter the star-formation properties of the galaxies.

All the BCMs in our sample reside in regions of very high galaxy density within their host clusters (section 5.3). The increasing ellipticities of their outermost regions could indicate that the BCMs are dynamically coupled to the elongated host clusters. Their rough alignment with the cluster X-ray emission and long axis of the galaxy distribution support conjectures that they respond to their local large-scale structure. these first-ranked galaxies have total luminosities ($M_V \approx -24$) similar to those of the cD/D galaxies that dominate the AWM/MKW poor clusters (TR81), which in turn are comparable to total luminosities of cD galaxies — excluding the envelopes — in rich clusters.

If these BCMs are stationed at the bottom of the host cluster potential well, a natural scenario for their formation and present special status necessarily invokes galaxy interactions and mergers. While the density of low-luminosity (fainter than M^*) galaxies in the cores of poor clusters are nearly as high as that of their rich counterparts, their velocity dispersions are likely to be lower. So, poor clusters may foster higher merger rates than their rich counterparts, which results in

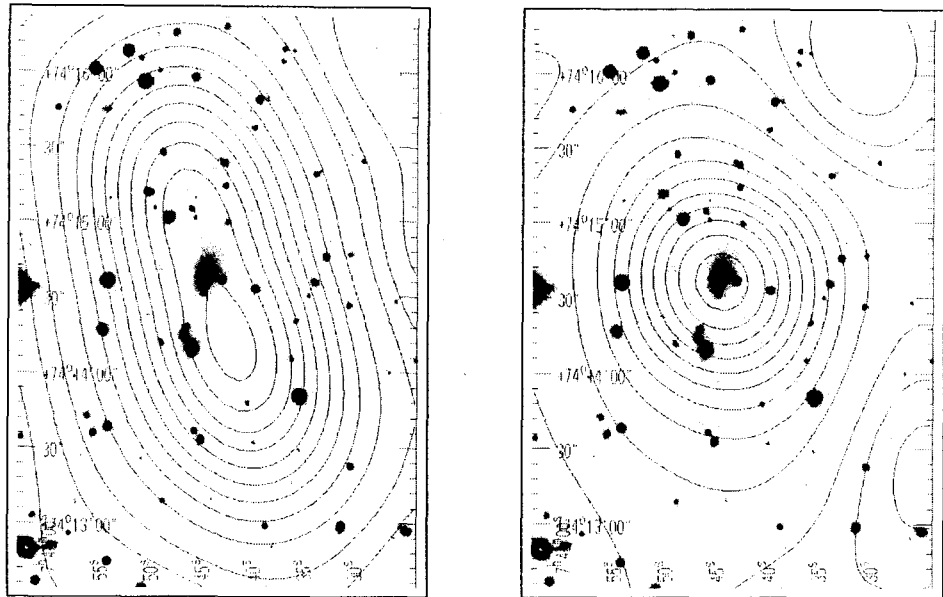


Figure 6.7: The radio maps of 4C +74.13 at 327 MHz (left) and 1.4 GHz overplotted on the optical image.

extremely large and massive galaxies. The abundance of nearby neighbors and dwarf galaxies in the closest environs of the BCMs indicate that gravitational encounters would continue throughout the lifetime of the central galaxy. The BCMs could cannibalize some of the smaller companions whose coalescence would further puff them up.

Evidence exists for these, for instance, in the color variations of the luminous BCM of MS1306, its tidal bridge with its northern (much smaller) neighbor and its rumpled appearance, and in the multiple nuclei of the cD of MS0735. Computer simulations show that tidal bridges are fragile and are destroyed when the galaxies come back together for repeated encounter, implying that the BCM of MS1306 is currently undergoing violent phenomena and the bridge may therefore usefully probe the form of the interaction. Galaxy interactions are likely to significantly affect the star formation or AGN activity in the galaxy central regions. We see that the BCM of MS0301 is too blue for its structural parameters, while that of MS1306 has a blue annulus and red envelop. Using radio continuum data from the 5 GHz survey of GL94, we calculate that our BCMs are moderate radio sources, with $\log P$ (5 GHz) between 22.5 and 23 W Hz^{-1} . Is the radio emission due to AGN or stellar contributions? Batuski et al. (1992) established that the starburst model is the best descriptor of the radio emission from interacting galaxies in poor clusters, but the “central monster” (AGN) model could be applied in a few cases. Further, the finding of a very steep-spectrum radio source in MS0735 indicates that the probability of a cluster containing such a source is unlikely to depend on cluster richness. The lack of strong absorption features in the residual color images indicates that there are no major dust lanes, or, if the galaxies are not really dust-free, then the dust is smoothly distributed.

The three BCMs studied through surface photometry have luminosity profiles well characterized by the de Vaucouleurs law for elliptical galaxies. This is in conformity with violent relaxation coming into play following major merger events. However, low-level deviations from purely ellip-

tical isophotes are ubiquitous, indicative in particular of weak embedded stellar disks. Further, the galaxies follow the equivalent Fundamental Plane relations for rich cluster ellipticals. Two of the three galaxies have de Vaucouleurs parameters at the very high end of the normal elliptical galaxies sequence; in the field, there are virtually no galaxies with such large effective radii as our BCMs. It may have been mergers of equal-mass galaxies that resulted in objects of such large dimensions. The various analyses indicate the occurrence of recent interactions and mergers of the BCMs with their neighbors but also signify that the galaxies are in equilibrium for the most part due to the last major merger having occurred at high-redshifts.

Though the mean surface brightness are as bright or brighter than that of cD galaxies in rich clusters, our BCMs lack an extended halo and are hence unlikely to be genuine cD galaxies. Now, the amount of tidal stripping of galaxies in poor clusters is smaller compared to that in rich agglomerations, due to the shallower potential well. This probably is the cause of the missing extended envelopes despite the cD-like luminosities of the BCMs (Thuan & Romanishin 1981).

The N-body simulations of Dubinski (1998) are particularly interesting to us since the galaxy system of his simulations can be classified as a poor cluster in terms of its galaxy population and velocity dispersion. Dubinski's suite of N-Body simulations posits rapid galaxy merging building up the bulk of the BCM luminosity during the initial collapse of the cluster along a filament. Strong cluster tidal fields strip stars from member galaxies and could account for the extended, very low surface brightness envelope of the nascent cD galaxy. The final product is a massive central galaxy with a flattened surface brightness profile and velocity dispersion similar to observed BCMs. The long axis of the intrinsically triaxial BCM aligns itself with the primordial filament and with the long axis of the cluster galaxy distribution, agreeing with observed trends for galaxy cluster alignment.³ The BCM continues, over its lifetime, to accrete satellites and nearby dwarf galaxies through dynamical friction; the small galaxies do not contribute much extra mass, but distend the cD halo further. Such mergers of gas-rich protogalactic units can feed a central black hole and activate the dominant cluster galaxy into a powerful radio source (West 1994). In the centers of cooling flows clusters, such radio sources may turn out to have very steep spectral indices, as is the case in MS0735.

Since the stellar population gradients are not very strong, in general, the brightness distributions are a pointer to the visible mass distribution of the galaxies. Extraordinary galaxies such as the X-ray overluminous elliptical galaxies (Vikhlinin et al. 1999) and ultra-luminous infra-red galaxies (Sanders & Mirabel 1996) appear to be luminous ellipticals in formation. There are indications that some of these reside in galaxy groups. Further, the luminosity of the brightest galaxy, in its privileged location at the poor cluster center, is correlated with the entire cluster X-ray emission (Yamagata & Maehara 1986). It would therefore be of great interest to observe a full sample of poor cluster BCMs at various redshifts and connect their origin and evolution with their environment as also with the cluster luminosity function.

³Dubinski's work does not explicitly include contributions from a cooling flow in the cluster.

Chapter 7

Conclusions

What the caterpillar calls the end of the world, the Master calls the butterfly.

– Richard Bach, “*Illusions: The Adventures of a Reluctant Messiah*”

The motivation for this work comes from the observed variations in properties of galaxies such as morphological fractions, star formation, etc., in different environments. The variations may have been set *ab initio*, and/or may arise due to the different relative impact of processes such as galaxy interactions and mergers, ram-pressure stripping or gas infall in the different environments. This is the so-called “nature vs. nurture” debate about galaxy properties. In this thesis, we examine the photometric properties and evolution of galaxies in poor clusters, and how they compare with their counterparts in isolation or in richer, denser neighborhoods.

In the literature there are many definitions of poor clusters; this class of galaxy systems spans the entire gamut of galaxy populations from triplets, through quintets, through systems like the Local Group, upto (and including) the threshold of rich clusters. Our working definition of a poor cluster is that its bright galaxy population within the central 0.5 Mpc must number > 5 but \leq the Abell (1958) richness 0 criterion of between 30 and 49 galaxies within two magnitudes of the third brightest cluster member.

7.1 Recapitulation of our Results

We study four poor clusters of galaxies selected as luminous X-ray sources ($L_X \geq 3 \times 10^{43} \text{ erg s}^{-1}$) at moderate redshifts ($0.08 < z < 0.22$). The objects, from the *Einstein* Medium Sensitivity Survey cluster catalog of Gioia & Luppino (1994) are: MS 0002.8+1556, MS 0301.7+1516, MS 0735.6+7421 and MS 1306.7-0121. We acquired multiband optical CCD images of these clusters (complete to $V \approx 21$ mag) using the 2.3-m Vainu Bappu Telescope operated by the Indian Institute of Astrophysics. We performed aperture photometry of the galaxies in the lines-of-sight to the cluster and placed it on the Johnson–Cousins standard.

How do star-formation properties of galaxies in poor clusters compare with those in the field and rich clusters? In Chapter 4, we study the colors (and, by inference, star-formation properties) of the poor cluster galaxies. The early-type galaxies in the EMSS poor clusters follow a well-defined color–magnitude relation (CMR). We have found that the slope and scatter of the CMR of early-type galaxies are roughly consistent with each other, and with the CMR of the Virgo cluster properly redshifted. We used the good definition and tightness of the CMR to cull cluster “sequence” members from the set of all the galaxies in each of the clusters. The fraction of “blue” objects — bluer than predicted by the CMR — is similar to those of low redshift richness 0 clusters,

which are themselves higher than those of rich clusters at similar redshifts. This reflects the red colors of the majority of disk galaxies, and the lack of very recent mergers.

What is the morphology of the poor clusters? What can we infer about their dynamical states? In Chapter 5 we present analyses related to the morphology of the four EMSS poor clusters. We study the cluster morphology at various levels: qualitatively by visual assessment and through a simple comparison of the optical image with the contours of X-ray emission; and in a quantitative manner using maps of the projected galaxy distribution. We find, not surprisingly, that the core and halo sizes for our poor clusters are typically one third and one quarter of the corresponding sizes for Abell clusters (Hickson 1977). Their concentration factor is smaller than the average for Abell clusters. The poor cluster morphologies (which we study in Chapter 5) are irregular and show some substructure, suggesting they are relatively unevolved. However, the dynamical youth of the cluster does not seem to rule out galaxy segregation by luminosity (for which the evidence is marginally significant). Further, luminosity segregation responds marginally more strongly to cluster-centric distance rather than to local environment, suggesting that its dominant driver is the global (dynamic) potential of the cluster. As for morphological segregation, the evidence is subtle and not very tractable to our analysis.

We examine the cluster richness and galaxian distribution in luminosity, i.e., luminosity function (LF) in Chapter 3. To test whether the galaxy LF is “universal”, i.e., independent of environment, (i) we compare the unbinned galaxy LFs created using galaxies belonging to the cluster color-magnitude “sequence” of the individual EMSS poor clusters among themselves and with a composite LF derived from the addition of the individual LFs, and (ii) perform fits of the binned weighted composite LFs in the B , V and R bands to the Schechter (1976) function and compare the Schechter parameters with the LFs of field and rich-cluster galaxies. In all these comparisons, we exclude the brightest cluster members which are thought to have “special”, i.e., non-statistical origins. Non-parametric statistical tests show that the sequence galaxy LFs of the individual poor clusters are not significantly different from each other to about $M_V = -18$, though there exist a few detailed variations especially at the brightest end. Schechter function fits to the binned composite LFs do not permit emphatic conclusions due to poor number statistics and lack of direct membership information. However, there are clear indications that the faint-end of the composite LFs are alike ($\alpha \approx -1$) in the different colors, and are similar to those of other poor galaxy clusters. The EMSS poor cluster LF is steeper than that of field galaxies (Lin et al. 1996) but not so steep as in either poor groups (Zabludoff & Mulchaey 2000) or richer clusters (e.g., Lugger 1986, Colless 1989).

All the poor clusters we study contain a dominantly bright galaxy close to the centroid of their X-ray emission. The luminosity difference between the first- and second-ranked galaxies ranges from 0.4 to 1.3 mag. The profiles of these brightest cluster members (BCMs) are well-described by the de Vaucouleurs $r^{1/4}$ law; the exception is the BCM of the $z = 0.2$ cooling-flow cluster, MS 0735.6+7421, which is a cD galaxy (and hosts the very steep spectrum radio source 4C +74.13). There is relatively little support for any recent episode of star formation in these galaxies. However, the BCM of MS 1306.7-0121 shows clear evidence of interactions with one or two of its smaller neighbors and has a color gradient reddening outwards, contrary to that observed in most other cluster dominant members (e.g., Mackie 1993). For the two clusters

with $L_X > 10^{44}$ erg s^{-1} , the optical long axis of the BCM is aligned to within 10° of the X-ray elongation. This behavior is seen in the dominant galaxies of other poor clusters (Fuller, West, & Bridges 1999), rich clusters (Rhee, van Haarlem, & Katgert 1992) as well as poor groups (Mulchaey & Zabludoff 1998). The surface-brightness profile, colors and color gradients of the BCMs, and their alignment with the isocontours of X-ray emission are consistent with a scenario in which the BCM forms by rapid mergers along a filament during the epoch of cluster formation (e.g., Dubinski 1998).

In summary, the poor clusters are of Abell richness class $r < 1$, exhibit central densities comparable to those of rich clusters and have widely different X-ray luminosities of the rich cluster range. It is most likely that galaxy-galaxy and galaxy-cluster relaxation processes are on-going in these dynamically complex environments that host both evolved and star-forming galaxies. If such galaxy interactions lead to starbursts, they might be part contributors to the blue galaxy fractions in poor clusters being higher than in the richer systems. Multiple mergers early in the history of the clusters could have been the origin of the brightest galaxies of the EMSS poor clusters that have enlarged core radii and lower surface brightnesses compared to their counterparts in rich clusters. In terms of the statistical properties of their galaxies, poor cluster therefore appear to be extensions of their rich counterparts to lower masses and lower or comparable X-ray luminosities.

7.2 Future Investigations

The important thing is not to stop questioning.

– A. Einstein

Far from being in splendid isolation from each other, galaxies interact among themselves and with their surroundings. Galaxies are most likely products of both nature and nurture. Thus, to understand the physical properties and the formation and evolution of galaxies, we have to take into account the interplay between galaxies and their environments. But despite much effort, even elementary questions about the influence of “nature” versus “nurture” regarding galaxies remain puzzling. Among the simple topics which are yet to throw up straight-forward answers are: (i) the mutual exchange of matter and energy between the components of galaxy aggregates — member galaxies the intra-cluster medium, and dark matter — which influences the properties and evolution of the whole system, (ii) the evolution of statistical properties of galaxy systems with redshift which has cosmological significance, and (iii) how small systems such as galaxy groups and poor clusters fit into the picture of large-scale structure.

The issue of “nature vs. nurture” has become one not of “either-or” but of “how much of each and when”. Disentangling the effects of birth and subsequent evolution is made more challenging by the conspiracy of the very different influences leading to similar outcomes on observable galaxian properties. Along with theoretical work, further observations are required to clarify these issues.

We should extend our current work to a much larger sample of poor clusters to characterize the optical, radio, and X-ray properties and evolution of poor systems of galaxies at moderate redshifts. Recent X-ray catalogs (e.g., Vikhlinin et al. 1998), which are large, complete and have

reasonably secure optical cross-identification, would allow creation of a statistically complete sample of poor clusters over a wide range of redshifts. Large datasets offer possibilities to better determine the galaxy luminosity functions (LFs) in a homogeneous way. Optical multi-color imaging data that are deep and cover a wide-field across the clusters would help push LF studies to faint regimes over the whole of the cluster extent. These would improve on LF studies even in the recent literature that appear fragmentary and often contradictory.

Acquiring deep spectroscopic data for the galaxies in the field of the poor clusters. These would provide membership information for the galaxies in the field of view, their spectroscopic types, i.e., whether they are emission-line galaxies or not. Many studies of environmental variations in galaxy morphology, luminosity functions, etc., make a case for in-depth exploration of galaxies separated into quiescent and actively star-forming. Detailed strengths of Balmer and metal absorption lines as functions of galaxy Hubble type and redshift help constrain the star-formation and morphological histories of the cluster populations. Spectroscopy would be essential in determining the internal kinematics of the clusters to characterize cluster substructure, and segregation by galaxy morphology, evolutionary state or velocity dispersion.

Larger samples of poor clusters, and detailed studies of their brightest cluster members could also yield answers about the way in which structure formed and grew in the Universe, and facilitate a number of other projects. If special mechanisms at the epoch of cluster formation create the BCM, and result in its alignment effects, then later processes in its dynamical evolution such as galactic cannibalism or cluster tidal fields should not affect it much. Here, it would be very productive to study the dwarf population that is closely associated with these brightest galaxies so as to derive the system masses, to map the outer potential wells of the latter, and to examine the objects in the context of hierarchical clustering and galaxy formation scenarios. It would also be important to check how the contrast of the brightest cluster galaxies with the second-ranked cluster galaxy affects the bright end of the LF. A small fraction of cD galaxies (including that of the poor cluster MS0735.6+7421 in our sample) host very steep spectrum radio sources (VSSS), especially if they reside at the centers of cooling flows. The fuelling of such highly luminous central radio sources is still a matter of debate. The role of dynamical activity in the larger cluster environs in creating the VSSS, and the reciprocal effect of the VSSS on the intracluster medium surrounding them are subjects of great interest. Radio observations would help map the cluster magnetic fields (e.g., using arguments of equipartition of energy between the radio-emitting plasma and the pressure of the ICM), and coronal lines in the optical spectra would provide estimates of the fraction of the cooling flow collected by the giant central galaxy.

The X-ray study of these systems is an obvious vehicle to revealing the processes that prevail in the material between the galaxies. Questions to be answered include: is the intracluster gas in hydrostatic equilibrium; what fraction of the high-energy emission has contribution due to discrete sources; how much of the plasma is pre-heated, etc.

It seems fair to say that only multi-frequency observations from the radio to the high-energy regime can provide insight into poor clusters which are among the most common environments for galaxies.

Bibliography

- [1] Abadi, M. G., Moore, B., & Bower, R. G. 1999, M.N.R.A.S, 308, 947
- [2] Abell, G. O. 1958, Ap.J.Supp.Series, 3, 211
- [3] Abell, G. O., Corwin, H. G., & Olowin, R. P. 1989, Ap.J.Supp.Series, 70, 1
- [4] Adami, C., Biviano, A., & Mazure, A. 1998, A.&A., 331, 439
- [5] Adami, C., Marcelin, M., Amram, P., & Russeil, D. 1999, A.&A., 349, 812
- [6] Albert, C.E., White, R.A., & Morgan, W.W. 1977, Ap.J., 211, 309
- [7] Allam, S. S., Tucker, D. L., Lin, H., & Hashimoto, Y. 1999, Ap.J.Lett., 522, L89
- [8] Allen, S. W., Fabian, A. C., Edge, A. C., Bohringer, H., & White, D. A. 1995, M.N.R.A.S, 275, 741
- [9] Allington-Smith, J.R., Ellis, R., Zirbel, E.L., & Oemler, A., Jr. 1993, Ap.J., 404, 521
- [10] Andreon, S., Garilli, B., & Maccagni, D. 1995, A.&A., 300, 711
- [11] Andreon, S. 1998, A.&A., 336, 98
- [12] Andreon, S. & Ettori, S. 1999, Ap.J., 516, 647
- [13] Aragon-Salamanca, A., Ellis, R. S., Couch, W. J., & Carter, D. 1993, M.N.R.A.S, 262, 764
- [14] Aragon-Salamanca, A., Baugh, C. M., & Kauffmann, G. 1998, M.N.R.A.S, 297, 427
- [15] Arimoto, N. & Yoshii, Y. 1987, A.&A., 173, 23
- [16] Arp, H. 1966, Ap.J.Supp.Series, 14, 1
- [17] Athanassoula, E., Makino, J., & Bosma, A. 1997, M.N.R.A.S, 286, 825
- [18] Athanassoula, E., Garijo, A., & García Gómez, C. 2001, M.N.R.A.S, 321, 353
- [19] Austin, T. B. & Peach, J. V. 1974, M.N.R.A.S, 167, 437
- [20] Bagchi, J. & Kapahi, V. K. 1994, Journal of Astroph. and Astronomy, 15, 275
- [21] Bahcall, N. A. 1975, Ap.J., 198, 249
- [22] Bahcall, N. A. 1977, A.R.A.&A., 15, 505
- [23] Bahcall N. A. 1977, Ap.J.Lett., 217, L77
- [24] Bahcall N. A. 1977, Ap.J.Lett., 218, L93
- [25] Bahcall N. A. 1980, Ap.J.Lett., 238, L117
- [26] Bahcall, N. A. 1981, Ap.J., 247, 787
- [27] Bahcall N. A. 1988, A.R.A.&A., 26, 631
- [28] Bahcall, J. N. & Soneira, R. M. 1981, Ap.J.Supp.Series, 47, 357
- [29] Baier, F. W., Lima Neto, G. B., Wipper, H., & Braun, M. 1996, Astronomische Nachrichten, 317, 77

- [30] Balkowski, C., 1992, in *Physics of nearby galaxies: Nature or nurture?*, eds. Thuan, Trinh Xuan; Balkowski, Chantal; Tran Thanh Van, J.
- [31] Balogh, M. L., Schade, D., Morris, S. L., Yee, H. K. C., Carlberg, R. G., & Ellingson, E. 1998, *Ap.J.Lett.*, 504, L75
- [32] Balogh, M. L., Morris, S. L., Yee, H. K. C., Carlberg, R. G., & Ellingson, E. 1999, *Ap.J.*, 527, 54
- [33] Barnes, J. 1985, *M.N.R.A.S*, 215, 517
- [34] Barnes, J. 1989, *Nature*, 338, 123
- [35] Barnes, J. E. & Hernquist, L. 1992, *A.R.A.&A.*, 30, 705
- [36] Barton, E. J., de Carvalho, R. R. & Geller, M. J. 1998, *A.J.*, 116, 1573
- [37] Batuski, D. J. & Burns, J. O. 1985, *A.J.*, 90, 1413
- [38] Batuski, D. J., Hanisch, R. J., & Burns, J. O. 1992, *A.J.*, 103, 1077
- [39] Baum, W. A. 1959, *P.A.S.P.*, 71, 106
- [40] Bautz L. P., Morgan W. W., 1970, *Ap.J.Lett.*, 162, L149
- [41] Beers, T. C. & Geller, M. J. 1983, *Ap.J.*, 274, 491
- [42] Beers, T.C., Kriessler, J.R., Bird, C.M., & Huchra, J.P. 1995, *A.J.*, 109, 874
- [43] Bekki, K. & Shioya, Y. 1997, *Ap.J.*, 486, 197
- [44] Bekki, K. 1999, *Ap.J.Lett.*, 510, L15
- [45] Bender, R., Saglia, R. P., Ziegler, B., Belloni, P., Greggio, L., Hopp, U., & Bruzual, G. 1998, *Ap.J.*, 493, 529
- [46] Bertola, F., Buson, L. M., & Zeilinger, W. W. 1988, *Nature*, 335, 705
- [47] Bhavsar, S. P. 1989, *Ap.J.*, 338, 718
- [48] Binggeli, B. 1982, *A.&A.*, 107, 338
- [49] Binggeli, B., Tammann, G. A., & Sandage, A. 1987, *A.J.*, 94, 251
- [50] Binggeli, B., Sandage, A., & Tammann, G. A. 1988, *A.R.A.&A.*, 26, 509
- [51] Binney, J. 1992, *A.R.A.&A.*, 30, 51
- [52] Binney, J., & Tremaine, S. 1987, *Galactic Dynamics*, Princeton Univ. Press
- [53] Biviano, A., Girardi, M., Giuricin, G., Mardirossian, F., & Mezzetti, M. 1992, *Ap.J.*, 396, 35
- [54] Biviano, A., Durret, F., Gerbal, D., Le Fevre, O., Lobo, C., Mazure, A., & Slezak, E. 1995, *A.&A.*, 297, 610
- [55] Bliton, M., Rizza, E., Burns, J. O., Owen, F. N., & Ledlow, M. J. 1998, *M.N.R.A.S*, 301, 609
- [56] Bode, P. W., Berrington, R. C., Cohn, H. N., & Lugger, P. M. 1994, *Ap.J.*, 433, 479
- [57] Bothun, G. D. , & Schombert, J. M. 1990, *Ap.J.*, 360, 436
- [58] Bothun, G. D. 1998, *Modern Cosmological Observations and Problems*, Taylor & Francis
- [59] Bower, R. G., Kodama, T., & Terlevich, A. 1998, *M.N.R.A.S*, 299, 1193

- [60] Bower, R. G., Lucey, J. R., & Ellis, R. S. 1992, M.N.R.A.S, 254, 601
- [61] Bridges, T. J. , & Hanes, D. A. 1994, Ap.J., 431, 625
- [62] Briel, U. G. & Henry, J. P. 1993, A.&A., 278, 37
- [63] Burke, D. J., Collins, C. A., & Mann, R. G. 2000, Ap.J.Lett., 532, L105
- [64] Burns, J. O., Hanisch, R. J., White, R. A., Nelson, E. R., Morrisette, K. A., & Moody, J. W., 1987, A.J., 94, 587
- [65] Burns, J. O., White, R. A., & Hough, D. H., 1981, A.J., 86, 1
- [66] Burns, J.O., Ledlow, M.J., Loken, C., Klypin, A., Voges, W., Bryan, G.L., Norman, M.L., & White, R.A. 1996, Ap.J., 467, L49
- [67] Burstein, D. & Heiles, C. 1982, A.J., 87, 1165
- [68] Bushouse, H. A. 1987, Ap.J., 320, 49
- [69] Butcher, H. & Oemler, A. 1978, Ap.J., 219, 18
- [70] Butcher, H. & Oemler, A., Jr. 1984, Ap.J., 285, 426
- [71] Caldwell, N. & Rose, J. 1997, A.J., 113, 492
- [72] Capelato, H. V., Gerbal, D., Salvador-Sole, E., Mathez, G., Mazure, A., & Sol, H. 1980, Ap.J., 241, 521
- [73] Cardelli, J.A., Clayton, G.C., & Mathis, J.S. 1989, Ap.J., 345, 245
- [74] Carlberg, R., Yee, H., Ellingson, E., Abraham, R., Gravel, P., Morris, S., & Pritchett, C.J. 1996, Ap.J., 462, 32.
- [75] Carlberg, R., Yee, H., & Ellingson, E. 1997, Ap.J., 478, 462.
- [76] Carter, D. 1978, M.N.R.A.S, 182, 797
- [77] Carter, D. & Metcalfe, N. 1980, M.N.R.A.S, 191, 325
- [78] Cayatte, V., Kotanyi, C., Balkowski, C., & van Gorkom, J. H. 1994, A.J., 107, 1003
- [79] Chambers, S. W., Melott, A. L., & Miller, C. J. 2000, Ap.J., 544, 104
- [80] Christlein, D. 2000, Ap.J., 545, 145
- [81] Cohen, J. G. 1986, A.J., 92, 1039
- [82] Colless M. 1989, M.N.R.A.S, 237, 799
- [83] Collins, C. A., Burke, D. J., Romer, A. K., Sharples, R. M., & Nichol, R. C. 1997, Ap.J.Lett., 479, L117
- [84] Condon, J. J., Cotton, W. D., Greisen, E. W., Yin, Q. F., Perley, R. A., Taylor, G. B., & Broderick, J. J. 1998, A.J., 115, 1693
- [85] Couch, W. J. & Newell, E. B. 1984, Ap.J.Supp.Series, 56, 143
- [86] Couch, W. J. & Sharples, R. M. 1987, M.N.R.A.S, 229, 423
- [87] Crawford, C. S., Allen, S. W., Ebeling, H., Edge, A. C., & Fabian, A. C. 1999, M.N.R.A.S, 306, 857
- [88] Dahlem, M. & Thiering, I. 2000, P.A.S.P., 112, 148
- [89] David, L. P., Jones, C., Forman, W., & Daines, S. 1994, Ap.J., 428, 544
- [90] Davis, D. S., Mulchaey, J. S., Mushotzky, R. F., & Burstein, D. 1996, Ap.J., 460, 601

- [91] de Carvalho, R. R. & Djorgovski, S. 1992, *Ap.J.Lett.*, 389, L49
- [92] Dekel, A. & Silk, J. 1986, *Ap.J.*, 303, 39
- [93] dell'Antonio, I. P., Geller, M. J., & Fabricant, D. G. 1994, *A.J.*, 107, 427
- [94] de Propris, R. & Pritchett, C. J. 1998, *A.J.*, 116, 1118
- [95] de Vaucouleurs, G. 1953, *M.N.R.A.S.*, 113, 134
- [96] de Vaucouleurs, G. 1975, in *Stars and Stellar Systems*, 9, 557 (1975), 9, 557
- [97] Diaferio, A., Geller, M., & Ramella, M. 1995, *A.J.*, 109, 2293
- [98] Dickinson, M. 1995, in *ASP Conf. Ser. 86: Fresh Views of Elliptical Galaxies*, eds. Buzzoni, A., Renzini, A., & Serrano, A., 283
- [99] Djorgovski S., Davis M., 1987, *Ap.J.*, 313 , 59
- [100] Doe, S.M., Ledlow, M.J., Burns, J.O., & White, R.A. 1995, *A.J.*, 110, 46
- [101] Dominguez-Tenreiro, R. & del Pozo-Sanz, R. 1988, *Ap.J.*, 324, 677
- [102] Donahue, M., Stocke, J., & Gioia, I. 1992, *Ap.J.*, 385, 49
- [103] Donahue, M. & Stocke, J. 1995, *Ap.J.*, 449, 554
- [104] Donahue, M. E. 1996, *Ap.J.*, 468, 79
- [105] Donahue, M. E., Voit, M., Gioia, I.M., Luppino, G.A., Hughes, J.H., & Stocke, J.T. 1998, *Ap.J.*, 552, 550
- [106] Donahue et al. 2001
- [107] Dressler, A. 1978, *Ap.J.*, 226, 55
- [108] Dressler, A. 1980, *Ap.J.*, 236, 351
- [109] Dressler, A. 1984, *A.R.A.&A.*, 22, 185
- [110] Dressler A., Lynden-Bell D., Burstein D., Davies R. L., Faber S. M., Terlevich R., Wegner G., 1987, *Ap.J.*, 313, 42
- [111] Dressler, A. & Shectman, S. A. 1988, *A.J.*, 95, 985
- [112] Dressler, A. & Gunn, J. E. 1992, *Ap.J.Supp.Series*, 78, 1
- [113] Dressler, A., Oemler, A. J., Sparks, W. B., & Lucas, R. A. 1994, *Ap.J.Lett.*, 435, L23
- [114] Dressler, A. et al. 1997, *Ap.J.*, 490, 577
- [115] Driver, S. P., Couch, W. J., & Phillipps, S. 1998, *M.N.R.A.S.*, 301, 369
- [116] Dubinski, J. 1998, *Ap.J.*, 502, 141
- [117] Duc, P.-A. & Mirabel, I. F. 1998, *A.&A.*, 333, 813
- [118] Durret, F., Gerbal, D., Lachieze-Rey, M., Lima-Neto, G., & Sadat, R. 1994, *A.&A.*, 287, 733
- [119] Ebeling, H., Voges, W., & Boehringer, H. 1994, *Ap.J.*, 436, 44
- [120] Ebeling, H., Edge, A. C., Fabian, A. C., Allen, S. W., Crawford, C. S., & Boehringer, H. 1997, *Ap.J.Lett.*, 479, L101
- [121] Edge, A. C. & Stewart, G. C. 1991, *M.N.R.A.S.*, 252, 428
- [122] Eggen, O. & Sandage, A. 1964, *Ap.J.*, 140, 130

- [123] Einasto M. 1990, M.N.R.A.S, 242, 56
- [124] Ellingson, E., Lin, H., Yee, H. K. C., & Carlberg, R. G. 2001, Ap.J., 547, 609
- [125] Ellis, R. S., Smail, I., Dressler, A., Couch, W. J., Oemler, A. Jr., Butcher, H., Sharples, R. M. 1997, Ap.J., 483, 582
- [126] Evrard, A. E. 1990, ApJ, 363, 349
- [127] Evrard, A. E. 1993, in *The Environment and Evolution of Galaxies*, eds. J. Michael Shull, Harley A. Thronson, Astrophysics and Space Science Library, Vol. 188, 69
- [128] Fabbiano, G., Kim, D.-W., & Trinchieri, G. 1992, Ap.J.Supp.Series, 80, 531
- [129] Faber, S.M. 1977, in *The Evolution of Galaxies and Stellar Populations*, eds. B. Tinsley, R. B. Larson, (New Haven, Yale Univ. Obs.), 157
- [130] Fabian, A. 1994, A.R.A.&A., 32, 277
- [131] Ferguson, H. C., & Sandage, A., 1991, A.J.101, 765
- [132] Ferguson, H. C. & Binggeli, B. 1994, Astron.and Astroph. Review, 6, 67
- [133] Flin, P. 1987, M.N.R.A.S, 228, 941
- [134] Folkes, S. et al. 1999, M.N.R.A.S, 308, 459
- [135] Forbes, D. A. & Thomson, R. C. 1992, M.N.R.A.S, 254, 723
- [136] Forman, W. & Jones, C. 1982, A.R.A.&A., 20, 547
- [137] Fort, B., LeFevre, O., Hammer, F. & Cailloux, M. 1992, Ap.J.Lett., 399, L125.
- ✓ [138] Franx, M., Illingworth, G., & Heckman, T. 1989, Ap.J., 344, 613
- [139] Frederic, J. J. 1995, Ap.J.Supp.Series, 97, 259
- [140] Freeman, K. C. 1970, Ap.J., 160, 811
- [141] Fukugita, M., Shimasaku, K., & Ichikawa, T. 1995, P.A.S.P., 107, 945
- [142] Fuller, T. M., West, M. J., & Bridges, T. J. 1999, Ap.J., 519, 22
- [143] Gaidos, E. J. 1997, A.J., 113, 117
- [144] Gaidos, E. J. 1997, A.J., 114, 474
- [145] Garcia, A. M., Paturel, G., Bottinelli, L., & Gouguenheim, L. 1993, A.&A.Supp.Series, 98, 7
- [146] Garilli B., Bottini D., Maccagni D., Carrasco L., & Recillas E. 1996, Ap.J.Supp.Series, 105, 191
- ✓ [147] Garilli, B., Maccagni, D., & Andreon, S. 1999, A.&A., 342, 408
- [148] Gavazzi, G. & Contursi, A. 1994, A.J., 108, 24
- [149] Geller, M. J. & Beers, T. C. 1982, P.A.S.P., 94, 421
- [150] Gioia, I. M., Henry, J. P., Maccacaro, T., Morris, S. L., Stocke, J. T., & Wolter, A. 1990, Ap.J.Lett., 356, L35
- [151] Gioia, I.M., Henry, I.M., Mullis, C.R., Ebeling, H., & Wolter, A. 1999, A.J., 117, 2608
- [152] Gioia, I. M. & Luppino, G. A. 1994, Ap.J.Supp.Series, 94, 583
- [153] Gioia, I.M., Shaya, E., LeFèvre, O., Falco, E.E., Luppino, G.A., & Hammer, F. 1998a, Ap.J., 497, 573.

- [154] Giovanelli, R., Haynes, M. P., & Chincarini, G. L. 1986, *Ap.J.*, 300, 77
- [155] Girardi, M., Fadda, D., Giuricin, G., Mardirossian, F., Mezzetti, M., & Biviano, A. 1996, *Ap.J.*, 457, 61
- [156] Girardi, M., Giuricin, G., Mardirossian, F., Mezzetti, M., & Boschin, W. 1998, *Ap.J.*, 505, 74
- [157] Gladders, M. D. & Yee, H. K. C. 2000, *A.J.*, 120, 2148
- [158] Gomez, P. L., Pinkney, J., Burns, J. O., Wang, Q., Owen, F. N., & Voges, W. 1997, *Ap.J.*, 474, 580
- [159] Goudfrooij, P., Hansen, L., Jorgensen, H. E., & Norgaard-Nielsen, H. U. 1994, *A.&A.Supp.Series*, 105, 341
- [160] Goudfrooij, P. & de Jong, T. 1995, *A.&A.*, 298, 784
- [161] Gourgoulhon, E., Chamaraux, P., & Fouque, P. 1992, *A.&A.*, 255, 69
- [162] Graham, A., Lauer, T. R., Colless, M., & Postman, M. 1996, *Ap.J.*, 465, 534
- [163] Guiderdoni, B. & Rocca-Volmerange, B. 1988, *A.&A.Supp.Series*, 74, 185
- [164] Giuricin, G., Marinoni, C., Ceriani, L., & Pisani, A. 2000, *Ap.J.*, 543, 178
- [165] Gunn, J. E. & Gott, J. R. I. 1972, *Ap.J.*, 176, 1
- [166] Hales, S. E. G., Mayer, C. J., Warner, P. J., & Baldwin, J. E. 1991, *M.N.R.A.S*, 251, 46
- [167] Hales, S. E. G., Waldram, E. M., Rees, N., & Warner, P. J. 1995, *M.N.R.A.S*, 274, 447
- [168] Hashimoto, Y. , Oemler, A. , Jr., Lin, H. & Tucker, D. L. 1998, *Ap.J.*, 499, 589
- [169] Hattori, M. et al. 1997, *Nature*, 388, 146
- [170] Helsdon, S. F. & Ponman, T. J. 2000, *M.N.R.A.S*, 319, 933
- [171] Henry, J. P., Gioia, I. M., Maccacaro, T., Morris, S. L., Stocke, J. T., & Wolter, A. 1992, *Ap.J.*, 386, 408.
- [172] Henry, J. P. et al. 1995, *Ap.J.*, 449, 422
- [173] Hernquist, L., Katz, N. & Weinberg, D. H. 1995, *Ap.J.* 442, 57-60
- [174] Hickson, P. 1977, *Ap.J.*, 217, 16
- [175] Hickson, P. 1982, *Ap.J.*, 255, 382
- [176] Hickson, P. 1997, *A.R.A.&A.*, 35, 357
- [177] Hoessel, J. G., Gunn, J. E., & Thuan, T. X. 1980, *Ap.J.*, 241, 486
- [178] Holmberg, E. 1941, *Ap.J.*, 94, 385
- [179] Huchra, J. P. & Geller, M. J. 1982, *Ap.J.*, 257, 423
- [180] Huchra, J. P. 1985, in the *ESO Workshop on the Virgo Cluster*, eds. Richter, O.-G. & Binggeli, B., 181
- [181] Hunsberger, S. D., Charlton, J. C. & Zaritsky, D. 1996, *Ap.J.*, 462, 50
- [182] Hwang, U., Mushotzky, R. F., Burns, J. O., Fukazawa, Y., & White, R. A. 1999, *Ap.J.*, 516, 604
- [183] Iglesias-Páramo, J. & Vílchez, J. M. 1999, *Ap.J.*, 518, 94

- [184] Ikebe, Y. et al. 1996, *Nature*, 379, 427
- [185] Impey, C., Bothun, G., & Malin, D. 1988, *Ap.J.*, 330, 634
- [186] Irwin, J. A. 1995, *P.A.S.P.*, 107, 715
- [187] James, P. A. & Mobasher, B. 2000, *M.N.R.A.S.*, 317, 259
- [188] Jarvis, J. F. & Tyson, J. A. 1981, *A.J.*, 86, 476
- [189] Jedrzejewski, R. I. 1987, *M.N.R.A.S.*, 226, 747
- [190] Jerjen, H., & Tammann, G. A., 1997, *A.&A.*321, 713
- [191] Johnstone, R. M. & Fabian, A. C. 1989, *M.N.R.A.S.*, 237, 27P
- [192] Joner, M. D. & Taylor, B. J. 1990, *P.A.S.P.*, 102, 1004
- [193] Jones, C. & Forman, W. 1984, *Ap.J.*, 276, 38
- [194] Jones, C. & Forman, W. 1992, in *NATO ASIC Proc. 366: Clusters and Superclusters of Galaxies*, ed. Fabian, A. C, 49
- [195] Jones, L. R., Scharf, C., Ebeling, H., Perlman, E., Wegner, G., Malkan, M., & Horner, D. 1998, *Ap.J.*, 495, 100
- [196] Joy, M., Prestwich, A. H., Burton, M., & Guimond, S. 1995, *Ap.J.Lett.*, 449, L113
- [197] Kaiser, N. 1984, *Ap.J.Lett.*, 284, L9
- [198] Kashikawa, N., Shimasaku, K., Yagi, M., Yasuda, N., Doi, M., Okamura, S., & Sekiguchi, M., 1995, *Ap.J.Lett.*452, L99
- [199] Kauffmann, G. 1995, *M.N.R.A.S.*, 274, 153
- [200] Kauffmann, G. & Charlot, S. 1998, *M.N.R.A.S.*, 297, L23
- [201] Kenney, J. D. P. & Young, J. S. 1989, *Ap.J.*, 344, 171
- [202] Kennicutt, R. C., Roettiger, K. A., Keel, W. C., van der Hulst, J. M., & Hummel, E. 1987, *A.J.*, 93, 1011
- [203] Kennicutt, R. C. 1989, *Ap.J.*, 344, 685
- [204] Kennicutt, R. C. 1998, *A.R.A.&A.*, 36, 189
- [205] Kennicutt, R. C. 1998, in *Saas-Fee Advanced Course 26: Galaxies: Interactions and Induced Star Formation*, eds. Kennicutt, R. C., Schweizer, F., Barnes, J. E., Friedli, D., Martinet, L., & Pfenniger, D., 1
- [206] King, I. 1962, *A.J.*, 67, 471
- [207] Kirshner, R. P., Oemler, A., Schechter, P. L., & Shectman, S. A. 1983, *A.J.*, 88, 1285
- [208] Knapp, G. R., Turner, E. L., & Cuncliffe, P. E. 1985, *A.J.*, 90, 454
- [209] Kodama, T., Arimoto, N., Barger, A. J., & Aragoń-Salamanca, A. 1998, *A.&A.*, 334, 99
- [210] Kodama, T., Bower, R. G., & Bell, E. F. 1999, *M.N.R.A.S.*, 306, 561
- [211] Koo, D. C. & Kron, R. G. 1992, *A.R.A.&A.*, 30, 613
- [212] Kormendy, J. 1977, *Ap.J.*, 218, 333
- [213] Kormendy, J. 1982, in *Morphology and Dynamics of Galaxies: Saas-Fee 12*, eds. Binney, J., Kormendy, J., & White, S. D. M., Martinet, L., Mayor, M., 115

- [214] Kormendy J., Djorgovski S., 1989, *A.R.A.&A.*, 27, 235
- [215] Kriss, G. A., D. F. Cioffi, & C. R. Canizares 1983, *Ap.J.*, 272, 439
- [216] Kundic, T., Hernquist, L., & Gunn, J. E. 1992, *American Astronomical Society Meeting*, 181, #118.10
- [217] Lambas, D. G., Groth, E. J., & Peebles, P. J. E. 1988, *A.J.*, 95, 975
- [218] Landolt A. 1992, *A.J.*, 104, 340
- [219] Larson, R. B. & Tinsley, B. M. 1974, *Ap.J.*, 192, 293
- [220] Larson, R. B. & Tinsley, B. M. 1978, *Ap.J.*, 219, 46
- [221] Larson, R. B., Tinsley, B. M., & Caldwell, C. N. 1980, *Ap.J.*, 237, 692
- [222] Lavery, R. J. & Henry, J. P. 1988, *Ap.J.*, 330, 596
- [223] Lavery, R. J. & Henry, J. P. 1994, *Ap.J.*, 426, 524
- [224] Ledlow, M.J., Loken, C., Burns, J.O., Hill, J.M., & White, R.A., 1996, *A.J.*, 112, 388
- [225] Le Fevre, O., Hammer, F., Angonin, M. C., Gioia, I. M., & Luppino, G. A. 1994, *Ap.J.Lett.*, 422, L5
- [226] Lima Neto, G. B. & Baier, F. W. 1997, *A.&A.*, 320, 717
- [227] Lin H., Kirshner L.P., Shechtman S.A., Landy S.D., Oemler A., Tucker D.L., & Schechter P.L. 1996, *Ap.J.*, 464, 60
- [228] Lopez-Cruz, O., Yee, H. K. C., Brown, J. P., Jones, C., & Forman, W., 1997, *Ap.J.Lett.* 475, L97
- [229] Loveday, J., Peterson, B. A., Efstathiou, G., & Maddox, S. J. 1992, *Ap.J.* 390, 338
- [230] Lubin, L. M. 1996, *A.J.*, 112, 23
- [231] Lubin, L. M., Postman, M., Oke, J. B., Ratnatunga, K. U., Gunn, J. E., Hoessel, J. G., & Schneider, D. P. 1998, *A.J.*, 116, 584
- [232] Lugger, P. M. 1986, *Ap.J.*, 303, 535
- [233] Lugger P. 1989, *Ap.J.*, 343, 572
- [234] Lumsden S.L., Collins C.A., Nichol R.C., Eke V.R., & Guzzo L. 1997, *M.N.R.A.S.*, 290, 119
- [235] Luppino, G.A. & Kaiser, N., 1997, *Ap.J.Lett.*, 475, L20
- [236] Luppino, G. A., Gioia, I. M., Hammer, F., Le Fèvre, O., & Annis, J. A. 1999, *A.&A.Supp.Series*, 136, 117
- [237] Maccacaro, T., Wolter, A., McLean, B., Gioia, I. M., Stocke, J. T., della Ceca, R., Burg, R., & Faccini, R. 1994, *Astrophys. Lett.*, 29, 267
- [238] Maccagni, D., Garilli, B., Gioia, I. M., Maccacaro, T., Vettolani, G., & Wolter, A. 1988, *Ap.J.Lett.*, 334, L1
- [239] Mackie, G., Visvanathan, N., & Carter, D. 1990, *Ap.J.Supp.Series*, 73, 637
- [240] Mahdavi, A., Boehringer, H., Geller, M. J., & Ramella, M. 1997, *Ap.J.*, 483, 68
- [241] Mahdavi, A., Böhringer, H., Geller, M. J., & Ramella, M. 2000, *Ap.J.*, 534, 114
- [242] Maia, M. A. G., Pastoriza, M. G., Bica, E. & Dottori, H. 1994, *Ap.J.Supp.Series*, 93, 425

- [243] Mamon, G. A. 1992, Ap.J.Lett., 401, L3
- [244] Margoniner, V. E. & de Carvalho, R. R. 2000, A.J., 119, 1562
- [245] Margoniner, V. E., de Carvalho, R. R., Gal, R. R., & Djorgovski, S. G. 2001, Ap.J.Lett., 548, L143
- [246] Martin, D. R., Nichol, R. C., Collins, C. A., Lumsden, S. A., & Guzzo, L. 1995, M.N.R.A.S, 274, 623
- [247] Marzke, R. O., Huchra, J. P., & Geller, M. J. 1994, Ap.J., 428, 43
- [248] Matsumoto, H., Koyama, K., et al, 1997, Ap.J., 482, 133
- [249] Matthews, T. A., Morgan, W. W., & Schmidt, M. 1964, Ap.J., 140, 35
- ✓ [250] Mehlert, D., Saglia, R.P., Bender, R., & Wegner, G., 1998, A.&A.Supp.Series, 141, 449
- [251] Mellier, Y. 1999, A.R.A.&A., 37, 127
- [252] Mendes de Oliveira, C. & Hickson, P. 1994, Ap.J., 427, 684
- [253] Merritt, D. 1984, Ap.J., 276, 26
- [254] Metcalfe, N., Godwin, J. G., & Peach, J. V. 1994, M.N.R.A.S, 267, 431
- [255] Metcalfe, N., Shanks, T., Fong, R., & Roche, N. 1995, M.N.R.A.S, 273, 257
- [256] Metevier, A. J., Romer, A. K., & Ulmer, M. P. 2000, A.J., 119, 1090
- [257] Mihalas, D. & Binney, J. 1981, *Galactic astronomy: Structure and Kinematics*, W. H. Freeman and Co.
- [258] Moles, M., del Olmo, A., Perea, J., Masegosa, J., Marquez, I., & Costa, V. 1994, A.&A., 285, 404
- [259] Molinari, E., Buzzoni, A., Chincarini, G., & Pedrana, M. D. 1995, Memorie della Societa Astronomica Italiana, 66, 275
- [260] Molinari, E., Chincarini, G., Moretti, A., & de Grandi, S. 1998, A.&A., 338, 874
- [261] Moore, B., Katz, N., Lake, G., Dressler, A., & Oemler, A., Jr. 1996, Nature 379, 613
- [262] Moretti, A., Molinari, E., Chincarini, G., & De Grandi, S. 1999, A.&A.Supp.Series, 140, 155
- [263] Morgan, W.W., Kayser, S., & White, R.A., 1975, Ap.J., 199, 545
- [264] Mulchaey, J. S., Davis, D. S., Mushotzky, R. F., & Burstein, D. 1993, Ap.J.Lett., 404, L9
- [265] Mulchaey, J., Davis, D., Mushotzky, R., & Burstein, D. 1996, Ap.J., 456, 80
- [266] Mulchaey, J.S. & Zabludoff, A.I. 1998, Ap.J., 496, 73
- [267] Mulchaey, J.S. & Zabludoff, A.I. 1999, Ap.J., 514, 133
- [268] Mulchaey, J. S. 2000, A.R.A.&A., 38, 289
- [269] Muriel, H. ;, Valotto, C. A., & Lambas, D. G. 1998, Ap.J., 506, 540
- [270] Neumann, D. M., & Boehringer, H. 1995, å, 301,865
- [271] Newberry, M. V., Kirshner, R. P., & Boroson, T. A. 1988, Ap.J., 335, 629
- [272] Odea, C. P. & Owen, F. N. 1985, A.J., 90, 9

- [273] Odewahn, S. C. 1995, P.A.S.P., 107, 770
- [274] Oegerle et al. 1987, A.J., 93, 519
- [275] Oegerle, W. R. & Hoessel, J. G. 1989, A.J., 98, 1523
- [276] Oemler A. Jr. 1974, Ap.J., 194, 1
- [277] Oemler, A. 1976, Ap.J., 209, 693
- [278] Oemler, A. 1992, in *Clusters and Superclusters of Galaxies*, (ed.) A.C. Fabian (Dordrecht: Kluwer), p. 29
- [279] Oemler, A. J., Dressler, A., & Butcher, H. R. 1997, Ap.J., 474, 561
- [280] Oort, J. 1983, A.R.A.&A., 21, 373
- [281] Oppenheimer, B. R., Helfand, D. J., & Gaidos, E. J. 1997, A.J., 113, 2134
- [282] Ostriker, J. & Tremaine, S. 1975, Ap.J., 202, L113
- [283] Ostriker, J. P., Lubin, L. M., & Hernquist, L. 1995, Ap.J.Lett., 444, L61
- [284] Paturel, G., Petit, C., Garnier, R., & Prugniel, P. 2000, A.&A.Supp.Series, 144, 475
- [285] Peletier, R. F., Davies, R. L., Illingworth, G. D., Davis, L. E., & Cawson, M. 1990, A.J., 100, 1091
- [286] Pennington, R. L., Humphreys, R. M., Odewahn, S. C., Zumach, W., & Thurmes, P. M. 1993, P.A.S.P., 105, 521
- [287] Phillipps, S., Driver, S. P., Couch, W. J., & Smith, R. M. 1998, Ap.J.Lett., 498, L119
- [288] Pierce, M. J. & Tully, R. B. 1992, Ap.J., 387, 47
- [289] Pierre, M. & Starck, J.-L. 1998, A.&A., 330, 801
- [290] Pildis, R. A., Bregman, J. N., & Schombert, J. M. 1995, A.J., 110, 1498
- [291] Plionis, M. 1994, Ap.J.Supp.Series, 95, 401
- [292] Poggianti, B. M. 1997, A.&A.Supp.Series, 122, 399
- [293] Poggianti, B. M., Smail, I., Dressler, A., Couch, W. J., Barger, A. J., Butcher, H., Ellis, R. S., & Oemler, A. J. 1999, Ap.J., 518, 576
- [294] Ponman, T. J. & Bertram, D. 1993, Nature, 363, 51
- [295] Ponman, T. J., Allan, D. J., Jones, L. R., Merrifield, M., McHardy, I. M., Lehto, H. J., & Luppino, G. A. 1994, Nature, 369, 462
- [296] Ponman, T., Bourner, P., Ebeling, H., & Bohringer, H. 1996, M.N.R.A.S, 283, 690
- [297] Postman, M. & Geller, M. J. 1984, Ap.J., 281, 95
- [298] Postman, M. & Lauer, T. R. 1995, Ap.J., 440, 28
- [299] Press, W. H. & Schechter, P. 1974, Ap.J., 187, 425
- [300] Price, R., Duric, N., Burns, J. O., & Newberry, M. V. 1991, A.J., 102, 14
- [301] Pritchett, C. J. & van den Bergh, S. 1999, A.J., 118, 883
- [302] Quintana, H. 1979, A.J., 84, 15
- [303] Rakos, K. D. & Schombert, J. M. 1995, Ap.J., 439, 47
- [304] Rakos, K. D., Odell, A. P., & Schombert, J. M. 1997, Ap.J., 490, 194

- [305] Ramella, M., Geller, M.J., Huchra, J.P. 1989, Ap.J., 344, 57
- [306] Ramella, M., Diaferio, A., Geller, M. J., & Huchra, J. P. 1994, A.J., 107, 1623
- [307] Ramella, M., Pisani, A., & Geller, M. J. 1997, A.J., 113, 483
- [308] Rector, T. A., Stocke, J. T., & Perlman, E. S. 1999, Ap.J., 516, 145
- [309] Rengelink, R. B., Tang, Y., de Bruyn, A. G., Miley, G. K., Bremer, M. N., Roettgering, H. J. A., & Bremer, M. A. R. 1997, A&AS, 124, 259
- [310] Rhee, G., van Haarlem, M., & Katgert, P. 1992, A.J., 103, 1721
- [311] Richstone, D. O. 1976, Ap.J., 204, 642
- [312] Roberts, M. S. & Haynes, M. P. 1994, A.R.A.&A., 32, 115
- [313] Rood H. J. 1988, A.R.A.&A., 26, 245
- [314] Rood H. J., Sastry G. N., 1971, P.A.S.P., 83, 313
- [315] Rose, J. A. 1977, Ap.J., 211, 311
- [316] Rose, J. A., Bower, R.G., Caldwell, N. , Ellis, R. S., Sharples, R. M., & Teague, P. 1994, A.J., 108, 2054
- [317] Saglia, R.P., Burstein, D., Baggle, G., Bertschinger, E., Colless, M.M., Davies, R.L., McMahan, R.K., & Wegner, G., 1997, M.N.R.A.S., 292, 499
- ✓ [318] Saglia, R. P., Maraston, C., Greggio, L., Bender, R., & Ziegler, B. 2000, A.&A., 360, 911
- [319] Sandage, A. 1976, Ap.J., 205, 6
- [320] Sandage, A. & Visvanathan, N. 1978, Ap.J., 223, 707
- [321] Sanders, D. B., Soifer, B. T., Elias, J. H., Madore, B. F., Matthews, K., Neugebauer, G., & Scoville, N. Z. 1988, Ap.J., 325, 74
- [322] Sanders, D. B., & Mirabel, I. F. 1996 A.R.A.&A., 34, 749
- [323] Sarazin, C. L. 1988, *X-ray Emission from Clusters of Galaxies*, Cambridge Astrophysics Series, Cambridge University Press.
- [324] Sarazin, C. L., Burns, J. O., Roettiger, K., & McNamara, B. R. 1995, Ap.J., 447, 559
- [325] Sastry, G. N. 1968, P.A.S.P., 80, 252
- [326] Scharf, C.A., Jones, L.R.L., Ebeling, H., Perlman, E., Malkam, M., & Wegner, G. 1997, Ap.J., 477, 79
- [327] Schechter P. 1976, Ap.J., 203, 297
- [328] Schlegel, D.J., Finkbeiner, D.P., & Davis, M. 1998, Ap.J., 500, 525
- [329] Schneider, S. E. 1996, in *The Minnesota Lectures on Extragalactic Neutral Hydrogen*, ASP Conf. Ser. 106, 323
- [330] Schombert, J. 1986, Ap.J.Supp.Series, 60, 603
- [331] Schombert, J. M. 1987, Ap.J.Supp.Series, 64, 643
- [332] Schombert, J. M. 1988, Ap.J., 328, 475
- [333] Schroeder, A. & Visvanathan, N. 1996, A.&A.Supp.Series, 118, 441
- [334] Schwartz, D. A., Griffiths, R. E. , Huchra, J. , Tonry, J. , Doxsey, R. E. , Johnston, M. D. , Mushotzky, R. F. , Swank, J. , & Davis, M. , 1980, Ap.J.Lett., 238, L53

- [335] Schweizer, F. : 1998, in *Saas-Fee Advanced Course 26: Galaxies: Interactions and Induced Star Formation*, 105
- [336] Schweizer, F. & Seitzer, P. 1992, A.J., 104, 1039
- [337] Shakhbazian, R. K. 1973, *Astrofizika*, 9, 495
- [338] Slezak, E., Durret, F., & Gerbal, D. 1994, A.J., 108, 1996
- [339] Slingo, A. 1974, M.N.R.A.S, 168, 307
- [340] Smail, I., Edge, A. C., Ellis, R. S., & Blandford, R. D. 1998, M.N.R.A.S, 293, 124
- ✓ [341] Sparks, W. B. 1988, A.J., 95, 1569
- [342] Sprayberry, D., Impey, C. D., Irwin, M. J., & Bothun, G. D. 1997, Ap.J., 482, 104
- [343] Stanford, S. A., Eisenhardt, P. R., & Dickinson, M. 1998, Ap.J., 492, 461
- [344] Stark, A. A., Gammie, C. F., Wilson, R. W., Bally, J., Linke, R. A., Heiles, C., & Hurwitz, M. 1992, Ap.J.Supp.Series, 79, 77
- [345] Stocke, J. T., Morris, S. L., Gioia, I. M., Maccacaro, T., Schild, R., Wolter, A., Fleming, T. A., & Henry, J. P. 1991, Ap.J.Supp.Series, 76, 813
- [346] Stocke, J. T., Perlman, E. S., Gioia, I. M., & Harvanek, M. 1999, A.J., 117, 1967
- [347] Struble, M. F. & Peebles, P. J. E. 1985, A.J., 90, 582
- [348] Struble, M. F. 1990, A.J., 99, 743
- [349] Struble, M. F. & Rood, H. J. 1991, Ap.J., 374, 395
- [350] Sulentic, J. W. 1987, Ap.J., 322, 605
- [351] Sulentic, J. W. & Rabaça, C. R. 1994, Ap.J., 429, 531
- [352] Sulentic, J. W., Pietsch, W., & Arp, H. 1995, A.&A., 298, 420
- [353] Szomoru, A., van Gorkom, J. H., Gregg, M. D., & Strauss, M. A. 1996, A.J., 111, 2150
- ✶ [354] Tamura, N., Kobayashi, C., Arimoto, N., Kodama, T., & Ohta, K. 2000, A.J., 119, 2134
- [355] Thompson, L. A. 1976, Ap.J., 209, 22
- [356] Thompson, L. A. & Gregory, S. A. 1993, A.J., 106, 2197
- ✓ [357] Thuan, T. X. & Romanishin, W., Ap.J., 248, 439
- [358] Thompson, L. A., & Gregory, S. A., 1980, Ap.J.242, 1
- [359] Toomre, A. & Toomre, J. 1972, Ap.J., 178, 623
- [360] Toth, G. & Ostriker, J. P. 1992, Ap.J., 389, 5
- [361] Trasarti-Battistoni, R. 1998, A.&A.Supp.Series, 130, 341
- [362] Trentham, N. 1997, M.N.R.A.S, 290, 334
- [363] Trentham, N. 1998, M.N.R.A.S, 294, 193
- [364] Trevese, D., Cirimele, G., & Flin, P. 1992, A.J., 104, 935
- [365] Tucker, D. L. et al. 2000, Ap.J.Supp.Series, 130, 237
- [366] Tully, R. B. 1987, Ap.J., 321, 280

- [367] Turner, E.L., & Gott, J.R. 1976, *Ap.J.Supp.Series*, 32, 409
- [368] Tyson, J. A. 1988, *A.J.*, 96, 1
- [369] Valdes, F. 1982a, *FOCAS User's Manual*, Kitt Peak National Observatory, Central Computer Services, Tucson, AZ, USA
- [370] Valdes, F. 1982b, *The Resolution Classifier*, in *Instrumentation in Astronomy IV*, SPIE Proceedings, 331
- [371] Valluri, M. & Jog, C. J. 1990, *Ap.J.*, 357, 367
- [372] Valotto C.A., Nicotra M.A., Muriel H., & Lambas D.G. 1997, *Ap.J.*, 479, 90
- [373] van Dokkum, P. G. & Franx, M. 1995, *A.J.*, 110, 2027
- [374] van Dokkum, P. G., Franx, M., Fabricant, D., Illingworth, G. D., & Kelson, D. D. 2000, *Ap.J.*, 541, 95
- [375] van Gorkom, J. 1996, in *ASP Conf. Ser. 106: The Minnesota Lectures on Extragalactic Neutral Hydrogen*, 293
- [376] van den Bergh, S., Abraham, R. G., Ellis, R. S., Tanvir, N. R., Santiago, B. X., & Glazebrook, K. G. 1996, *A.J.*, 112, 359
- [377] Venkatesan, T. C. A., Batuski, D. J., Hanisch, R. J., & Burns, J. O. 1994, *Ap.J.*, 436, 67
- [378] Vikhlinin, A., McNamara, B. R., Forman, W., Jones, C., Quintana, H., & Hornstrup, A. 1998, *Ap.J.*, 502, 558
- [379] Vikhlinin, A., McNamara, B. R., Hornstrup, A., Quintana, H., Forman, W., Jones, C., & Way, M. 1999, *Ap.J.Lett.*, 520, L1
- [380] Visvanathan, N. & Sandage, A. 1977, *Ap.J.*, 216, 214
- [381] Vorontsov-Velyaminov, B. A. 1959, *Atlas and catalog of interacting galaxies*
- [382] Walke, D. G. & Mamon, G. A. 1989, *A.&A.*, 225, 291
- [383] Wall, J. V. 1996, *QJRAS*, 37, 519
- [384] Weedman, D. W. 1986, *Quasar astronomy*, Cambridge University Press
- [385] West, M. J., Dekel, A., & Oemler, A. J. 1989, *Ap.J.*, 336, 46
- [386] West, M. J. 1989, *Ap.J.*, 344, 535
- [387] West, M. J., Villumsen, J. V., & Dekel, A. 1991, *Ap.J.*, 369, 287
- [388] West, M. J. 1994, *M.N.R.A.S.*, 268, 79
- [389] White, S. D. M. 1982, in *Saas-Fee Advanced Course 12: Morphology and Dynamics of Galaxies*, 291
- [390] White, R. A., Bliton, M., Bhavsar, S. P., Bornmann, P., Burns, J. O., Ledlow, M. J., & Loken, C. 1999, *A.J.*, 118, 2014
- [391] White, D. A., Jones, C., & Forman, W. 1997, *M.N.R.A.S.*, 292, 419
- [392] Whitmore B., Forbes D., Rubin V. 1988, *Ap.J.*, 333, 542
- [393] Whitmore, B., 1992, in *Physics of nearby galaxies: Nature or nurture?*, eds. Thuan, Trinh Xuan; Balkowski, Chantal; Tran Thanh Van, J.
- [394] Whitmore, B., Gilmore, D., Jones, C. 1993, *Ap.J.*, 407, 489
- [395] Wilson, G., Smail, I., Ellis, R. S., & Couch, W. J. 1997, *M.N.R.A.S.*, 284, 915

- [396] Wise, M. W. & Silva, D. R. 1996, *Ap.J.*, 461, 155
- [397] Worthey, G. 1994, *Ap.J.Supp.Series*, 95, 107
- [398] Yamagata, T. & Maehara, H. 1986, *Astrophysics and Space Science*, 118, 459
- [399] Yee, H. K. C., Ellingson, E., Morris, S.L., Abraham, R., & Carlberg, R. G. 1998, *Ap.J.Supp.Series*, 116, 211.
- [400] Yepes, G., Dominguez-Tenreiro, R., & del Pozo-Sanz, R. 1991, *Ap.J.*, 373, 336
- [401] Zabludoff, A. I., Zaritsky, D., Lin, H., Tucker, D., Hashimoto, Y., Sheckman, S. A., Oemler, A., & Kirshner, R. P. 1996, *Ap.J.*, 466, 104
- [402] Zabludoff, A.I. & Mulchaey, J.S. 1998a, *Ap.J.*, 496, 39
- [403] Zabludoff, A.I., Mulchaey, J.S. 1998b, *Ap.J.Lett.*, 498, L5
- [404] Zabludoff, A. I. & Mulchaey, J. S. 2000, *Ap.J.*, 539, 136
- [405] Zaritsky, D., Smith, R., Frenk, C., & White, S. D. M. 1993, *Ap.J.*, 405, 464
- [406] Zel'Dovich, Y. B. 1970, *A.&A.*, 5, 84
- [407] Zepf, S. E. & Whitmore, B. C. 1991, *Ap.J.*, 383, 542
- [408] Zepf, S. E. & Whitmore, B. C. 1993, *Ap.J.*, 418, 72
- [409] Zhang, X., Zheng, Y., Chen, H., Wang, S., Cao, A., Peng, B., & Nan, R. 1997, *A.&A.Supp.Series*, 121, 59
- [410] Zombeck, M. V. 1990, *Handbook of Astronomy and Astrophysics*, Second Edition, Cambridge University Press.
- [411] Zwicky, F. 1957, *Morphological Astronomy*, Berlin: Springer
- [412] Zwicky, F., Herzog, E., Karpowicz, M., Kowal, C.T., & Wild, P. 1961-1968, *Catalogue of Galaxies & Clusters of Galaxies* (Caltech, Pasadena)

Appendix A

Catalog of Galaxies

Here we provide the photometric catalog of *galaxies* in the line-of-sight to the poor clusters. The columns are the position (right ascension and declination in J2000.0 co-ordinates), V magnitude, $(B - V)$, $(V - R)$ and $(R - I)$ colors in 11 arcsec apertures, corrected for Galactic extinction.

Galaxies in the field of MS0002					
RA (2000)	Dec (2000)	V	$B-V$	$V-R$	$R-I$
0: 5: 2.6	16:14:58	19.51	-	0.43	-
0: 5: 2.9	16:15:24	21.67	-	-0.11	-
0: 5: 3.0	16:14:34	21.76	-	0.53	-
0: 5: 3.3	16: 9:41	21.75	-	0.68	-
0: 5: 3.3	16:13:24	21.59	-	0.93	-
0: 5: 3.3	16:17:17	21.37	-	0.08	-
0: 5: 3.4	16:14:42	20.14	-	0.56	-
0: 5: 3.4	16:14:50	18.73	-	0.56	-
0: 5: 3.7	16: 9:22	20.64	-	0.67	-
0: 5: 4.7	16:16:15	20.70	-	0.37	-
0: 5: 4.8	16:10:55	22.34	-	0.26	-
0: 5: 5.2	16: 9:26	22.66	-	0.54	-
0: 5: 5.2	16:15:29	21.51	-	0.46	-
0: 5: 5.4	16:10:58	22.28	-	1.59	-
0: 5: 5.6	16:12:25	19.62	-	0.84	-
0: 5: 5.7	16:10:42	19.38	-	0.62	-
0: 5: 5.7	16:11:23	22.95	-	1.04	-
0: 5: 5.7	16:11:42	22.65	-	0.74	-
0: 5: 5.7	16:15:55	21.53	-	0.39	-
0: 5: 6.0	16:16:40	20.25	-	0.43	-
0: 5: 6.2	16:10:44	22.85	-	1.48	-
0: 5: 6.2	16:14:25	21.59	-	0.87	-
0: 5: 6.2	16:15: 0	20.63	-	0.62	-
0: 5: 6.3	16: 9:10	21.89	-	0.39	-
0: 5: 6.6	16:11:35	24.16	-	1.04	-
0: 5: 6.6	16:12:20	21.24	-	1.13	-
0: 5: 6.6	16:15:42	20.25	-	0.41	-
0: 5: 7.2	16:15:42	20.82	-	0.40	-
0: 5: 7.4	16: 8:30	21.50	-	1.03	-
0: 5: 7.4	16:14:10	21.36	-	0.89	-
0: 5: 7.5	16:15:36	22.17	-	0.78	-
0: 5: 8.2	16:11:41	24.82	-	2.97	-
0: 5: 8.4	16:14: 9	21.87	-	1.07	-
0: 5: 8.5	16:11:55	24.46	-	2.84	-
0: 5: 8.5	16:12:33	18.61	-	0.68	-
0: 5: 8.7	16:14:30	20.08	-	0.64	-
0: 5: 8.7	16:15:43	22.45	-	0.87	-
0: 5: 8.7	16:16: 5	21.73	-	0.73	-
0: 5: 9.2	16: 8:41	19.26	-	0.54	-
0: 5: 9.7	16: 8:53	22.32	-	0.54	-
0: 5: 9.9	16: 8:58	23.29	-	1.30	-
0: 5: 9.9	16:11:18	21.87	-	0.94	-
0: 5: 9.9	16:16:57	20.52	-	0.44	-
0: 5:10.0	16: 9:13	19.11	-	0.59	-
0: 5:10.1	16: 8: 0	22.66	-	0.65	-
0: 5:10.1	16:13:35	23.11	-	1.72	-
0: 5:10.2	16: 8:33	28.01	-	-	-
0: 5:10.2	16:13:25	21.16	-	0.90	-
0: 5:10.2	16:16:53	21.63	-	0.65	-
0: 5:10.2	16:17:43	20.70	-	-0.30	-
0: 5:10.4	16:14:40	23.02	-	1.16	-

continued

MS0002					
0: 5:10.5	16:13:48	21.79	-	1.26	-
0: 5:10.7	16:14: 3	22.24	-	0.92	-
0: 5:10.7	16:16:11	21.81	-	0.63	-
0: 5:10.8	16:10:36	19.84	-	0.61	-
0: 5:10.8	16:11:56	22.25	-	0.52	-
0: 5:10.9	16:17: 4	20.34	-	0.55	-
0: 5:11.1	16: 8:45	21.23	-	0.71	-
0: 5:11.1	16:17:21	21.20	-	0.21	-
0: 5:11.4	16:11:16	19.26	-	0.42	-
0: 5:11.6	16:16:30	20.40	-	0.31	-
0: 5:11.7	16: 8:40	21.39	-	0.66	-
0: 5:11.7	16:17: 8	21.21	-	0.40	-
0: 5:11.9	16:15:36	20.45	-	0.39	-
0: 5:12.4	16: 9:32	22.58	-	0.70	-
0: 5:12.6	16: 8: 3	22.23	-	-0.66	-
0: 5:12.6	16:13:48	21.06	-	1.55	-
0: 5:12.7	16: 9:12	18.86	-	0.65	-
0: 5:12.7	16:16:49	21.09	-	0.59	-
0: 5:12.8	16: 9: 7	18.19	-	0.39	-
0: 5:13.1	16:11: 9	20.98	-	0.48	-
0: 5:13.3	16:15:48	22.23	-	0.66	-
0: 5:13.7	16:14:29	20.30	-	0.64	-
0: 5:13.7	16:15:14	22.53	-	1.09	-
0: 5:14.0	16: 9: 1	22.11	-	0.19	-
0: 5:14.1	16:12: 3	23.73	-	2.19	-
0: 5:14.1	16:13: 8	22.16	-	1.28	-
0: 5:14.3	16:17: 5	20.64	-	0.45	-
0: 5:14.4	16: 9:41	21.61	-	0.55	-
0: 5:14.5	16:14:45	21.87	-	0.67	-
0: 5:14.6	16:12:54	20.48	-	0.65	-
0: 5:14.6	16:13: 3	19.54	-	0.69	-
0: 5:14.8	16:17:38	20.82	-	0.56	-
0: 5:14.9	16:13: 0	19.63	-	0.62	-
0: 5:15.1	16:16:24	20.41	-	0.54	-
0: 5:15.3	16:10:30	22.88	-	1.28	-
0: 5:15.4	16:14: 0	23.25	-	2.20	-
0: 5:15.4	16:14:14	22.72	-	0.64	-
0: 5:15.5	16:14:41	22.87	-	0.97	-
0: 5:15.6	16: 8: 1	21.42	-	0.23	-
0: 5:15.6	16:13:44	19.91	-	0.62	-
0: 5:15.9	16:16:17	18.43	-	0.60	-
0: 5:16.1	16:13: 9	23.16	-	1.29	-
0: 5:16.2	16:11:23	19.60	-	0.47	-
0: 5:16.2	16:15:51	21.90	-	0.42	-
0: 5:16.5	16: 9: 7	23.14	-	-0.46	-
0: 5:16.5	16:12:27	25.72	-	2.99	-
0: 5:16.6	16:15: 4	21.64	-	0.70	-
0: 5:16.7	16: 9:17	21.17	-	0.45	-
0: 5:16.7	16:10:33	22.05	-	0.28	-
0: 5:16.8	16:17:18	20.70	-	0.36	-
0: 5:16.9	16:15:35	22.28	-	0.42	-
0: 5:17.1	16:10:16	21.81	-	0.51	-
0: 5:17.1	16:14:27	24.23	-	1.46	-
0: 5:17.2	16:10:31	21.15	-	0.47	-
0: 5:17.4	16: 8:50	22.66	-	-0.22	-
0: 5:17.4	16:11:11	22.04	-	0.36	-
0: 5:17.4	16:13:42	21.82	-	1.55	-
0: 5:17.5	16:12: 6	22.51	-	0.83	-
0: 5:17.7	16:14:35	18.17	-	0.71	-
0: 5:17.8	16:13:46	20.94	-	0.73	-
0: 5:17.8	16:14:45	18.47	-	0.67	-

continued

MS0002				
0: 5:17.8	16:15:26	21.53	- 1.02	--
0: 5:18.1	16: 8:20	21.09	- 0.50	--
0: 5:18.1	16:10:42	19.95	- 0.39	--
0: 5:18.2	16:13: 2	21.68	- 0.79	--
0: 5:18.2	16:15: 2	22.45	- 0.54	--
0: 5:18.3	16:13:30	20.31	- 0.70	--
0: 5:18.3	16:16:30	19.79	- 0.57	--
0: 5:18.4	16:10: 7	20.69	- 0.51	--
0: 5:18.4	16:12:56	23.71	- 1.49	--
0: 5:18.5	16:11:25	21.74	- 0.62	--
0: 5:18.5	16:12:20	24.16	- 1.91	--
0: 5:18.5	16:12:43	24.50	- 2.23	--
0: 5:18.8	16:16:20	21.25	- 0.80	--
0: 5:18.9	16: 9: 5	19.12	- 0.56	--
0: 5:19.0	16:13:54	23.57	- 1.65	--
0: 5:19.2	16:10:29	18.97	- 0.25	--
0: 5:19.6	16:12: 2	22.80	- 0.79	--
0: 5:20.0	16: 9:56	20.23	- 0.77	--
0: 5:20.1	16:17:43	20.59	- 0.35	--
0: 5:20.2	16: 8:25	17.80	- 0.61	--
0: 5:20.5	16: 9: 1	18.13	- 0.64	--
0: 5:20.5	16:11:22	21.50	- 0.40	--
0: 5:20.5	16:14:30	23.54	- 1.03	--
0: 5:20.8	16: 9:15	22.07	- 0.55	--
0: 5:20.8	16: 9:33	21.43	- 0.39	--
0: 5:20.8	16:17:14	19.05	- 0.46	--
0: 5:20.9	16: 9: 1	20.21	- 0.91	--
0: 5:20.9	16:12:29	21.68	- 1.55	--
0: 5:21.0	16:12: 7	19.58	- 0.64	--
0: 5:21.1	16:14:37	23.25	- 1.14	--
0: 5:21.2	16:10:20	18.91	- 0.63	--
0: 5:21.2	16:15:38	20.51	- 0.59	--
0: 5:21.4	16:11: 6	18.65	- 0.54	--
0: 5:21.7	16: 9: 2	18.95	- 0.60	--
0: 5:21.9	16:13:18	20.85	- 0.62	--
0: 5:22.0	16:13:10	18.35	- 0.69	--
0: 5:22.1	16:14:11	20.89	- 0.47	--
0: 5:22.3	16:10:45	18.33	- 0.42	--
0: 5:22.7	16:17: 9	18.89	- 0.51	--
0: 5:22.8	16:12:59	18.80	- 0.69	--
0: 5:22.8	16:16:55	20.99	- 0.73	--
0: 5:23.0	16:11:56	22.64	- 0.59	--
0: 5:23.1	16:10:10	20.58	- 0.55	--
0: 5:23.1	16:10:25	19.72	- 0.74	--
0: 5:23.1	16:17: 6	19.83	- 0.66	--
0: 5:23.2	16:11:42	19.10	- 0.47	--
0: 5:23.4	16:12:49	20.51	- 0.70	--
0: 5:23.4	16:16:31	20.81	- 0.52	--
0: 5:23.4	16:16:35	21.05	- 0.65	--
0: 5:23.8	16:11:47	19.41	- 0.66	--
0: 5:23.9	16:15:13	20.15	- 0.35	--
0: 5:24.0	16:10:44	20.16	- 0.53	--
0: 5:24.0	16:13: 9	16.53	- 0.69	--
0: 5:24.0	16:13:18	18.99	- 0.74	--
0: 5:24.1	16:11:10	19.55	- 0.58	--
0: 5:24.1	16:12:11	22.38	- 0.21	--
0: 5:24.1	16:15:19	21.27	- 0.63	--
0: 5:24.2	16:11:19	20.54	- 0.67	--
0: 5:24.5	16:14:16	20.55	- 0.62	--
0: 5:25.0	16: 8:13	19.29	- 1.12	--
0: 5:25.0	16: 9: 2	24.25	- -0.26	--
0: 5:25.0	16:13:28	20.40	- 0.64	--
0: 5:25.0	16:14:40	21.70	- 0.24	--
0: 5:25.4	16:13:46	20.33	- 1.03	--
0: 5:25.5	16:11:11	22.40	- 1.11	--
0: 5:25.5	16:15:13	21.50	- 0.58	--
0: 5:25.6	16: 9:51	23.06	- -1.24	--
0: 5:25.6	16:13:29	21.50	- 0.67	--
0: 5:25.6	16:14:27	20.59	- 0.98	--

continued

MS0002				
0: 5:25.7	16: 9:24	20.58	- 0.72	--
0: 5:25.8	16:12:35	22.83	- 0.61	--
0: 5:25.9	16:12: 0	21.82	- 0.89	--
0: 5:25.9	16:13:40	21.40	- 0.86	--
0: 5:25.9	16:17:33	20.70	- 0.42	--
0: 5:26.1	16:13:19	21.44	- 0.84	--
0: 5:26.1	16:13:30	21.42	- 0.76	--
0: 5:26.2	16: 9:32	23.09	- 1.11	--
0: 5:26.2	16:10: 3	18.39	- 0.60	--
0: 5:26.2	16:15:39	21.38	- 0.72	--
0: 5:26.2	16:16:53	20.18	- 0.45	--
0: 5:26.6	16:17:15	21.14	- 0.28	--
0: 5:26.7	16: 9:21	22.57	- 0.58	--
0: 5:26.7	16:12:32	21.61	- 0.84	--
0: 5:26.9	16:11:53	19.43	- 0.67	--
0: 5:26.9	16:15:12	21.77	- 0.25	--
0: 5:27.0	16:11:31	25.54	- 1.98	--
0: 5:27.0	16:13:17	20.16	- 0.64	--
0: 5:27.3	16:10:22	22.64	- 0.41	--
0: 5:27.4	16: 9:35	22.86	- 0.48	--
0: 5:27.4	16:16:57	21.39	- 0.55	--
0: 5:27.6	16:12:58	20.27	- 0.60	--
0: 5:27.6	16:14:54	19.12	- 0.68	--
0: 5:27.7	16: 8: 5	17.97	- 0.60	--
0: 5:27.7	16:11:27	21.40	- 0.99	--
0: 5:27.9	16: 8:16	19.50	- 0.46	--
0: 5:27.9	16:12:32	24.14	- 1.62	--
0: 5:27.9	16:12:48	22.48	- 0.80	--
0: 5:28.0	16:16:19	21.14	- 0.22	--
0: 5:28.4	16:14: 2	18.20	- 0.70	--
0: 5:28.5	16:10:46	20.04	- 0.29	--
0: 5:28.8	16: 9:11	20.92	- 0.28	--
0: 5:28.8	16:10:31	19.41	- 0.44	--
0: 5:28.8	16:11:51	21.18	- 0.71	--
0: 5:28.8	16:12:55	23.05	- 1.12	--
0: 5:28.9	16:13:30	20.52	- 0.72	--
0: 5:28.9	16:14: 8	21.34	- 0.67	--
0: 5:28.9	16:14:34	21.44	- 0.60	--
0: 5:29.0	16:14:46	22.27	- 0.49	--
0: 5:29.0	16:16:22	21.46	- 0.41	--
0: 5:29.1	16:15: 5	22.16	- 0.19	--
0: 5:29.3	16:12:23	18.87	- 0.65	--
0: 5:29.4	16:13:58	21.17	- 1.30	--
0: 5:29.4	16:17:40	20.68	- 0.76	--
0: 5:29.5	16: 8:27	21.60	- 0.19	--
0: 5:29.7	16:14:16	21.98	- 0.56	--
0: 5:29.8	16:13:47	22.21	- 0.49	--
0: 5:29.9	16:13:57	19.43	- 0.65	--
0: 5:30.0	16: 8:43	21.93	- -0.14	--
0: 5:30.0	16:12:19	21.81	- 0.73	--
0: 5:30.1	16:13: 7	17.83	- 0.66	--
0: 5:30.1	16:16:37	18.26	- 0.61	--
0: 5:30.2	16:11:48	20.52	- 0.82	--
0: 5:30.4	16:14:40	20.73	- 0.21	--
0: 5:30.6	16:12: 4	21.85	- 0.68	--
0: 5:30.7	16:17:15	21.03	- 0.35	--
0: 5:30.8	16:13:10	20.27	- 0.72	--
0: 5:30.8	16:17:17	21.00	- 0.36	--
0: 5:31.0	16:12: 7	21.57	- 0.40	--
0: 5:31.1	16:11:49	18.53	- 0.73	--
0: 5:31.2	16:16:18	20.65	- 0.81	--
0: 5:31.4	16:12:22	22.00	- 1.15	--
0: 5:31.5	16: 8:52	22.20	- -0.53	--
0: 5:31.5	16:16:27	21.40	- 0.11	--
0: 5:31.5	16:16:46	21.43	- 0.42	--
0: 5:31.7	16:12:47	24.78	- 2.96	--
0: 5:31.7	16:13:51	20.04	- 0.68	--
0: 5:31.7	16:14: 3	21.88	- 0.78	--
0: 5:31.7	16:17:27	18.73	- 1.18	--

continued

<i>MS0002</i>				
0: 5:31.8	16:14:59	18.80	-	0.52
0: 5:32.0	16: 8:57	21.00	-	0.13
0: 5:32.0	16: 9:45	21.10	-	0.54
0: 5:32.0	16:10:10	21.61	-	0.15
0: 5:32.1	16: 9:26	23.46	-	0.79
0: 5:32.2	16:13: 8	22.24	-	0.87
0: 5:32.3	16:14: 4	20.43	-	0.75
0: 5:32.3	16:14:31	20.67	-	0.68
0: 5:32.3	16:14:54	20.17	-	0.90
0: 5:32.3	16:16:55	20.98	-	0.25
0: 5:32.4	16:10:53	19.90	-	0.60
0: 5:32.5	16: 9:19	21.01	-	0.89
0: 5:32.7	16: 8: 8	21.82	-	0.07
0: 5:32.7	16:10:26	20.21	-	0.56
0: 5:32.8	16: 8:49	21.35	-	0.40
0: 5:33.0	16:12: 0	20.52	-	0.51
0: 5:33.1	16:14:21	20.69	-	0.67
0: 5:33.1	16:16: 8	21.45	-	0.24
0: 5:33.2	16: 9:53	22.96	-	-0.26
0: 5:33.3	16: 8:46	22.79	-	0.61
0: 5:33.5	16:12:41	20.23	-	0.76
0: 5:33.5	16:16:53	21.22	-	0.29
0: 5:33.5	16:17: 5	21.40	-	0.57
0: 5:33.7	16:14:26	19.53	-	0.78
0: 5:33.8	16:11: 9	20.01	-	1.22
0: 5:33.8	16:12:37	22.80	-	0.98
0: 5:33.9	16:12: 8	21.81	-	0.37
0: 5:34.0	16:15: 6	18.76	-	0.65
0: 5:34.0	16:16:56	20.61	-	0.37
0: 5:34.2	16: 9:24	23.06	-	0.73
0: 5:34.3	16:11:49	23.00	-	0.05
0: 5:34.3	16:12:22	19.62	-	0.55
0: 5:34.3	16:14:18	21.51	-	0.74
0: 5:34.4	16:14: 3	18.77	-	0.64
0: 5:34.5	16:13:41	22.09	-	0.49
0: 5:34.6	16: 8:45	22.63	-	-0.10
0: 5:34.8	16:10:54	20.49	-	0.88
0: 5:34.8	16:14: 1	20.87	-	0.66
0: 5:35.1	16: 8:54	21.31	-	0.28
0: 5:35.3	16:17:48	18.73	-	0.77
0: 5:35.4	16:14:38	19.92	-	0.59
0: 5:36.1	16:16:14	19.95	-	0.44
0: 5:36.1	16:16:42	19.91	-	0.53
0: 5:36.3	16: 8:24	20.82	-	0.17
0: 5:36.5	16:15:41	21.02	-	0.16
0: 5:36.7	16:12:35	19.44	-	0.61
0: 5:36.9	16:11:17	19.57	-	1.13
0: 5:37.2	16:13:47	18.26	-	0.63
0: 5:37.3	16:14: 5	21.67	-	0.38
0: 5:37.3	16:15:32	21.35	-	0.68
0: 5:37.6	16: 9:21	19.47	-	0.29
0: 5:37.8	16: 8:59	20.62	-	0.42
0: 5:37.8	16:11:36	22.26	-	0.60
0: 5:37.8	16:13:38	17.81	-	0.64
0: 5:37.8	16:14:40	21.29	-	0.48
0: 5:38.0	16:16:42	18.75	-	0.54
0: 5:38.1	16:12:30	19.85	-	0.33
0: 5:38.1	16:13:28	19.95	-	0.51
0: 5:38.1	16:14:50	22.40	-	0.16
0: 5:38.1	16:15: 3	22.27	-	1.06
0: 5:38.4	16:10:45	18.04	-	0.62
0: 5:38.5	16:12:47	22.21	-	0.20
0: 5:38.6	16:10:23	20.67	-	0.53
0: 5:38.6	16:15:12	19.55	-	0.55
0: 5:38.7	16: 9:14	22.61	-	-0.23
0: 5:38.7	16:11:50	22.25	-	1.15
0: 5:38.8	16:11:59	20.87	-	0.50
0: 5:39.0	16:15: 6	21.77	-	0.74
0: 5:39.3	16:10:25	22.91	-	-1.93

continued

<i>MS0002</i>				
0: 5:39.3	16:15:59	21.00	-	0.42
0: 5:39.7	16:14:52	20.94	-	0.71
0: 5:39.7	16:17:19	20.91	-	0.41
0: 5:39.8	16:17:46	21.28	-	0.35
0: 5:39.9	16:16:42	19.74	-	0.50
0: 5:40.1	16: 8:57	21.78	-	-1.47
0: 5:40.1	16:15:48	20.34	-	0.43
0: 5:40.5	16:15: 8	21.19	-	0.27
0: 5:40.6	16:14:45	21.24	-	0.11
0: 5:40.7	16: 9:39	20.83	-	0.38
0: 5:40.8	16:12:19	18.55	-	0.59
0: 5:41.0	16:15:19	21.26	-	0.23
0: 5:41.2	16: 9:51	20.22	-	0.95
0: 5:41.4	16:11:11	22.25	-	-0.08
0: 5:41.4	16:14:41	21.96	-	0.51
0: 5:41.7	16:11:35	20.20	-	0.95
0: 5:41.7	16:15:26	19.80	-	0.51
0: 5:41.8	16: 9:47	20.56	-	0.55
0: 5:43.0	16:17:33	20.06	-	0.43
0: 5:43.1	16:15: 2	21.79	-	-0.13
0: 5:43.1	16:17:39	18.67	-	0.65
0: 5:43.3	16:12:19	21.93	-	0.56
0: 5:43.3	16:16:17	17.14	-	0.60
0: 5:43.4	16: 9:54	22.01	-	-0.75
0: 5:43.5	16:10: 3	20.20	-	0.81
0: 5:43.5	16:11: 7	21.46	-	0.66
0: 5:43.6	16:12:46	19.85	-	0.31
0: 5:43.7	16:11:37	21.23	-	0.46
0: 5:43.8	16:10:28	21.58	-	0.76
0: 5:44.0	16:12:17	19.74	-	0.56
0: 5:44.0	16:15:43	20.51	-	0.40
0: 5:44.1	16:13:43	21.74	-	0.10
0: 5:44.3	16:16:46	21.19	-	0.02
0: 5:44.7	16: 8:39	21.37	-	-0.27
0: 5:44.7	16:17:45	20.38	-	0.09
0: 5:44.8	16: 9:17	22.09	-	0.40
0: 5:45.0	16:13:37	20.57	-	0.52
0: 5:45.1	16: 8:53	18.33	-	0.32
0: 5:45.1	16:14:37	19.50	-	1.06
0: 5:45.3	16:12: 5	18.98	-	1.29
0: 5:45.4	16: 9:51	20.02	-	0.41
0: 5:45.7	16: 8:34	20.98	-	-0.27

Table A.1: Catalog of galaxies in the field of MS0002.

Galaxies in the field of MS0301					
RA (2000)	Dec (2000)	V	B-V	V-R	R-I
3: 4:10.9	15:22:59	19.46	-	0.55	-
3: 4:11.7	15:28:10	18.49	0.31	0.64	0.63
3: 4:12.4	15:25:42	17.40	0.69	0.61	1.00
3: 4:12.6	15:25:35	19.46	-0.15	1.01	1.23
3: 4:12.6	15:31: 9	19.26	0.38	0.82	0.53
3: 4:13.6	15:25:15	18.38	0.77	0.81	1.22
3: 4:13.7	15:23:54	17.83	0.82	0.45	1.54
3: 4:13.9	15:31: 9	18.77	0.49	0.67	0.77
3: 4:14.3	15:29:21	19.66	0.21	0.80	0.04
3: 4:14.3	15:30: 9	18.82	0.26	0.68	0.84
3: 4:14.5	15:24:57	18.40	0.83	0.78	1.15
3: 4:15.1	15:28:50	17.18	0.86	0.48	0.76
3: 4:15.4	15:26:31	18.54	0.15	0.53	0.58
3: 4:15.4	15:27:54	17.19	0.85	0.46	0.84
3: 4:15.5	15:31:28	21.82	-	1.43	0.45
3: 4:15.6	15:23:30	18.10	0.76	0.19	1.63
3: 4:16.0	15:29:42	16.74	0.92	0.49	0.84
3: 4:16.4	15:26: 5	20.42	-0.73	1.31	0.52
3: 4:16.6	15:26:54	18.63	0.12	0.21	1.17
3: 4:16.6	15:27: 5	17.96	0.04	0.04	1.13
3: 4:16.9	15:25:53	19.77	-0.27	0.72	0.08
3: 4:16.9	15:29:39	20.54	-0.27	0.79	-0.29
3: 4:17.2	15:28:50	20.15	0.10	0.97	1.01
3: 4:17.3	15:29:51	21.14	-0.06	1.02	-0.68
3: 4:17.4	15:23: 7	19.15	-	-0.04	-
3: 4:17.6	15:26:12	19.59	-0.02	0.49	0.47
3: 4:17.7	15:27:41	17.97	0.16	0.03	1.27
3: 4:17.9	15:26:31	18.57	0.43	0.47	0.77
3: 4:18.0	15:29:36	21.89	-0.84	1.44	1.27
3: 4:18.3	15:29:43	19.11	0.56	0.46	0.72
3: 4:18.4	15:25:30	20.47	-0.81	1.07	-0.15
3: 4:18.4	15:26:11	19.32	0.37	0.60	0.45
3: 4:18.7	15:28:27	20.25	-0.03	0.64	0.65
3: 4:18.9	15:30:47	17.99	0.12	0.15	0.81
3: 4:19.1	15:26:48	18.66	0.41	0.34	0.83
3: 4:19.1	15:30:28	20.22	-	1.04	1.69
3: 4:19.2	15:28:58	21.06	-0.44	0.44	0.38
3: 4:19.3	15:22:53	17.81	-	-0.27	-
3: 4:19.3	15:24:31	18.56	0.27	0.47	0.89
3: 4:19.3	15:27:30	18.03	0.51	-0.13	1.23
3: 4:19.5	15:28:37	21.23	-0.15	0.87	0.83
3: 4:19.8	15:26:31	19.65	0.08	0.43	0.33
3: 4:19.8	15:29: 7	18.84	0.55	0.39	0.67
3: 4:19.9	15:26:41	19.17	0.44	0.49	0.78
3: 4:20.3	15:31:45	20.20	-	0.67	1.72
3: 4:20.4	15:26:48	19.74	-0.03	0.60	0.79
3: 4:20.4	15:31: 8	19.24	0.89	0.62	1.22
3: 4:20.5	15:28:41	21.24	-0.84	0.49	-0.46
3: 4:20.9	15:27:56	20.25	0.50	0.50	0.80
3: 4:21.0	15:28:18	19.97	0.55	0.39	0.76
3: 4:21.2	15:26:41	20.38	-0.05	0.61	0.05
3: 4:21.2	15:28:52	20.40	0.50	0.09	1.00
3: 4:21.3	15:29:49	20.85	0.29	0.29	-0.88
3: 4:21.6	15:28:54	20.91	-0.36	0.32	-0.44
3: 4:21.8	15:27:30	17.43	0.62	0.39	0.82
3: 4:21.9	15:22:52	18.86	-	-0.41	-
3: 4:22.2	15:25:51	16.45	1.01	0.52	0.78
3: 4:22.5	15:25:35	18.70	0.47	0.39	0.47
3: 4:22.7	15:27: 4	20.45	-0.15	0.33	-0.25
3: 4:22.8	15:25:47	16.93	1.06	0.47	0.79
3: 4:22.9	15:22:27	19.27	-	-0.21	-
3: 4:23.4	15:24:16	20.25	-0.55	0.89	0.51
3: 4:23.6	15:25:34	21.01	-0.53	0.93	-1.70
3: 4:23.6	15:30:19	18.09	0.83	0.38	0.86
3: 4:23.7	15:29:25	20.19	0.39	-0.11	2.02
3: 4:23.8	15:24:57	20.94	-0.47	1.37	0.20
3: 4:24.0	15:30: 1	20.05	0.38	0.22	0.16

continued

MS0301					
3: 4:24.2	15:24:50	21.14	-0.47	1.56	0.21
3: 4:24.3	15:26:50	20.30	0.05	0.28	0.16
3: 4:24.3	15:27:59	19.38	0.48	0.11	0.62
3: 4:24.3	15:28: 5	18.27	0.82	0.37	0.78
3: 4:24.5	15:26:52	19.87	0.09	0.26	0.17
3: 4:25.6	15:27:59	20.24	0.29	-0.04	1.24
3: 4:25.6	15:28:40	21.08	0.10	0.88	-0.17
3: 4:25.7	15:27:35	20.68	-0.01	0.56	-0.01
3: 4:26.0	15:24:33	19.09	0.41	0.37	-0.08
3: 4:26.1	15:26: 9	17.20	0.84	0.41	0.75
3: 4:26.1	15:26:45	17.39	0.90	0.46	0.84
3: 4:26.1	15:28: 3	18.44	1.36	0.50	0.96
3: 4:26.6	15:27:57	20.20	0.37	0.53	0.29
3: 4:26.8	15:27:11	19.37	0.63	0.19	0.60
3: 4:27.2	15:28:49	17.41	0.94	0.40	0.86
3: 4:27.4	15:27:29	19.18	0.77	0.37	0.95
3: 4:27.4	15:29: 3	19.10	0.73	0.28	1.00
3: 4:27.7	15:27:33	20.57	0.31	0.50	1.42
3: 4:27.8	15:23:27	19.92	0.54	1.07	1.13
3: 4:28.1	15:30:22	20.02	0.41	0.20	0.19
3: 4:28.4	15:28:14	16.19	0.98	0.45	0.87
3: 4:28.4	15:31:50	19.71	-	0.07	-
3: 4:28.6	15:29:21	20.65	0.13	0.63	0.07
3: 4:28.8	15:28:37	18.59	0.46	0.84	0.05
3: 4:28.9	15:28:17	18.88	1.29	0.43	1.15
3: 4:29.0	15:27:46	19.69	0.72	0.30	1.06
3: 4:29.0	15:28: 5	19.93	0.51	0.12	1.53
3: 4:29.0	15:28:11	18.95	1.32	0.32	0.98
3: 4:29.4	15:28:24	18.06	1.52	0.49	0.95
3: 4:29.4	15:30: 6	20.09	0.45	0.28	0.34
3: 4:29.5	15:22:49	19.01	1.47	0.52	0.70
3: 4:29.6	15:28: 9	18.38	0.90	0.40	0.86
3: 4:29.6	15:29:34	20.17	0.74	0.44	0.22
3: 4:29.7	15:30:21	18.82	1.64	0.42	1.02
3: 4:30.1	15:27:34	15.76	1.01	0.46	0.88
3: 4:30.1	15:30:55	19.66	0.99	-0.11	1.41
3: 4:30.3	15:28:44	18.62	0.99	0.28	0.92
3: 4:30.4	15:25: 2	21.20	-0.32	0.92	-0.14
3: 4:30.6	15:29:17	18.70	1.18	0.32	0.95
3: 4:30.7	15:29:31	20.83	0.34	0.52	-0.01
3: 4:30.8	15:25:53	20.43	0.62	0.41	-0.60
3: 4:31.0	15:23:31	21.20	-0.15	1.29	-0.19
3: 4:31.1	15:30:58	20.62	0.49	0.53	0.63
3: 4:31.3	15:27:44	19.17	0.96	0.22	0.97
3: 4:31.3	15:30:20	17.27	0.63	0.39	0.81
3: 4:31.6	15:31:14	20.76	-0.75	1.19	0.48
3: 4:32.0	15:29:12	18.61	1.02	0.31	0.85
3: 4:32.1	15:25:45	18.96	0.94	0.37	0.57
3: 4:32.2	15:28:23	20.91	0.31	0.57	0.15
3: 4:32.3	15:29:47	18.66	1.28	0.41	0.95
3: 4:32.3	15:31:20	17.97	0.71	0.26	0.83
3: 4:32.8	15:29: 5	21.44	-0.14	1.15	0.01
3: 4:33.7	15:26:41	18.60	1.42	0.47	0.98
3: 4:33.8	15:28:42	19.85	1.27	0.35	0.38
3: 4:33.9	15:32:26	19.42	-	-0.06	-
3: 4:34.1	15:26:43	18.43	1.34	0.39	0.90
3: 4:34.4	15:23:57	21.08	1.04	1.24	0.08
3: 4:34.8	15:27:53	19.95	0.69	-0.43	1.13
3: 4:34.9	15:29:59	20.94	0.00	0.30	0.18
3: 4:35.1	15:29:17	16.99	0.97	0.41	0.78
3: 4:35.4	15:25: 8	20.86	0.35	0.97	0.29
3: 4:35.6	15:25:15	18.68	1.98	0.53	0.65
3: 4:35.7	15:24:50	20.25	1.44	0.63	0.39
3: 4:36.1	15:32:18	18.38	-	0.17	0.88
3: 4:36.7	15:29:53	21.31	0.87	0.85	0.16
3: 4:36.9	15:23:31	20.53	0.87	0.62	-0.85
3: 4:36.9	15:31:54	20.19	-	0.35	-
3: 4:37.3	15:24:14	20.97	0.78	0.55	0.89
3: 4:37.4	15:30:36	21.04	1.26	1.19	0.91

continued

MS0301					
3: 4:37.5	15:25:50	20.86	0.81	0.75	0.61
3: 4:37.6	15:27:40	20.34	-0.12	0.30	0.31
3: 4:37.7	15:25:14	19.43	1.04	0.19	0.43
3: 4:37.8	15:31:14	20.44	1.16	0.49	1.49
3: 4:38.0	15:31:37	21.29	0.80	0.86	0.88
3: 4:38.1	15:27:16	20.35	1.60	0.66	1.37
3: 4:38.1	15:29:21	20.93	0.45	0.40	0.21
3: 4:38.9	15:29:26	20.86	1.34	1.14	0.80
3: 4:39.0	15:30:46	21.94	0.08	1.83	0.77
3: 4:39.3	15:22:51	20.63	1.47	0.63	-0.08
3: 4:39.6	15:28:24	19.64	0.87	-0.51	0.74
3: 4:39.9	15:31: 6	20.37	0.80	0.51	0.28
3: 4:40.0	15:26:16	21.13	-0.31	0.51	0.01
3: 4:40.1	15:26:52	20.22	0.54	0.32	0.62
3: 4:40.1	15:29:30	20.83	1.27	1.09	0.83
3: 4:40.4	15:30:42	20.98	0.87	1.02	0.78
3: 4:40.9	15:30:19	21.43	-0.38	0.90	-0.57
3: 4:41.0	15:27:49	20.28	1.13	0.57	0.77
3: 4:41.3	15:22:48	19.15	0.57	0.29	0.71
3: 4:41.4	15:31:44	20.22	0.07	0.04	-0.45
3: 4:42.3	15:26:34	20.16	0.83	0.47	0.72
3: 4:42.7	15:29:13	21.25	1.16	1.04	0.67
3: 4:43.0	15:27:46	20.29	1.54	0.98	0.95
3: 4:43.1	15:30:58	19.56	0.43	0.43	0.26
3: 4:43.3	15:29: 5	18.78	0.72	-0.21	-0.03
3: 4:43.4	15:29:10	20.25	0.64	0.33	0.39
3: 4:44.0	15:31:59	19.49	0.65	0.16	0.15
3: 4:44.1	15:31:49	20.31	1.48	0.85	0.73
3: 4:44.2	15:29: 9	20.40	1.26	0.90	0.80
3: 4:44.6	15:22:58	19.59	1.05	0.10	0.09
3: 4:44.9	15:29:12	20.06	0.62	0.29	0.43
3: 4:45.3	15:28:47	19.34	0.83	0.38	0.65
3: 4:45.3	15:32:22	20.58	0.72	0.27	-0.51
3: 4:45.7	15:22:32	20.17	3.02	0.04	-0.19
3: 4:45.8	15:28:26	20.57	1.58	1.03	0.93
3: 4:46.0	15:28:13	20.69	1.00	1.09	0.78
3: 4:46.4	15:28:36	18.79	0.51	-0.75	0.65
3: 4:46.5	15:29:16	20.55	1.17	0.91	0.66
3: 4:46.7	15:28:22	20.44	0.33	0.27	0.48
3: 4:46.8	15:28:31	20.59	0.64	0.76	0.80
3: 4:47.2	15:28:58	21.24	-	1.01	0.77
3: 4:47.4	15:25:13	19.13	0.70	0.16	1.15
3: 4:47.4	15:29: 3	21.02	2.23	0.85	0.52
3: 4:47.6	15:22:58	18.99	0.71	0.10	0.59
3: 4:47.6	15:28:47	20.10	1.08	0.65	0.79
3: 4:47.9	15:26:15	22.45	0.72	1.38	0.18
3: 4:48.2	15:28:24	20.74	2.54	0.96	0.89
3: 4:48.3	15:23:27	20.18	0.55	-0.10	0.57
3: 4:48.5	15:31:34	20.34	0.86	0.50	0.32
3: 4:48.6	15:30:46	18.99	1.25	0.39	0.52
3: 4:49.1	15:28: 6	21.59	0.32	0.98	0.33
3: 4:49.5	15:29:35	20.11	1.00	0.28	0.38
3: 4:49.7	15:28:14	18.91	0.62	0.17	0.54
3: 4:49.8	15:27:57	20.60	0.96	0.48	0.38
3: 4:49.8	15:31:26	19.03	0.55	0.12	0.22
3: 4:50.0	15:31:56	19.90	0.54	0.23	-1.48
3: 4:50.1	15:29:23	18.88	1.51	-0.57	0.70
3: 4:50.1	15:29:28	19.78	0.71	0.22	0.27
3: 4:50.1	15:31:10	20.39	1.50	0.70	0.45
3: 4:50.4	15:26:18	20.46	0.80	0.60	0.42
3: 4:50.8	15:26:14	17.94	1.66	0.26	0.02
3: 4:50.8	15:27:48	20.52	1.29	0.46	0.50
3: 4:51.0	15:27:13	21.33	-	1.06	0.24
3: 4:51.1	15:31:21	17.54	1.52	0.22	0.52
3: 4:51.7	15:29:24	22.13	0.98	0.09	-1.27
3: 4:51.9	15:29: 0	20.88	0.65	0.18	-0.68
3: 4:51.9	15:31: 7	19.79	1.28	0.60	0.66
3: 4:52.1	15:27:14	20.38	0.40	0.96	0.71
3: 4:52.1	15:28:27	19.99	0.65	0.11	0.19

continued

MS0301					
3: 4:52.5	15:26:25	21.02	0.47	0.07	-0.24
3: 4:52.6	15:22:56	18.29	1.44	0.42	0.84
3: 4:52.6	15:24:52	17.94	0.79	0.26	0.68
3: 4:52.7	15:32:10	18.68	-	0.40	0.42
3: 4:52.9	15:29: 7	19.16	1.42	0.44	0.63
3: 4:52.9	15:30:39	21.09	2.46	0.06	-
3: 4:52.9	15:31: 3	20.78	1.76	0.09	-0.14
3: 4:53.0	15:30:46	20.38	1.47	0.27	0.19
3: 4:53.8	15:31:21	19.71	-	-0.06	-0.09
3: 4:53.9	15:30:40	19.29	1.20	0.30	0.63
3: 4:54.6	15:31:51	18.09	-	0.37	0.09
3: 4:55.6	15:28: 1	18.94	1.68	0.51	0.70
3: 4:55.8	15:23:20	19.57	1.31	-0.27	0.20
3: 4:56.0	15:24:38	18.36	1.53	0.31	0.84
3: 4:56.3	15:22:32	18.75	0.92	-0.01	0.64
3: 4:56.3	15:22:57	16.96	1.00	0.35	0.86
3: 4:57.7	15:22:43	19.79	1.71	-0.04	1.03
3: 4:58.8	15:27:52	20.83	-	0.18	0.20
3: 4:59.0	15:27: 8	20.37	1.04	-0.14	-0.53

Table A.2: Catalog of galaxies in the field of MS0301.

Galaxies in the field of MS0735					
RA (2000)	Dec (2000)	V	B-V	V-R	R-I
7:40:39.1	74:16:19	20.84	1.47	0.64	0.81
7:40:44.7	74:14:36	20.57	0.37	0.02	0.08
7:40:45.6	74:16:31	21.61	1.10	0.70	1.41
7:40:48.0	74:13:31	22.05	1.72	0.70	2.23
7:40:49.0	74:10:24	20.65	1.43	1.00	0.82
7:40:50.8	74:12:38	21.22	1.80	1.19	1.24
7:40:51.6	74:11:38	22.28	0.92	1.05	0.93
7:40:51.7	74:15:34	21.94	1.49	1.51	1.21
7:40:52.4	74: 9:41	19.88	1.56	0.97	0.92
7:40:53.0	74:14: 7	21.30	1.43	1.54	1.20
7:40:53.3	74:17:42	19.66	1.68	0.93	3.14
7:40:53.8	74:12:52	22.94	—	2.06	1.58
7:40:53.8	74:17:11	21.51	1.21	1.10	-0.38
7:40:54.7	74:11:36	21.23	0.97	0.85	0.19
7:40:55.1	74:12:17	21.98	0.12	0.68	-2.78
7:40:56.4	74:14:46	22.19	2.94	1.14	0.58
7:40:56.4	74:15:24	21.39	0.75	1.18	0.58
7:40:57.3	74:15: 0	20.33	0.81	0.87	0.53
7:40:58.3	74: 9:29	21.41	0.93	1.65	0.44
7:40:59.6	74:17: 1	21.01	1.32	1.26	1.34
7:41: 1.0	74:11:41	21.08	2.23	0.88	1.07
7:41: 1.0	74:13: 8	22.09	0.38	1.46	0.73
7:41: 1.0	74:15:36	22.49	—	1.81	1.19
7:41: 1.5	74:12:30	19.24	0.96	0.81	0.57
7:41: 1.6	74:12:56	20.34	1.27	1.03	0.67
7:41: 1.7	74:16:40	20.50	1.57	0.96	0.84
7:41: 2.2	74:16: 8	20.76	4.01	1.23	0.97
7:41: 3.0	74:11:53	21.95	1.06	0.97	0.19
7:41: 5.4	74:17:10	22.35	0.75	1.42	1.19
7:41: 5.9	74:16:43	22.13	1.07	0.91	1.79
7:41: 6.3	74:14:58	19.89	1.65	0.95	0.71
7:41: 6.3	74:15: 4	20.31	2.29	0.78	0.73
7:41: 7.4	74:11:33	22.86	-0.78	1.59	0.25
7:41: 7.7	74:15: 2	20.93	1.72	1.03	0.55
7:41: 8.1	74:13: 4	20.39	1.26	1.07	0.75
7:41: 8.2	74:14:21	20.14	1.64	0.95	0.75
7:41: 9.2	74:12: 7	20.21	1.87	1.04	0.74
7:41:12.4	74:13:50	22.09	1.75	1.55	0.80
7:41:12.9	74:11:34	21.02	1.23	0.88	0.62
7:41:13.0	74:17:52	21.85	0.43	0.94	-0.32
7:41:14.1	74:18:19	18.95	1.84	0.93	—
7:41:14.2	74:18:12	20.20	2.11	0.87	—
7:41:14.8	74:12: 7	22.22	0.72	1.05	0.65
7:41:15.2	74:14:26	21.48	1.50	1.52	1.34
7:41:15.7	74: 9:31	19.87	1.72	0.68	0.64
7:41:15.9	74:11:34	21.25	0.53	0.58	0.13
7:41:15.9	74:16:23	22.00	1.51	1.57	1.56
7:41:17.2	74:13:53	20.73	1.10	0.92	0.51
7:41:17.5	74:18:41	20.72	1.45	0.71	—
7:41:17.7	74:13:36	21.25	0.44	0.87	0.15
7:41:18.4	74:16:22	21.37	1.70	0.65	0.77
7:41:18.9	74:12:12	20.73	0.83	0.74	0.40
7:41:20.5	74:16:41	21.58	0.85	0.91	1.27
7:41:21.0	74:15:26	19.26	1.51	0.95	0.72
7:41:22.0	74:14:31	20.74	1.88	1.00	0.80
7:41:22.0	74:14:54	21.16	1.32	1.08	0.60
7:41:22.1	74:12:58	20.69	1.39	1.02	0.46
7:41:22.2	74: 9:45	20.39	2.00	1.69	1.78
7:41:25.0	74:12:53	19.89	1.47	0.95	0.74
7:41:25.8	74:18:10	21.15	1.35	1.11	—
7:41:25.9	74:17: 0	20.40	1.32	0.96	0.96
7:41:26.1	74:14:26	22.17	0.74	0.63	0.00
7:41:26.8	74:10: 0	22.62	1.04	1.87	0.73
7:41:27.2	74:10:33	20.86	1.04	0.78	0.41
7:41:28.6	74:17:25	21.73	0.60	1.35	0.98
7:41:30.4	74:16:43	19.62	1.78	0.94	0.85
7:41:31.1	74:17:57	19.75	1.44	0.91	2.43

continued

MS0735					
7:41:31.3	74:18:30	19.47	1.69	0.79	—
7:41:31.5	74:12:55	19.72	1.66	0.96	0.74
7:41:32.4	74:10:45	21.68	1.44	1.26	1.24
7:41:33.7	74:15:18	21.05	1.89	1.18	0.56
7:41:34.7	74:11: 5	20.75	1.48	0.84	0.81
7:41:34.7	74:14:28	22.12	0.70	0.78	0.35
7:41:36.2	74:17:40	21.51	1.09	0.95	1.23
7:41:36.4	74:13:13	21.97	1.62	0.90	0.01
7:41:36.8	74:16: 9	21.05	1.46	0.96	0.97
7:41:36.9	74:16:40	21.25	1.92	0.97	1.22
7:41:37.1	74:16: 4	21.53	1.26	0.93	0.82
7:41:38.6	74:18:15	21.18	1.21	1.14	—
7:41:39.2	74:11:54	22.42	3.89	1.72	1.65
7:41:39.2	74:16:29	21.22	0.68	1.26	1.16
7:41:39.5	74:15:48	20.24	1.03	0.94	0.68
7:41:39.8	74:15:37	21.21	1.63	0.95	0.65
7:41:40.0	74:13:29	21.82	1.34	0.95	0.68
7:41:41.1	74:18:22	21.30	1.91	-0.80	—
7:41:42.0	74:10: 9	19.76	1.65	0.94	0.76
7:41:42.6	74:14:58	21.31	1.60	1.09	0.44
7:41:42.7	74:15:23	20.84	1.35	1.21	0.73
7:41:42.8	74:16:26	19.39	1.28	0.79	0.58
7:41:43.1	74:14:36	19.81	2.13	0.85	0.74
7:41:43.4	74:17:41	20.37	1.61	0.91	0.90
7:41:43.5	74:10:38	22.54	—	1.77	1.67
7:41:44.6	74:14:38	18.53	1.62	0.95	0.79
7:41:45.0	74:10:40	20.09	1.64	1.06	0.72
7:41:45.1	74:13:31	20.31	1.14	1.01	0.72
7:41:45.7	74:13:34	20.93	1.54	1.26	1.31
7:41:45.7	74:15:57	20.01	2.67	0.95	0.73
7:41:46.0	74:15: 4	21.15	1.02	1.15	0.45
7:41:46.1	74:14: 8	18.86	1.58	0.95	0.75
7:41:46.4	74:10:52	19.39	1.78	0.74	0.75
7:41:46.7	74:14:12	19.54	1.68	0.85	0.84
7:41:47.5	74:16:16	20.85	2.27	1.06	0.75
7:41:48.3	74:17:55	19.69	1.65	0.81	0.57
7:41:48.7	74:15:27	20.67	2.01	0.94	0.62
7:41:48.7	74:18: 3	21.08	1.34	0.97	2.44
7:41:48.9	74:13: 6	23.54	0.17	2.90	1.75
7:41:49.1	74:14:10	21.36	1.22	0.69	0.56
7:41:49.1	74:14:40	23.40	-0.52	2.36	0.93
7:41:49.2	74:18:43	20.86	1.96	0.88	—
7:41:49.6	74:12: 8	20.36	1.59	0.94	0.77
7:41:49.7	74:12:16	20.97	1.88	0.93	0.63
7:41:50.9	74:12:30	19.78	1.35	0.93	0.71
7:41:50.9	74:18:21	18.60	0.80	0.68	—
7:41:51.0	74:18:51	21.14	1.70	0.77	—
7:41:51.6	74:15:16	22.53	-0.56	1.22	0.68
7:41:52.2	74:10:53	20.71	2.94	0.60	0.47
7:41:52.4	74:12:13	19.53	1.91	0.91	0.75
7:41:53.2	74:12:12	19.86	2.24	0.83	0.79
7:41:53.3	74:17: 0	21.74	0.40	1.27	1.06
7:41:53.6	74:11: 0	20.73	2.60	0.75	0.57
7:41:53.7	74:18:14	22.58	0.91	1.56	—
7:41:53.9	74:15: 8	22.40	1.47	1.27	0.80
7:41:54.0	74:17:28	19.37	1.71	1.00	0.74
7:41:54.1	74:13:36	20.48	1.44	1.62	1.66
7:41:54.1	74:15:45	21.47	0.23	0.67	0.54
7:41:54.7	74: 9:32	21.11	0.50	0.77	0.80
7:41:54.7	74:14:16	19.49	1.36	0.93	0.74
7:41:55.0	74:11:54	21.10	1.24	0.47	0.91
7:41:55.3	74:18: 9	21.36	1.01	1.26	—
7:41:55.6	74:13:34	20.42	1.59	1.04	0.76
7:41:56.3	74:12: 8	20.44	3.15	1.00	0.84
7:41:56.4	74:13:41	20.62	2.65	0.89	0.75
7:41:56.5	74:11:53	19.90	1.59	0.93	0.77
7:41:57.3	74:13: 6	21.96	0.95	1.18	0.44
7:41:57.4	74:13:57	21.96	1.14	1.08	0.92
7:41:57.9	74:12:53	21.40	2.08	0.99	0.71

continued

MS0735					
7:41:58.0	74:10:19	19.67	1.38	0.89	0.77
7:41:58.5	74: 9:33	20.04	1.83	0.90	0.64
7:41:58.7	74:16:45	19.74	2.10	0.91	0.73
7:41:58.9	74: 9:42	20.00	1.90	0.88	0.86
7:41:59.1	74:15:46	20.79	1.51	0.96	0.73
7:41:59.2	74:11:48	20.14	1.85	0.97	0.75
7:41:59.3	74:10:21	21.19	1.68	0.61	0.77
7:41:59.5	74: 9:51	19.38	1.75	0.90	0.74
7:41:59.6	74:12: 1	21.60	0.90	0.71	0.75
7:41:59.7	74:12:49	20.45	1.22	0.97	0.95
7:42: 2.6	74:11:30	22.58	0.66	1.27	1.31
7:42: 2.7	74:13:33	21.60	1.34	1.07	0.73
7:42: 3.3	74:15: 0	21.10	1.33	0.88	0.41
7:42: 3.8	74:17:22	20.65	1.32	0.91	0.34
7:42: 5.1	74:15:58	21.81	1.58	0.87	0.56
7:42: 5.8	74:13:12	20.85	1.11	0.99	0.66
7:42: 6.6	74:15:38	19.74	1.22	0.71	0.62
7:42: 6.8	74:17:18	21.51	1.85	1.39	0.78
7:42: 7.2	74:12:26	21.29	1.20	0.82	0.70
7:42: 8.5	74:10: 9	21.34	3.13	0.50	0.39
7:42: 8.8	74:10:48	21.42	1.38	0.67	0.71
7:42:10.4	74: 9:45	21.24	1.76	1.08	0.43
7:42:11.7	74:11:32	20.24	1.40	0.87	0.71
7:42:12.6	74:12:33	21.31	1.87	0.96	1.04
7:42:12.7	74:15:18	19.33	1.83	0.91	0.79
7:42:15.3	74:18:40	19.88	1.65	1.11	-
7:42:16.1	74: 9:43	19.76	2.46	1.03	0.77
7:42:17.0	74: 9:34	21.48	2.03	1.49	-0.11
7:42:17.1	74:12: 4	22.00	0.74	1.08	0.43
7:42:17.5	74:13:40	22.30	0.56	0.95	1.18
7:42:18.1	74:10:22	20.50	2.43	0.91	0.22
7:42:18.9	74:12:37	21.70	1.20	0.66	0.63
7:42:20.7	74:12:35	21.76	-	0.30	0.14
7:42:21.1	74:11:39	22.21	1.88	1.35	1.09
7:42:21.3	74:16: 4	22.76	2.31	1.53	1.66
7:42:21.5	74:15:31	21.67	3.78	0.66	-0.09
7:42:22.1	74:10:17	19.73	2.56	0.86	0.55
7:42:22.8	74:12:45	21.83	1.64	1.22	1.46
7:42:23.6	74:11:32	19.05	1.23	0.73	0.66
7:42:23.7	74:14:13	22.08	1.63	1.24	0.60
7:42:24.0	74:10:13	20.43	4.11	0.75	0.37
7:42:26.6	74:15:36	18.64	0.82	0.53	0.51
7:42:27.3	74:11:18	20.81	0.85	0.77	0.51
7:42:27.4	74:12:50	19.80	1.65	0.85	0.66
7:42:27.5	74:12: 3	19.01	1.55	0.79	0.73
7:42:28.6	74:13:16	19.70	1.52	1.10	1.16
7:42:28.6	74:13:23	18.71	1.79	0.88	0.77
7:42:30.1	74:13:30	20.88	1.25	0.96	0.65
7:42:30.7	74:14:13	20.72	1.66	0.97	0.61
7:42:30.7	74:15:31	20.49	0.89	0.67	0.75
7:42:31.0	74:11:58	20.29	1.27	0.76	0.65
7:42:31.1	74:16:25	21.87	1.37	0.72	0.96
7:42:31.4	74:13:57	22.84	0.90	1.39	1.27
7:42:31.6	74:13: 0	21.97	0.67	0.81	0.14
7:42:32.0	74:12:38	20.90	1.23	1.18	0.67
7:42:33.0	74:16:58	21.09	0.84	0.77	0.20
7:42:33.3	74:11: 2	20.00	1.58	0.82	0.71
7:42:34.0	74:11:38	21.39	1.87	0.94	0.55
7:42:34.6	74:17:51	21.77	1.20	0.51	-
7:42:34.7	74:10:44	22.20	1.64	1.30	1.66
7:42:34.8	74:13:25	21.86	2.17	1.29	1.27
7:42:35.6	74:16:41	21.46	0.65	0.72	0.50
7:42:37.3	74:11:12	20.43	1.04	0.51	0.57
7:42:37.8	74:10:33	22.34	1.01	0.89	1.26
7:42:38.0	74:17:16	20.65	0.83	0.68	0.53
7:42:38.3	74:14: 7	19.52	1.27	0.75	0.71
7:42:38.4	74:14:43	22.09	0.76	1.19	1.60
7:42:38.6	74:10:47	21.81	-	1.02	1.66
7:42:38.9	74:15: 2	20.08	1.63	0.90	0.78

continued

MS0735					
7:42:39.6	74:15:21	20.01	1.22	0.59	0.59
7:42:39.7	74:14: 8	21.74	0.51	0.78	0.97
7:42:40.0	74:12: 2	19.59	1.19	0.82	0.76
7:42:40.4	74:12:13	21.24	1.25	1.06	1.09
7:42:42.1	74:16:39	21.54	1.13	1.35	0.90
7:42:43.2	74:10:55	22.04	1.58	1.01	0.32
7:42:43.8	74:15:54	20.85	1.71	0.91	0.95
7:42:44.5	74:11:38	22.00	0.41	1.08	1.07
7:42:46.0	74:16:15	21.93	-	1.05	1.05
7:42:46.1	74:17:51	21.59	1.19	0.40	-
7:42:46.5	74:15:32	19.40	1.62	0.92	0.75
7:42:46.5	74:17:38	22.65	-0.19	1.76	1.64
7:42:46.8	74:14:32	20.79	0.80	0.62	0.76
7:42:47.6	74:10:59	19.99	2.02	0.51	0.98
7:42:48.1	74:11: 4	18.52	1.85	0.85	0.80
7:42:48.5	74:15:47	20.34	0.91	0.67	0.41
7:42:49.0	74: 9:39	20.05	0.63	0.60	0.34
7:42:49.5	74:17:41	21.32	1.56	0.82	-0.41
7:42:49.6	74:11:56	19.94	1.85	0.97	0.74
7:42:50.4	74:11:30	21.47	0.75	0.80	0.28
7:42:51.2	74: 9:46	20.39	1.89	0.72	0.62
7:42:51.8	74:12:43	21.77	-	1.21	1.39
7:42:53.1	74:14:23	21.34	3.01	1.17	1.23
7:42:53.3	74:13:31	22.15	-	1.20	1.17
7:42:54.4	74:12:48	19.03	1.74	1.10	1.20
7:42:54.8	74:14:16	21.12	0.87	0.74	0.45
7:42:54.9	74:14:39	20.64	1.25	0.76	0.56
7:42:55.8	74:11:25	20.34	1.61	0.61	0.78
7:42:55.9	74:10:13	20.31	2.25	0.95	0.71
7:42:57.3	74:12: 5	19.22	1.67	0.90	0.79
7:42:57.9	74:10:49	21.02	0.35	1.07	0.43
7:42:59.2	74:12:45	20.00	-	0.77	0.45
7:42:59.9	74: 9:47	20.33	-	0.93	0.42
7:42:60.0	74:15: 0	19.70	-	0.72	0.42

Table A.3: Catalog of galaxies in the field of MS0735

Galaxies in the field of MS1306					
RA (2000)	Dec (2000)	V	B-V	V-R	R-I
13: 8:57.5	-1:35:14	20.99	1.02	0.75	0.36
13: 8:57.5	-1:36:59	20.94	1.70	0.94	0.20
13: 8:57.8	-1:33:27	19.24	1.32	0.93	0.85
13: 8:57.8	-1:38:18	19.83	1.48	1.20	1.56
13: 8:58.2	-1:35:10	20.50	1.06	1.26	1.46
13: 8:58.2	-1:40:50	20.66	0.27	0.06	0.01
13: 8:58.9	-1:32:25	20.39	1.17	0.34	-
13: 8:58.9	-1:41:46	20.25	0.08	0.39	0.42
13: 8:60.0	-1:39:24	21.20	1.08	1.09	0.64
13: 9: 0.4	-1:37:53	19.28	0.32	0.69	0.24
13: 9: 0.7	-1:36:29	19.31	1.41	1.13	1.16
13: 9: 0.7	-1:36:42	21.24	0.72	1.20	0.44
13: 9: 0.7	-1:39:25	20.30	0.87	0.81	0.48
13: 9: 0.7	-1:41: 0	20.18	0.46	0.43	0.40
13: 9: 1.1	-1:34:54	20.81	1.25	1.49	1.57
13: 9: 1.1	-1:41:24	20.38	1.22	1.17	1.61
13: 9: 1.4	-1:36:50	21.09	0.72	1.60	1.05
13: 9: 1.4	-1:40: 5	20.55	1.26	0.42	0.43
13: 9: 2.5	-1:34:13	20.57	0.30	0.74	0.87
13: 9: 2.5	-1:37:37	20.13	0.51	0.88	0.44
13: 9: 2.9	-1:34:40	18.75	1.08	0.80	0.64
13: 9: 3.2	-1:39:11	24.56	-2.20	4.03	1.80
13: 9: 3.6	-1:40: 8	21.20	0.19	1.17	0.96
13: 9: 3.6	-1:41:57	19.38	1.13	0.65	0.91
13: 9: 4.3	-1:31:59	19.84	1.28	0.17	-
13: 9: 4.7	-1:37:17	19.90	0.15	0.62	0.73
13: 9: 5.0	-1:31:56	18.03	1.65	0.96	-
13: 9: 5.0	-1:36:22	20.35	0.54	0.95	0.95
13: 9: 5.0	-1:36:43	16.96	0.73	0.43	0.69
13: 9: 5.4	-1:35:59	21.29	0.35	0.96	1.20
13: 9: 5.8	-1:34:18	22.75	0.79	2.53	1.51
13: 9: 5.8	-1:37:49	22.20	-0.66	2.03	0.91
13: 9: 6.1	-1:33:29	20.83	2.07	1.18	1.23
13: 9: 6.1	-1:33:53	18.28	1.36	0.78	0.86
13: 9: 6.5	-1:35: 8	19.34	0.83	0.72	0.94
13: 9: 6.5	-1:38: 5	19.20	0.48	0.65	0.45
13: 9: 6.5	-1:38:21	19.31	1.05	0.86	0.72
13: 9: 6.8	-1:34:35	19.45	0.82	0.84	0.75
13: 9: 7.2	-1:37: 1	19.38	1.16	0.98	0.94
13: 9: 7.2	-1:40:42	21.58	0.01	0.83	0.13
13: 9: 7.6	-1:35:39	17.00	0.62	0.42	0.71
13: 9: 7.6	-1:38:38	19.27	0.98	0.82	0.62
13: 9: 7.6	-1:41:15	18.67	1.22	0.81	0.60
13: 9: 7.9	-1:37:15	17.06	1.13	0.67	0.83
13: 9: 8.3	-1:39: 5	20.85	-0.28	1.03	-0.27
13: 9: 8.3	-1:42:14	20.61	0.66	0.77	0.01
13: 9: 8.6	-1:32:15	19.24	0.82	0.31	-
13: 9: 8.6	-1:39:59	19.99	0.73	0.80	0.36
13: 9: 9.0	-1:33:41	18.51	1.06	0.74	0.81
13: 9: 9.0	-1:34:52	20.17	1.64	1.29	1.03
13: 9: 9.4	-1:34:29	22.03	-0.32	2.15	1.38
13: 9: 9.4	-1:39:53	22.44	-0.14	2.06	0.12
13: 9: 9.4	-1:40:12	20.60	0.80	0.78	-0.08
13: 9: 9.7	-1:32: 9	16.38	1.25	0.67	-
13: 9: 9.7	-1:34:31	23.42	-0.31	3.31	1.55
13: 9: 9.7	-1:36:25	18.31	1.02	0.74	0.75
13: 9: 9.7	-1:36:59	16.49	1.87	-0.37	1.15
13: 9:10.1	-1:33:38	20.72	1.34	1.63	1.28
13: 9:10.1	-1:34: 9	20.56	1.39	1.74	1.16
13: 9:10.4	-1:33:23	19.51	0.98	0.58	0.80
13: 9:10.4	-1:33:44	22.01	1.36	2.03	1.32
13: 9:11.2	-1:36: 4	20.86	0.92	1.11	1.17
13: 9:11.2	-1:41: 7	21.18	1.50	1.31	-0.57
13: 9:11.5	-1:33:52	20.16	0.86	0.84	0.90
13: 9:11.5	-1:39:41	20.91	0.89	1.21	0.57
13: 9:11.5	-1:42: 3	21.97	-0.06	1.61	-0.26
13: 9:11.9	-1:38:35	20.97	0.80	0.92	0.42

continued

MS1306					
13: 9:12.2	-1:36:18	20.98	1.29	1.18	0.85
13: 9:12.6	-1:38:52	21.47	1.19	1.71	0.71
13: 9:12.6	-1:39:56	22.05	0.04	1.65	-0.64
13: 9:13.0	-1:36:15	21.16	1.75	1.72	1.12
13: 9:13.3	-1:35:47	23.50	-0.37	3.06	1.39
13: 9:13.3	-1:36: 7	17.88	1.14	0.71	0.84
13: 9:13.7	-1:35: 1	21.91	1.56	2.10	1.27
13: 9:13.7	-1:36:48	20.14	0.83	0.91	0.93
13: 9:13.7	-1:39: 3	19.42	1.08	0.89	0.59
13: 9:14.0	-1:36:33	16.89	1.20	0.66	0.85
13: 9:14.4	-1:32:52	21.29	0.20	0.91	1.19
13: 9:14.4	-1:33:12	21.36	0.07	0.75	1.44
13: 9:14.4	-1:41:38	21.57	-0.24	1.19	-0.77
13: 9:14.8	-1:39:15	22.03	0.94	1.61	0.51
13: 9:15.1	-1:34: 8	21.67	0.16	1.39	1.04
13: 9:15.5	-1:32:28	19.51	1.69	1.09	-
13: 9:15.8	-1:35:56	17.25	1.18	0.69	0.86
13: 9:15.8	-1:41:55	21.26	0.28	1.15	-0.17
13: 9:16.2	-1:34:30	17.09	1.20	0.69	0.88
13: 9:16.9	-1:38:22	20.52	1.53	1.11	1.56
13: 9:16.9	-1:40:26	19.07	1.71	1.13	0.82
13: 9:17.3	-1:37: 7	19.99	0.89	0.82	1.19
13: 9:17.6	-1:33:23	19.91	1.17	1.19	0.88
13: 9:17.6	-1:34: 5	21.53	0.04	1.53	0.81
13: 9:17.6	-1:36:54	16.34	1.22	0.63	0.87
13: 9:17.6	-1:39: 1	20.75	0.66	0.82	0.85
13: 9:18.0	-1:33:15	21.20	0.39	1.10	0.83
13: 9:18.0	-1:41:32	20.62	0.97	1.17	0.45
13: 9:18.4	-1:42:12	21.73	0.87	1.52	0.57
13: 9:19.1	-1:32:52	18.14	0.91	0.66	0.78
13: 9:19.1	-1:34:17	19.31	0.93	0.95	0.77
13: 9:19.1	-1:34:53	20.16	0.68	0.95	0.81
13: 9:19.1	-1:36: 9	19.81	1.01	0.64	1.06
13: 9:19.1	-1:37: 9	17.71	1.28	0.29	1.09
13: 9:19.1	-1:37:22	14.89	1.24	0.62	0.86
13: 9:19.1	-1:38:22	19.87	1.16	0.67	0.94
13: 9:19.1	-1:38:30	20.06	1.58	0.78	0.87
13: 9:19.4	-1:37:49	19.89	1.24	0.30	1.35
13: 9:19.4	-1:39:41	19.06	0.87	0.76	0.50
13: 9:19.4	-1:41:33	19.22	1.19	0.83	0.67
13: 9:19.8	-1:37:37	19.35	1.05	0.47	1.00
13: 9:19.8	-1:37:43	20.01	0.92	0.50	1.52
13: 9:20.2	-1:35:46	20.01	1.13	1.12	1.02
13: 9:20.2	-1:36:17	16.56	1.18	0.63	0.89
13: 9:20.2	-1:42: 9	20.69	1.64	1.11	1.14
13: 9:20.5	-1:32:12	20.31	0.84	0.03	-
13: 9:20.5	-1:32:42	20.85	0.81	0.27	-0.79
13: 9:20.5	-1:34:56	18.15	0.53	0.39	0.58
13: 9:20.5	-1:35: 7	17.75	1.11	0.65	0.83
13: 9:20.5	-1:37:34	20.02	1.00	0.55	1.07
13: 9:20.5	-1:42:12	20.48	1.14	0.68	0.34
13: 9:20.9	-1:37:24	17.99	1.13	0.67	0.85
13: 9:20.9	-1:40:31	19.90	0.79	0.97	0.41
13: 9:20.9	-1:42:10	20.29	0.76	0.72	0.25
13: 9:20.9	-1:42:20	19.57	1.27	0.68	0.66
13: 9:21.2	-1:37:59	16.98	1.18	0.63	0.86
13: 9:21.2	-1:42: 4	18.91	1.33	0.73	0.70
13: 9:21.6	-1:38:28	18.80	1.16	0.79	0.71
13: 9:21.6	-1:39:52	19.99	0.61	1.02	0.56
13: 9:21.6	-1:40:58	18.98	1.07	0.91	0.56
13: 9:22.0	-1:34:47	20.16	1.40	1.16	0.90
13: 9:22.3	-1:37: 6	20.31	0.26	0.51	0.74
13: 9:22.3	-1:38:52	19.89	0.46	0.85	0.40
13: 9:22.3	-1:39:42	21.36	-0.01	1.21	-0.18
13: 9:23.0	-1:36:18	20.76	0.43	0.87	0.83
13: 9:23.0	-1:36:39	21.12	0.06	0.93	0.92
13: 9:23.4	-1:32:26	19.47	1.54	0.56	-
13: 9:23.4	-1:34:18	21.30	0.44	1.30	0.91
13: 9:23.4	-1:35:50	22.31	-0.44	1.87	1.23

continued

MS1306					
13: 9:23.4	-1:40:49	21.08	1.44	1.38	0.40
13: 9:23.8	-1:33:35	18.98	1.06	0.74	0.64
13: 9:23.8	-1:33:44	19.84	0.97	0.76	0.44
13: 9:23.8	-1:34:12	21.04	1.01	0.92	0.24
13: 9:24.1	-1:33:46	19.69	0.90	0.74	0.43
13: 9:24.1	-1:36:36	22.84	-0.35	2.69	1.51
13: 9:24.1	-1:38:43	19.86	0.97	0.94	0.54
13: 9:24.1	-1:41:29	20.90	0.79	1.03	-0.81
13: 9:24.5	-1:39: 1	21.27	0.11	1.31	0.05
13: 9:24.5	-1:40:53	20.46	1.39	1.46	0.68
13: 9:24.8	-1:32:38	16.42	0.98	0.64	-
13: 9:24.8	-1:34:46	19.78	0.88	0.34	0.28
13: 9:24.8	-1:36:42	19.08	0.88	0.81	0.60
13: 9:24.8	-1:36:56	18.15	1.06	0.70	0.76
13: 9:25.2	-1:32:59	20.63	1.04	0.58	0.99
13: 9:25.9	-1:33:59	19.11	0.78	0.56	0.36
13: 9:26.6	-1:34:22	17.24	1.18	0.63	0.82
13: 9:26.6	-1:40: 8	21.61	1.56	1.86	0.21
13: 9:26.6	-1:40:41	20.06	0.58	0.89	0.00
13: 9:27.4	-1:32:50	16.84	1.27	0.63	0.82
13: 9:27.4	-1:34: 5	20.81	1.15	0.67	0.10
13: 9:27.4	-1:37:55	17.68	1.13	0.65	0.76
13: 9:27.4	-1:38: 0	18.61	1.11	0.67	0.63
13: 9:27.4	-1:41:20	21.29	1.08	-	-
13: 9:27.7	-1:32:33	20.50	1.94	0.32	-
13: 9:27.7	-1:36:29	20.42	0.69	0.74	-0.03
13: 9:27.7	-1:38:19	21.71	-0.30	1.58	0.04
13: 9:28.1	-1:36:25	21.03	0.89	0.81	-0.89
13: 9:28.1	-1:37:50	20.01	1.05	0.97	0.31
13: 9:28.1	-1:39:23	17.84	1.07	0.67	0.73
13: 9:28.8	-1:33: 9	20.46	3.20	0.64	1.09
13: 9:28.8	-1:37:23	19.58	1.10	0.87	0.43
13: 9:29.2	-1:32: 5	20.36	1.96	-0.11	-
13: 9:29.5	-1:33:21	19.93	2.75	-0.17	-0.27
13: 9:29.9	-1:32:29	20.33	2.29	-0.25	-
13: 9:29.9	-1:33:20	20.55	1.55	-0.04	-
13: 9:29.9	-1:36: 0	20.69	2.60	0.95	0.96
13: 9:29.9	-1:36:32	20.90	0.72	0.87	-1.10
13: 9:29.9	-1:38:46	22.52	-0.51	1.89	-
13: 9:30.2	-1:35: 9	17.89	1.23	0.63	0.73
13: 9:30.2	-1:38:20	18.40	1.08	0.70	0.70
13: 9:30.2	-1:42: 2	20.31	1.05	0.28	-0.06
13: 9:30.6	-1:37:46	20.34	0.66	0.59	-0.75
13: 9:30.6	-1:37:51	18.78	0.40	0.40	0.12
13: 9:30.6	-1:38:21	17.98	1.48	0.92	1.05
13: 9:31.0	-1:37:22	23.70	-0.09	3.20	0.14
13: 9:31.3	-1:32:57	19.66	2.98	0.65	0.16
13: 9:31.3	-1:38:52	19.07	1.35	0.56	0.68
13: 9:31.3	-1:39: 3	18.76	1.01	0.54	0.53
13: 9:31.7	-1:34:53	20.37	1.45	0.99	0.79
13: 9:31.7	-1:35:34	20.21	1.34	0.40	0.34
13: 9:31.7	-1:36:50	19.85	1.07	0.76	0.17
13: 9:32.0	-1:32: 9	20.23	1.71	-0.27	-
13: 9:32.0	-1:37:36	20.52	1.78	1.15	0.16
13: 9:32.0	-1:41:50	21.37	2.54	1.10	-0.61
13: 9:32.4	-1:34:38	17.18	1.29	0.66	0.80
13: 9:32.8	-1:36:33	20.78	3.96	1.00	0.92
13: 9:32.8	-1:36:59	20.52	1.11	0.57	-0.93
13: 9:33.1	-1:36:34	21.15	4.01	1.05	-0.60
13: 9:33.1	-1:37: 0	21.38	-	1.11	-0.43
13: 9:33.1	-1:38:45	17.93	0.02	-0.07	-0.01
13: 9:33.5	-1:33:57	20.54	2.07	-0.27	-
13: 9:33.5	-1:34:53	16.99	1.24	0.63	0.81
13: 9:33.5	-1:35:35	19.05	1.18	0.62	0.49
13: 9:33.5	-1:40:45	20.02	1.85	1.38	2.14
13: 9:33.8	-1:41:59	20.35	1.70	-	-0.32
13: 9:34.2	-1:34:23	20.41	2.26	0.12	-
13: 9:34.6	-1:38:37	21.26	1.72	0.63	-
13: 9:34.6	-1:40:39	19.20	0.92	0.43	-0.05

continued

MS1306					
13: 9:34.9	-1:33:23	19.24	1.48	0.45	-0.57
13: 9:34.9	-1:37:35	20.58	1.01	0.40	-
13: 9:35.3	-1:35: 1	20.33	2.49	0.22	-
13: 9:35.3	-1:37: 0	19.95	1.04	0.35	-1.29
13: 9:35.3	-1:38:11	19.50	1.87	0.94	0.91
13: 9:35.6	-1:40:22	20.37	1.18	-	-0.32
13: 9:36.0	-1:33: 4	18.02	0.98	0.44	-
13: 9:36.0	-1:35:33	19.55	1.72	0.64	-
13: 9:36.4	-1:39:56	20.14	2.12	0.33	-
13: 9:36.7	-1:34:34	19.97	1.97	0.63	-
13: 9:36.7	-1:38: 4	21.19	0.98	0.62	-
13: 9:36.7	-1:41:50	18.66	0.65	0.40	-
13: 9:37.1	-1:37: 2	20.05	1.35	0.14	-
13: 9:37.4	-1:38:18	19.50	1.21	0.32	-
13: 9:37.8	-1:36:12	19.76	1.51	-0.03	-
13: 9:37.8	-1:38:27	20.38	2.23	-0.04	-
13: 9:38.2	-1:35:19	19.77	2.00	-0.23	-
13: 9:38.2	-1:35:35	20.12	1.66	0.05	-
13: 9:38.2	-1:36: 0	17.55	0.89	0.50	-
13: 9:38.5	-1:38:25	18.49	1.21	0.54	-
13: 9:38.5	-1:38:32	20.23	1.98	-	-0.32
13: 9:38.5	-1:41:39	18.64	0.71	0.33	-
13: 9:38.9	-1:36:54	19.04	0.96	0.27	-
13: 9:39.2	-1:38: 2	19.28	1.09	0.10	-

Table A.4: Catalog of galaxies in the field of MS1306.

Appendix B

Cosmological Parameters

This presents graphically the variation of distance, the distance modulus, the angular size subtended, and the linear scale.

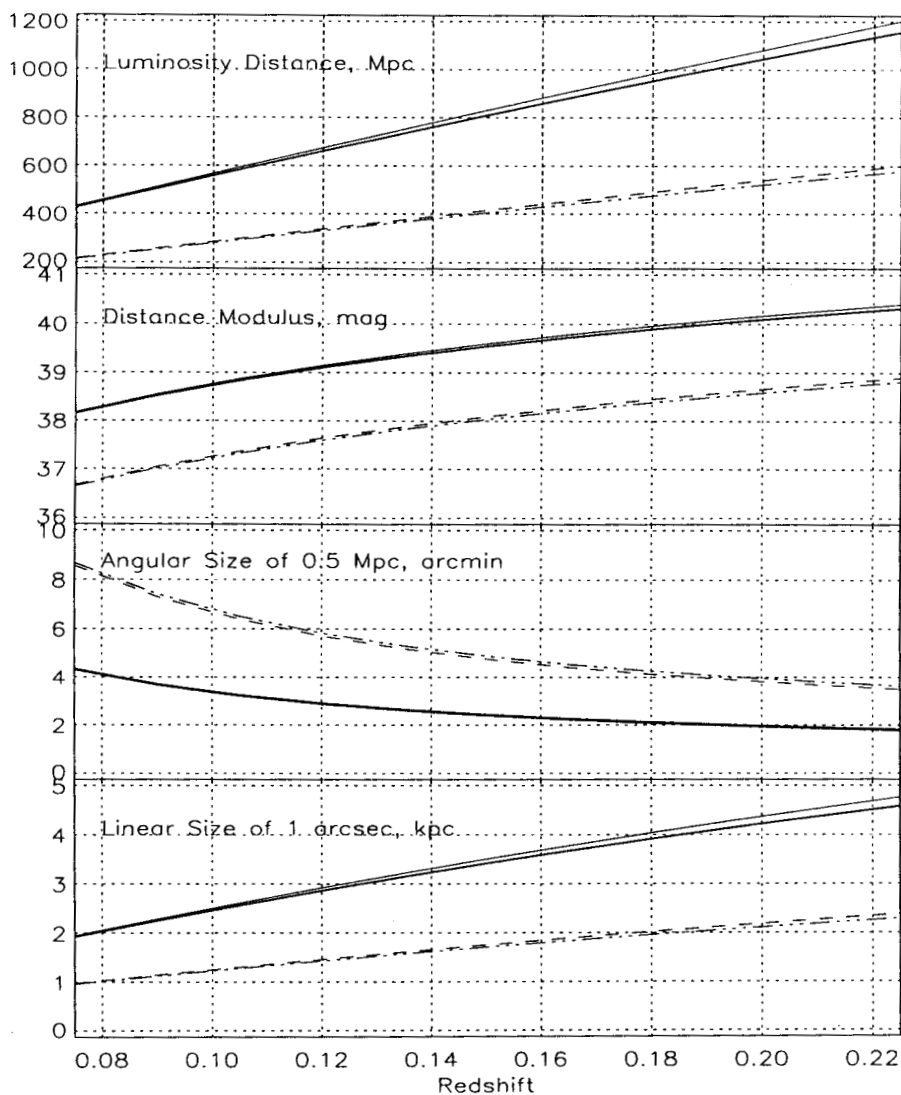


Figure B.1: Luminosity distance, distance modulus, angular size and linear size in different cosmologies. Thick solid lines are for $H_0 = 50 \text{ km s}^{-1} \text{ Mpc}^{-1}$ and $q_0 = 0.5$, thin solid lines for $H_0 = 50 \text{ km s}^{-1} \text{ Mpc}^{-1}$ and $q_0 = 0$, dashed lines for $H_0 = 100 \text{ km s}^{-1} \text{ Mpc}^{-1}$ and $q_0 = 0.5$, dashed-dotted lines for $H_0 = 100 \text{ km s}^{-1} \text{ Mpc}^{-1}$ and $q_0 = 0$.

Appendix C

Image Reduction Software

Here we present a synopsis of the software packages, and a listing of the most important tasks within them, that we have used to reduce and analyze the CCD data.

Image Reduction and Analysis Facility ¹ (IRAF) includes programs for general image processing and graphics, plus a large number of programs specially for the reduction and analysis of optical and Infra-Red astronomical data, both image and spectroscopic. It also has layered onto its packages to analyze data in other wavelength regimes such as Ultra-Violet and X-ray.

Space Telescope Science Data Analysis System (STSDAS) is a software package for reducing and analyzing data from the Hubble Space Telescope but can be used on essentially any astronomical data. Its tasks are designed to make use of IRAF images and the package itself is integrated onto IRAF. STSDAS includes packages for fitting image features e.g., 2-dimensional galaxy brightness profiles with elliptical isophotes, and for image deconvolution and restoration, etc.

Faint Object Classification and Analysis System (FOCAS, Jarvis and Tyson 1981, Valdes 1982) is a suite of programs for the detection and classification of objects on astronomical images. FOCAS acts to reduce the digitized image to a catalog containing the magnitude, position and classification data for objects in the image field. The cataloging process includes the segmentation of objects to a limiting isophote, estimation of object dimensions, and object listing. FOCAS classifies objects as noise, stars or galaxies proceeds by fitting the PSF to the object light distribution using nonparametric statistical pattern recognition techniques. If one uses optimal parameters to ensure detection of the faintest objects without significant contamination from spurious sources, one can routinely achieve detection efficiencies of $\approx 90\%$ and classification accuracies of $\approx 80\%$ for apparent magnitudes as faint as 24.

We used, among others, the following IRAF/STSDAS packages and the commands within them:
images.tv

display - Load an image or image section into the display

imedit - Examine and edit pixels in images

imexamine - Examine images using image display, graphics, and text

tvmark - Mark objects on the image display

images.imgeom

blkavg - Block average or sum a list of N-D images

magnify - Magnify a list of 1-D or 2-D images

rotate - Rotate and shift a list of 2-D images

¹IRAF is distributed by the National Optical Astronomical Observatories operated by the Association of Universities for Research in Astronomy, Inc., USA, under co-operative agreement with the National Science Foundation.

images.imcoords

ccmap - Compute image plate solutions using matched coordinate lists
ccsetwcs - Create an image celestial wcs from the ccmap plate solution
ccxymatch - Match celestial and pixel coordinate lists

images.immatch

imalign - Align and register 2-D images using a reference pixel list
imcentroid - Compute and print relative shifts for a list of 2-D images
imcombine - Combine images pixel-by-pixel using various algorithms
psfmatch - Match the point-spread functions of 1-D or 2-D images
wregister - Register 1-D or 2-D images using the image wcs

images.imutil

chpixtype - Change the pixel type of a list of images
hedit - Header editor
imarith - Simple image arithmetic
imstatistics - Compute and print statistics for a list of images

noao.apphot and noao.daophot

phot - Measure magnitudes for a list of stars
psf - Compute the point spread function

noao.artdata

mkobjects - Make/add artificial stars and galaxies to 2D images
mkpattern - Make/add patterns to images

stsdas.analysis.isophote

bmodel - Build a model image from isophotal analysis data
ellipse - Fit elliptical isophotes

stsdas.analysis.fitting

gfit1d - Interactive 1-d linear curve fit to images, tables or lists

NB 4315